The ATLAS liquid argon calorimeter high-voltage system: commissioning, optimisation, and LHC relative luminosity measurement

Samir. S. Arfaoui

▶ **To cite this version:**

Samir. S. Arfaoui. The ATLAS liquid argon calorimeter high-voltage system: commissioning, optimisation, and LHC relative luminosity measurement. Instrumentation and Detectors [physics.ins-det]. Université de la Méditerranée - Aix-Marseille II, 2011. English. NNT : . tel-00658194

HAL Id: tel-00658194

https://theses.hal.science/tel-00658194

Submitted on 10 Jan 2012

HAL is a multi-disciplinary open access archive for the deposit and dissemination of scientific research documents, whether they are published or not. The documents may come from teaching and research institutions in France or abroad, or from public or private research centers.

L'archive ouverte pluridisciplinaire **HAL**, est destinée au dépôt et à la diffusion de documents scientifiques de niveau recherche, publiés ou non, émanant des établissements d'enseignement et de recherche français ou étrangers, des laboratoires publics ou privés.

CPPM-T-2011-05

Université de la Méditerranée Aix-Marseille II
Faculté des Sciences de Luminy

Centre de Physique des Particules de Marseille

Organisation Européenne pour la Recherche Nucléaire

Thèse de Doctorat
spécialité
Instrumentation

présentée par
Samir Arfaoui

pour l'obtention du titre de
Docteur en Sciences

Système haute-tension du calorimètre à argon liquide du détecteur ATLAS: mise en œuvre, optimisation, et mesure de luminosité du LHC

---

soutenue le 14 Octobre 2011 devant le jury composé de:

Walter Bonivento	Examinateur
Beate Heinemann	Rapporteuse
Luis Hervas	Co-directeur / Superviseur CERN
Eric Kajfasz	Président du jury
Emmanuel Monnier	Directeur de thèse
Patrick Puzo	Rapporteur

2

CPPM-T-2011-05

Université de la Méditerranée Aix-Marseille II
Faculté des Sciences de Luminy

Centre de Physique des Particules de Marseille

European Organisation for Nuclear Research

Ph.D. Thesis

speciality

Instrumentation

presented by

Samir Arfaoui

for the title

Docteur en Sciences

The ATLAS liquid argon calorimeter high-voltage system: commissioning, optimisation, and LHC relative luminosity measurement

---

defended on October 14, 2011 before the committee comprised of:

Walter Bonivento	Examinateur
Beate Heinemann	Rapporteuse
Luis Hervas	Co-directeur / Superviseur CERN
Eric Kajfasz	Président du jury
Emmanuel Monnier	Directeur de thèse
Patrick Puzo	Rapporteur

2

To Helmut Braun

Acknowledgements

First and foremost, I would like to thank my supervisors Emmanuel Monnier and Luis Hervas for their continuous support during the fours years I have spent at CERN.

I would also like to thank CERN for providing me with financial support as part of the Doctoral Student Programme for the past three years.

The work presented in this thesis would not have been possible without the support of all my colleagues of the ATLAS Liquid Argon Calorimeter group. In particular I would like to thank Francesco Tartarelli and Valerio Grassi for the invaluable advice during my work on the high-voltage system. I would also like to thank Jessica Leveque for her support and analysis advice. A particular thanks goes to Peter Krieger who provided me with invaluable knowledge on the FCal inner workings.

Thanks also to the members of my defence committee: Walter Bonivento, Beate Heinemann, Eric Kajfasz, and Patrick Puzo for accepting to review my work.

Finally I would like to thank all my friends, at CERN and beyond, for all the great moments we spent together during all these years.

Contents

Introduction 2

1 The ATLAS experiment at the Large Hadron Collider 3

1.1 Physics motivations . . . 3

1.2 The Large Hadron Collider . . . 7

1.3 The ATLAS detector . . . 11

1.3.1 Magnet system . . . 15

1.3.2 Inner detector . . . 16

1.3.2.1 Pixel detector . . . 16

1.3.2.2 Semi-Conductor Tracker . . . 18

1.3.2.3 Transition Radiation Tracker . . . 18

1.3.2.4 Beam Condition Monitor . . . 20

1.3.3 Forward detectors . . . 21

1.3.3.1 LUCID . . . 22

1.3.3.2 ZDC . . . 23

1.3.3.3 ALFA . . . 24

1.3.4 Calorimeters . . . 25

1.3.4.1 Electromagnetic calorimeters . . . 26

1.3.4.2 Hadronic calorimeters . . . 28

1.3.5 Muon spectrometer . . . 29

1.3.5.1 Resistive Plate Chambers and Thin Gap Chambers 30
1.3.5.2 Monitored Drift Tubes and Cathode Strip Chambers 31
1.3.6 Trigger and Data acquisition 32

2 The ATLAS liquid argon calorimeters 35
2.1 Introduction 35
2.2 Electromagnetic calorimeters 36
2.2.1 Geometry and granularity 36
2.2.2 Liquid argon gap 39
2.3 Hadronic calorimeters 40
2.4 Forward calorimeters 41
2.5 From the ionization signal to the digitized samples 44
2.6 Performance 48
2.7 Conclusion 50

3 The LAr high-voltage system 53
3.1 Introduction 53
3.2 High-voltage distribution 54
3.3 High-voltage corrections 56
3.4 Hardware 59
3.4.1 Feedthroughs 59
3.4.2 Modules 60
3.4.3 Crates 64
3.4.4 Return current measurement 65
3.5 Slow control 71
3.5.1 Software 71
3.5.2 Archiving and visualization of the high-voltage system data 75
3.6 Operation of the high-voltage system 76

3.6.1 High-voltage trips . . . 77
3.6.2 Miscellaneous HV issues . . . 77
3.6.2.1 Hospital lines . . . 78
3.6.2.2 Channel 14 . . . 80
3.6.2.3 CAN-bus communication . . . 80
3.6.2.4 OPC server . . . 81
3.7 DCS and data quality . . . 81
3.8 Conclusion . . . 82

4 Luminosity determination with the ATLAS forward calorimeters 83
4.1 Introduction . . . 83
4.2 Linearity assessment in test beam . . . 84
4.2.1 Protvino test beam setup . . . 84
4.2.2 Estimation of the non-linearity . . . 85
4.3 Simulation . . . 86
4.3.1 Collision data . . . 87
4.3.2 PSpice simulation . . . 89
4.4 Luminosity calibration . . . 93
4.4.1 Luminosity algorithms . . . 93
4.4.2 van der Meer calibration . . . 94
4.5 FCal high-voltage power supplies currents . . . 98
4.5.1 Shorted tubes . . . 98
4.5.2 Pedestal measurability . . . 98
4.5.3 Pedestal noise . . . 100
4.6 Luminosity calibration of the FCal high-voltage currents in 2010 . . . 102
4.6.1 Comparing LUCID and FCal data . . . 102
4.6.2 Systematic uncertainties . . . 107

4.7 FCal luminosity in 2011 . . . 110
4.7.1 Early 2011 data . . . 111
4.7.2 After new LUCID RX cards . . . 113
4.7.3 BCM thresholds changes . . . 113
4.7.4 Rescaling of the 2011 early BCM and LUCID data . . . 116
4.7.5 Cross-comparisons after the May 2011 vdM calibration . . . 117
4.8 Conclusion . . . 118

Conclusions and outlook 120

Bibliography 120

A High-voltage system technical specifications i

B FCal high-voltage power supply datasheet xxiii

C High-voltage crates manual xxix

D OPC server manual xxxvii

E Power supply calibration manual lxxi

List of Figures

1.1 Observed and expected 95% C.L. upper limits on the ratios to the SM cross section, as functions of the Higgs boson mass for the combined CDF and D0 analyses [16]. 6

1.2 The combined upper limit on the Standard Model Higgs boson production cross section divided by the Standard Model expectation as a function of m_H. 6

1.3 The CERN accelerator complex. 8

1.4 Cross section of an LHC dipole magnet showing the two separate vacuum chambers [17]. 9

1.5 Production cross-section times branching ratio of the Higgs boson decay channels as a function of its mass. 11

1.6 Peak instantaneous luminosity delivered by the LHC at IP1 per day in 2011. 12

1.7 Cumulative integrated luminosity versus day in 2011. 12

1.8 Overview of the ATLAS detector. It is 25 m in diameter and 44 m in length, and weighs approximately 7000 tonnes. 14

1.9 Barrel toroid magnet 15

1.10 Endcap toroid magnet 15

1.11 The ATLAS Inner detector. It is approximately 7 m in length and 1.2 m in diameter. 16

1.12 Section of the ATLAS Inner detector barrel region. 16

1.13 Distribution of the local x unbiased residuals of the pixel barrel modules. Plot produced with tracks ($p_T > 2GeV$) reconstructed in LHC Minimum Bias events at centre-of-mass energy 7 TeV. Full blue circles show the real data residuals after the detector alignment, and the open red circles show the residuals using Monte Carlo with a perfectly aligned detector (normalized to the number of entries in the data distribution). The local x coordinate of the pixels is along the most precise pixel direction. 17

1.14 Semi-Conductor Tracker barrel module 18

1.15 The TRT unbiased residuals, as obtained from 7 TeV LHC collision data after detector alignment and Monte Carlo (perfectly aligned detector) for the TRT barrel. The Monte Carlo distributions (open red circles) are normalized to the number of entries in the data (full blue circles). Tracks are required to have $p_T > 2\ GeV$. For low-momentum tracks, the width of the residual distribution is expected to be larger than the intrinsic accuracy per hit as predicted from the drifttime measurement because of the contribution from multiple scattering. 19

1.16 BCM station, with its four modules, mounted inside the inner detector. . . 20

1.17 Location of the LUCID, ZDC, and ALFA forward detectors along the beam line on one side of the ATLAS detector. The same set of detectors are place symmetrically with respect to the interaction point. 21

1.18 Computer-generated view of the LUCID Cerenkov tubes and their arrangement around the beam pipe. 22

1.19 ZDC electromagnetic module. 23

1.20 ZDC hadronic module. 23

1.21 (a) Schematic view of an ALFA roman pot - (b) ALFA scintillating fibres - (c) ALFA readout electronics. 25

1.22 The ATLAS calorimeters. 26

1.23 Schematic of a Tile calorimeter module. 29

1.24 Rendered 3D view of the ATLAS muon spectrometer. 30

2.1 The fours types of electrodes of the electromagnetic calorimeter. The two top ones correspond to barrel electrodes: $|\eta| < 0.8$ (left) and $|\eta| > 0.8$ (right). The bottom left is an endcap inner wheel electrode and the bottom right is the outer wheel. Dimensions are in mm. 37

2.2 Sketch of the granularity and segmentation of electromagnetic calorimeter cells. 38

2.3 Sketch of an electromagnetic calorimeter liquid argon gap. 40

2.4 Schematic transverse (left) and lateral (right) views of the hadronic endcap calorimeter. 41

2.5 Schematic view of a hadronic endcap liquid argon gap. 42

2.6 Lateral view of the positioning of the forward calorimeters inside the endcap cryostats. 43

2.7 Transverse view the forward calorimeter tube matrix. 44

2.8 Cold cabling of four forward calorimeter tube groups. The high-voltage feed, analogue summing, and feedthrough connection are also represented. 44

2.9 Transverse view of the three FCal-A modules. The tiles, consisting of tube groups, represent readout channels. 45

2.10 Front-End Board schematic 47

2.11 LAr signal before and after shaping. The black markers represent the 40 MHz sampling of the pulse. 47

2.12 Schematic view of a calorimeter cell (equivalent to a capacitor) being traversed by a charged particle. As the ionisation current i_S flows out to the readout chain (right) for the energy deposition measurement. The high-voltage power supply (left) injects the current i_{HV} to maintain the potential U constant across the liquid argon gap. 48

2.13 Average time per Front-End Board in the electromagnetic barrel and endcap calorimeters extracted from 7 TeV collision data in 2011 49

2.14 Average time per Front-End Board in the hadronic endcap and forward calorimeters extracted from 7 TeV collision data in 2011 50

3.1 High-voltage distribution as a function of $|\eta|$ for the EMEC. A uniform calorimeter response requires a high-voltage which varies continuously as a function of $|\eta|$ (open circles), which has been approximated by a set of discrete values (full triangles) corresponding the nine high-voltage sectors. 56

3.2 Electromagnetic calorimeter high-voltage correction factor in the middle layer versus (η, ϕ) coordinates of the calorimeter cells. Status at the beginning of October 2009. The current situation does not differ significantly. 58

3.3 The six high-voltage feedthroughs sitting on top the calorimeter cryostats. 60

3.4 Schematic of a high-voltage feedthrough. 61

3.5 A 32-channel high-voltage power supply unit. 63

3.6 Layout of a high-voltage power supply and its connection to the cryostat. 63

3.7 High-voltage cable connectors. 64

3.8 High-voltage cable connector and its counterpart on the HV power supply unit. 64

3.9 Overview of the ATLAS technical cavern, USA15. Shown are the five HV racks (red), the low voltage power supplies racks (purple), and the DCS and ROD racks (blue). This dynamic panel reflects the status of the racks by monitoring their temperatures, the humidity, and the main power supplies. 66

3.10 High-voltage power supply crates in USA15. 67

3.11 Schematic of the grounding monitoring of the liquid argon calorimeter cryostats 68

3.12 Return current measurement coils. 69

3.13 Return current data acquisition setup. 69

3.14 Layout of the return current measurements. 70

3.15 Return currents. 70

3.16 Crate control PVSS panel. 72

3.17 Main HV control software panels. 73

3.18 Single HV line control panel. 74

3.19 Dataflow of the high-voltage system. Shown are the path of the data readout and storage (blue) and the commands (red). 75

3.20 EMBA hospital 79

3.21 EMBC hospital 79

4.1 Test beam setup of the high luminosity project in Protvino. 85

4.2 Measured HV current summed over three FCal prototype channels versus beam intensity compared to a non-linear fit [56]. 87

4.3 Average energy deposited in the FCal1 A (left) and C (right) by minimum bias events versus the (i_η, i_ϕ) indices of the readout channels. 88

4.4 Spice model schematic of an FCal high-voltage line (left) connected to an HV sector (middle right). Also shown are the HV filter box (middle left) and the current pulse generator (right). See text for details. 90

4.5 Shape of the Spice simulation signal. The amplitude A corresponds to the current induced by one minimum bias event and the period P average duration between two such events. 90

4.6 Current response at the power supply level for a single FCal-1 high-voltage line in simulation with fixed pulse amplitude. The four curves correspond to the four simulations with different P-values. See text for details. 91

4.7 Current response at the power supply level for a single FCal-1 high-voltage line in the simulation with μ-dependent pulse amplitude. The four curves correspond to the four simulations with different A-values. See text for details. 92

4.8 Specific interaction rate versus nominal beam separation for the BCM Event_OR algorithm during the May 2011 vdM scan. The residual deviation of the data from the Gaussian plus constant background fit assuming statistical errors only is shown in the bottom panel [58]. 96

4.9 Gap $g_{ch} = \langle I_{ch} \rangle - 3 \cdot \sigma_{ch}$ distribution of the 128 EM-FCal high-voltage lines currents during periods with no LHC beam. The vertical line at zero indicates the cut applied on the gap for an HV line to be eligible for the luminosity measurement. Only positive values of g are allowed. 99

4.10 One FCal high-voltage line current versus time during periods with no LHC beam presence. Top: Before ADC offset implementation, only the positive tail of the noise fluctuations are read and the pedestal cannot be estimated. Bottom: After new ADC offset, current fluctuates around a positive value and pedestal can be measured. 100

4.11 Root mean square distribution of the 128 EM-FCal high-voltage lines currents during periods with no LHC beam. The vertical lines at 0.001 μA and 0.015 μA indicate the cuts applied on the noise for an HV line to be eligible for the luminosity measurement. 101

4.12 Current pedestal versus time for a selection of typical FCal-C HV lines during a one hour period prior to LHC beam injection. 104

4.13 Current versus luminosity for a selection of FCal HV lines. 105

4.14 Ratio $\mathcal{L}_{LUCID}/\mathcal{L}_{FCal}$ for 17 ATLAS runs in 2010. The ratios are computed and displayed per luminosity block. 106

4.15 Distribution of the ratio $\mathcal{L}_{LUCID}/\mathcal{L}_{FCal}$ for 17 ATLAS runs in 2010. One ratio is computed per luminosity block and high-voltage line. 107

4.16 Average ratio per run $\langle \mathcal{L}_{LUCID}/\mathcal{L}_{FCal} \rangle_{run}$ for 17 ATLAS runs in 2010. 108

4.17 FCal calibrated instantaneous luminosity (red) for an ATLAS run taken in 2010. Superimposed is the ATLAS preferred instantaneous luminosity (blue). 108

4.18 Current of one FCal-C HV line versus time for a typical LHC fill on June 5 2011. The left graph, from 8.00AM to 9.45AM, is a zoom of the beginning of the fill from injection to stable beams. The right graph, from 23.00pm to 1.00am, is a zoom of the end of fill and after the beam dump. 110

4.19 Average ratio between FCal A and C HV lines luminosities to the offline preferred luminosity (here LUCID_EventOR) versus the ϕ index of the line in 2011. The calibration of the FCal HV lines is extracted from 2010 data, hence the ϕ modulation. The amplitude of the modulation is approximately 2%. 112

4.20 Average ratios of LUCID and BCM luminosities to FCal for a set of ATLAS runs recorded in April 2011, after the installation of the new LUCID receiver cards and the BCM thresholds changes. The horizontal axis represents the ATLAS run number. 116

4.21 FCal-based LUCID and BCM 2011 rescaling factors for different ATLAS data-taking periods, corresponding to different detector statuses. 117

4.22 Ratios of LUCID and BCM luminosities after FCal-based rescaling, compared to the number of interactions per bunch crossing measured by LUCID. 117

4.23 Fractional deviation in the integrated luminosity obtained using different algorithms with respect to the BCM_H_EventOR value as a function of time. Each point shows the average deviation for a single ATLAS run. Statistical uncertainties per point are negligible. Extracted from [58]. . . . 118

4.24 Fractional deviation in the average number of interactions per bunch crossing (averaged over BCIDs) obtained using different algorithms with respect to the BCM_H_EventOR value as a function of $\langle \mu \rangle$. Statistical uncertainties per point are negligible. Extracted from [58]. 118

List of Tables

1.1 Quarks and leptons properties [13]. 5

1.2 Gauge bosons properties [13]. 6

1.3 LHC design and 2011 operational parameters. 11

1.4 Design performance and coverage of the ATLAS detectors. p_T denotes the transverse momentum of particles traversing the detector, i.e. the momentum projection on the x-y plane. 13

2.1 Granularity and coverage of the electromagnetic calorimeters. 39

2.2 Granularity and coverage of the hadronic endcap calorimeter. 40

2.3 Granularity and coverage of the forward calorimeter. Cell sizes are expressed in cm in the transverse plane $\Delta x \times \Delta y$. 43

2.4 LAr calorimeter faulty channels as of July 2011. The percentages are dominated by dead channels and extremely noisy channels that need to be masked out of the readout chain. 50

3.1 Coverage, gap size, and operative voltage of the liquid argon calorimeters. 55

3.2 Number of non-nominal LAr high-voltage lines as of 12/07/2011. 58

3.3 Number of hospitalised high-voltage lines as of 12/07/2011. 79

4.1 Test beam intensities and their LHC equivalent luminosity. 86

4.2 Parameters and results of fixed amplitude simulation. The pulse amplitude A is fixed at 12.4 μA. The period P between each pulse is related to the luminosity by the relation $P = 1/(\mathcal{L}\sigma_{inel})$. The DC current expected is for a single FCal-1 high-voltage line. ATLAS uses the PYTHIA value of 71.5 mb for σ_{inel}. 90

4.3 Parameters and results of fixed period simulation. The period P between each pulse is fixed at 50 ns. The amplitude A corresponds to an average current induced at $\mu = 1$ weighted by μ_{eq}. The DC current expected is for a single FCal-1 high-voltage line. 92

4.4 LUCID and BCM algorithms descriptions. With the x-axis of the ATLAS coordinate system pointing towards the inside of the LHC ring, the C-side corresponds to positive z and the A- side to negative z. 94

4.5 Average ratios of LUCID and BCM luminosities to FCal. These two ATLAS runs were recorded on March 22nd and 23rd before the 2011 LUCID and BCM modifications. Ratios labelled *All* are taken over all the BCIDs, and *Phys* only the BCIDs colliding at IP1. 113

4.6 Average ratios of LUCID and BCM luminosities to FCal for two ATLAS runs recorded on April 15th and 16th 2011. These runs were taken after the replacement of the LUCID receiver cards and before the BCM threshold changes. Ratios labelled *All* are taken over all the BCIDs, and *Phys* only the BCIDs colliding at IP1. 114

4.7 Average ratios of LUCID and BCM luminosities to FCal for a set of ATLAS runs recorded in April 2011, after the installation of the new LUCID receiver cards and the BCM thresholds changes. The algorithms used include data from all BCIDs. 115

4.8 Average ratios of LUCID and BCM luminosities to FCal for a set of ATLAS runs recorded in April 2011, after the installation of the new LUCID receiver cards and the BCM thresholds changes. The algorithms used include only data from colliding BCIDs. 115

Introduction

The main goals of the ATLAS [1] scientific programme are the observation or exclusion of physics beyond the Standard Model (SM), as well as the measurement of production cross-sections of SM processes. As the rate of events N of a given physics process is linked to the cross-section σ by the relation $N = \mathcal{L} \cdot \sigma$, where $\mathcal{L}$ is the luminosity at the interaction point, it is important to measure the luminosity with great precision.

The ATLAS experiment has two major luminosity monitors, LUCID (Luminosity measurement Using Cerenkov Integrating Detector), which consists of Cerenkov tubes located around the beam axis 17 m away from the interaction point, and BCM (Beam Condition Monitor) which is a diamond-based detector and has both beam-abort and luminosity capabilities. As these detectors provide a relative luminosity measurement, they were absolutely calibrated in 2010 using the van der Meer procedure, achieving a total systematic uncertainty of 3.4%. The ultimate plan is to provide an absolute calibration using the ALFA detector during a run with special beam optics.

In order to provide more cross-checks and a better control on the systematic uncertainties, other luminosity handles are always needed. In particular, an independent measurement using the liquid argon forward calorimeter (FCal), based on the readout current of its high-voltage system, has been developed.

This document starts, in Chapter 1, by laying out the physics motivations behind the construction of the LHC and the ATLAS detector before describing their layout and performance. Chapter 2 offers a detailed description of the ATLAS liquid argon calorimeter,

and Chapter 3 focuses on its high-voltage system, which is used to perform the luminosity determination presented in Chapter 4.

Chapter 1

The ATLAS experiment at the Large Hadron Collider

After a description of the Standard Model of particle physics and the scientific motivations behind the construction of the Large Hadron Collider (LHC) and its experiments in Section 1.1, Section 1.2 details the LHC layout and main characteristics, followed by a description of the ATLAS experiment in Section 1.3.

1.1 Physics motivations

Theoretical and experimental progress has lead to the formulation of the standard model of particle physics, which describes elementary particles and their interaction via the electromagnetic, weak, and strong forces. Gravity is not included in the model. For the past 40 years, many experimental results have helped build up and strengthen the validity of this model, particularly at high energy particle physics colliders. These results include, in chronological order:

- observation of neutral currents in the Gargamelle detector in 1973 [2],
- observation of the W and Z bosons in $p\bar{p}$ collisions at the CERN SPS by the UA1

([3], [4]) and UA2 experiments [5] in 1983,

- determination of the number of light neutrino species by the LEP experiments [6, 7, 8],
- precise measurement of the W mass at the CERN LEP [9] and Fermilab Tevatron [10],
- observation of the top quark in $p\bar{p}$ collisions by the CDF [11] and D0 [12] at the Fermilab Tevatron in 1995.

Thanks to the data gathered by operating the SPS and LEP at CERN and the Tevatron at Fermilab, we now know that the Standard Model of particle physics correctly describes the observed phenomena up to energies of $\mathcal{O}$(100 GeV). However, the Standard Model has its limits. Firstly, it does not include the gravitational interaction and general relativity. Secondly there are 19 free parameters in the model, including the fermions masses, which values are not predicted. Three parameters should be added to these 19 to include the neutrino masses, following experimental evidence of neutrino oscillations. Thirdly, the Standard Model does not explain why there are three generations of fermions or why their masses cover such a large range. Finally, from a cosmological viewpoint, no explanation on the nature of cold dark matter, which seems to occupy most of the universe, has been provided. An extension of the standard model predicts the existence of the Higgs boson, which is believed to give other particles their masses, but has yet to be observed experimentally. For instance, its involvement in WW scattering implies that its mass must be lower than $\sim$ 1 TeV in order to maintain unitarity. Theories beyond the Standard Model, such as Supersymmetry, Technicolor, Extra-Dimensions models have been trying to take on these issues.

It was therefore decided to build a collider giving access to mass domains up to a few TeV in order to cover all the searches for new physics. Finding evidence of the Higgs boson and search for new physics beyond the Standard Model are the main goal of the ATLAS and CMS experiments installed on the LHC collider.

The quark model allows for a classification of the elementary constituents of matter with three generations of fermions: six quarks, six leptons and their antimatter counter-

parts. The quarks are constituents of hadrons, e.g. protons and neutrons, and are confined to these bound states: free quarks have not been observed experimentally. They carry fractional electric charges (-2/3, 1/3) and have very different masses. The six leptons are divided into three charged and three neutral particles. Properties of these elementary particles are listed in Table 1.1. The lightest quark and leptons pairs, the up and down quarks, the electron, and the electron neutrino, are responsible for all the stable matter in the universe.

	Quarks		Leptons	
First generation	u up Q = 2/3 e m = 1.5 - 4.5 MeV	d down Q = -1/3 e m = 5 - 8.5 MeV	e^- electron Q = -e m = 0.511 MeV	ν_e electron neutrino Q = 0 m < 3 eV
Second generation	c charm Q = 2/3 e m = 1 - 1.4 GeV	s strange Q = -1/3 e m = 80 - 155 MeV	μ^- muon Q = -e m = 105.7 MeV	ν_μ muon neutrino Q = 0 m < 0.19 eV
Third generation	t top Q = 2/3 e m = 174.3 GeV	b bottom Q = -1/3 e m = 4 - 4.5 GeV	τ^- tau Q = -e m = 1777 MeV	ν_τ tau neutrino Q = 0 m < 18.2 eV

Table 1.1: Quarks and leptons properties [13].

In the standard model, the interaction between two elementary particles is described by the exchange of messenger particles associated with each of the three forces included in the model. The electromagnetic interaction governs the interaction between two charged particles. It is carried out by the photon, which is massless, hence the infinite range of its extent. It manifests macroscopically as electromagnetic waves, electric currents, and attractive of repulsive phenomena depending on the electric charge. The strong interaction acts as the binding force in hadrons and atomic nuclei. Its range is approximately 10^{-15} m. It is carried out by gluons, which have neither mass nor electric charge but another charge named *colour*. The weak interaction is responsible for the decay of heavy quarks and leptons into lighter ones, which has for consequence that all stable matter in comprised of solely first generation fermions. It is also responsible for the flavour change of the up quark to a down quark during proton-proton fusion, which occurs in the Sun. It is carried by the massive W and Z vector bosons. The range of the

Particle	γ	$W^{\pm}$	Z^0	g
Force	Electromagnetic	Weak	Weak	Strong
Charge	Q = 0	Q = ± e	Q = 0	Q = 0
Mass	m < $2 \cdot 10^{-16}$ eV	m = 80.2 GeV	m = 91.2 GeV	m = 0

Table 1.2: Gauge bosons properties [13].

weak interaction is approximately 10^{-17} m. The charges and masses of the four vector bosons of the standard model are listed in Table 1.2.

The electroweak theory, which unifies the electromagnetic and weak interactions, predicts the existence of the photon, the neutral Z^0 and the charged W^+ and W^- bosons. The fact that the photon has zero mass and the W and Z are massive is however an issue as the theory requires the gauge bosons to be massless. The mechanism of spontaneous symmetry breaking [14, 15] describes how these four massless gauge bosons couple with a new field, called the Higgs field, giving three of them their masses. The particle associated with the Higgs field is called the Higgs boson, and has yet to be observed experimentally. However data collected at the Tevatron $p\bar{p}$ collider allowed physicist to put boundaries on its mass, as shown on Figure 1.1, which illustrates the latest results [16]. Additionally, the data collected in 2011 by the ATLAS collaboration allowed a similar study, of which the summary is depicted in Figure 1.2. These results exclude the Standard Model Higgs with a 95% confidence level in the [155,190] and [295,450] GeV mass ranges.

1.2 The Large Hadron Collider

The Large Hadron Collider (LHC, [17]) is aimed at colliding protons (lead ions) at the design energy of 7 TeV (2.76 TeV/nucleon). It is installed in the tunnel that used to host the Large Electron-Positron collider (LEP) at CERN until 2000.

The centre-of-mass energy of 14 TeV has been chosen due to theoretical motivations as well as results from the LEP and Tevatron experiments indicating new physics at the TeV-scale. Despite the fact that the standard model predicts the existence of the Higgs

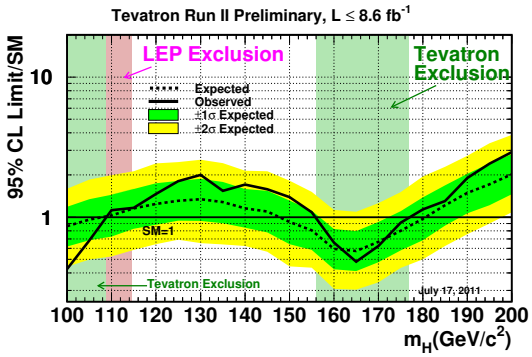

Figure 1.1: Observed and expected 95% C.L. upper limits on the ratios to the SM cross section, as functions of the Higgs boson mass for the combined CDF and D0 analyses [16].

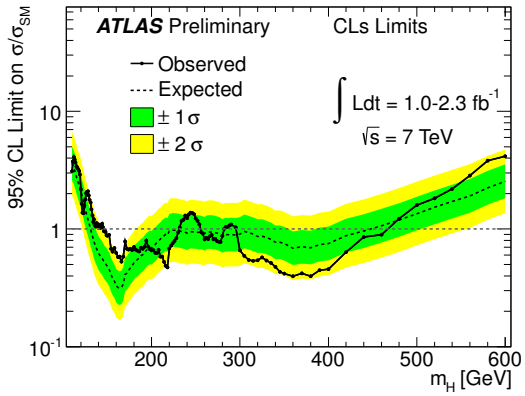

Figure 1.2: The combined upper limit on the Standard Model Higgs boson production cross section divided by the Standard Model expectation as a function of m_H.

boson, there is no indication on its mass. This is the main reason why a hadron collider was chosen to discover it. Indeed, by colliding protons at a centre-of-mass energy of 14 TeV, the energy available in each collision ranges from 0 to 14 TeV, because of the proton compositeness. This leads to the production of a wide spectrum of decay products, thus increasing the potential for discovery. Moreover, an electron collider with 7 TeV per beam in the existing 27 km tunnel would not be efficient because of energy losses due to synchrotron radiation, which scales as m^{-4}. As protons are ~2000 times heavier than electrons, these losses are much smaller, allowing for a favourable yield between the energy given to the proton during acceleration and the amount lost by synchrotron radiation at each turn.

The CERN accelerator complex is illustrated in Figure 1.3. The 26.7 km tunnel of the LHC lies between 45 m and 170 m below France and Switzerland and was built between 1984 and 1989. Protons are provided by a hydrogen source at the Linac2 linear accelerator, accelerated to 50 MeV and sent to the Proton Synchrotron Booster (PSB) where their energy is increased to 1.4 GeV. After the PSB, the protons reach the Super Proton Synchrotron (SPS) where they are accelerated to 450 GeV, before being injected as two bunched beams into the LHC. The Radio Frequency (RF) cavities of the LHC finally accelerates both beams up to their nominal energies of 7 TeV. The beams circulating in

the LHC are not continuous: the protons are packed into bunches nominally 25 ns apart and form *bunch trains*, up to the design maximum number of filled bunches of 2808. The LHC is also able to collide lead ions at 2.76 TeV/nucleon centre-of-mass: the ions are provided by a lead source and injected by the Linac3 into the Low Energy Ion Ring (LEIR) before reaching the PSB from where they follow the same chain as protons.

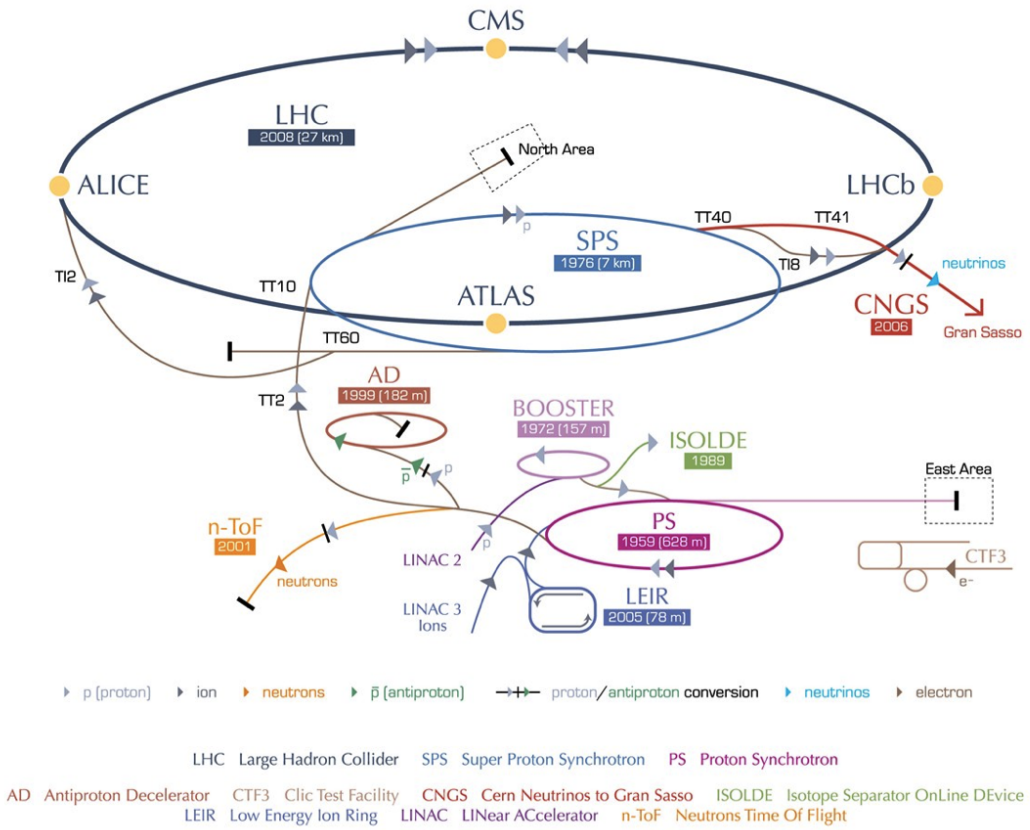

Figure 1.3: The CERN accelerator complex.

Because two proton beams cannot circulate in opposite directions in the same vacuum chamber with a single bending magnetic field, a twin-bore design was chosen for the 1232 dipole magnets, as illustrated in Figure 1.4. Two superconducting dipole magnets and two beam pipes lie in a single cryostat cooled down to the superfluid Helium temperature of 1.9 K. The magnets are made NbTi and a current of $\sim$ 12 kA allows for magnetic fields up to 8.4 T. Additionally, the LHC is equipped with quadrupole magnets that provide focusing, as well as higher multipole magnets for corrections.

The LHC is divided into eight straight sections with different purposes:

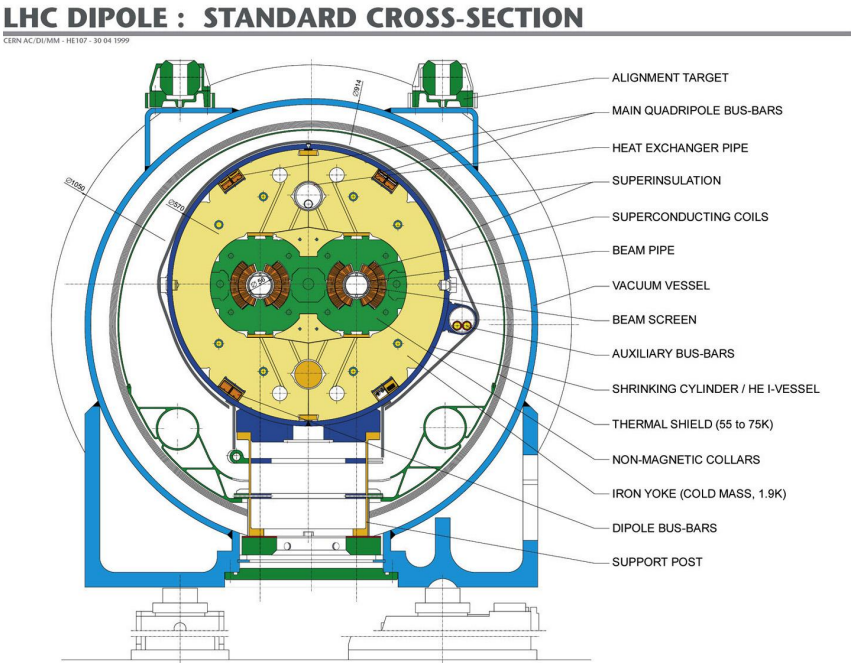

Figure 1.4: Cross section of an LHC dipole magnet showing the two separate vacuum chambers [17].

Beam dump Beams are dumped into large graphite cylinders to protect the machine and the experiments.

Radio Frequency cavities Particles circulating in the LHC are accelerated to their nominal energy.

Momentum cleaning Particles with a too large momentum dispersion with respect to nominal are cleaned up by a dedicated set of magnets and collimators .

Betatron cleaning Particles which drift too much from their nominal orbit are cleaned up by a specific collimation configuration.

ATLAS A Toroidal LHC ApparatuS [1]. General purpose detector designed to achieve the main LHC goals: Higgs, SUSY, extra dimensions, ...

CMS Compact Muon Solenoid [18]. Same goals as ATLAS, but uses different detector technologies.

ALICE A Large Ion Collider Experiment [19]. Specifically designed to observe heavy ion collisions, its main physics goal is understanding the properties of the quark-gluon plasma.

LHCb Large Hadron collider beauty experiment [20]. Designed to measure differences

in the properties of matter and antimatter, primarily through the observation of CP violation in B mesons, and more generally B physics studies.

One of the main features that characterises a machine like the LHC is its ability to produce collisions, described by a parameter called the *luminosity*. For two bunches containing N_1 and N_2 protons meeting at the revolution frequency f_r, the *instantaneous luminosity*, expressed in $cm^{-2}s^{-1}$, can be written as follows [21]:

$$\mathcal{L} = \frac{N_1 N_2 f_r}{4\pi\sigma_x\sigma_y}$$

where $\sigma_{x,y}$ are the transverse beam sizes at the interaction point. Furthermore, as the rate of events N of a given physics process is linked to the cross-section σ by the relation $N = \mathcal{L} \cdot \sigma$, one needs to measure the luminosity with great precision. For instance, Figure 1.5 depicts the evolution of the production cross-sections times the branching ratio of the Higgs boson as a function of its mass, which illustrates the importance of precise cross-section measurements and therefore precise luminosity determination.

In the above expression of the luminosity with the beam parameters, the measurement of the number of proton per beam is performed by measuring their currents using current transformers placed around the beam pipes. As of summer 2011, the uncertainty on the beam current measurements dominate the total uncertainty on the luminosity. A detailed review of the luminosity determination in ATLAS is given in Chapter 4.

In 2011 the LHC has been colliding protons with half the designed energy because of the consolidation work and additional magnet training required to safely operate the machine higher than 3.5 TeV per beam. This work will be performed during the 2012-2013 shutdown period. In 2011, the LHC successfully managed to collide up to 1331 proton bunches at IP1, where the ATLAS experiment is located, achieving a peak instantaneous luminosity of 3.3 10^{33} $cm^{-2}s^{-1}$ and an average number of 16 inelastic p-p collisions per bunch crossing. These achievements, as well as the LHC design parameters, are listed in Table 1.3.

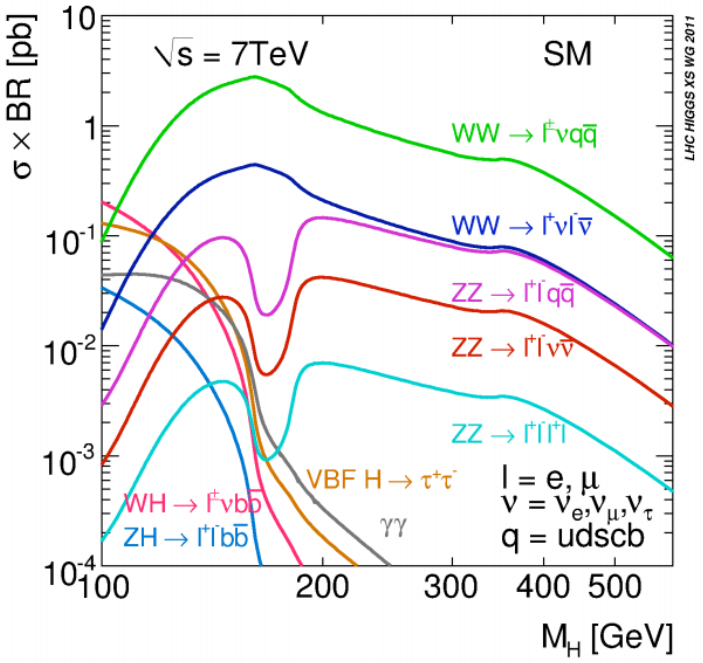

Figure 1.5: Production cross-section times branching ratio of the Higgs boson decay channels as a function of its mass.

	September 2011	Nominal
Collision proton energy [GeV]	3500	7000
Centre-of-mass energy [GeV]	7000	14000
Number of filled bunches	1380	2808
Number of particles per bunch	$1.15\ 10^{11}$	$1.15\ 10^{11}$
Distance between two filled bunches [ns]	50	25
Peak luminosity at ATLAS [$cm^{-2}\ s^{-1}$]	$3.3\ 10^{33}$	10^{34}
Average number of *p-p* collisions per bunch crossing	16	23

Table 1.3: LHC design and 2011 operational parameters.

The evolution of the peak instantaneous luminosity and the delivered integrated luminosity in 2011 are illustrated on Figures 1.6 and 1.7[1].

1.3 The ATLAS detector

The ATLAS [1] detector construction started in 1997, and its installation in the 80 m deep dedicated experimental cavern began in 2003. Test beams studies, followed by extensive

[1] https://twiki.cern.ch/twiki/bin/view/AtlasPublic/LuminosityPublicResults#2011_pp_Collisions

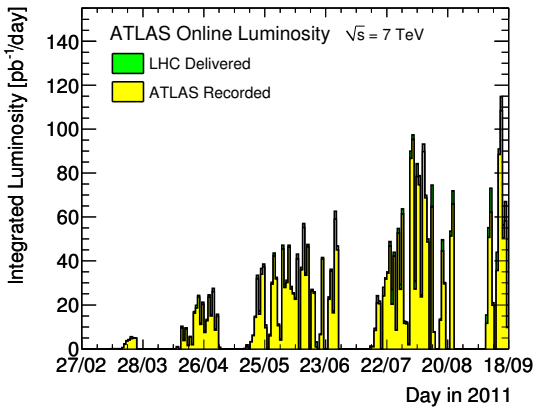

Figure 1.6: Peak instantaneous luminosity delivered by the LHC at IP1 per day in 2011.

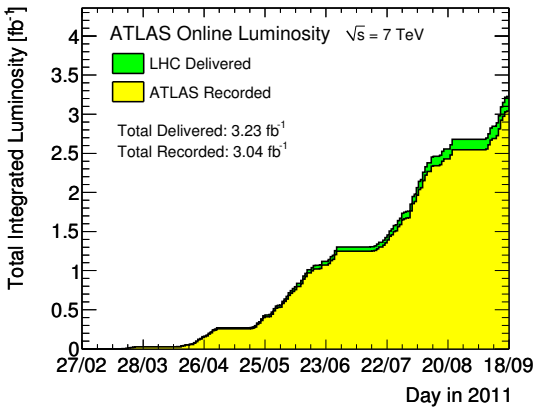

Figure 1.7: Cumulative integrated luminosity versus day in 2011.

commissioning with cosmic muons [22, 23, 24, 25], allowed the ATLAS collaboration to be ready for the first LHC circulating beams in 2008. The year 2009 saw the first proton-proton collisions at 900 GeV of center-of-mass energy, and in 2010 the first 7 TeV collisions. The detector layout is presented on Figure 1.8.

In order to satisfy its performance requirements with respect to LHC collision products, it has three-fold structure with a tracking system, a calorimetry system, and a muon spectrometer surrounding the interaction point with maximum coverage.

The inner detector system, surrounded by a 2 T solenoidal magnetic field used to bend charged particle tracks, is composed of a high granularity Pixel detector, a silicon micro-strip (SCT) detector, and a Transition Radiation Tracker (TRT). It provides high precision tracking of charged particles, vertex measurements, as well as electron identification with the TRT.

The calorimetry system consists of a liquid argon sampling calorimeter (LAr) surrounded by a scintillating tiles hadronic calorimeter in the barrel region. Its main goal is to provide trigger capabilities on electrons, photons, jets, and missing transverse energy as well as particle identification (electrons, photons) and energy measurements.

Strong bending power in the volume of the muon spectrometer is provided by three large air-core toroid systems (one barrel and two end-cap superconductive magnets). The muon spectrometer consists of chambers placed all around the toroid magnets, to

both trigger and perform high precision tracking of muons, the only charged particles remaining outside of the calorimetry system.

The ATLAS coordinate system is defined with the interaction point as its origin. The x-axis is pointing towards the center of the LHC ring, and the y-axis upwards. The detector is separated in two sides along the z-axis, the A-side for $z > 0$ and the C-side for $z < 0$. The azimuthal angle ϕ spans around the beam axis in the transverse plane, and the polar angle θ is defined from the z-axis. In collider experiments, the *pseudo-rapidity* coordinate η is generally used instead of the polar angle since particle production from collisions is rather constant as a function of pseudo-rapidity in the range covered by the main detectors (around $|\eta| < 5$). It is defined as follows:

$$\eta = -\ln \left| \tan \left(\frac{\theta}{2} \right) \right|$$

The η coverage, as well as the design performance of each sub-detector, is summarized in table 1.4.

Detector component	Required resolution	η coverage	
		Measurement	Trigger (Level-1)
Inner detector	$\sigma_{p_T}/p_T = 0.05\%\ p_T \oplus 1\%$	± 2.5	
EM calorimeter	$\sigma_E/E = 10\%/\sqrt{E} \oplus 0.7\%$	± 3.2	± 2.5
Hadronic calorimeter			
barrel and end-cap	$\sigma_E/E = 50\%/\sqrt{E} \oplus 3\%$	± 3.2	± 3.2
forward	$\sigma_E/E = 100\%/\sqrt{E} \oplus 10\%$	$3.1 < \lvert\eta\rvert < 4.9$	$3.1 < \lvert\eta\rvert < 4.9$
Muon spectrometer	$\sigma_{p_T}/p_T = 10\%$ at $p_T = 1$ TeV	± 2.7	± 2.4

Table 1.4: Design performance and coverage of the ATLAS detectors. p_T denotes the transverse momentum of particles traversing the detector, i.e. the momentum projection on the x-y plane.

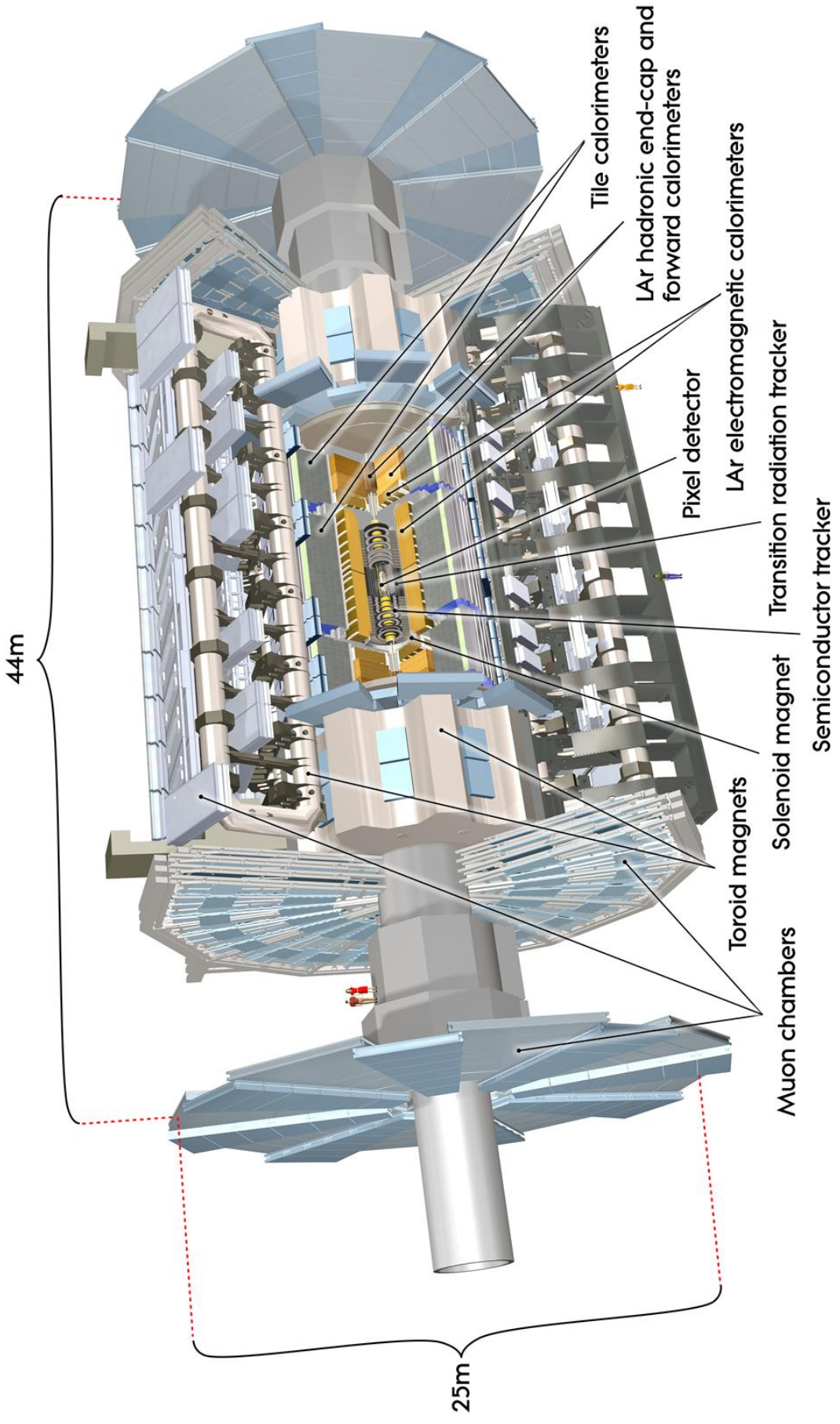

Figure 1.8: Overview of the ATLAS detector. It is 25 m in diameter and 44 m in length, and weighs approximately 7000 tonnes.

1.3.1 Magnet system

The ATLAS magnet system [26] is aimed at providing bending power for charged particles momentum measurements. Around the Inner Detector lies a Nb/Ti/Cu superconductive solenoid providing a 2 T magnetic field parallel, for $|z| < 2$ m, to the beam axis. Its thin design is crucial for minimizing the material in front of the barrel calorimeter, with which it shares the cold cryostat vessel. Three large air-core toroid magnets surround the calorimeters: one barrel (Figure 1.9), providing a maximum field of 0.5 T at its centre; two end-caps (Figure 1.10), providing a 1 T field. All magnets are operated at a temperature of 4.5 K and operative currents of 7.73 kA for the solenoid and 20.4 kA for the toroids. As the toroid magnets follow an eight-fold structure, the magnetic fields are not homogeneous in ϕ. Therefore, approximately 1800 Hall probes are mounted on the muon spectrometer to measure and monitor the field intensity in the ATLAS cavern. This ensures good knowledge of the magnetic field intensity in the cavern in order to satisfy the performance requirement on the momentum resolution.

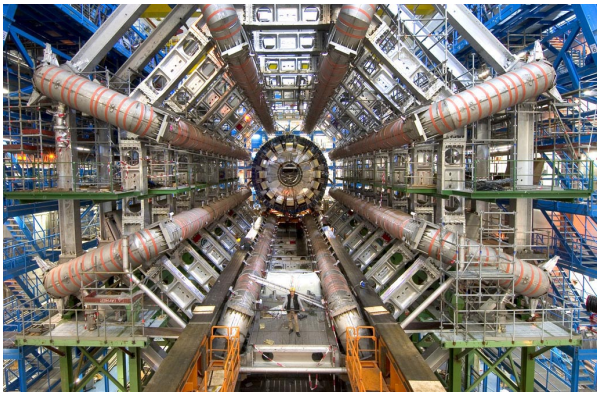

Figure 1.9: Barrel toroid magnet

Figure 1.10: Endcap toroid magnet

1.3.2 Inner detector

In order to perform high precision tracking of charged particles and accurate vertex reconstruction, three detectors comprise the innermost layer of the ATLAS detector [27, 28]. From the interaction point: a silicon pixel detector (Pixel), a silicon microstrip detector (SCT) and a Transition Radiation Tracker (TRT). The global layout, as well as a section of the Inner Detector, are shown on Figures 1.11 and 1.12. Additionally, the Inner Detector is equipped with the Beam Condition Monitor, a set of diamond detectors which act as a protection system from unstable LHC beams and also have luminosity monitoring capabilities.

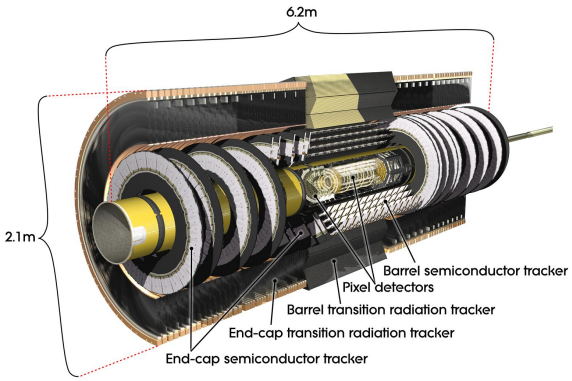

Figure 1.11: The ATLAS Inner detector. It is approximately 7 m in length and 1.2 m in diameter.

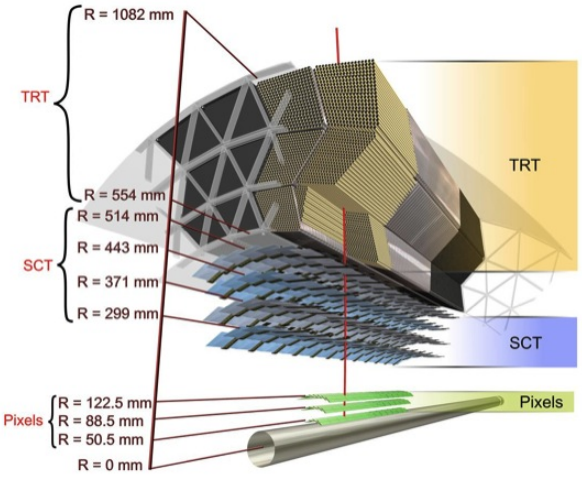

Figure 1.12: Section of the ATLAS Inner detector barrel region.

1.3.2.1 Pixel detector

The Pixel detector [27, 28] is the closest to the interaction point and covers $|\eta| < 2.5$ in pseudo-rapidity. The charge collected in a pixel over a certain threshold is used to determine if a charged particle went through. In the high-multiplicity environment of the LHC, it must provide excellent spatial resolution for measurements such as secondary vertices and impact parameters. Its 80.4 million 50×400 μm^2 silicon pixels are divided among three cylindrical barrel layers and three end-cap disks on each side. The design intrinsic accuracy is 10 μm in the $R - \phi$ direction and 115 μm in z. Measurements with

collision data have shown that the pixels alignment is very close to the design, as shown on Figure 1.13 for the x direction, which shows a FWHM (Full Width Half-Maximum) of 19 μm. The three barrel layers are located at respectively 5.05 cm, 8.85 cm, and 12.25 cm of the beam axis, and the end-cap disks at $|z| = 49.5$ cm, 58.0 cm and 65.0 cm. The high radiation environment causes the effective doping concentration of the silicon sensors to increase with time, hence requiring a higher bias voltage. As this phenomenon is temperature-dependant, the Pixel detector is operated at temperatures ranging between -5 °C and -10 °C.

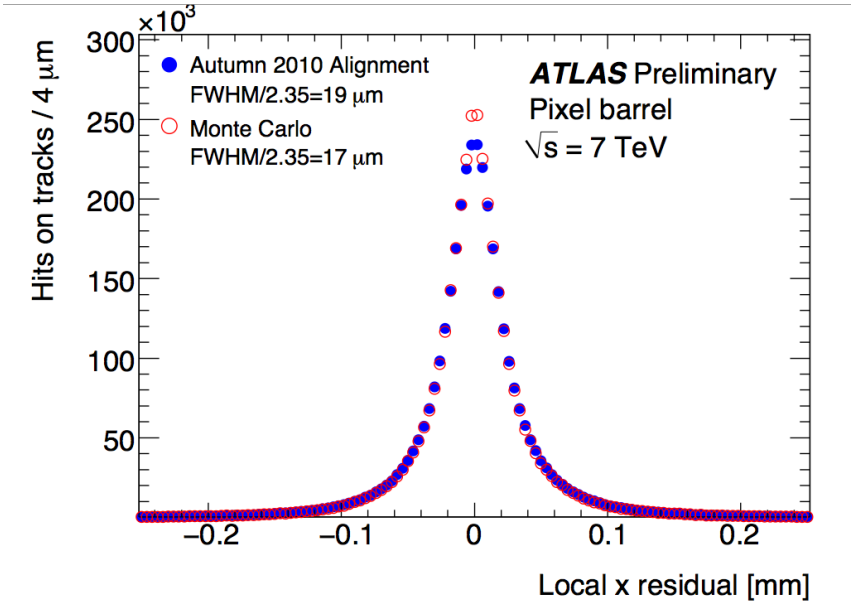

Figure 1.13: Distribution of the local x unbiased residuals of the pixel barrel modules. Plot produced with tracks ($p_T > 2GeV$) reconstructed in LHC Minimum Bias events at centre-of-mass energy 7 TeV. Full blue circles show the real data residuals after the detector alignment, and the open red circles show the residuals using Monte Carlo with a perfectly aligned detector (normalized to the number of entries in the data distribution). The local x coordinate of the pixels is along the most precise pixel direction.

In the next long-term LHC shutdown, in 2013-2014, the addition of inner barrel layer is planned. The project, called Insertable B-Layer [29], aims at extending the lifetime of the Pixel detector at the LHC design luminosity, as well as improving secondary vertex reconstruction, essential for b-tagging in Higgs searches.

1.3.2.2 Semi-Conductor Tracker

The Semi-Conductor Tracker (SCT, [27, 28]) surrounds the Pixel detector for charged particle tracking. It is comprised of four barrel layers ($|\eta| < 1.4$) and nine end-cap disks ($1.1 < |\eta| < 2.5$) on each side. One of the 4088 SCT modules, as shown on Figure 1.14, consists of two pairs of silicon microstrip planes glued together back-to-back. The planes are rotated with respect to each other by a 40 mrad angle, which allows measurements along the length of a strip. The microstrip pitch is approximately 80 μm, and the intrinsic accuracy is 16 μm (R $-$ ϕ) $\times$ 580 μm (z). The SCT contains approximately 6.2 million read-out channels.

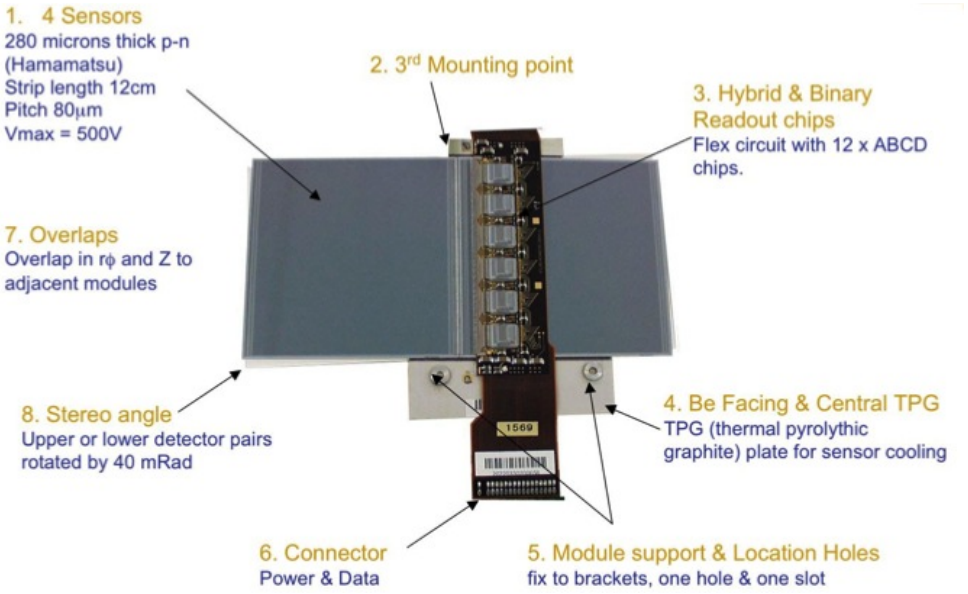

Figure 1.14: Semi-Conductor Tracker barrel module

1.3.2.3 Transition Radiation Tracker

The Transition Radiation Tracker (TRT, [27, 28]) is the outermost part of the Inner detector. It is made of 351000 individually read out straw tubes of 4 mm in diameter. In the three barrel layers, the 144 cm tubes are aligned along the beam axis; in the three end-cap disks, the 37 cm tubes are arranged radially. Each tube is filled with a gas mixture of $Xe/CO_2/O_2$ and contains a gold plated tungsten anode at its center. The operative voltage

of 1530 V applied to the cathode yields to a gain of approximately 2.5×10^4.

When a charged particle goes through a tube, it ionizes the gas producing electron-ions pairs; the electrons drift induces a current on the anode as the signal. Moreover, the drift time (duration of the current pulse) allows the determination of the distance of the track with respect to the center of the tube. A minimum of 36 straws will be traversed in the barrel region (22 in the end-caps), and the intrinsic resolution is designed to be 130 μm in $R-\phi$. Measurements with collision data show for instance a FWHM of 138 μm in the x direction in the TRT barrel, as illustrated on Figure 1.15.

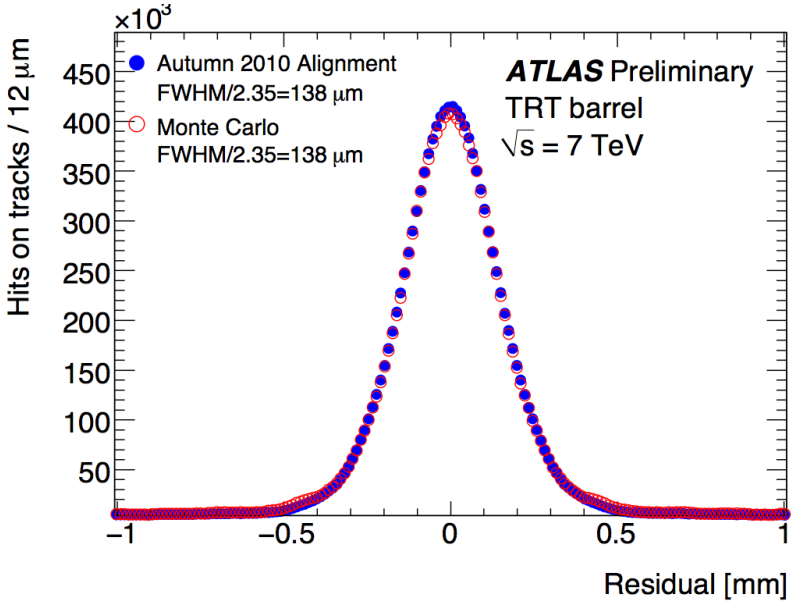

Figure 1.15: The TRT unbiased residuals, as obtained from 7 TeV LHC collision data after detector alignment and Monte Carlo (perfectly aligned detector) for the TRT barrel. The Monte Carlo distributions (open red circles) are normalized to the number of entries in the data (full blue circles). Tracks are required to have $p_T > 2$ GeV. For low-momentum tracks, the width of the residual distribution is expected to be larger than the intrinsic accuracy per hit as predicted from the drifttime measurement because of the contribution from multiple scattering.

The transition radiation emitted in the TRT allows for the separation of electrons and pions, providing an additional handle for electron identification in the electromagnetic calorimeter. The photons produced at the transition are absorbed by the gas mixture, inducing a much larger signal than the standard ionization process. Therefore, both tracking and particle identification are made possible by setting two separate thresholds on a tube-by-tube basis.

1.3.2.4 Beam Condition Monitor

The ATLAS Beam Condition Monitor [30] is designed as the experiment's way to detect unstable LHC beams and trigger safety beam dumps in order to protect the inner detector. It is comprised of two stations, located at $z \pm 184$ cm of the ATLAS interaction point. One BCM station is made of four radiation hard diamond-based sensors, as seen on Figure 1.16, each module sitting at a radius of 5.5 cm from the beam axis. By using time-of-flight information between the two stations, the BCM is capable of distinguishing collision-like events, i.e. in-time coincidences, from beam induced background, and, if the conditions are met, is capable of sending a beam abort trigger to the LHC. In addition to its beam abort capabilities, the BCM has access to information related to the luminosity, as it effectively measures a collision rate. Therefore by adjusting the detector thresholds and calibrating it using similar techniques as developed in the next section, it has been successfully used as a luminosity monitor during the 2011 data-taking period. The BCM calibration and luminosity algorithms are discussed in Chapter 4.

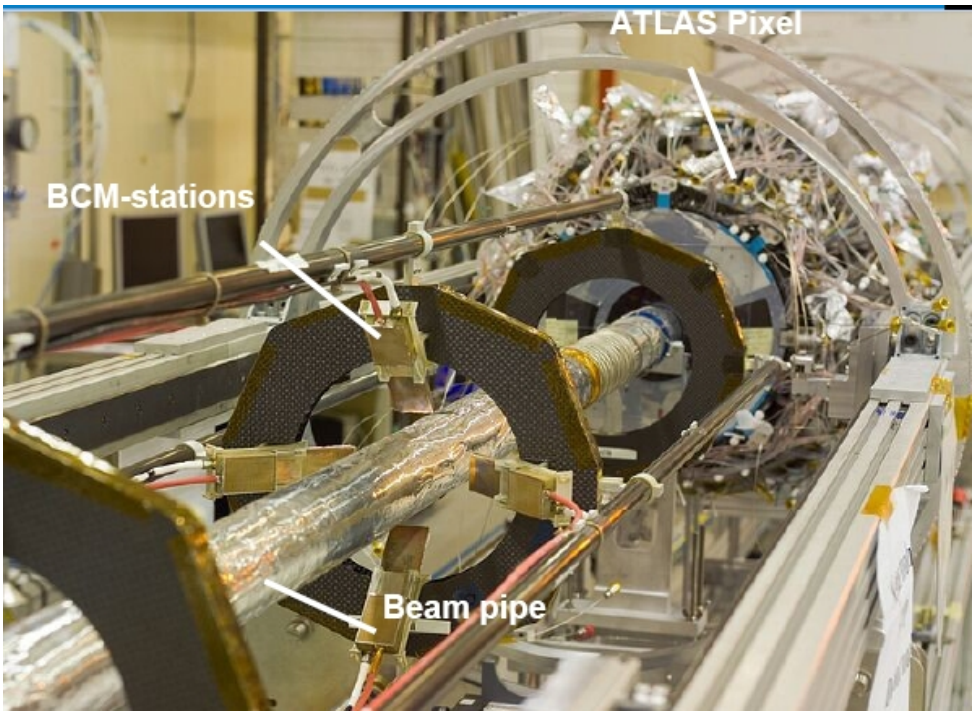

Figure 1.16: BCM station, with its four modules, mounted inside the inner detector.

1.3.3 Forward detectors

Three additional detectors cover the forward region of ATLAS. Their location with respect to ATLAS is shown on Figure 1.17. LUCID (LUminosity measurement using Cerenkov Integrating Detector, [31]) is located at ± 17 m of the interaction point (IP) and measures proton-proton inelastic scattering. It consists of an array of Cerenkov tubes surrounding the beam pipe and read out by photomultiplier tubes. It is one of the main handles on relative luminosity monitoring. The Zero Degree Calorimeter (ZDC, [32]) is located ± 140 m from the IP, just before the two independent LHC beam pipes merge into a single one for ATLAS. Its main goal is to detect forward neutrons for heavy-ions centrality measurements up to $|\eta| = 8.3$. ALFA (Absolute Luminosity For ATLAS, [31]) consists of scintillating fibre trackers located in eight roman pot stations ± 240 m from the IP. Its purpose is to provide an absolute luminosity calibration to the other luminosity detectors during dedicated data-taking periods with special machine optics.

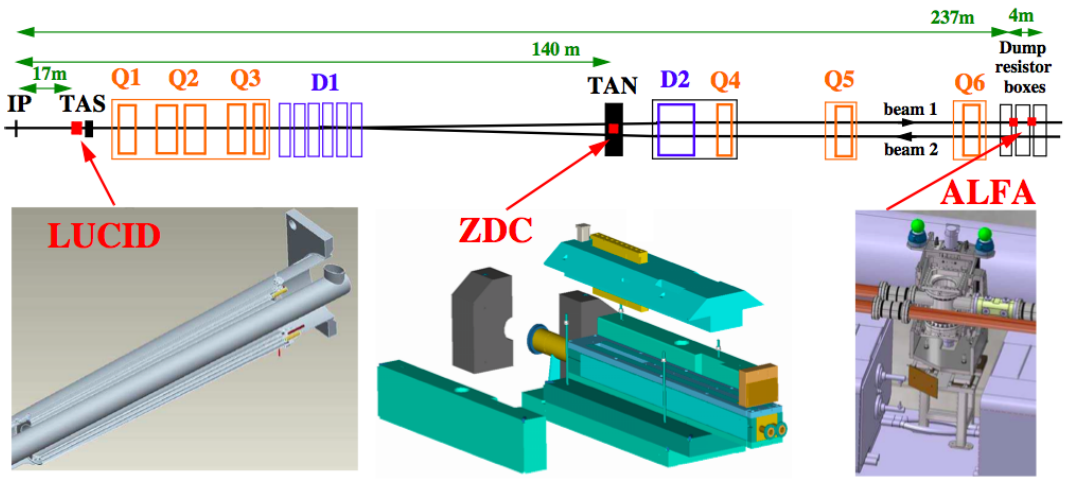

Figure 1.17: Location of the LUCID, ZDC, and ALFA forward detectors along the beam line on one side of the ATLAS detector. The same set of detectors are place symmetrically with respect to the interaction point.

1.3.3.1 LUCID

The LUCID [31] detector surrounds the LHC beam pipe on both sides of the ATLAS interaction point at a distance of 17 m. Its layout and position are illustrated on Figure 1.18. One vessel contains 20 aluminium tubes pointing towards the interaction point approximately 10 cm from the beam axis. Each vessel is filled with C_4F_{10} at 1.3 bar for Cerenkov light measurement. Sixteen of the 20 tubes are read out through 15 mm photomultipliers (PMT) and 4 tubes have their collected light transmitted through quartz fibers outside of the forward shielding to be read out by multi-anode photomultiplier tubes.

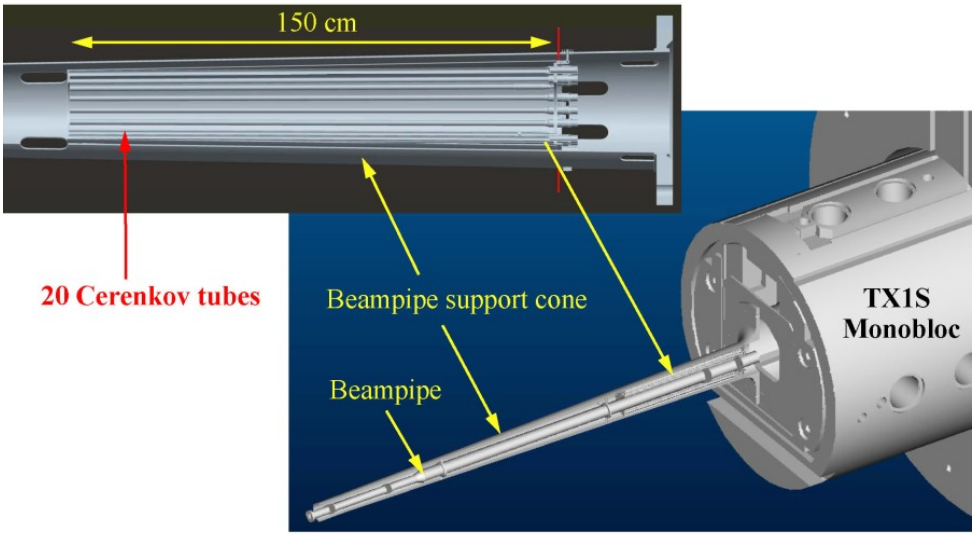

Figure 1.18: Computer-generated view of the LUCID Cerenkov tubes and their arrangement around the beam pipe.

The 16 photomultipliers signals are individually sent to the front-end electronics and, if they pass a predefined threshold, the considered tube is registered to have been hit. In addition to providing trigger capabilities, the signals from both sides are sent to LUMAT cards programmed with luminosity algorithms and calibration constants, which allows for an online luminosity determination for each LHC bunch crossing. The algorithms are predefined as coincidence (*AND*), exclusive, and inclusive *OR* between the two LUCID detectors. The calibrations can be derived from Monte Carlo studies [33], van der Meer scans [33, 34], or ultimately using the ALFA detectors.

1.3.3.2 ZDC

The ZDC [32] is comprised of four modules, one electromagnetic and three hadronic. The EM module, depicted on Figure 1.19, consists of eleven 10 mm thick tungsten plates, extended by steel plates, traversed by 96 quartz rods forming an 8×12 matrix perpendicular to the beam axis. On the front face of the module the rods are bent upwards and read out at the top by multi-anode photomultiplier tubes. Therefore, the Cerenkov light induced by particle showers traversing the module provides both position (rods hit) and energy (light intensity) measurements. In order to get an improved measurement of the incident particle energy over that of the position measuring rods, quartz strips are installed between the plates and read out from the top by photomultiplier tubes. The hadronic module, shown in Figure 1.20, is similar to the electromagnetic module except that four rods (instead of one) are mapped to one pixel of the multi-anode photomultiplier tube and not that all hadronic modules have position sensing rods.

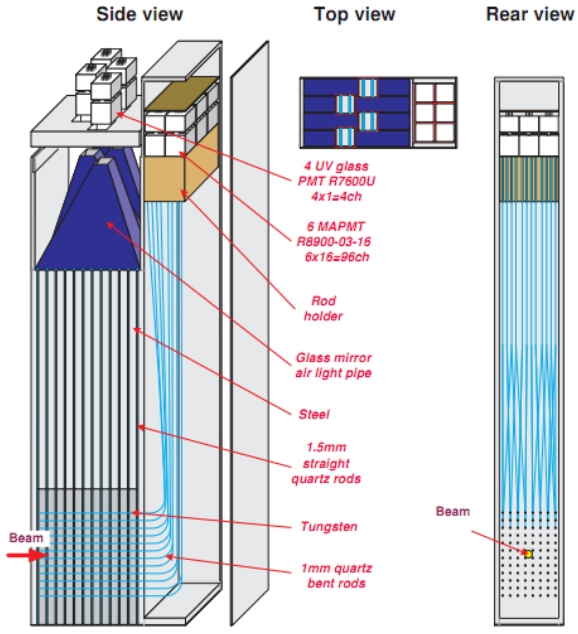

Figure 1.19: ZDC electromagnetic module.

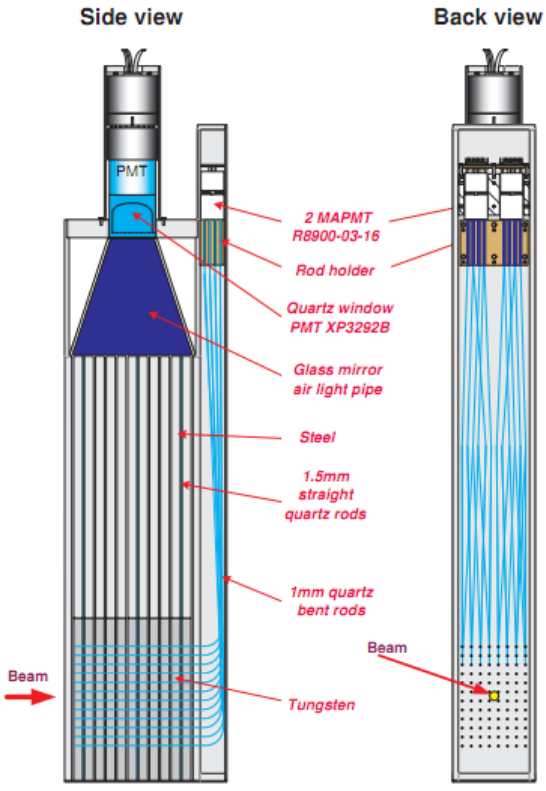

Figure 1.20: ZDC hadronic module.

For p-p collisions, the ZDC single-side signals and coincidence rates provides trigger capabilities as well as, similarly to LUCID, the possibility to monitor relative luminosity. Since 2011, LUMAT cards have been installed on the ZDC readout chain in order to provide an online, bunch-by-bunch luminosity measurement. The calibration is performed the same way, using van der Meer scans.

1.3.3.3 ALFA

The ALFA [31] detector is designed to measure elastic scattering at small angles - and the total elastic p-p cross-section - in order to obtain an absolute luminosity calibration independent from the LHC machine parameters. The goal is to achieve an uncertainty of 1% on the absolute calibration of the luminosity. The detector consists of four roman pot stations (Figure 1.21-a) placed at 240 m on each side of the ATLAS interaction point. The very small scattering angle ($\sim$ 3.5 μrad) requires the active detector parts to be very close ($<$2 mm) to the proton beams. Therefore, set of scintillating fibres (Figure 1.21-b) are mounted on the top a bottom half-pots and are allowed to move very close to the beams through bellows with direct access to the beam pipe vacuum. One module consists of ten layers of 64 scintillating fibres, alternating with a 90° angle. The light from each layer is collected and routed to a dedicated 64-channel multi-anode photomultiplier tube on the base of the roman pot, before being sent to the readout electronics (Figure 1.21-c). Additionally, for triggering, each module is equipped with two dedicated scintillating tiles read out by photomultiplier tubes.

As mentioned previously, the ALFA detectors aim at measuring p-p elastic scattering at very small angles. In order to achieve this, it uses parallel-to-point focusing optics: the protons scattered at the same angle at the ATLAS interaction point will end up at the same y-position of the ALFA tracker, regardless of their collision vertex position. For scattering angles as small as 3.5 μrad, a machine requirement is that the beam angular divergence must be smaller than the angle to be measured. This leads to a set of machine parameters very different from those of nominal p-p collisions. Therefore, ALFA will have

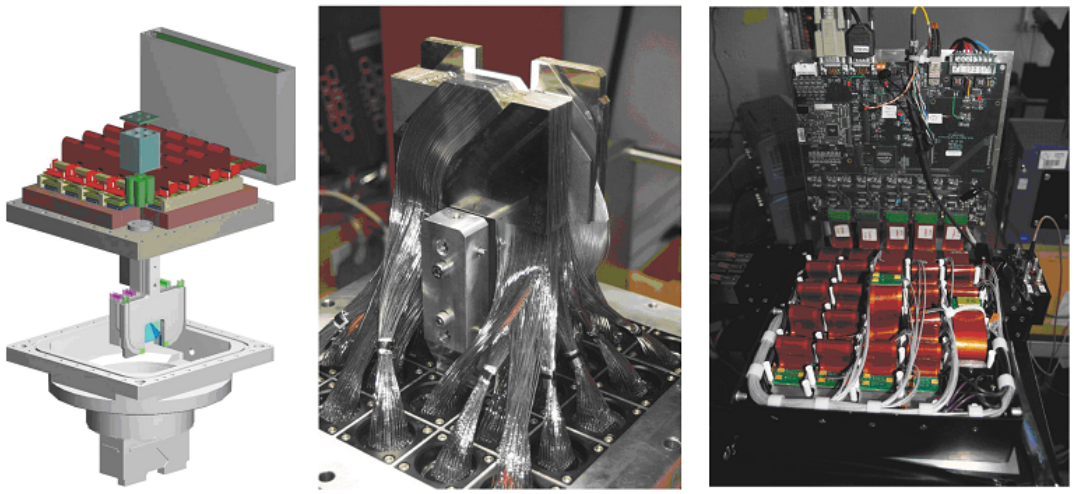

Figure 1.21: (a) Schematic view of an ALFA roman pot - (b) ALFA scintillating fibres - (c) ALFA readout electronics.

dedicated runs in the LHC machine schedule in order to perform its measurements, the first of which, somewhat intermediary, being in the fall 2011 [35].

As of the 2010 winter shutdown, the complete ALFA detectors are installed in the LHC tunnel. Their Detector Control System infrastructure is in place, as well as their integration in the ATLAS Trigger and Data Acquisition chain. Commissioning is continuing, pending interesting results from their special run in the fall 2011.

1.3.4 Calorimeters

The ATLAS calorimeters (see Figure 1.22) cover the large pseudo-rapidity range $|\eta| < 4.9$ and will be described in detail in Chapter 2. Their design is dictated by physics searches such as $H \rightarrow \gamma\gamma$ or Z' and W' bosons, which involve electrons, photons and constraint their performance requirements as shown in Table 1.4. With those requirements in mind, the calorimeters role is therefore to provide trigger capabilities, electron/photon/jet identification, as well as energy measurements for electrons, photons, jets, and missing transverse energy (E_T^{miss}). The electromagnetic and end-cap hadronic calorimeters are sampling calorimeters [36] with liquid argon (LAr) as an active medium, and will be detailed in

chapter 2. The barrel and extended barrels of the hadronic are also sampling calorimeters, made of scintillating plastic tiles.

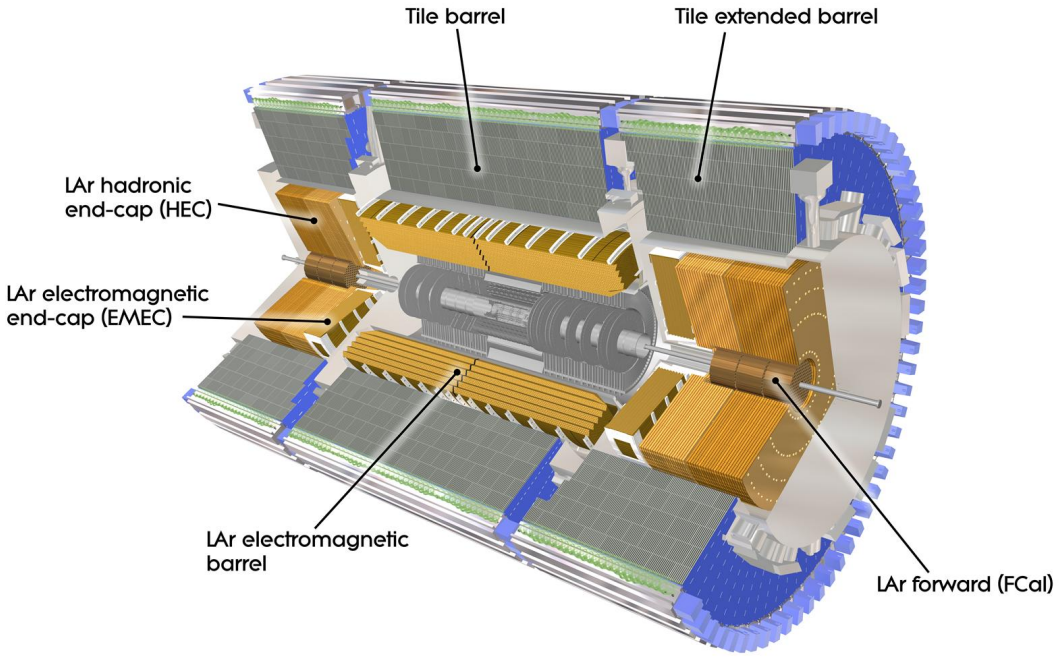

Figure 1.22: The ATLAS calorimeters.

1.3.4.1 Electromagnetic calorimeters

The electromagnetic (EM) calorimeter is divided into a central barrel ($|\eta| < 1.475$) and two end-caps ($1.375 < |\eta| < 3.2$). In the forward region ($3.15 < |\eta| < 4.30$), the first module of the forward calorimeter (FCal) is part of the EM calorimeter. The EM barrel and end-caps are made of a succession of lead absorbers and copper electrodes, with gaps of liquid argon in between. Each gap harbours an electric field provided by a dedicated high-voltage system, which will be described in detail in chapter 3. The FCal layout consists of electrode tubes in a copper-tungsten matrix (absorber) arranged along the beam axis.

Barrel The *accordion* geometry of the electrodes allows fast signal extraction and full ϕ-coverage with no gap. The barrel is segmented in three compartments in depth (layers 1,2, and 3) with different cell sizes. The first layer (as seen from the interaction point) is very finely segmented in η (0.0031), which is crucial for discriminating photons coming from a π^0 meson decay and so-called *prompt* photons (i.e. coming from a p-p collision product). This is particularly useful for physics searches such as $H \to \gamma\gamma$, where the photon background is extremely large. An additional detector layer is installed in front of the EM barrel: the Pre-Sampler (PS). Its purpose is to allow for an estimate of the energy lost by the charged particles before entering the calorimeter, mainly in the solenoid magnet and cryostat vessel.

End-cap The electromagnetic end-caps (EMEC) extends the EM calorimetry further in pseudo-rapidity. The EMEC is divided in two coaxial wheels: the outer wheel (OW) covers $1.375 < |\eta| < 2.5$ and the inner wheel (IW) covers $2.5 < |\eta| < 3.2$. The OW is segmented into three layers in depth whereas the IW is two-layers deep. The main feature of the EMEC is its variable gap size: the LAr gap varies with the radius and, in order to obtain a uniform response across the EMEC, the high-voltage applied to the different η-sectors varies accordingly.

Forward The Forward Calorimeter (FCal) is the innermost calorimeter in the end-cap cryostats and is made of three modules. They share the same design: an absorber matrix filled with electrode tubes arranged along the beam axis. For the first module (FCal-1), aimed at forward electrons and photons energy measurements, the absorber is copper; the two other modules, optimized for hadronic energy measurments (FCal-2 and 3) are made of tungsten. Inside each tube is a rod, where the high-voltage is applied; the gap between the rod and its tube is filled with liquid argon.

1.3.4.2 Hadronic calorimeters

Tile calorimeter The Tile calorimeters (TileCal, [37]) surround the barrel and end-cap cryostats and are aimed at measuring jet and hadron energies. The TileCal is divided into three parts: a barrel ($|\eta| < 1$) and two extended barrels on each side ($0.8 < |\eta| < 1.7$). It is a sampling calorimeter with steel absorbers and scintillating plastic tiles as an active material. Each tile as read by a pair of wavelength shifting optical fibres connected to photomultiplier tubes. One of the modules (or ϕ-wedge) is represented on Figure 1.23.

The calibration of the readout electronics, photomultiplier tubes, and scintillating tiles are performed with three dedicated systems. The first is calibrated by injecting a known charge in the front-end electronics and measure the response, the photomultiplier tubes are calibrated by a laser system, and the tiles are calibrated by scanning the modules with a ^{137}Cs source through small tubes in the modules arranged along the beam axis.

In radius, the tile calorimeter ranges from 2.28 m to 4.25 m. The pseudo-projective segmentation (longitudinally and in depth) lead to cell sizes of $\Delta\eta \times \Delta\Phi = 0.1 \times 0.1$ in the first two compartments and $\Delta\eta \times \Delta\Phi = 0.1 \times 0.2$ in the last; the TileCal has approximately 9600 read-out channels. The energy resolution, determined during test beam studies, can be written as follows:

$$\frac{\Delta E}{E} = \frac{53\%}{\sqrt{E}} \oplus 5.7\%$$

Hadronic End-cap The Hadronic End-Cap (HEC) calorimeter shares the end-cap cryostats along with the EMEC and FCal and cover the pseudo-rapidity range $1.5 < |\eta| < 3.2$. It is a sampling calorimeter with copper absorbers and liquid argon as an active medium. The electrode planes are flat and arranged orthogonally with respect to the beam axis. The HEC is divided in two wheels, each segmented in two layers in depth.

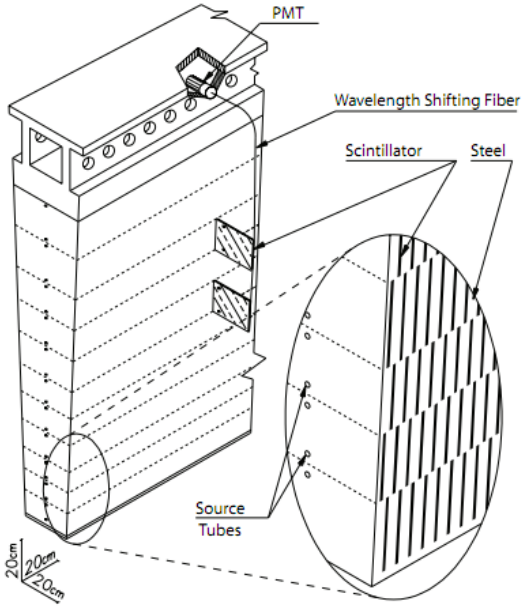

Figure 1.23: Schematic of a Tile calorimeter module.

1.3.5 Muon spectrometer

The outermost layers of the ATLAS detector consist of a scattering of different types of detectors forming the muon spectrometer [38] as shown on Figure 1.24. Its purpose is to perform trigger and precision tracking of muons, as well as measure their momentum with an aim of $\sigma_{p_T}/p_T = 10\%$ for $p_T = 1\ TeV$. The muon tracking can be extended by combining tracks from both the inner detector and the muon spectrometer. The momentum measurement is made possible by the bending power of the three toroidal fields, whose geometry has been chosen so that the fields are almost always perpendicular the muon trajectory, hence improving the momentum resolution of the spectrometer. The relation between a charged particle's momentum p, the intensity of the magnetic field B, and the radius of curvature of its track r can be written as follows:

$$p\ [GeV] = 0.3 \times B\ [T] \times r\ [m]$$

Two types of chambers are used for measurements, and two other for trigger. All the chambers are aligned with respect to each other using a grid of 5800 triplets of infrared

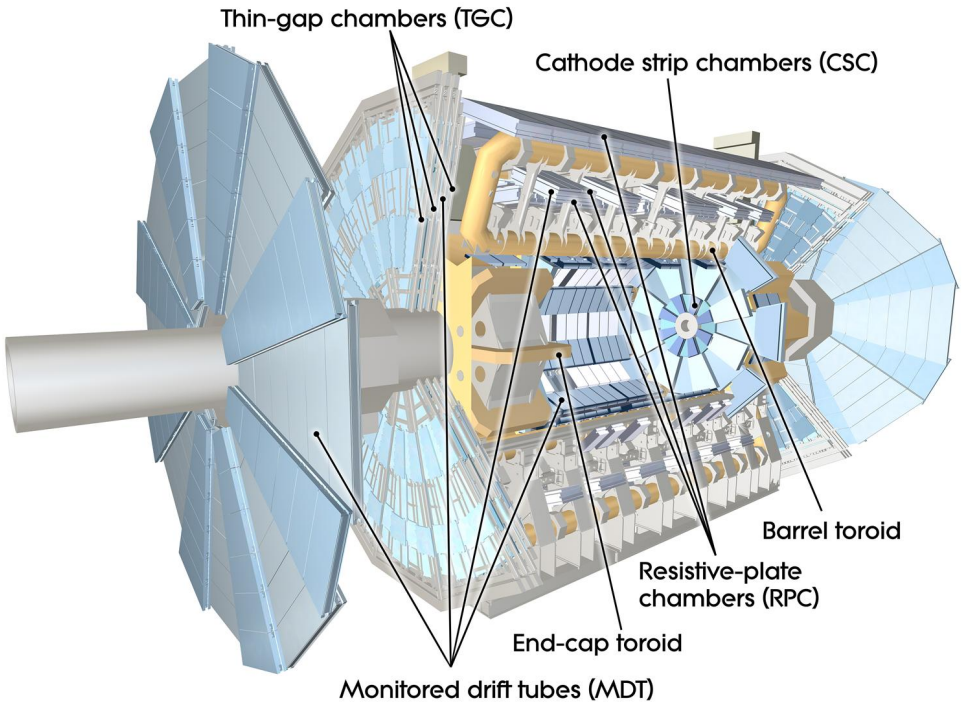

Figure 1.24: Rendered 3D view of the ATLAS muon spectrometer.

optical sensors, allowing a constant monitoring of the detectors' position in the cavern and achieving a 30 μm precision on the relative position of the chambers.

1.3.5.1 Resistive Plate Chambers and Thin Gap Chambers

The Muon Spectrometer uses two types of chambers for trigger purposes. The requirements for such a setup include:

- discrimination of transverse momentum
- bunch-crossing identification
- fast tracking information to be used by high-level trigger

Two different technologies have been chosen: Resistive Plate Chambers (RPC) and Thin Gap Chambers (TGC).

The RPC, which covers the pseudo-rapidity range $|\eta| < 1.05$, consists of three concentric cylindrical layers in the barrel region. The layer spacing allows for high-transverse

momentum (p_T) and low-p_T trigger capabilities. The RPC is a gaseous parallel electrode-plate detector. Two plastic resistive plates are separated by a 2 mm gas mixture ($C_2H_2F_4/Iso-C_4H_{10}/SF_6$) where lies an electric field of 4.9 kV/mm. The signal is read out by capacitive coupling to metallic strips placed on the outer faces of the resistive plates.

The TGC provides the measurement of the second coordinate in the range $1.05 < |\eta| < 2.7$ as well as muon trigger capabilities in the range $1.05 < |\eta| < 2.4$. Seven layers complement the MDT in the middle end-cap wheel, and two in the innermost η region. The TGC's requirements include good timing resolution for bunch-crossing identification and good granularity for a trigger dependent on momentum resolution. The TGC are multiwire proportional chambers operated in quasi-saturated mode: the wires, 1.4 mm away from the graphite cathodes, are put at a potential of 2.9 kV and are surrounded by a highly quenching gas mixture of CO_2 / $n-C_5H_{12}$, resulting in an amplification gain of $\sim 3 \times 10^5$. This leads to an overall very good timing resolution.

1.3.5.2 Monitored Drift Tubes and Cathode Strip Chambers

The Monitored Drift Tubes (MDT) are chambers comprised of aluminium tubes of 30 mm in diameter filled with an Ar/CO_2 gas mixture and a tungsten anode. The tubes are operated at a pressure of 3 bar and a voltage of 3080 V, resulting in an amplification gain of 2×10^4. The average spatial resolution of one of the 350000 tubes of the MDT is approximately 80 μm. The chambers are placed in three cylindrical layers in the barrel and three axial disks around the end-caps. The MDT covers the pseudo-rapidity range $|\eta| < 2.7$, except for the innermost layer of the end-cap ($2.0 < |\eta| < 2.7$), where Cathode Strip Chambers (CSC) are installed. At $|\eta| > 2$, the particle rate exceeds the MDT maximum allowed counting rate of 100 Hz/cm^2, whereas the CSC can safely operate at rates approaching 1 kHz/cm^2. The CSC are multiwire proportional chambers with cathodes segmented into strips; wires perpendicular to the strips provide the precision coordinate and wires parallel to the strips provide the transverse coordinate. The design resolution of one CSC plane is 60 μm.

1.3.6 Trigger and Data acquisition

The ATLAS trigger system is divided into three stages: L1, L2, and Event Filter. The two latter form the High Level Trigger (HLT). The calorimetry and muons systems front-end electronics acquire the lowest level of signals, gathers them, and sends them to the L1 trigger. The L1 then looks for basic patterns that could identify muons, electrons, photons, jets, or missing transverse energy and makes a decision: the *L1 Accept* (L1A). The time needed by the L1 to provide the L1A (2.5 μs) is limited by the overall L1 ouput rate of ~75 kHz, by design. Once the L1A has been issued, the buffered data is sent to the L2 along with regions of interest (RoI), which are $\eta - \phi$ regions of the detector where information has been deemed interesting, to be processed further by applying more refined algorithms. This process takes ~40 ms and the L2 maximum rate is limited to ~3.5 kHz. If an event passes the L2 stage, it is sent to the Event Filter to be permanently stored as raw data, at a maximum rate of 300 Hz. The raw data is then available offline to be fully reconstructed by dedicated algorithms and made available to the users for analysis.

Since 2010, a 36 h calibration loop has been implemented between the recording of the raw data and their reconstruction, in order to allow for data quality assessment and appropriate actions if necessary (e.g. masking of noisy readout channels, adjusting alignment). Immediately after data-taking, a data stream (Express Stream) containing 10% of the total amount is reconstructed and used to identify and define action items. After 36 hours, the reconstruction is performed on the entire dataset (Bulk) taking into account all these corrections.

Infrastructure-wise, the different elements of the chain just described are as follows: the L1 is a purely hardware trigger (necessary for speed) located in the ATLAS technical cavern; the L2 and Event Filter are handled by a computer farm located at the surface above the ATLAS cavern; the data are stored in the CERN Computer Centre and reconstructed there. The latter stage, also known as Tier-0 (first stage of the LHC Computing

Grid), is where all the data are made available to eleven Tier-1 sites in the world, which in turn make the data available to all the Tier-2 sites and so on. This allows optimal availability of data and best usage of the computing resources of all the ATLAS institutes around the world.

Chapter 2

The ATLAS liquid argon calorimeters

2.1 Introduction

As mentioned in the previous chapter the ATLAS liquid argon (LAr) calorimeters are a set of sampling calorimeters installed in three cryostats in between the trackers and the toroid magnets. Their goal is to provide Level-1 trigger capabilities along with Tile calorimeter, as well as electron/photon identification with very good γ / $\pi^0 \rightarrow \gamma\gamma$ separation, crucial for the $H \rightarrow \gamma\gamma$ analyses, and EM energy measurements with a good linearity up to 1.5 TeV (Z' and W' searches).. Reconstruction of jets and measurements of missing transverse energy and total transverse energy are also part of the calorimeters' tasks.

When a particle such as an electron or a photon traverses matter, it interacts and loses part of its energy though different processes. At high energies, two processes govern these energy losses: a charged particle will lose energy by emitting radiation (*Bremsstrahlung*) as it crosses material, and photon will produce electron-positron pairs by interacting with the high-Z absorber material. The combination of these two processes give birth to an electromagnetic shower, with a cascade of *Bremsstrahlung* radiation and pair production until the products reach very low energies and are absorbed.

Liquid argon has been chosen as an active medium because of the linearity of its

response, its stability, and its radiation hardness. A liquid argon gap functions as an ionisation chamber: when a charged particle traverses the gap it ionises the liquid argon and the presence of an electric field allows for the drift of the electron-ion pairs produced. The electron drift induces a current proportional the energy lost in the gap. The signal generation will be detailed in Section 2.5.

The LAr calorimeters are housed in three cryostats, one barrel and two endcaps. The electromagnetic barrel calorimeter (EMB) lies in the barrel cryostat and one endcap cryostat contains the electromagnetic endcap calorimeter (EMEC), the hadronic endcap calorimeter (HEC), and the forward calorimeter (FCal).

After a description of the main characteristics of the liquid argon calorimeters in Sections 2.2, 2.3, and 2.4, Section 2.5 summarises how an energy measurement is extracted from the detector. Finally, Section 2.6 describes their performance and status as of 2011.

2.2 Electromagnetic calorimeters

2.2.1 Geometry and granularity

In order to provide full ϕ-coverage without crack and fast extraction of the signal, an accordion geometry has been chosen for the electrodes and absorbers for the electromagnetic barrel (EMB) and endcap (EMEC) calorimeters, as shown on Figure 2.1. This geometry also ensures that a particle will cross multiple gaps/absorbers on its path allowing the development of an electromagnetic shower.

In the barrel the accordion waves are parallel to the beam axis and their folding angle varies along the radius in order to keep the liquid argon gap as constant as possible. In the electromagnetic endcaps, the accordion waves run axially and the folding angle varies with radius. As it will be discussed in Chapter 3, the constant liquid argon gap in the barrel leads to a uniform setting of the high-voltage applied, whereas in the endcaps, as the gap varies with radius, a segmentation into high-voltage sectors with different

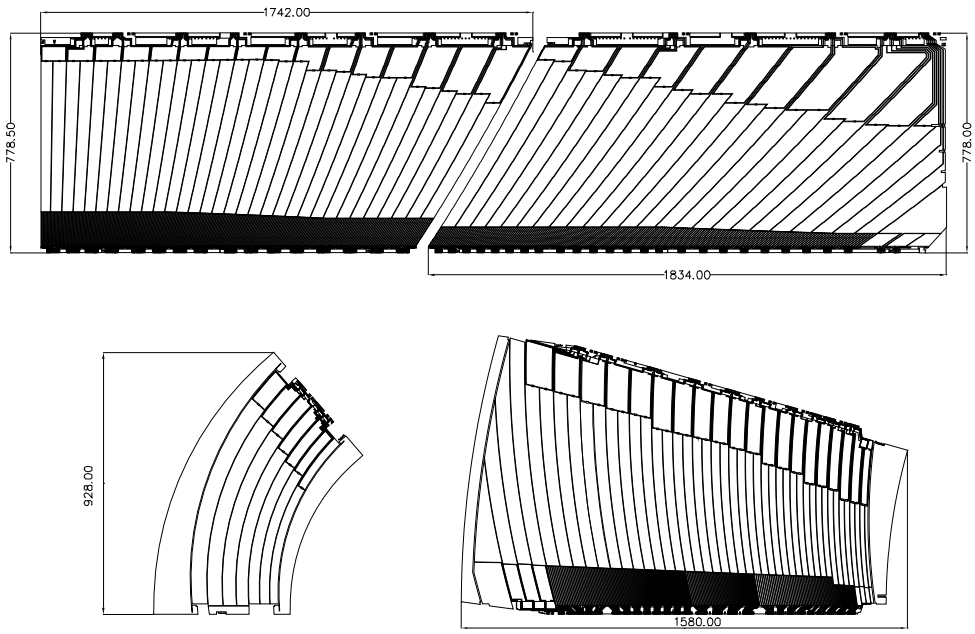

Figure 2.1: The fours types of electrodes of the electromagnetic calorimeter. The two top ones correspond to barrel electrodes: $|\eta| < 0.8$ (left) and $|\eta| > 0.8$ (right). The bottom left is an endcap inner wheel electrode and the bottom right is the outer wheel. Dimensions are in mm.

settings was chosen in order to obtain a uniform response.

The barrel calorimeter [39] is divided into two half-barrels, each consisting of 16 modules in ϕ build for practical assembly reasons. It is 6.4 m in length, 4 m in diameter and covers the pseudo-rapidity range $0 < |\eta| < 1.475$. One half-barrel module contains 64 absorber planes interleaved with readout electrodes. Each lead/stainless steel absorber is fixated on a glass-fibre composite bars at its extremities, which allows for the accurate positioning and protection of the connectors, and maintains the liquid argon gap size of 2.1 mm. In addition, honeycomb spacers have been installed between the absorber and electrode planes to help maintain the gap and limit sagging effects due to material weight. Additionally, the barrel is equipped with a presampler [40] module which role is to measure the energy lost in front of the calorimeter, which consists mainly of the solenoid and the cryostat wall. It shares the same cryostat and is placed front of the barrel as seen from the interaction point. The presampler is made of 32 azimuthal sectors, 11 mm deep, each divided into eight modules in pseudo-rapidity, providing a coverage of $\Delta\eta \times \Delta\phi = 1.52 \times 0.2$.

The endcap calorimeter [41] covers the pseudo-rapidity range $1.375 < |\eta| < 3.2$ and is made of two coaxial wheels, each wheel itself divided into eight ϕ-wedges. Each endcap contains 768 absorber-electrode planes in the outer wheel and 256 in the inner wheel. In the region $1.5 < |\eta| < 1.8$, a presampler layer in installed against the cryostat wall, and is made of 32 azimuthal sectors made of 2 mm thick liquid argon active layers.

As seen from the interaction point, the electromagnetic calorimeters are segmented into depth layers (Figure 2.2): in the precision region ($|\eta| < 2.4$, the front layer is finely segmented in η primarily to allow for the distinction between *prompt* photons (i.e. coming from a pp collision) and photons due to the decay of π^0 mesons; the middle layer, which is the largest, collects most of the energy deposited by the shower; the back layer (up to $|\eta| = 2.5$), sees the tail of the electromagnetic shower and contributes to the separation of electromagnetic and hadronic showers.

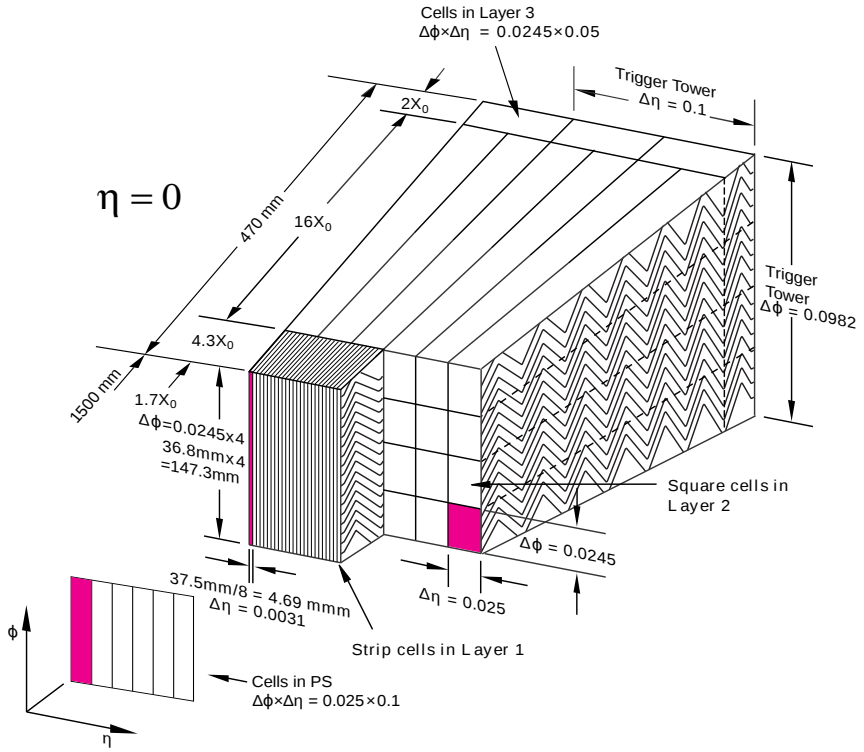

Figure 2.2: Sketch of the granularity and segmentation of electromagnetic calorimeter cells.

The granularity and pseudo-rapidity coverage of the electromagnetic calorimeters are listed in Table 2.1.

	Barrel		Endcap	
Presampler	0.025×0.1	$\lvert\eta\rvert < 1.52$	0.025×0.1	$1.5 < \lvert\eta\rvert < 1.8$
Layer 1 (front)	$0.025/8 \times 0.1$	$\lvert\eta\rvert < 1.40$	0.050×0.1	$1.375 < \lvert\eta\rvert < 1.425$
	0.025×0.025	$1.40 < \lvert\eta\rvert < 1.475$	0.025×0.1	$1.425 < \lvert\eta\rvert < 1.5$
			$0.025/8 \times 0.1$	$1.5 < \lvert\eta\rvert < 1.8$
			$0.025/6 \times 0.1$	$1.8 < \lvert\eta\rvert < 2.0$
			$0.025/4 \times 0.1$	$2.0 < \lvert\eta\rvert < 2.4$
			0.025×0.1	$2.4 < \lvert\eta\rvert < 2.5$
			0.1×0.1	$2.5 < \lvert\eta\rvert < 3.2$
Layer 2 (middle)	0.025×0.025	$\lvert\eta\rvert < 1.40$	0.050×0.025	$1.375 < \lvert\eta\rvert < 1.425$
	0.075×0.025	$1.40 < \lvert\eta\rvert < 1.475$	0.025×0.025	$1.425 < \lvert\eta\rvert < 2.5$
			0.1×0.1	$2.5 < \lvert\eta\rvert < 3.2$
Layer 3 (back)	0.050×0.025	$\lvert\eta\rvert < 1.35$	0.050×0.025	$1.5 < \lvert\eta\rvert < 2.5$
Total number of readout channels	109568		63744 (both sides)	

Table 2.1: Granularity and coverage of the electromagnetic calorimeters.

2.2.2 Liquid argon gap

Figure 2.3 illustrates the layout of an electromagnetic calorimeter readout cell. One lead absorber is surrounded by two steel plates glued on each side to provide mechanical strength. The absorbers are connected to the common cryostat ground at the calorimeter inner and outer edges. The copper readout electrode is surrounded by two copper high-voltage electrodes using layers of insulating kapton. One of the key features of this calorimeter is highlighted by this layout, indeed one readout electrode effectively sees two liquid argon half-gaps, with their independently fed electric fields. This ensure redundancy in the occurrence of the loss of one of the two high-voltage sources. The EMB electrodes are uniformly set to a of 2000 V potential, and the EMEC electrodes, because of the varying gaps, are set to voltages ranging from 1000 V to 2500 V and - 2000 V in the EMEC presampler. The high-voltage system and its distribution inside the calorimeter will be described in Chapter 3. The signal induced by the ionisation electron drift in the liquid argon gap is collected by capacitive coupling in the readout electrode and transmitted to the electronic readout chain for amplification and processing, as discussed in Section 2.5.

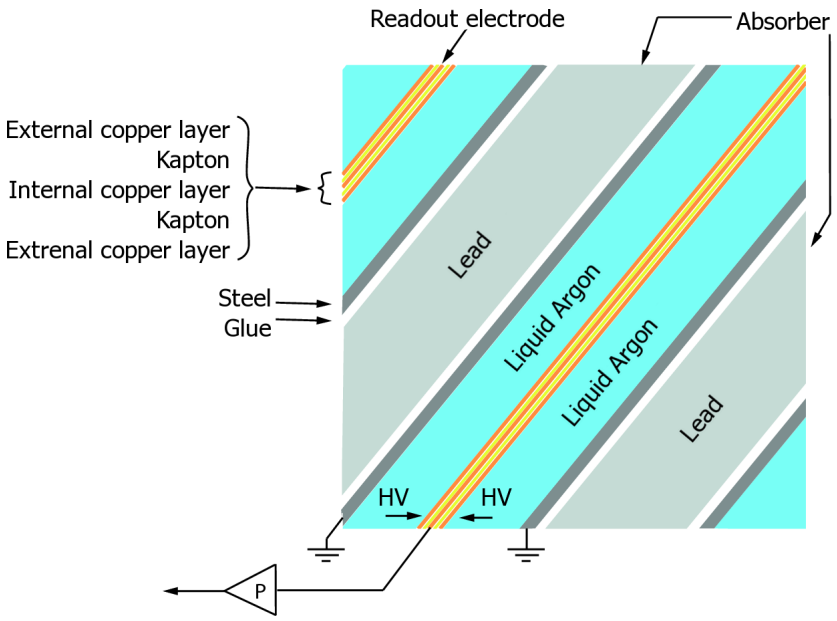

Figure 2.3: Sketch of an electromagnetic calorimeter liquid argon gap.

	Hadronic endcap	
$\Delta\eta \times \Delta\phi$	0.1×0.1	$1.5 < \lvert\eta\rvert < 2.5$
	0.2×0.2	$2.5 < \lvert\eta\rvert < 3.2$
# of readout channels	5632 (both sides)	

Table 2.2: Granularity and coverage of the hadronic endcap calorimeter.

2.3 Hadronic calorimeters

The hadronic endcap calorimeter (HEC) [42] shares the endcap cryostat along with the EMEC and forward calorimeter. As illustrated on Figure 2.4, it is made of two modules, each divided into two longitudinal wheels. Each wheel consists of 32 ϕ-wedges. There is a total of 26 flat absorber copper plates in the two front wheels and 16 in the two rear wheels. A distance of 8.5 mm is maintained between the plates where lies four distinct 1.8 mm liquid argon gaps. The HEC granularity, coverage, and number of readout channels is detailed in Table 2.2.

As shown on Figure 2.5, four electrodes divide the gap between two copper plates into four liquid argon gaps. The two central electrodes are back to back and separated from the central copper readout electrode by insulating kapton. These *PAD* layers define the

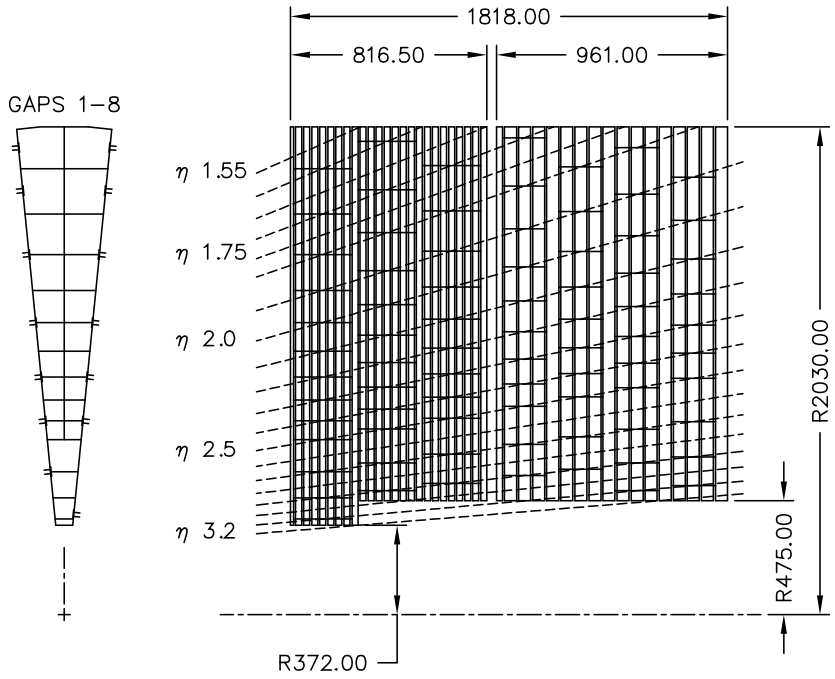

Figure 2.4: Schematic transverse (left) and lateral (right) views of the hadronic endcap calorimeter.

lateral segmentation of the HEC by a high-resistivity padding and are independently fed high-voltage. The outermost electrodes, or *EST* for electrostatic transformers, have their high-resistivity side facing the *PAD* with a high-voltage applied to the other side. This layout effectively creates four distinct drift gaps, each independently fed by a different high-voltage line. The nominal voltage applied to the HEC electrodes is 1800 V, which corresponds to a 1 kV/mm electric field and an average electron drift time of 430 ns.

2.4 Forward calorimeters

The forward calorimeter (FCal) [43] is a sampling calorimeter that covers the pseudo-rapidity range $3.2 < |\eta| < 4.9$ and is housed in the two end-cap cryostats along with the electromagnetic end-cap (EMEC) and the hadronic end-cap (HEC) calorimeters, as illustrated on Figure 2.6. Each of the two FCal modules (FCal A and FCal C) is divided into three longitudinal absorber matrices, one made of copper (FCal-1) and the other two of tungsten (FCal-2/3). Each matrix, contains tubes arranged along the beam axis

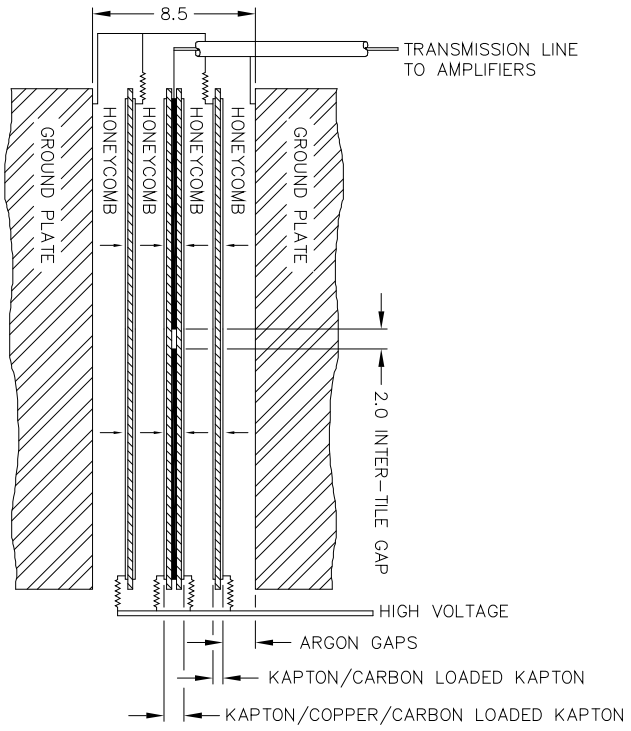

Figure 2.5: Schematic view of a hadronic endcap liquid argon gap.

	Forward calorimeter	
FCal-1 (EM)	3.0×2.6	$3.15 < \lvert\eta\rvert < 4.30$
	$(3.0 \times 2.6)/4$	$3.10 < \lvert\eta\rvert < 3.15$
	$(3.0 \times 2.6)/4$	$4.30 < \lvert\eta\rvert < 4.83$
FCal-2 (Had)	3.3×4.2	$3.24 < \lvert\eta\rvert < 4.50$
	$(3.3 \times 4.2)/4$	$3.20 < \lvert\eta\rvert < 3.24$
	$(3.3 \times 4.2)/4$	$4.50 < \lvert\eta\rvert < 4.81$
FCal-3 (Had)	5.4×4.7	$3.32 < \lvert\eta\rvert < 4.60$
	$(5.4 \times 4.7)/4$	$3.29 < \lvert\eta\rvert < 3.32$
	$(5.4 \times 4.7)/4$	$4.60 < \lvert\eta\rvert < 4.75$
# of readout channels	3524 (both sides)	

Table 2.3: Granularity and coverage of the forward calorimeter. Cell sizes are expressed in cm in the transverse plane $\Delta x \times \Delta y$.

which are filled with liquid argon, the active medium. Figure 2.7 shows the section of an FCal matrix and its tube arrangement. An FCal tube houses a central rod on which a high-voltage (HV) is applied to drift ionisation electrons by the effective electric field of approximately 1 kV/mm. As per its design, the FCal granularity is better expressed in the x-y plane: the readout cell segmentation is detailed in Table 2.3.

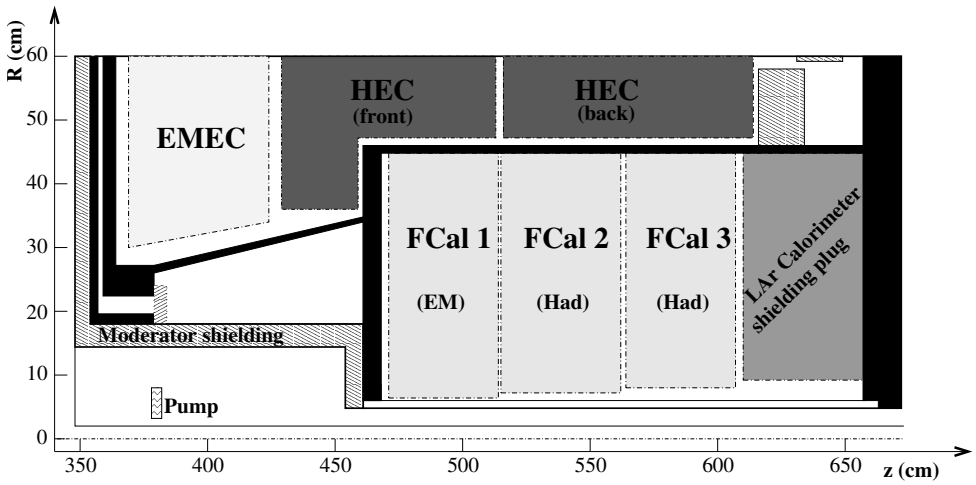

Figure 2.6: Lateral view of the positioning of the forward calorimeters inside the endcap cryostats.

Each FCal-1 matrix is divided into 16 ϕ-sectors, each of them fed by four independent high-voltage lines. There are two types of readout channels: summed channels are made of 4 groups of 4 tubes and unsummed channels which consist of a single 4-tube group. The latter type only covers the inner and outer edges of the FCal modules. In the case

of summed channels (see Figure 2.8, each of the 4 tube groups is fed by one of the four HV lines in this sector. This ensures redundancy in the event of HV-related issues, and allows for an offline correction of the cell energy in case of a failure of one of the HV lines. The two hadronic matrices, FCal-2 and FCal-3, follow a similar layout. The three FCal-A matrices are illustrated in Figure 2.9.

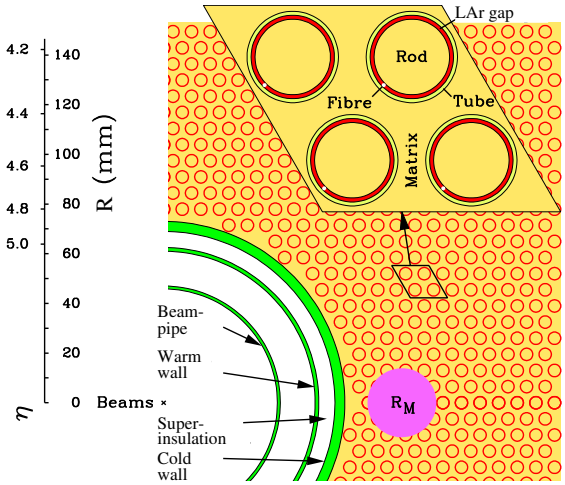

Figure 2.7: Transverse view the forward calorimeter tube matrix.

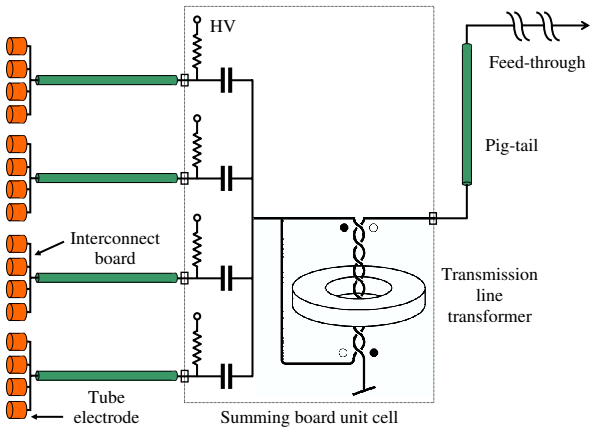

Figure 2.8: Cold cabling of four forward calorimeter tube groups. The high-voltage feed, analogue summing, and feedthrough connection are also represented.

2.5 From the ionization signal to the digitized samples

The ultimate goal of the calorimeter is to provide energy measurement from the ionisation signals produces in the different liquid argon gaps previously described, the following section details the signal extraction and processing by the electronics chain, as well as the calibration of the calorimeters readout electronics.

As mentioned previously, when a charged particle traverses a gap, it ionises the liquid argon, producing electron-ion pairs which drift in the electric field provided by the high-voltage system. The ions drift speed being negligible compared to that of electrons, their contribution can be ignored. If we consider a single charge q drifting in a liquid argon gap harbouring a electric field $\vec{E}$ provided by a constant potential U_0, the power it is

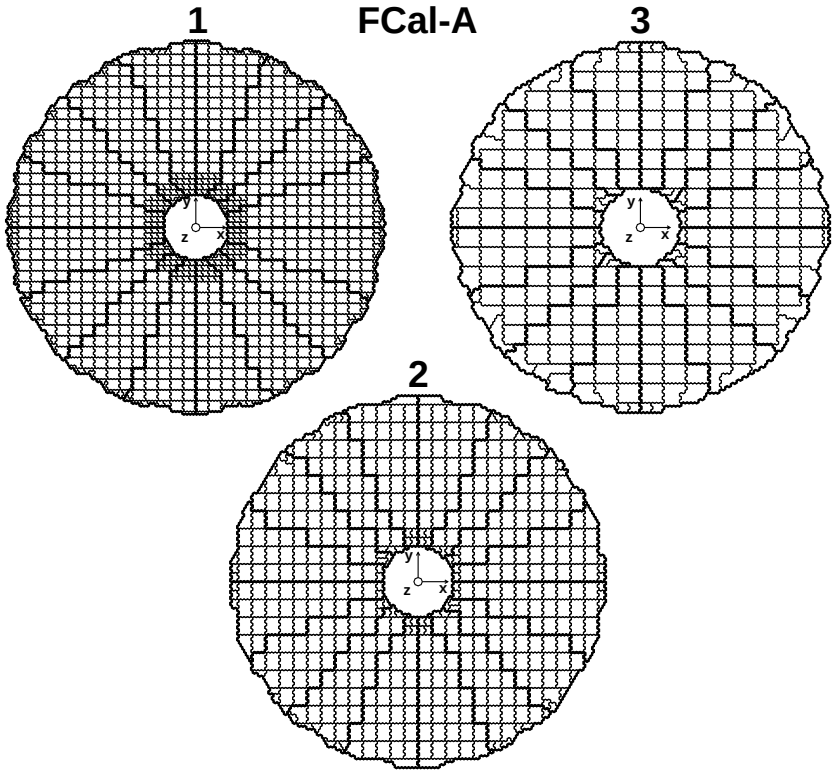

Figure 2.9: Transverse view of the three FCal-A modules. The tiles, consisting of tube groups, represent readout channels.

supplied can be expressed as follows:

$$P = q\ \vec{E} \cdot \vec{v_d}$$

where $\vec{v_d}$ is the charge drift velocity. With g denoting the liquid argon gap width, the current induced by the drifting charge can be written:

$$i(t) = \frac{P}{U_0} = \frac{|q| \cdot E \cdot v_d}{U_0} = \frac{|q| \cdot v_d}{g}$$

Back to the case when a charge particle instantly and uniformly ionises a liquid argon gap. Creating N electron-ion pairs and considering that the maximum total current induced at $t = 0$ is I_0 and is null when all the electrons are collected after $\tau_d = v_d/g$ (drift time):

$$I(t) = N\ e\ \left(1 - \frac{t}{\tau_d}\right) = I_0\ \left(1 - \frac{t}{\tau_d}\right)$$

An electron drift velocity in the liquid argon of approximately 4.5 mm/μs, an electric field of 1 kV/mm and a drift gap $g \sim 2.1$ mm, the drift time is $\sim$ 450 ns. This duration is long compared to the LHC design bunch crossing frequency: 1/25 ns. Therefore this signal has to be processed properly in the electronic readout chain [44].

The signal is then extracted to the front-end electronic boards [45] located outside the cryostats, as shown of Figure 2.10.

Here it first meets the pre-amplifiers where it is amplified away from the electronic noise. The signal is then shaped through a bipolar $CR-(RC)^2$ filter which outputs a pulse with an early narrow peak, reflecting the I_0 current, and a longer, negative, undershoot. The goal of the shaping is to minimise the out-of-time pile-up, and the bipolarity ensure that the pulses average to zero. Both triangular and shaped signal are illustrated in figure 2.11. Each of the three outputs - for the three gains - of the shaper is analogically sampled at 40 MHz and sent to be temporarily buffered in the Switch Capacitor Arrays (SCA). The SCA allows for the storage of 144 pulses, corresponding to a duration of

approximately 3.6 μs, awaiting a signal from the Level-1 trigger to send the selected pulses further down the chain, which shouldn't take more than 2.5 μs.

In parallel, the shaper outputs are analogically summed and sent to the Level-1 trigger for decision. If an event is selected, five samples are digitised around the Level-1 Accept time at 40 MHz by the 12 bits ADC and sent via optical fibres to the back-end electronics [46] located in the ATLAS technical cavern, USA15.

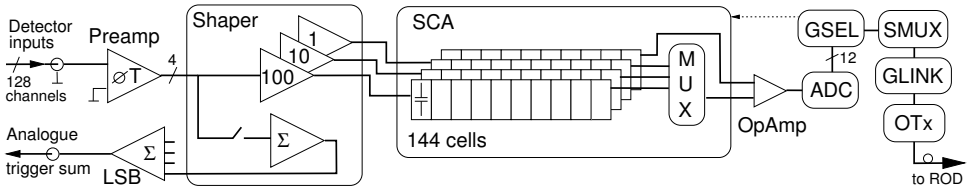

Figure 2.10: Front-End Board schematic

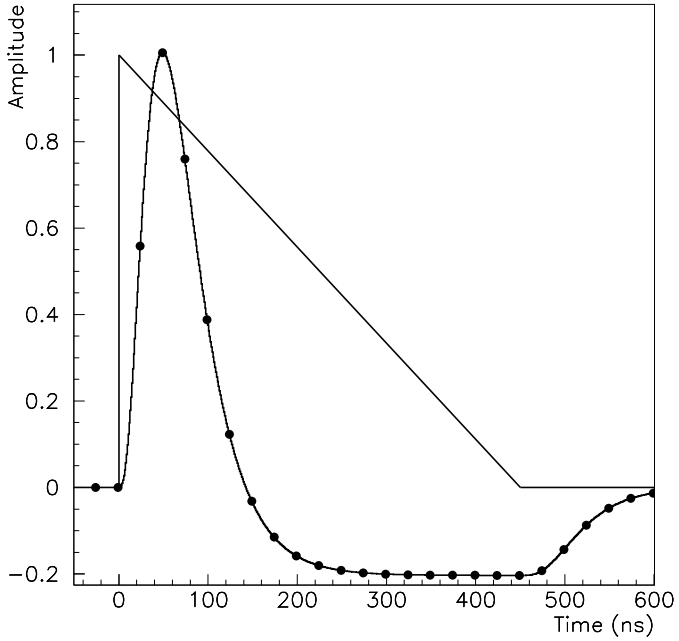

Figure 2.11: LAr signal before and after shaping. The black markers represent the 40 MHz sampling of the pulse.

The back-end electronics process the signals sent from the front-end and provide the ATLAS data acquisition (DAQ) system energy and time measurements for each of the calorimeter readout channels. The Read-Out Drivers (ROD) [47] receive the digitised

samples and Digital Processor Units (DSP) compute the energy and time as follows:

$$E = \sum_{i=0}^{N_{samples}} a_i \, (s_i - p) \qquad \tau = \frac{1}{E} \sum_{i=0}^{N_{samples}} b_i \, (s_i - p)$$

where $N_{samples}$ is the number of digitised samples, s_i the number of ADC counts of sample i, p the pedestal - i.e. the number of ADC counts in the absence of signal, and a_i and b_i a set of coefficients extracted from the calibration of the calorimeter.

Going back to the ionisation current induced in the liquid argon gap. Every time a charge particle traverses a gap, charges are lost, inducing a voltage drop. To compensate for the voltage drop, the high-voltage system has to inject a number of charges equivalent to the amount lost due to ionisation. A schematic view of the process is illustrated in Figure 2.12.

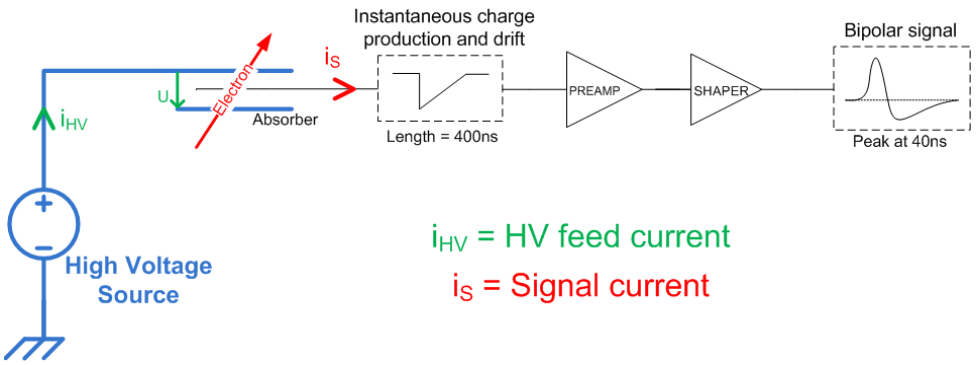

Figure 2.12: Schematic view of a calorimeter cell (equivalent to a capacitor) being traversed by a charged particle. As the ionisation current i_S flows out to the readout chain (right) for the energy deposition measurement. The high-voltage power supply (left) injects the current i_{HV} to maintain the potential U constant across the liquid argon gap.

2.6 Performance

The expected performance of the liquid argon calorimeters [48] is mostly governed by physics searches involving the Higgs boson, such as the $H \to \gamma\gamma$ and $H \to 4e$ decays channels, as well as searches for the Z' and W' which produce very high energy electrons. The performance requirements involve a good energy resolution as well as a good angular

resolution between the two photons in case of the di-photon decay channel of the Higgs. Test beam results have led to the following expression of the energy resolution:

$$\frac{\Delta E}{E} = \frac{a}{\sqrt{E}} \oplus \frac{b}{E} \oplus c$$

The first term corresponds to the sampling term, related to the shower across the calorimeter gaps. The value of a is approximately 10% in the electromagnetic calorimeters, 50% in the hadronic calorimeters, and 100% in the forward calorimeters. The second term corresponds to the noise contribution, dominated by the noise of the electronic readout. The noise term grows with the pile-up noise due to the increase of the luminosity. The last term reflects the effects of the non-uniformity of the calorimeter response as well as quality of the detector calibration. It must be maintained below 0.7% as per the calorimeter design requirements. The angular resolution is provided by the fine segmentation of the electromagnetic calorimeters first layer is found to be approximately $50\mu rad/\sqrt{E[GeV]}$ overall. Finally, for searches such as long-lived ionising particles, a good timing resolution is required, with an achieved resolution of 100 to 170 ps across the calorimeters, as shown on Figures 2.13 and 2.14.

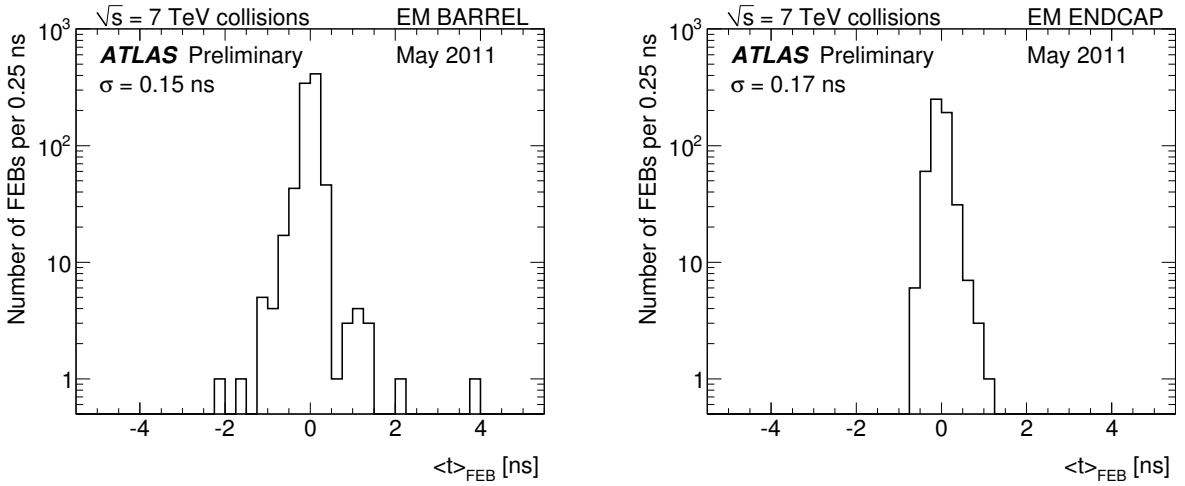

Figure 2.13: Average time per Front-End Board in the electromagnetic barrel and endcap calorimeters extracted from 7 TeV collision data in 2011

Table 2.4 illustrates the status of the LAr calorimeter readout as of July 2011. Overall, 99.79% of the readout channels are usable for data-taking. The faulty channels are

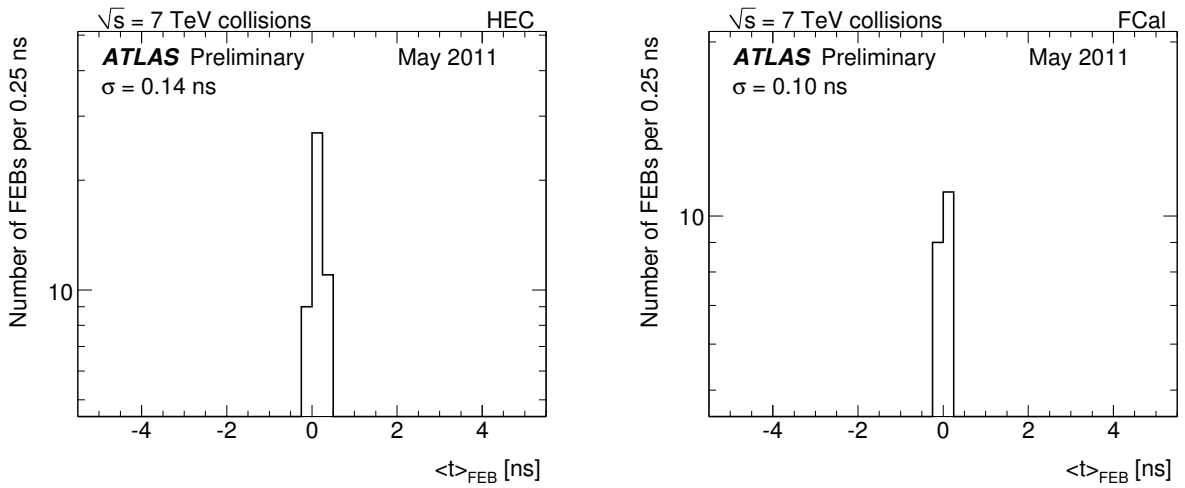

Figure 2.14: Average time per Front-End Board in the hadronic endcap and forward calorimeters extracted from 7 TeV collision data in 2011

Detector	# readout channels	Percentage of faulty channels
EM	173312	0.29%
HEC	5632	0.37%
FCal	3524	0.23%
Overall LAr	182468	0.21%

Table 2.4: LAr calorimeter faulty channels as of July 2011. The percentages are dominated by dead channels and extremely noisy channels that need to be masked out of the readout chain.

mostly due to dead or disconnected channels, either at the time of assembly or during commissioning, and very noisy channels that need to be masked out of the readout.

Overall, the LAr calorimeter performance is under control and well within its design parameters.

2.7 Conclusion

The ATLAS liquid argon calorimeters, their main characteristics and performance have been described in this chapter. As discussed, the high-voltage system feeding the liquid argon gaps is a crucial part of the calorimeter. The high-voltage system and its operation will therefore be described in Chapter 3 and a relative luminosity measurement, using the currents injected by the HV system due to ionisations losses, will be discussed in

Chapter 4.

Chapter 3

The LAr high-voltage system

3.1 Introduction

As mentioned in Chapter 2, the LAr high-voltage system is designed to feed the calorimeter liquid argon gaps with electric fields allowing for the drift of ionisation electrons induced by charged particles passing through. Without the drift field, the electron-ion pairs produced would recombine, thus preventing the creation of the drift current and any energy measurement.

The installation of the LAr HV system in the ATLAS technical cavern was performed between 2004 and 2007 following a series of studies with prototypes at the CERN North Area test beam lines. At my arrival in the group in 2007, approximately half of the system was installed and cabled. I consequently contributed to the finalisation of the power supplies installation and cabling, and actively helped in the development of the control system framework. I then continued my work as high-voltage expert during which time I assisted in the daily maintenance of the system, as well as continuing developments.

The choice of the operational regime of the HV system is motivated by two reasons: the drift time of the ionisation electrons and the breakdown voltage of the liquid argon. As the drift velocity of the electrons in the liquid argon gap is found to be approximately

proportional to $E^{\frac{1}{3}}$, a too low electric field will increase the drift time of the electrons and challenge the electronic readout through pile-up effect of the shaped signals. Furthermore, if the electric field is too intense, the risk of causing sparks in the gaps rises, hence disturbing the operation of the calorimeter and compromising the gap integrity. These considerations have led to the setting of an operational field of approximately 1 kV/mm across all the calorimeters, with various operating voltages depending on the liquid argon gap sizes.

Additionally, the requirements of the high-voltage system include constraints on features such as the grounding scheme and safety systems to protect the detector as well as the HV system.

3.2 High-voltage distribution

Table 3.1 lists the granularity, gap size, and nominal high-voltage settings of the liquid argon calorimeters.

In the barrel, each high-voltage line supplies one side of all the electrodes in a HV sector of $\Delta\eta \times \Delta\phi = 0.2 \times 0.2$, corresponding to 32 electrodes in ϕ. As the gap size is constant, the applied voltage is the same across the entire barrel, +2000 V.

In the electromagnetic endcap calorimeter, each HV line feeds one side of all the electrodes in a sector of $\Delta\phi = 0.2$ and $\Delta\eta$ varying from 0.1 to 0.4. Because of the gap size variation, the high-voltage settings have to be adapted in order to keep a uniform response of the EMEC. If a continuous variation of the high-voltage settings would have been ideal, for practical reasons a variation by steps was chosen. A total of seven HV sectors in the outer wheel and two in the inner wheel have different nominal high-voltage settings. These variations are illustrated on Figure 3.1.

In the hadronic endcap calorimeters, the high-voltage is fed to the PAD and EST boards through HV patch panels mounted on the HEC modules inside the cryostats [49].

Detector						
$\|\eta\|$						
Gap [mm]						
Voltage [V]						
EMB Presampler						
$0 - 1.52$						
1.9 - 2.0						
+2000						
EMB						
$0 - 1.475$						
2.1						
+2000						
EMEC Presampler						
$1.5 - 1.8$						
2.0						
-2000						
EMEC outer wheel						
$1.375 - 1.5$	$1.5 - 1.6$	$1.6 - 1.8$	$1.8 - 2.0$	$2.0 - 2.1$	$2.1 - 2.3$	$2.3 - 2.5$
2.7	2.5	2.2	1.9	1.6	1.4	1.2
+2500	+2300	+2100	+1700	+1400	+1250	+1000
EMEC inner wheel						
$2.5 - 2.8$				$2.8 - 3.2$		
2.5				2.0		
+2300				+1800		
HEC						
$1.5 - 3.2$						
8.5						
+1800						
FCAL						
$3.1 - 4.9$						
0.25 - 0.375 - 0.5						
+250 / +375 / +500						

Table 3.1: Coverage, gap size, and operative voltage of the liquid argon calorimeters.

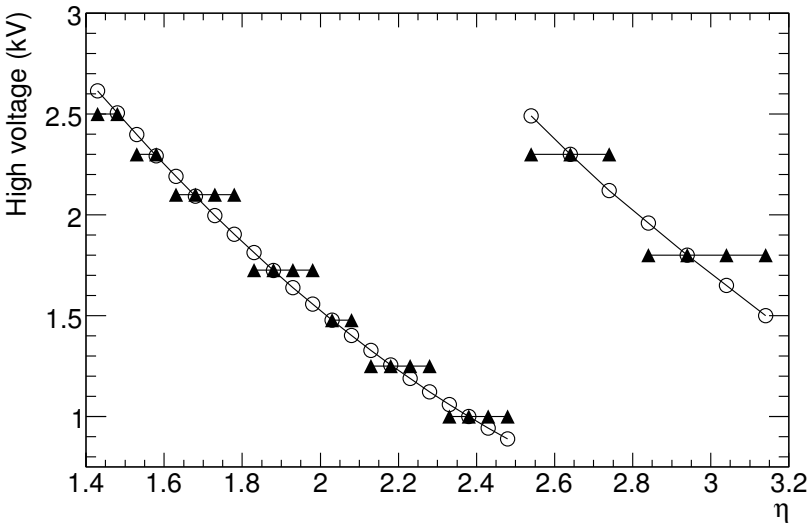

Figure 3.1: High-voltage distribution as a function of $|\eta|$ for the EMEC. A uniform calorimeter response requires a high-voltage which varies continuously as a function of $|\eta|$ (open circles), which has been approximated by a set of discrete values (full triangles) corresponding the nine high-voltage sectors.

Via strip-line connectors, the HV is distributed on the electrode with highly resistive polyimide layers, which helps reducing the noise induced by the high-voltage system and limits the risk of electric discharges.

The forward calorimeter high-voltage distribution is performed via summing boards mounted on the faces of the absorber matrices. One FCal readout cell is divided into four tubes groups, each fed by separate HV lines. This ensures that in case of HV failure, a fourth of the signal will be lost at most.

The following section describes how the calorimeter cell energy is corrected with respect to changes in the high-voltage settings.

3.3 High-voltage corrections

From the high-voltage system viewpoint, two reasons can lead to the correction for the measured energy [50].

The first, as illustrated in the previous section, is inherent to the EMEC, is permanent

and is by construction due to the fact that the high-voltage varies by steps whereas the EMEC gap sizes varies continuously. Therefore, the cell energy in a specific HV sector has to be corrected depending on its η position within that sector. The corrected cell energy in the HV sector S can be expressed as follows:

$$E_{corr}(\eta, S) = E_{meas} \cdot \frac{\beta^S}{1 + \alpha^S(\eta - \eta^S_{centre})}$$

where η^S_{centre} is the η position at the centre of HV sector S. The parameters α^S and β^S originate from the linear dependence of the energy with η.

The second type of high-voltage correction has to be performed when one or more high-voltage lines are Off or at a voltage lower than their nominal value. Test beam results have shown that the measured energy is proportional to $\sim V^{0.38}$. Therefore, if two sides an electrode group are at a reduced by identical voltage, the corrected energy is:

$$E_{corr} = E_{meas} \cdot \left(\frac{V_{nom}}{V_{op}} \right)^{0.38}$$

where V_{nom} is the nominal voltage and V_{op} the reduced, operative voltage.

Finally, in the more general case where the two HV lines are at two different operative voltages V_{op1} and V_{op2}, the corrected energy becomes:

$$E_{corr} = \frac{2 \cdot E_{meas}}{\left(\frac{V_{op1}}{V_{nom}} \right)^{0.38} + \left(\frac{V_{op2}}{V_{nom}} \right)^{0.38}}$$

As of the 12th of July 2011, 244 out of the 4320 liquid argon high-voltage lines are operated at a non-nominal voltage. The breakdown by sub-detector is listed in Table 3.2, and the geometrical location of the correction factors in the electromagnetic calorimeters are illustrated on Figure 3.2.

The cause of high-voltage reduction comes mostly from observation of effects on the calorimeter trigger rates and related noisy readout channels which leads to the manual

Detector	A-side	C-side
EMEC	32	29
EMEC PS	1	3
EMB	24	21
EMB PS	24	28
HEC	27	54
FCAL	1	0

Table 3.2: Number of non-nominal LAr high-voltage lines as of 12/07/2011.

setting of a lower operative value. Noise hunting campaigns were performed where HV and L1Calo trigger experts worked in the ATLAS control room to identify noise induced by the high-voltage system. By looking at Level-1 trigger rates coming from the calorimeter analogue sums and changing the high-voltage settings, they were able to identify several HV lines inducing noise at their nominal voltage. Therefore, these lines are operated at a lower voltage. These campaigns mainly took place in the HEC and EMBPS.

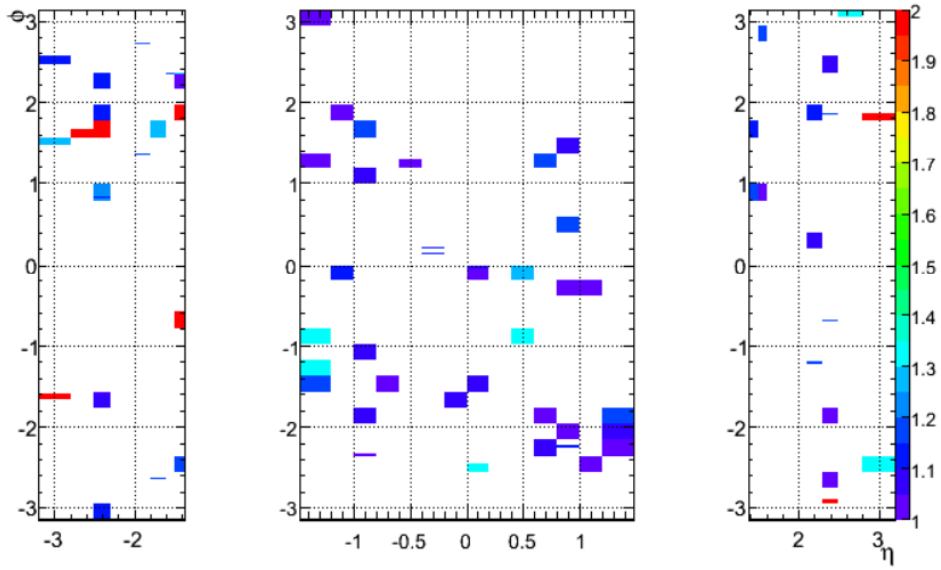

Figure 3.2: Electromagnetic calorimeter high-voltage correction factor in the middle layer versus (η, ϕ) coordinates of the calorimeter cells. Status at the beginning of October 2009. The current situation does not differ significantly.

Another source of non-nominal voltage are HV lines that draw large amounts of current. This is caused by shorts in the calorimeter, which leads to the power supply injecting a DC current. If the power supply feeding that particular short cannot inject enough cur-

rent to maintain the nominal voltage, or if the power dissipation exceeds the limit of the filter box resistor, the operative voltage is decreased accordingly.

The following section describes the layout the high-voltage system hardware, from the electrodes to the power supplies.

3.4 Hardware

This section describes the hardware equipment constituting the LAr high-voltage system. The feedthroughs, allowing the passage of the HV lines into the liquid argon cold cryostat, as well as the high-voltage power supplies and their crates are detailed. Finally, the grounding scheme and return current measurements are described.

3.4.1 Feedthroughs

The high-voltage is carried out of the technical cavern to the experimental cavern, where lies the ATLAS detector, by $\sim$ 120 m cables. The 168 cables coming from the power supply units are connected to the 3 cryostats onto 6 high-voltage feedthroughs (HVFT, [51]), two for the barrel and two for each endcap cryostat, as illustrated on Figure 3.3. The role of the HVFT is to allow the transfer of the warm HV lines into the the liquid argon cryostats at 88 K. The HVFT is kept at room temperature, and the wires pass through a buffer of gaseous argon before entering the cryostat vessel.

The schematic design of a HVFT is shown on Figure 3.4. The HV wire is first connected to an RC filter, the purpose of which is to reduce the noise entering the cryostat, it then goes through the wire feedthrough plane and down into a stainless steel bellow sitting within the cryostat wall. The bellow's role is to accommodate the mechanical strains between the cold and warm cryostat wall, especially during the cryostat cooldown. At the bellow level also lies the interface between the gaseous argon buffer and the cryostat's liquid argon. The HV wires are finally distributed to the calorimeter electrodes through

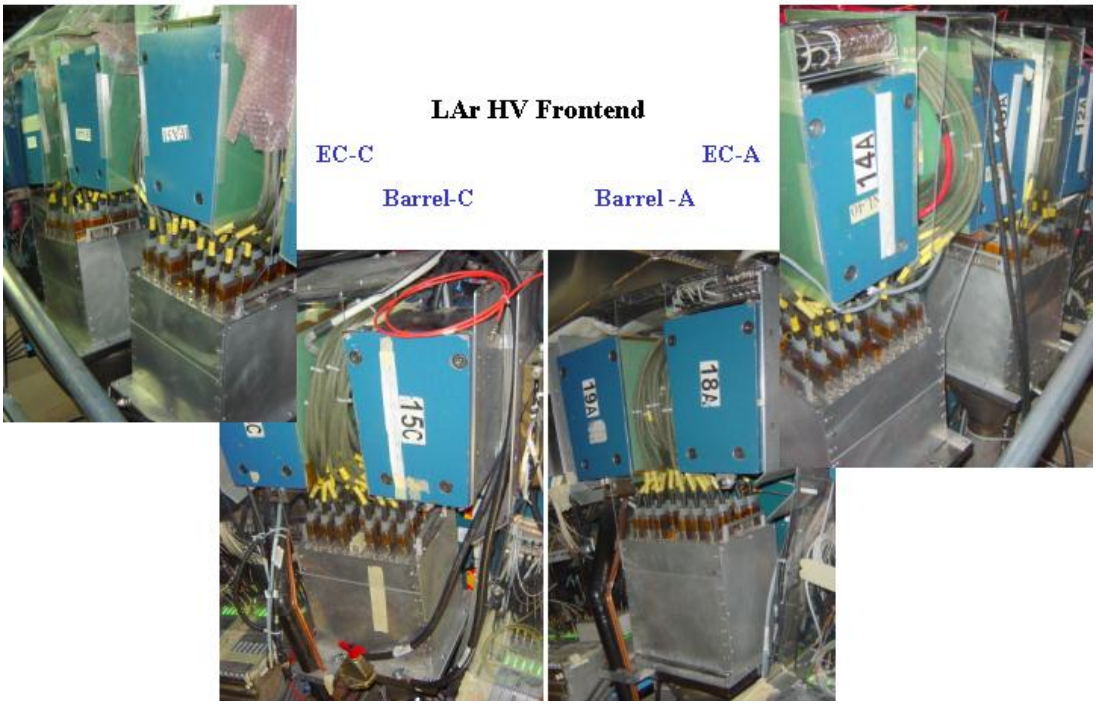

Figure 3.3: The six high-voltage feedthroughs sitting on top the calorimeter cryostats.

different patch panels.

3.4.2 Modules

The HV power supply system hardware was manufactured by the Iseg Spezialelektronik GmbH[1] company, located in Dresden, Germany. The technical specifications are listed in Appendix A.

A high-voltage power supply unit must comply to comply to a set of requirements, including:

- the unit and connector housings, as well as the cable shield, must be connected to the HV return to the cryostat ground, whilst being separated from the crate connection to the safety ground grid, therefore ensuring that the HV supply remains floating

[1] http://www.iseg-hv.com

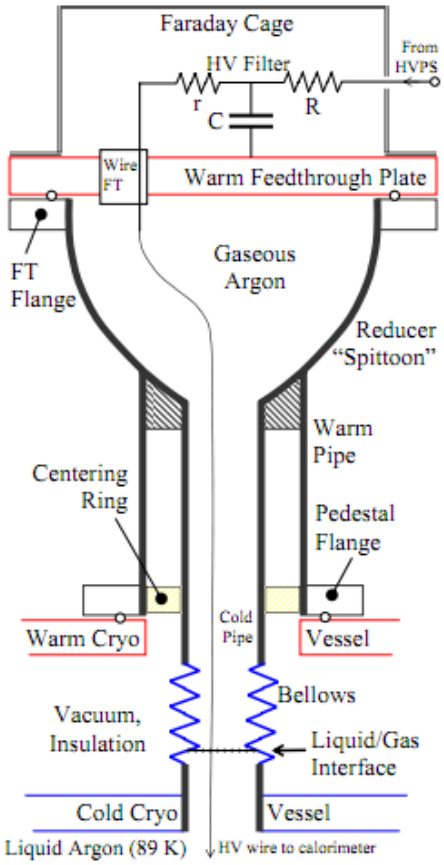

Figure 3.4: Schematic of a high-voltage feedthrough.

- each high-voltage line voltage must be individually settable and regulated from 0 V up to its nominal value
- the voltage setting and regulation must be better than 100 mV
- the maximum current output must comply with the estimations derived from the expected particle fluxes at the LHC design luminosity, ranging from 75 μA to 6 mA depending on the subdetector
- each unit must possess an interlock system to allow for the safe discharge of the calorimeter in case of emergency, such as cooling or power failures

Each HV power supply unit contains two boards of 8 (FCal) or 16 (everything but the FCal) channels, as shown on Figure 3.5. A unit is insertable on rails into a 19"-6U-Eurocrate chassis and connected via its backplane to the crate communication bus and the primary 24 V power supply. The front face displays each board's status on LED, and exhibits the following features:

- two potentiometers that allow for the setting of the hardware voltage and current limits over the whole module range, above which the entire unit is automatically switched off
- the safety loop connector, illustrated on Figure 3.6, which is connected to the interlock system for safety controls
- a 32 pin connector, illustrated on Figures 3.8 and 3.7, which carries out the high-voltage to the detector, contains the HV return lines, as well as interlock pins that, being different for each module type depending on the subdetector fed, prevents accidentally connecting detector parts to HV lines with improper characteristics; additionally, the interlock pins act as ground pins

The high-voltage is generated per channel, regulated around the set value via a voltage comparator and current is injected towards the detector whenever a voltage drop

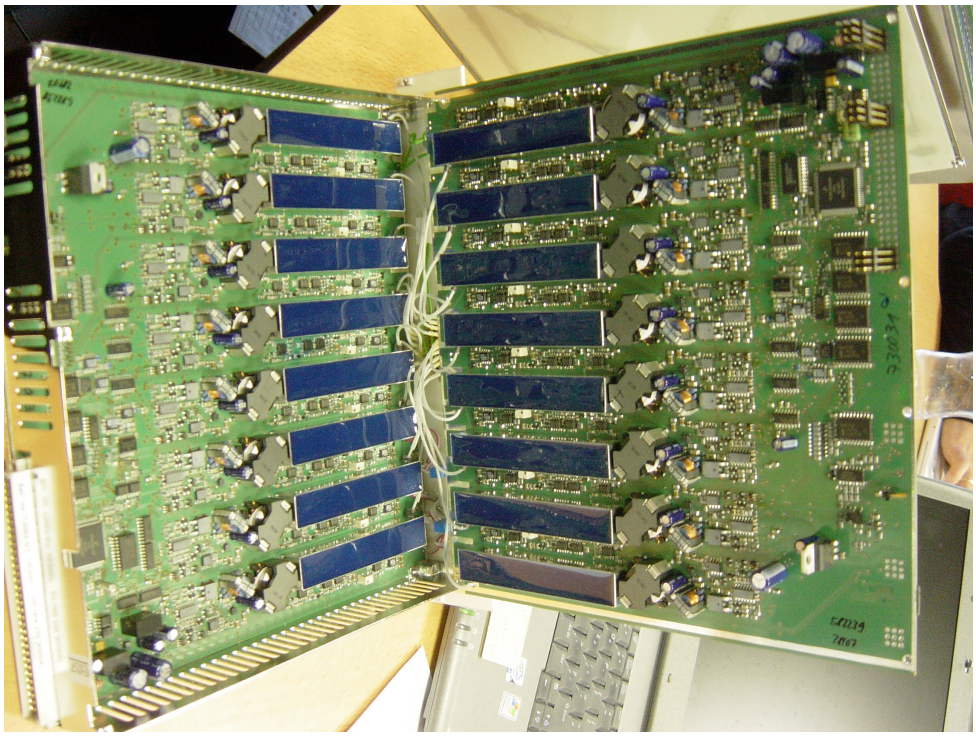

Figure 3.5: A 32-channel high-voltage power supply unit.

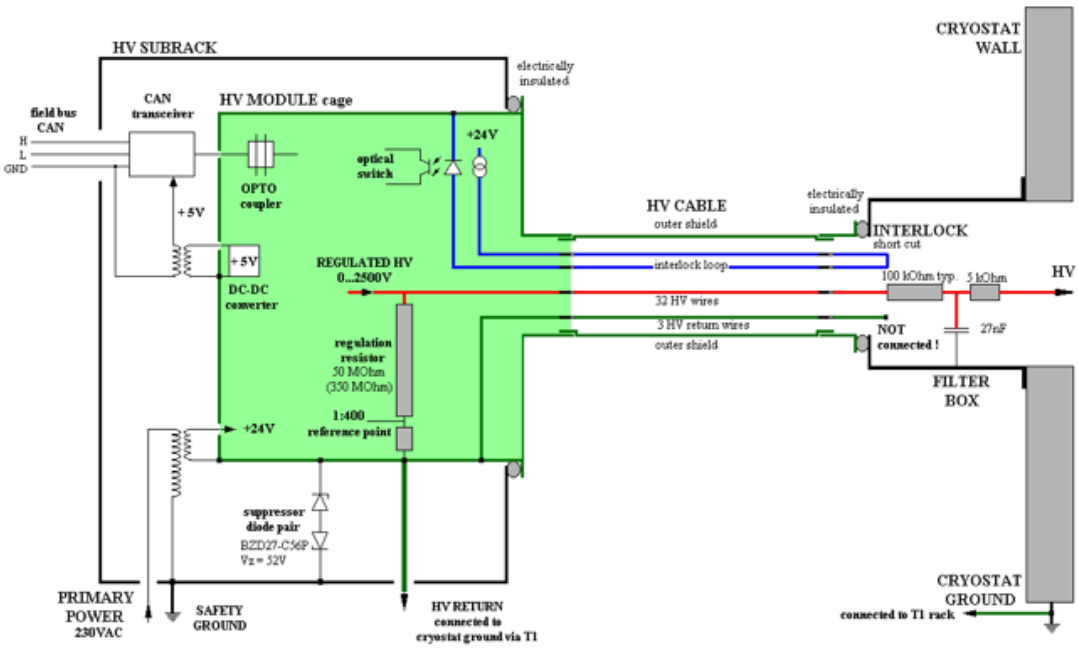

Figure 3.6: Layout of a high-voltage power supply and its connection to the cryostat.

Figure 3.7: High-voltage cable connectors.

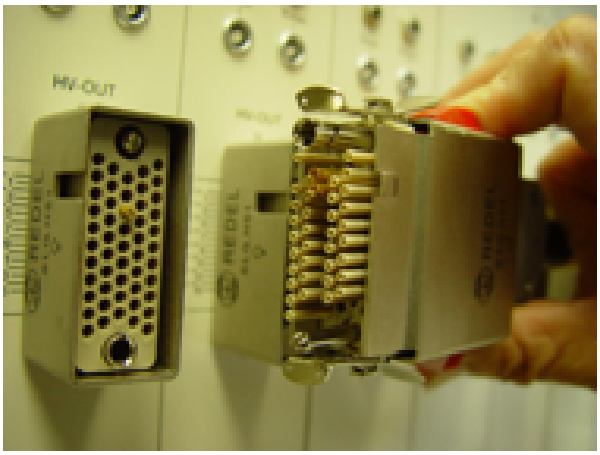

Figure 3.8: High-voltage cable connector and its counterpart on the HV power supply unit.

occurs in any of the liquid argon gaps fed by the HV channel. In order to limit the power dissipation in the filter resistor of the filter box (3.4), the maximum allowed current can be set via software. But as a failsafe, a hardware current limit can be adjusted via a potentiometer located on the HVPS unit. The maximum voltage allowed can similarly be adjusted, i.e. if a part of the calorimeter is normally fed 1800 V, one can use standard 2500 V power supplies but limit their voltage output to allow safe operation. To ensure the integrity of the circuit and protect the power supplies, a internal interlock loop is present on each unit, which is closed only if an HV cable is plugged in the unit. This way if a cable is accidentally disconnected from the unit, the power supply will ramp down to 0 V. Since different modules feed different parts of the calorimeter with different operative voltages, it is important to categorise the connectors to avoid plugging the wrong cable to the wrong unit. This is done by an interlock pin configuration on the connector, which is different for each subdetector, and will not allow the cable connector to enter the unit connector.

3.4.3 Crates

The LAr HV crates are located in the ATLAS underground technical cavern, USA15, along with all the ATLAS backend electronic infrastructure. The crates are describes in length

in Appendix C. An overview of the USA15 counting room with the LAr racks is shown on Figure 3.9. As illustrated on Figure 3.10, there are a total of 20 crates installed in five racks. Each rack contains four crates separated by heat exchangers and fans to control the temperature and air flow, additionally to a cooling water circuit. The cooling water circuit is protected by a redundant tap water circuit in case of a failure of the cooling system of technical cavern. The crates are powered individually through the ATLAS Uninterruptable Power Supply (UPS) system, and each is connected to the safety ground grid of the ATLAS cavern. The connection to the UPS serves as a protection against disturbances of the general power grid. A single crate houses up to eight power supply units, and possesses its own crate controller unit. All the crate controllers are linked together in chain via CAN[2] lines to a dedicated computer to allow for their control and monitoring.

3.4.4 Return current measurement

In order to safely operate the detector and minimise electromagnetic interferences to the readout electronics, the grounding of the entire ATLAS experiment must be done in a well controlled manner. The grounding strategy, described in great detail in [52], follows the CERN safety instructions and electrical code, as well French, Swiss, and European regulations. The grounding guidelines include requirements regarding the electrical insulation of all the detectors with a single connection to the ATLAS "Safety Network", as well as floating power supply systems. The latter, described previously, includes the liquid argon calorimeter high-voltage power supply system, which therefore was designed to be floating.

Concerning the liquid argon calorimeters, they have been designed to be entirely insulated from the ground of the experimental cavern, as well as other subdetectors. The safety grounding of the calorimeter cryostats is performed via dedicated ground cables leading to the technical cavern USA15, some 100 m away. Two cables (for redundancy)

[2] http://www.dcd.pl/dcdpdf/can2spec.pdf

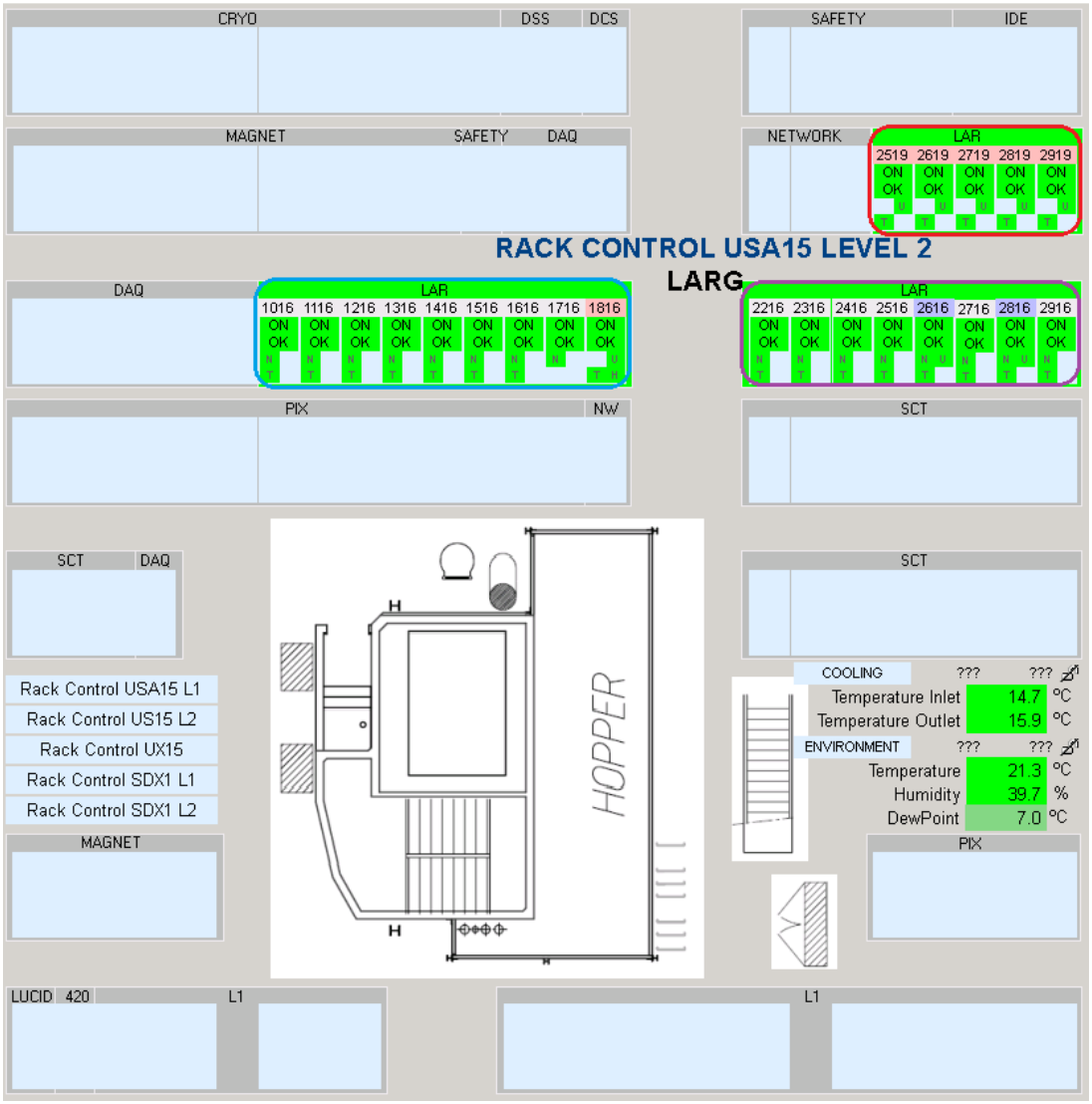

Figure 3.9: Overview of the ATLAS technical cavern, USA15. Shown are the five HV racks (red), the low voltage power supplies racks (purple), and the DCS and ROD racks (blue). This dynamic panel reflects the status of the racks by monitoring their temperatures, the humidity, and the main power supplies.

Figure 3.10: High-voltage power supply crates in USA15.

per cryostat (the barrel and the two endcaps) end up connected to one of the racks in USA15 (one of the L1 racks as seen on Figure 3.9), which is itself connected to the Safety Ground. In order to detect possible current leaks due accidental contacts between the LAr system and other detectors or services, a DC current monitoring system has been put in place. As illustrated on Figure 3.11, the principle is to inject a reference 500 mA DC current to each cryostat, let it come back through the ground, and measure the difference. This is achieved by using and Integrated Parametric Current Transformer (IPCT), a high precision contactless DC measurement coil[3]. The IPCT has a resolution of 12 μA over its full dynamic range of $\pm$ 10 mA, enough to detect small leakage currents. The IPCT data is readout and can be visualised via a web trending display and included into an alarm system.

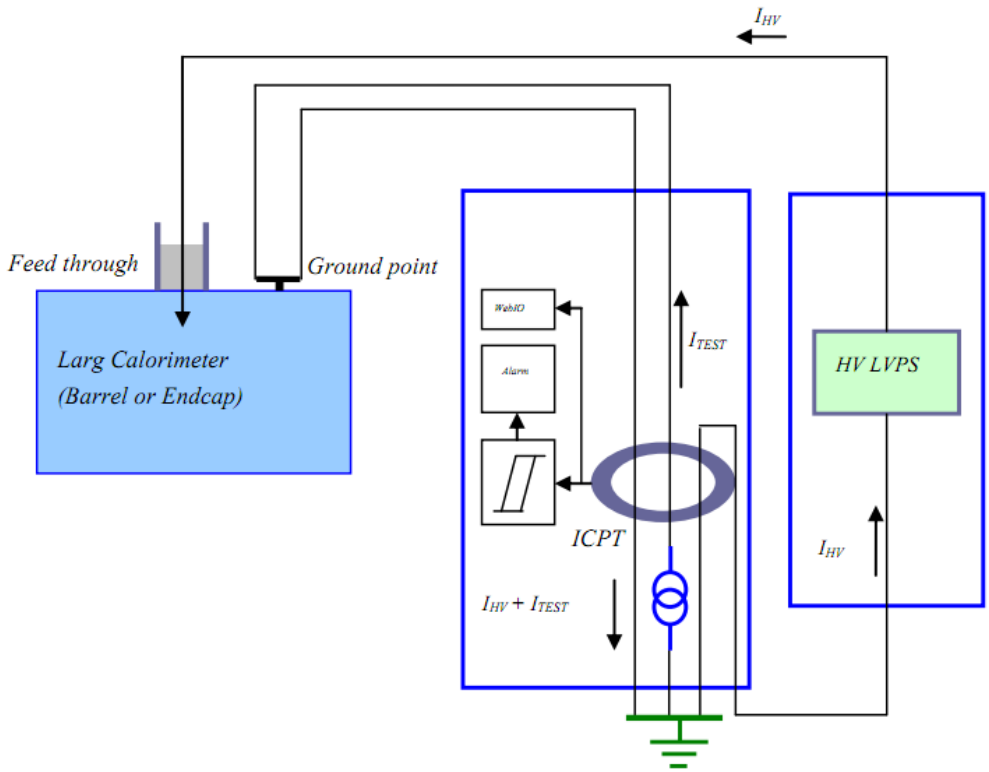

Figure 3.11: Schematic of the grounding monitoring of the liquid argon calorimeter cryostats

As shown on Figure 3.11, the return current from the high-voltage system also also goes through the IPCT monitoring coil. The HV return current reflects the voltage drops in

[3] http://www.bergoz.com

the calorimeter gaps as charged particles ionise the liquid argon, as illustrated on Figure 2.12 of the previous Chapter. Measuring this return current for each HV subsystem could therefore give interesting handles on the amount of current induced by collision products in the calorimeters, as well as performing a more localised monitoring of the HV system grounding. For those reasons, a set of six additional IPCT coils were installed on the different return lines of the HV crates. The coil installation, data acquisition setup, and complete layout can be seen on Figures 3.12, 3.13 and 3.14. The six coils measure the return currents corresponding to the following sub-detectors: EMEC-FCal-A, EMEC-FCal-C, HEC-A, HEC-C, EMB-EMBPS, and finally the total return current of the three cryostats. The IPCT having a resolution of 12 μA, they are not sensitive enough to provide a competitive handle on the luminosity at the current state. The IPCT data are read out through 12 bit ADCs and sent to one of the high-voltage control machine (Figure 3.15, where they are archived in the DCS Oracle database, as well as displayed on the LAr FSM.

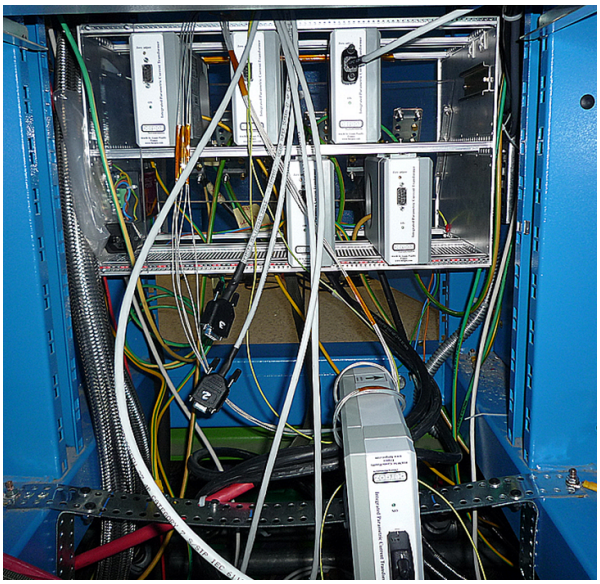

Figure 3.12: Return current measurement coils.

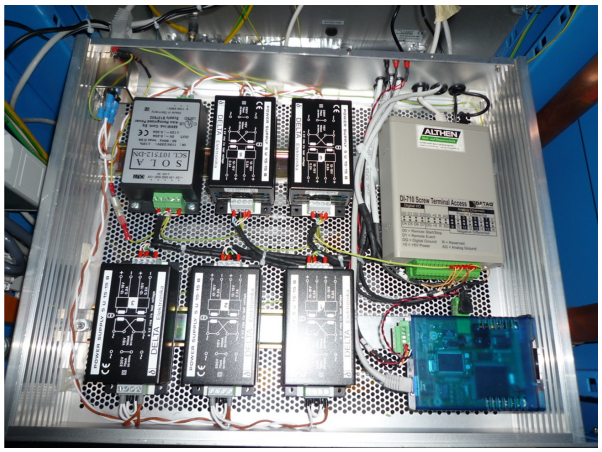

Figure 3.13: Return current data acquisition setup.

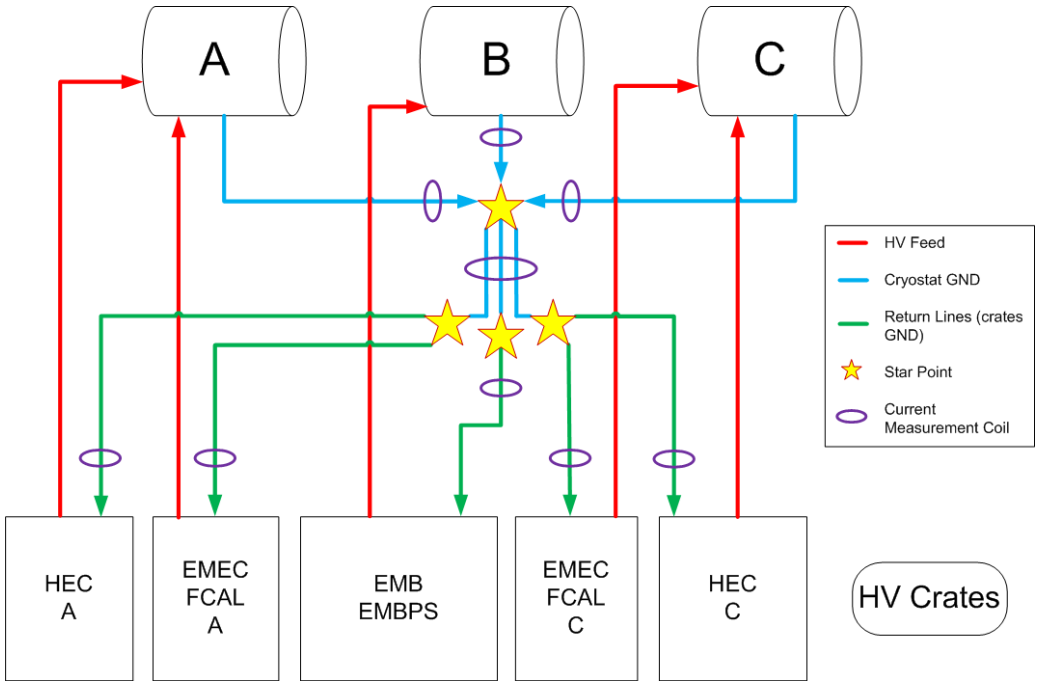

Figure 3.14: Layout of the return current measurements.

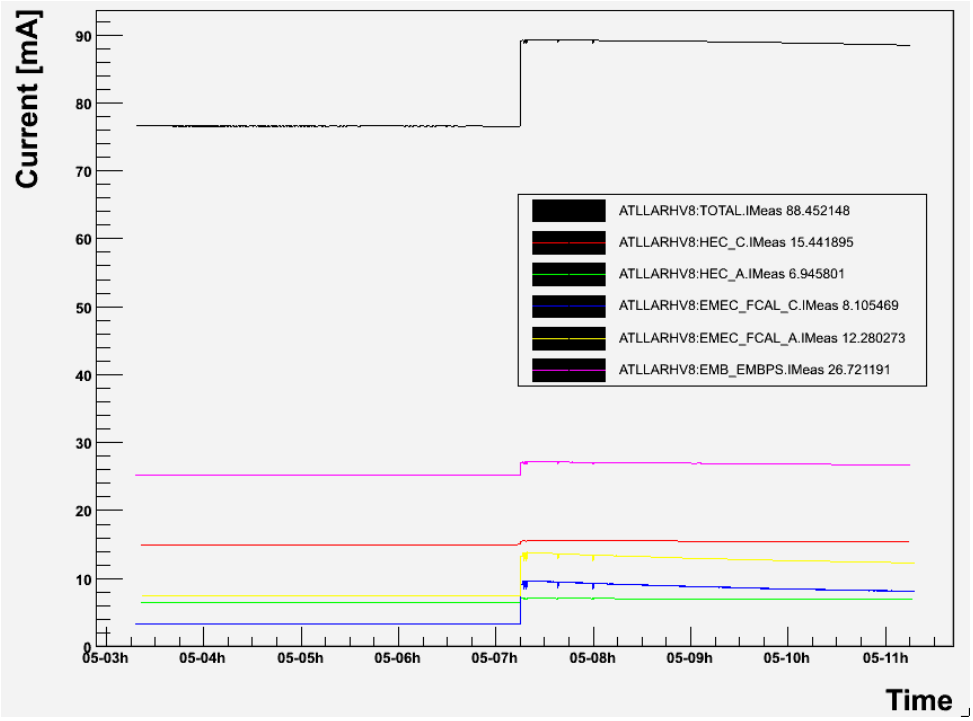

Figure 3.15: Return currents.

3.5 Slow control

A major requirement of the LAr high-voltage system is the ability to control and monitor all its operational parameters. To achieve this, a software layer has been developed to read out and control the system on top of a proprietary software that communicates with the hardware. The deployment of the software infrastructure was done according to the ATLAS central Detector Control System (DCS, [53]) recommendations, which aims at harmonising all the ATLAS DCS systems under a common framework.

3.5.1 Software

The lowest layer is the Object Linking and Embedding for Process Control (OPC) software, which handles the real-time communication with the hardware. An OPC server has been developed by the HV power supply manufacturer, Iseg Spezialelektronik GmbH, and is maintained by their engineers as per its proprietary status. Its role is to provide direct access to data items related to the control and monitoring of the HV crates and power supply units. The OPC server manual is attached in Appendix D.

The next software layers were developed by the ATLAS collaboration using the PVSS[4] framework, a distributed software used for real-time control and monitoring of large scale hardware installations. In the PVSS framework, the OPC client's purpose it to communicate with OPC server, linking hardware data items to so-called datapoint elements within PVSS. These datapoint elements can be grouped by device, and setting or reading them out defines the communication with the HV system. Therefore, items such as module temperatures, HV line voltage, current and status can be read-out and items such as the set voltage and the current limits can be controlled, all directly from PVSS in a uniform manner.

As an example, Figure 3.16 shows the PVSS crate control panel. As mentioned previously, all the crate controllers are linked by a CAN line to a single control computer.

[4] http://www.etm.at

On this computer, a PVSS instance is running, and this panel allows for the control and monitoring of the crate parameters:

- crate general information such as serial number, power supply unit contained, rack/subrack names
- environmental parameters like temperature and humidity
- crate status, including interlock alerts, main power supply status, communication status
- switching each crate On/Off, which consequently switches Off the main power supply, hence all the modules inside

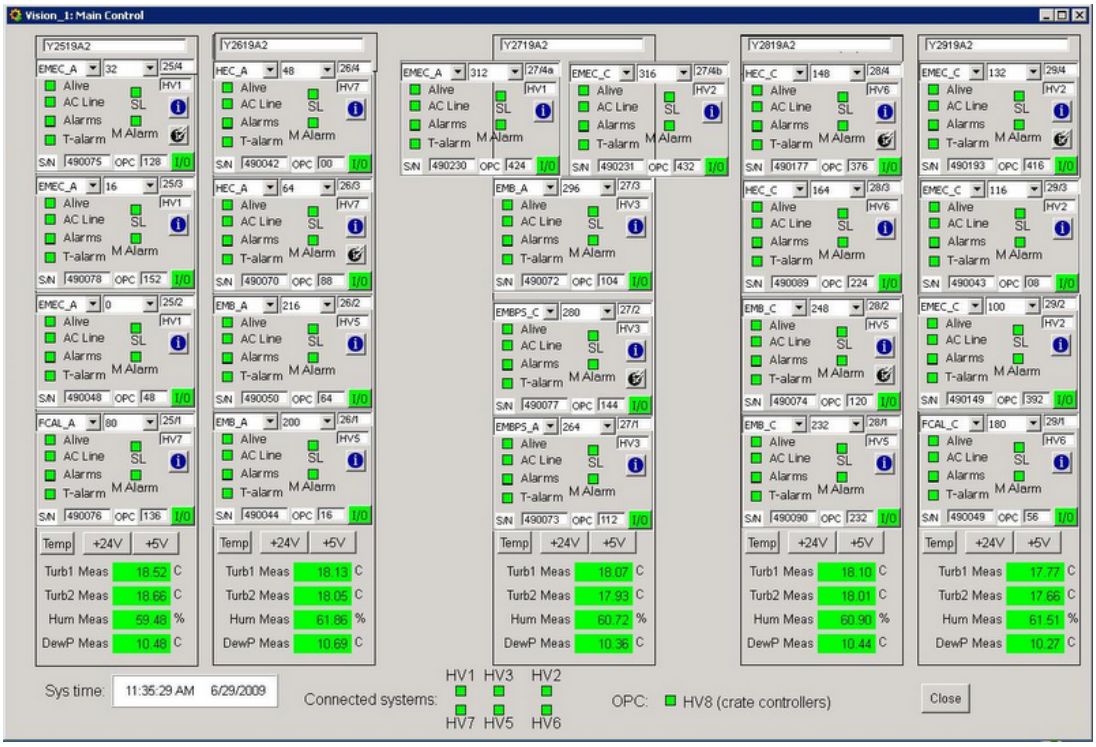

Figure 3.16: Crate control PVSS panel.

A total of seven computers run the control software of the high-voltage system, each independently connected a to a set of crates organised per subdetector. On each computer runs an instance of the PVSS software, with its own OPC server/client, as well as its

own datapoint element structure. However a generic set of control panels, as shown on Figure 3.17 were designed and run on each machine. These panels allow for the control of parameters of the OPC server, which in turn sets the parameters in the hardware, such as the OPC deadband, which filter numerical values like voltages and currents to reduce the CAN traffic and module general parameters like the fine adjustment, a parameter which improves the voltage regulation around the set value. Furthermore, control of entire crates/modules is possible through a panel which allows loading a set of parameters from a configuration database. This eases the operation of the HV system when group commands are required, for instance when the entire system needs to be switched Off/On before and after a technical stop for maintenance.

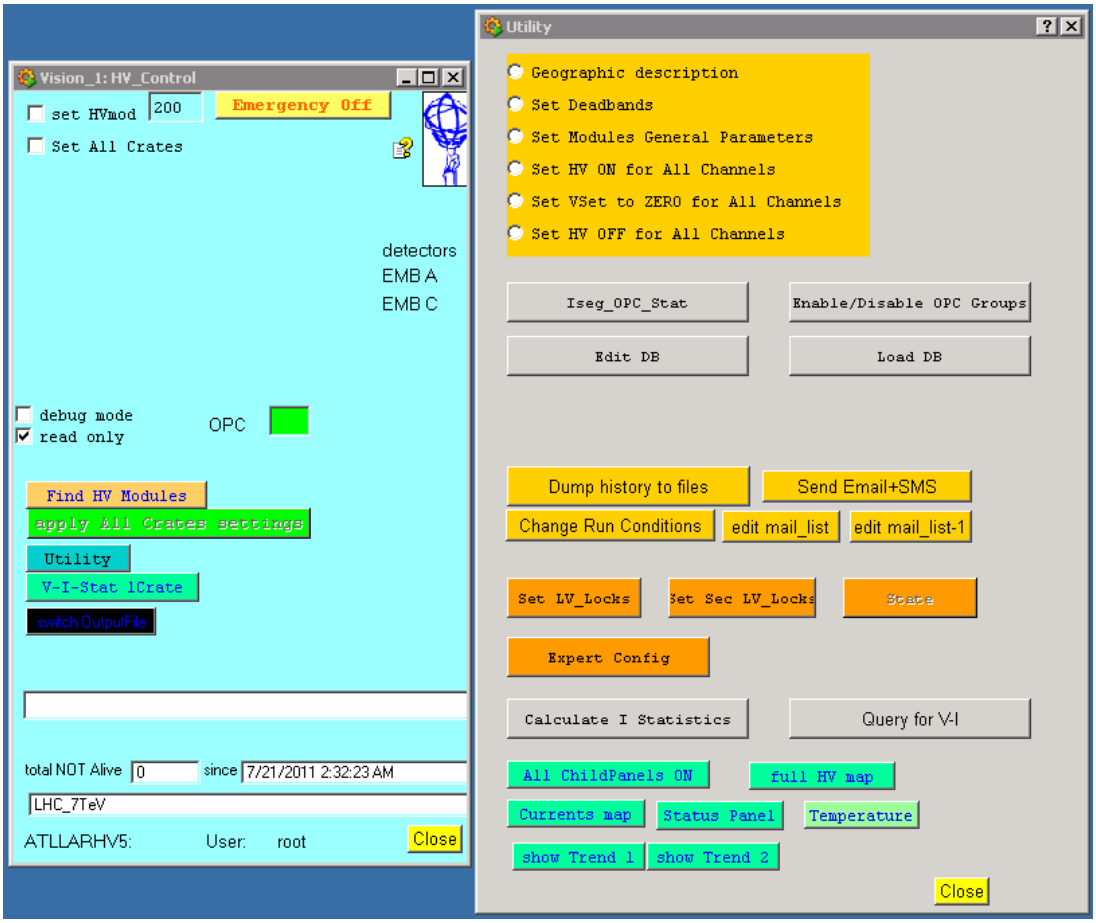

Figure 3.17: Main HV control software panels.

Additionally, visualisations of all the power supplies and each of their channels is available. This provides the ability to control a single line as illustrated on Figure 3.18,

with features such as:

- switching On/Off an HV line
- setting the operative voltage and software current limit
- setting the voltage ramp speed
- reading out the module/channel information, e.g. measured voltage, current, status, temperature
- displaying module/channel general information, e.g. serial number, geometrical location

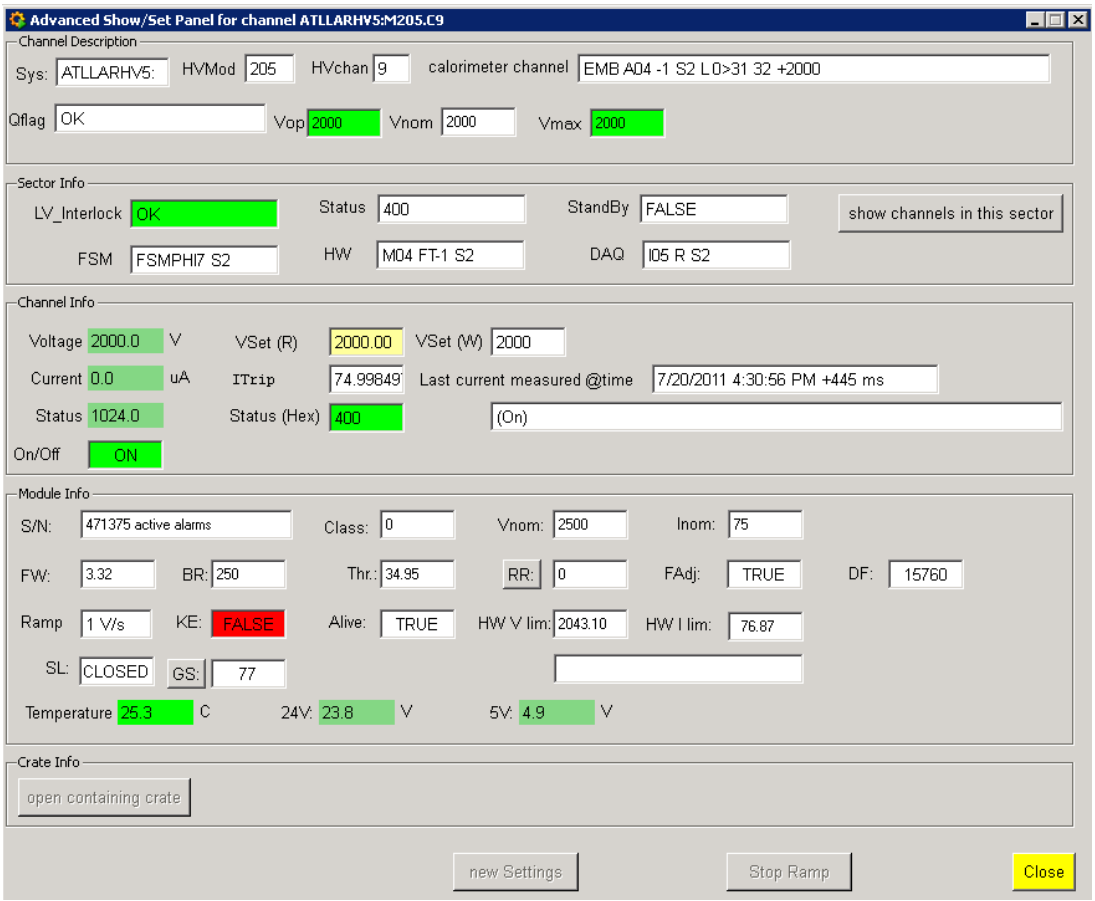

Figure 3.18: Single HV line control panel.

Some of the data being read out is needed offline for reasons such as calorimeter energy correction due to voltage variations, luminosity measurement using the HV line

currents, data quality assessments that requires knowledge of each HV line's status, to general long-term analyses of temperature trends or calibration drifts. The permanent storage is performed within the PVSS environment to centralised databases common to all the ATLAS detectors. The storage and handling of the HV information is discussed in the following section.

3.5.2 Archiving and visualization of the high-voltage system data

The high-voltage dataflow is illustrated on Figure 3.19.

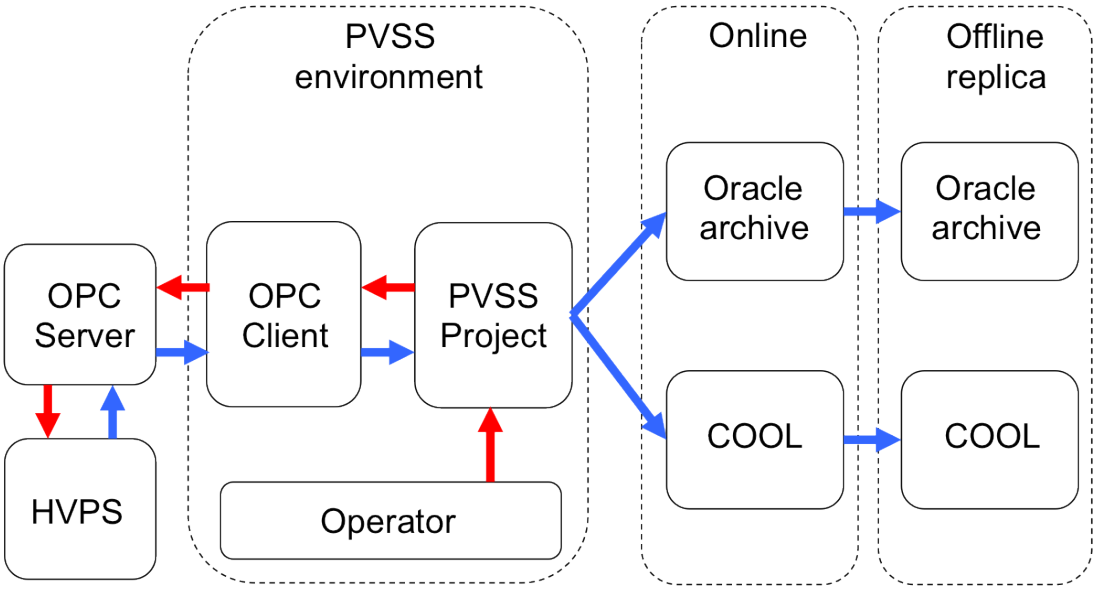

Figure 3.19: Dataflow of the high-voltage system. Shown are the path of the data readout and storage (blue) and the commands (red).

The PVSS instances running on each high-voltage machine have, in addition to their control and monitoring capabilities, a module that archives a set of selected datapoint values to an Oracle database inside the ATLAS technical network. Any standard data type can be archived, such as floats (e.g. voltages, temperatures) or booleans (e.g. status). Due to the large amount of data requiring archiving, smoothing can be applied to reduce the throughput. The online database contents are subsequently replicated to an offline database outside the technical network, and made available to the ATLAS collaboration. This precaution is taken in order to protect the online database integrity, as it sits in the

firewall-protected technical network.

DCS data needed for by the ATLAS reconstruction software can in parallel by stored in the COOL configuration database. In particular, the calorimeter reconstruction software includes a instance that corrects the energy of cells fed by high-voltage lines that are not at nominal voltage, as described previously. This requires the voltage of every single line to be continuously stored in COOL.

The following section will describe some of the aspects of the operation of the high-voltage system.

3.6 Operation of the high-voltage system

Standard operation of the high-voltage system include switching all or part of the power supplies On/Off, which, as mentioned previously, is achieved by bulk loading prepared settings from a database. Modifications of the operational parameters, such as operative voltages, current limits, deadbands, ramp speed, and archiving settings, are also part of the daily activity, following discussions with the liquid argon operation community. In an effort to maintain a consistent operation of the calorimeter, interventions on the high-voltage system are kept to a minimum during data-taking periods, except during system malfunctions when experts need to act on either the hardware of the software. All the interventions are thoroughly documented in the ATLAS electronic logbook system.

During technical stops or shutdown periods, deeper interventions on the system can be performed. Typically, the entire high-voltage system is switched off, and maintenance can be done on the hardware and software. Maintenance includes replacement of faulty power supply units in case of hardware failures (one or more faulty HV lines) or firmware malfunctions. The replacement of a power supply unit can also be performed with the rest of the system On, with a "hot swap" procedure: the faulty PS is switched off, the software infrastructure halted, and the PS unit can be exchanged.

3.6.1 High-voltage trips

During physics data-taking, the high-voltage system is principally prone to one type of problem: high-voltage trips. Trips occur when a calorimeter liquid argon gap temporarily asks for more current – in order to keep the voltage constant – than the power supply is able to feed. Trips cause the affected HV line to switch off and ramp down to 0 V. As the power supply tries to inject current into the calorimeter, it crosses either the software or hardware (usually higher) current limit, and trips as a safety measure. Additionally, as observed during the 2010 and 2011 data-taking periods, the trip occurrence seems to be influenced by magnetic field activity (when the magnets are ramped up or down) but is dominated by the increase of instantaneous luminosity. Naturally, when the luminosity increases, the particle flux traversing the calorimeter gains in intensity, which increases the strain on the power supplies to keep the liquid argon gap electric fields constant. Before the 2010 winter shutdown, high-voltage on-call experts, of which I was part of, had to manually ramp up tripped HV lines as soon as possible, which happened more often as the instantaneous luminosity increased. It was therefore decided to implement a feature in the power supplies that would automatically ramp up the high-voltage after a trip. This feature is in place since spring 2011 and eased the load on the HV experts, but, more importantly, reduced the amount of collected data that had to be deemed unusable for physics analyses by decreasing the duration of voltage variations.

3.6.2 Miscellaneous HV issues

Over the four years that I have worked on the high-voltage system, we encountered many issues disturbing normal operation: the "hospitalisation" of HV lines feeding detector regions containing shorts, the infamous "channel 14" issue which turned out to be a construction defect, and issues with the communication with the hardware via the CAN lines and the OPC server.

3.6.2.1 Hospital lines

As mentioned previously, liquid argon gaps are susceptible to shorts, which are believed to be impurities in the argon. When a short occurs, the high-voltage power supply, trying to maintain the voltage around the set value, injects a DC current. However this current can exceed the maximum current output of the standard power supplies, e.g. 1 mA in the EMB compared to the 75 μA allowed. This prevents feeding an entire high-voltage sector (32 gaps in the EMB), including the other liquid argon gaps with no short. The solution to this issue has been to bypass the affected HV lines so that their corresponding HV region can be fed by a special type of power supply, custom made for this purpose, up to currents of 3 mA. The cabling in the HV racks had to be entirely redesigned to accommodate this feature. In the barrel, the 16 cables from each side, instead of going directly to the feedthrough, are redirected to custom-made panels in the back of the racks, as illustrated on Figures 3.20 and 3.21. From there 16 cables make their way normally to the detector. On each panel, a 32 pin connector from a 3 mA power supply comes in and its cable is stripped of its housing to enable picking single lines. Each hospital "patient" is then pulled out of its original connector and replaced with one of the hospital lines. From this point on, the affected detector region is fed by the 3 mA power supply instead of the standard one. However, in most cases, even though a higher current output is allowed, operating at nominal voltage is impossible due to the limit on power dissipation at the level of the filer box resistor. Therefore the majority of hospital lines are operated at reduced voltages. In the endcap C, the EMEC and a fourth of the HEC are connected to the C backplane. In the endcap A, only the EMEC is connected. This is mainly due to historical reasons related to the lack of HEC hospital candidates.

The number of hospital lines as of July 2011 are listed in Table 3.3.

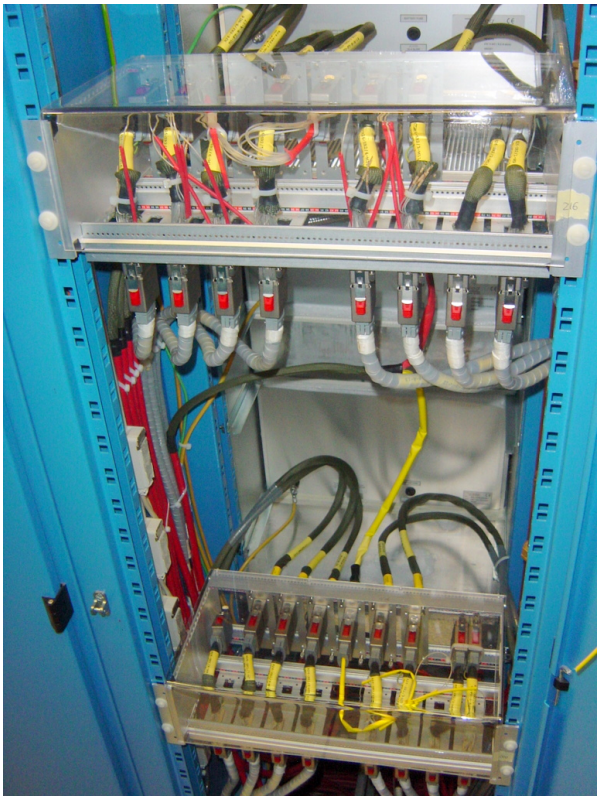

Figure 3.20: EMBA hospital

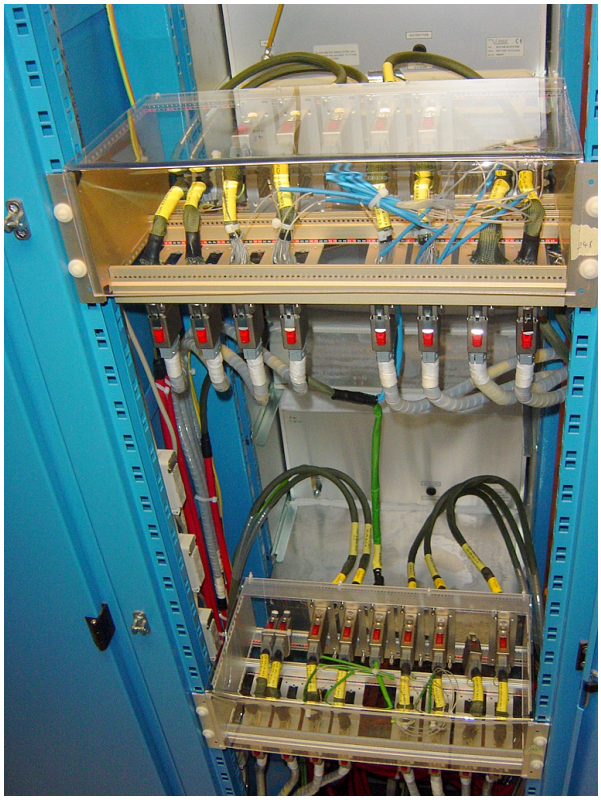

Figure 3.21: EMBC hospital

Detector	A-side	C-side
EMEC	18	16
EMB	16	16
HEC	N/A	7

Table 3.3: Number of hospitalised high-voltage lines as of 12/07/2011.

3.6.2.2 Channel 14

During my work on the monitoring of the power supplies readout, I came across a feature exhibited by a specific module type. Even though they performed normally in terms of voltage regulation, the 2kV/75μA units populating the EMB and EMBPS showed excessive noise ($\sim 1\mu A$ compared to the "normal" $\sim 100nA$) in their current readout, systematically on one channel out of the 16 per board. Always channel 14, in most modules. In order to disentangle a possible detector effect, measurements were performed before and after swapping HV cables feeding completely different parts of the detector. The results confirmed that the source of the noise was in the power supplies and after providing the constructor with a report, they found a design flaw on their boards. The affected power supplies were consequently shipped off by small batches, replacing them with healthy ones. The refurbished units were received and tested in our test setup and confirmed to have been fixed. Even though this event did not jeopardise the operation of the system, it allowed us to gain experience in the understanding of the power supplies, and helped the constructor in their own developments.

3.6.2.3 CAN-bus communication

Each high-voltage control machine continuously communicates with a few dozen power supply units, with the exception of the crate control machine which handles all of the 21 crates. This implies having a stable and reliable communication throughput. In the past few years we have encountered, on many occasions, cases where commands were not properly sent to the hardware, or data not correctly readout. After investigating the CAN lines connections with and communication, a few CAN buses were found to be faulty, thus impeding on the overall performance of the control. Replacing them, and carefully verifying the quality of the transmitted signals, allowed us to improve the readout and control performance.

3.6.2.4 OPC server

Along with fixing the hardware communication issues, a lot of developments have occurred on the OPC server[5] side. The OPC server, as mentioned previously, acts as a bridge between our PVSS control software and the high-voltage system. During operation, many issues with crashes, lost commands, hangs, were experienced with the OPC server. A continuous effort to document and transmit reports to the constructor have led to many improvements in the code behind the OPC server. Since the beginning of 2011, we have reached a state with very few OPC communications issues, especially because of the implementation of a cache mechanism that optimises the way commands are sent to the hardware and how parameters are read-out.

3.7 DCS and data quality

In order to ensure the usability of the data recorded by the ATLAS experiment for physics analyses, constant monitoring of the detector systems is required. The Detector Control System data quality (DCSDQ) assessment [54] is the lowest level of the data validation process and therefore provides early information about detector-related issues which can be acted upon by either offline correction or data samples rejection.

The liquid argon calorimeter data quality strategy aims at identifying and classifying detector problems and their possible solutions, with a duty to provide ATLAS with the status of the data recorded by the calorimeter. Concerning the LAr DCS data quality, the sole source of issues stems from high-voltage trips, mentioned in the previous section. Indeed, during HV trips the voltage applied varies, affecting the gap electric fields hence the measured energy. Because the recorded data is cut into 1 min slices (luminosity blocks) and the computing resources only allow one set of calibration parameters (including high-voltage corrections) per luminosity block, if the voltage across the liquid argon gaps varies during a luminosity block because of a trip, the measured energy can-

[5] http://www.iseg-hv.de

not be corrected properly. Therefore the data recorded by the calorimeter in the affected subdetector needs to be flagged "unusable" for physics analyses. Offline data quality teams appointed by the LAr DQ group are in charge the daily reporting, investigation, and flagging of the data affected by trips, with the help of a series of dedicated software tools. Finally, the autorecovery feature described in the previous section helps in diminishing the duration of high-voltage trips, and ongoing studies are investigating the effect of a slow voltage variation (ramp-up) during a luminosity block on the reconstructed energy, which if demonstrated negligible, would decrease the amount of unusable data.

3.8 Conclusion

This chapter described the liquid argon calorimeter high-voltage system hardware layout and characteristics, its control software and operation, as well as its influence of the data recorded by the calorimeters. Even though the high-voltage system is primarily designed as support system to the calorimeters, it can also be used to perform a luminosity measurement. Indeed, as mentioned before, the current induced in the liquid argon gaps by ionising particles is compensated by the high-voltage power supplies in order to keep the voltage constant. This current is found to be directly proportional to the number of electron-ion pair produced during the ionisation process, hence to the instantaneous luminosity at the ATLAS interaction point.

The next chapter will describe how a relative luminosity measurement can be performed by measuring and calibrating the high-voltage power supply currents of the forward calorimeters.

Chapter 4

Luminosity determination with the ATLAS forward calorimeters

4.1 Introduction

During proton-proton collisions at the LHC, a large flux of minimum bias particles traverses the detector forward regions. Minimum bias events stem from soft *pp* interactions and consist of mostly $\pi^0/\pi^\pm$ mesons with low transverse momentum. Most of their energy is deposited in the electromagnetic forward calorimeter as electromagnetic showers of photon pairs from π^0 decays. The induced particle flux intensity is directly proportional to the interaction rate, so to the luminosity. The current injected by the FCal-1 high-voltage system to compensate for ionisation losses from minimum bias events is correlated to the flux, and therefore gives a direct handle on the luminosity [55].

This approach has two advantages. The response is linear with the luminosity and it is independent from the ATLAS trigger and data acquisition (DAQ) system hence does not suffer from event selection biases and DAQ downtime. However, as the currents measurement from the power supplies is part of a slow control environment, it prevents the possibility of distinguishing individual LHC bunch crossings. Finally, this method is

not capable of rejecting beam background, e.g. by performing A/C coincidences.

The following will describe the linearity assessment in test beam in Section 4.2, before detailing results obtained from simulations in Section 4.3. Section 4.4 will detail the different luminosity handles and their absolute calibration. Finally Sections 4.5, 4.6, 4.7 will discuss how the FCal high-voltage lines have been monitored, selected and calibrated in order to perform a luminosity determination in 2010 and 2011.

4.2 Linearity assessment in test beam

The linearity has been demonstrated during test beams for the high luminosity LHC R&D phase in Protvino. Using a 50 GeVproton beam and a prototype of the FCal, the non-linear fraction of the response was shown to be 0.36% up to 10^{34} cm^2s^{-1}, the LHC design instantaneous luminosity [56].

4.2.1 Protvino test beam setup

The goal of the HiLum project is to assess the performance of the liquid argon calorimeters under the high particle rate expected at the sLHC luminosity of 10^{35} $cm^{-2}s^{-1}$. This has been performed at the 60 GeV proton beam at the Institute for High Energy Physics (IHEP) in Protvino, Russia, using FCal, EM, and HEC prototypes. The experimental setup is depicted on Figure 4.1. In addition the calorimeter prototypes and their iron absorbers, the test beam line is equipped with instruments to measure the beam position (secondary emission chamber), beam profile (hodoscope), and beam intensity (ionisation chamber and six scintillation counters for cross-checks).

One of the three prototypes is a miniature version of the electromagnetic section of the ATLAS forward calorimeter. It consists of an copper matrix containing 16 electrodes with a 250 μm (similar to the ATLAS FCal) liquid argon gap adjacent to 16 electrodes with a 100 μm gap, one of the foreseen configurations for a cold FCal at HL-LHC. The electrodes

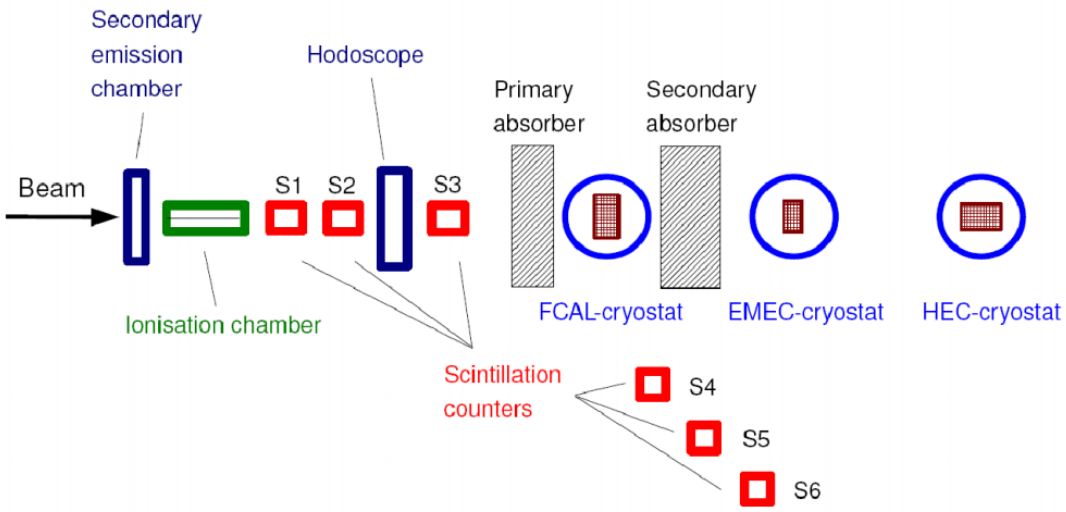

Figure 4.1: Test beam setup of the high luminosity project in Protvino.

are grouped by four, each group having its own readout and high-voltage wires. Similarly to the ATLAS LAr production system, the high-voltage power supply used during this test beam is manufactured by Iseg, with 250 V operative voltage and a maximum allowed current of 10 mA. The study of the current response of the FCal prototype high-voltage lines was performed by illuminating either group of 16 electrodes and simultaneously measuring the beam intensity and HV currents.

4.2.2 Estimation of the non-linearity

The proton beam is structured as 116 ns long bunches separated by 990 ns, and is extracted onto the targets as 1.2 s "spills". Therefore, each spill contains approximately 10^6 proton bunches. By varying the bunch intensities (number of protons per bunch), the total number of protons per spill can span the range between 10^7 to 10^{11} p/spill. In order to construct an analogy to the LHC luminosity, let us consider the inelastic collision rate $N_{inel} = \mathcal{L}\sigma_{inel}$, where σ_{inel} is the p-p inelastic cross-section (71.5 mb, [57]). Now to find the LHC luminosity equivalent to a certain number N_{pps} of protons per spill at the test

beam, one can rewrite N_{inel} as follows:

$$N_{inel} = \frac{N_{pps}}{\tau_{spill}}$$

where τ_{spill} is the spill duration, 1.2 s. This effectively gives the particle rates in both cases. Now, the LHC equivalent luminosity can be written:

$$\mathcal{L} = \frac{N_{inel}}{\sigma_{inel}} = \frac{N_{pps}}{\tau_{spill} \cdot \sigma_{inel}}$$

Therefore, as shown in Table 4.1, the LHC equivalent luminosities can be expressed for all the beam intensities measured in Protvino and can be used to extrapolate the analysis results to ATLAS.

Protons per spill	10^7	10^8	10^9	10^{10}	10^{11}
LHC equivalent luminosity $[cm^{-2}\ s^{-1}]$	10^{32}	10^{33}	10^{34}	10^{35}	10^{36}

Table 4.1: Test beam intensities and their LHC equivalent luminosity.

For each spill, the high-voltage power supply currents were measured every 100 ms and all the measurements integrated over the spill duration, providing one measurement per spill per HV line. To measure currents at this speed, a 24-bit ADC was specifically designed by the HiLum group. The internal power supply ADC only allows a maximum measurement rate of 0.2 Hz. Every HV measurement was matched with a beam current measurement using the ionisation chamber and consequently compared. By fitting the beam intensities versus HV integrated currents per spill with a second degree polynomial, one can then estimate the non-linearity of the response. The data collected as well as the fit are illustrated on Figure 4.2. Assuming an uncertainty on the beam intensity measurement by the ionisation chamber of 1.2%, a non-linear fraction of 0.36% was measured for 10^9 protons/spill, equivalent to an LHC luminosity of 10^{34} $cm^{-2}s^{-1}$.

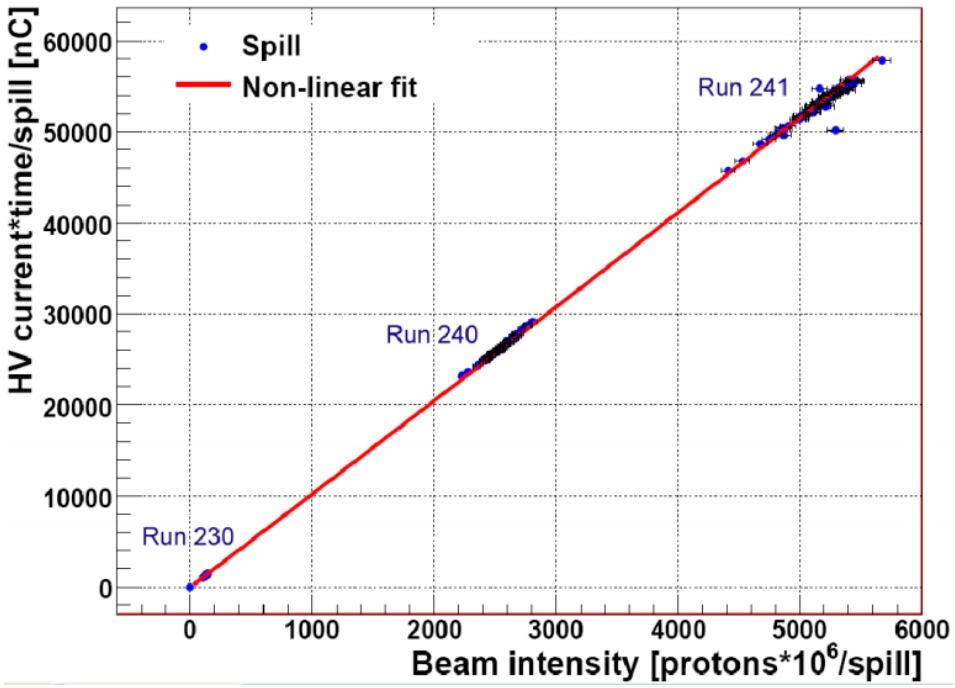

Figure 4.2: Measured HV current summed over three FCal prototype channels versus beam intensity compared to a non-linear fit [56].

4.3 Simulation

This section describes a study performed in order to have an idea of the currents expected in the forward calorimeter in the presence of p-p collisions. A study of the minimum bias energy deposition in the FCal with data can be used to run a simulation of the electronic chain separating the FCal and its high-voltage power supplies, thus providing a rough estimate of the DC currents expected as well as the minimum instantaneous luminosity required to measure them.

4.3.1 Collision data

Prior to running the simulation, one must first determine the average amount of energy deposited in the forward calorimeter by minimum bias events and particularly the amount of energy as seen by a single high-voltage line. In the FCal-1, each of the sixteen ϕ-sectors is fed by four separate HV lines, each either feeding a fourth of a summed channel

(four electrode groups) or a single unsummed channel (a single electrode group). Hence, depending of the case, the energy "seen" by an HV line will either be the energy measured in on unsummed channel or a fourth of the energy of a summed channel. Therefore it is important to look at the average energy deposited in each FCal-1 cell in order to estimate the energy seen by a single HV line.

Figure 4.3 illustrate the average energy deposited in each FCal-1 cell during a *p-p* run at 7 TeV. The energy is plotted versus the (i_η, i_ϕ) indices of the calorimeter readout channels. There are 1008 readout channels per side, so a 16×64 map is enough to identify them all. The data is from the minimum bias stream and the run (166786[1]) was recorded in October 2010. During this run, with 233 colliding bunches at IP1, the average number of inelastic interactions per bunch crossing μ was 2.7 for a peak instantaneous luminosity of approximately 10^{32} $cm^{-2}s^{-1}$.

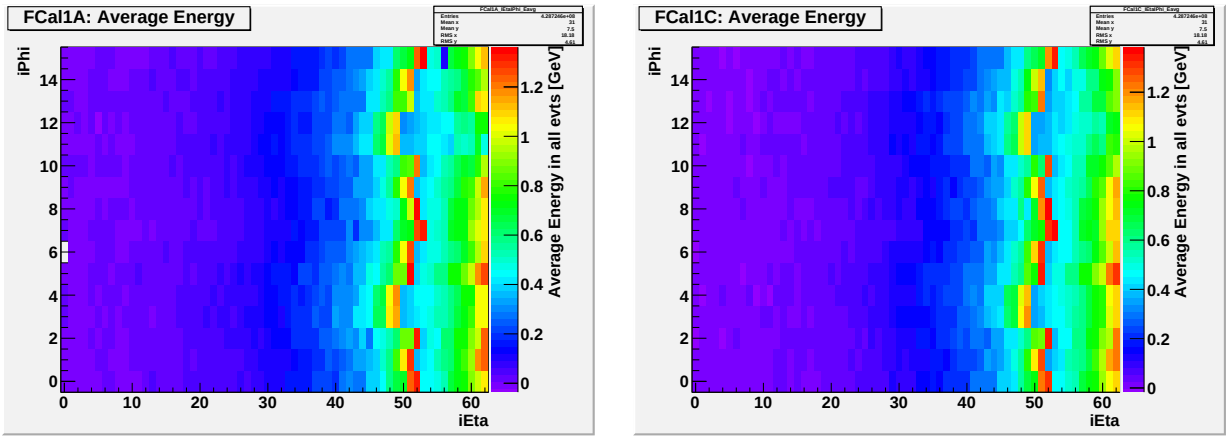

Figure 4.3: Average energy deposited in the FCal1 A (left) and C (right) by minimum bias events versus the (i_η, i_ϕ) indices of the readout channels.

The induced current in an FCal cell can be derived from the measured energy using the $\mu A2MeV$[2] conversion factor, which has been determined during test beam, as follows:

$$\langle I_{cell} \rangle = \frac{\langle E_{cell} \rangle}{\mu A2MeV} \times 2$$

where the factor 2 represents the contribution from the ions drift.

[1] http://atlas-runquery.cern.ch/query.py?q=find+run+166786+%2F+show+lhc
[2] $\mu A2MeV = 669\ MeV/\mu A$ in the FCal-1

Finally, by matching each of the FCal-1 high-voltage lines to their respective readout channels and adding up the induced currents contributions, the current seen by a single HV line is expressed as follows:

$$I_{HV} = \sum \frac{\langle I_{cell} \rangle_{summed}}{4} + \sum \langle I_{cell} \rangle_{unsummed}$$

Averaging across the 128 FCal-1 high-voltage lines leads to $\langle I_{HV} \rangle = 12.4 \pm 1.7\ \mu A$. This value is used as an input to the simulation described in the next section.

4.3.2 PSpice simulation

The idea behind this simulation is to demonstrate the rise of the DC current induced by minimum bias interactions in the calorimeter. For this study, the PSpice[3] software was used to model the electronic chain between an FCal-1 high-voltage line and the electrodes it feeds.

As depicted on Figure 4.4, the model consists of four parts. The high-voltage line is modelled by an ideal voltage source set at 250 V. Then the HV lines connect to its filter box, consisting of an RC filter (10 kΩ, 200 nF) and a blocking resistor (1 kΩ), which purpose is to limit the noise induced in the cryostat by the HV system. The next section consists of 48 FCal cells arranged in parallel. One FCal cell can be modelled by a 1.5 nF capacitive load with its own protection resistor. Most FCal cells have a 1 MΩ protection resistor, however the innermost (closest to the beam pipe) cells have 2 MΩ resistor in order to cope with the higher particle flux by limiting the voltage drop. Putting those cells in parallel leads $R_{//} = 21$ kΩ and $C_{//} = 72$ nF. The final part, on the right-hand side of Figure 4.4, consists of a pulsed current source which purpose is to emulate the current induced by energy deposition in the calorimeter. It is modelled by a triangular signal (Figure 4.5) whose amplitude is proportional to the amount of current induced by one minimum bias event. The pulse rate relates to how often such events occur.

[3] http://www.electronics-lab.com/downloads/schematic/013/

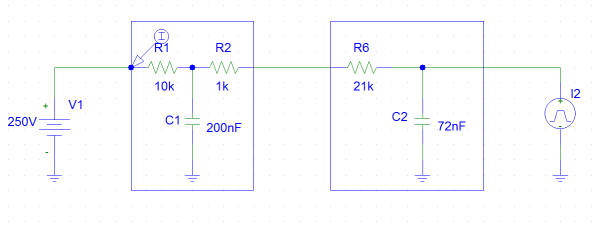

Figure 4.4: Spice model schematic of an FCal high-voltage line (left) connected to an HV sector (middle right). Also shown are the HV filter box (middle left) and the current pulse generator (right). See text for details.

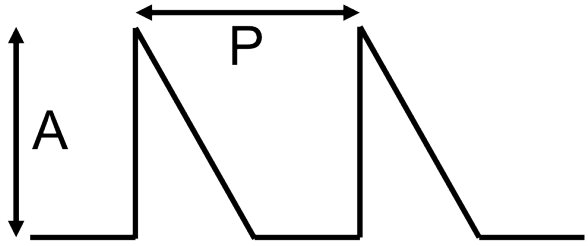

Figure 4.5: Shape of the Spice simulation signal. The amplitude A corresponds to the current induced by one minimum bias event and the period P average duration between two such events.

The simulation was performed during a 30 ms period, where all the values of the circuits are calculated every 5 ms. This proved to be enough to see the rise of the DC current at the level of the power supply. In order to compare the outputs, this simulation was performed using two different parametrisations of the current pulse.

The first uses a fixed amplitude and varying pulse frequency. This is motivated by the fact that the inelastic interaction rate can be expressed as $N = \mathcal{L}\sigma_{inel}$. So, on average, one interaction will occur every 1/N seconds. This of course is not true at high luminosity because of pile-up, however this model is reasonable at low luminosity. In this approach we use the current extracted from data as the amplitude, and run the simulation for four values of the period, corresponding to four luminosity values. The results of the simulation are shown on Figure 4.6 and summarised in Table 4.2. The curves represent the current I_{ch} measured at the power supply level (one high-voltage line) for the four luminosities.

P $[\mu s]$	14000	1400	140	14
$\mathcal{L}_{eq}$ $[cm^{-2}s^{-1}]$	10^{30}	10^{31}	10^{32}	10^{33}
I_{ch} $[\mu A]$	0.024	0.235	2.35	10.9

Table 4.2: Parameters and results of fixed amplitude simulation. The pulse amplitude A is fixed at 12.4 μA. The period P between each pulse is related to the luminosity by the relation $P = 1/(\mathcal{L}\sigma_{inel})$. The DC current expected is for a single FCal-1 high-voltage line. ATLAS uses the Pythia value of 71.5 mb for σ_{inel}.

The second simulation is based on a more realistic approach, using pile-up to parametrise the pulse amplitude. Therefore, as the average number of inelastic interactions per bunch crossing increases, the pulse amplitude can be weighted by the μ-value. In this case the

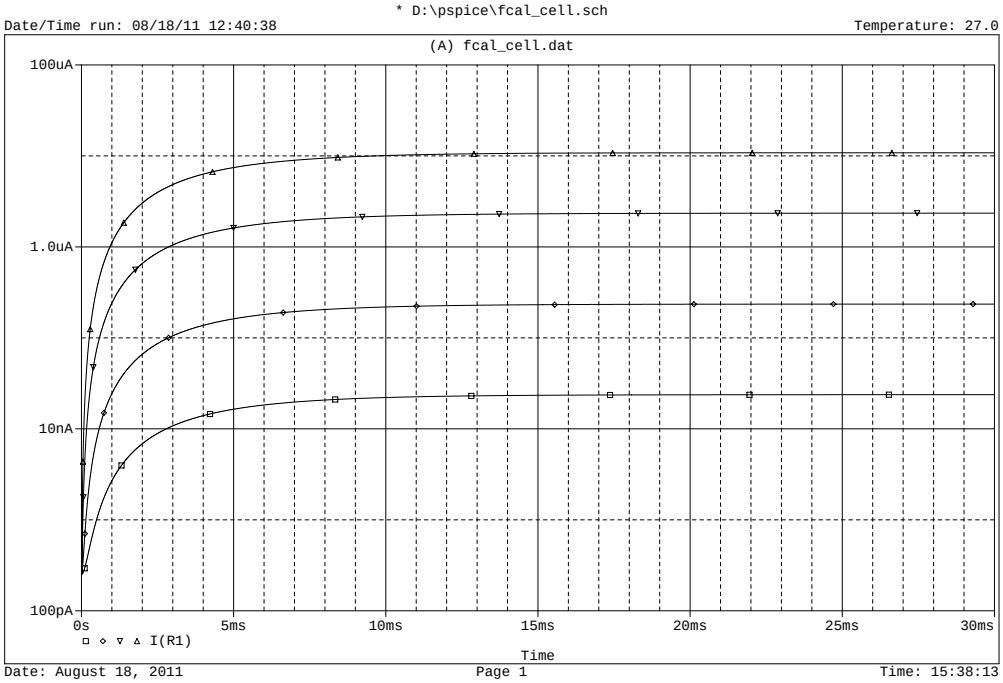

Figure 4.6: Current response at the power supply level for a single FCal-1 high-voltage line in simulation with fixed pulse amplitude. The four curves correspond to the four simulations with different P-values. See text for details.

duration between two consecutive pulses is kept constant at 50 ns. The average current induced by one minimum bias event in the FCal-1 is determined in the previous section and amounts to approximately 12.4 μA for a fill with an average μ was about 2.7. The parametrisation of the simulation has been chosen to scan four μ values: 0.01, 0.1, 1, and 10. Therefore, in order to obtain the base current value at, let us say, $\mu = 1$, one must rescale the value of the current, which brings it to 4.6 μA. Finally, the amplitude of the pulse can be set to be $A = 4.6 \times \mu$ for each case. The current responses are depicted on Figure 4.7 and summarised in Table 4.3.

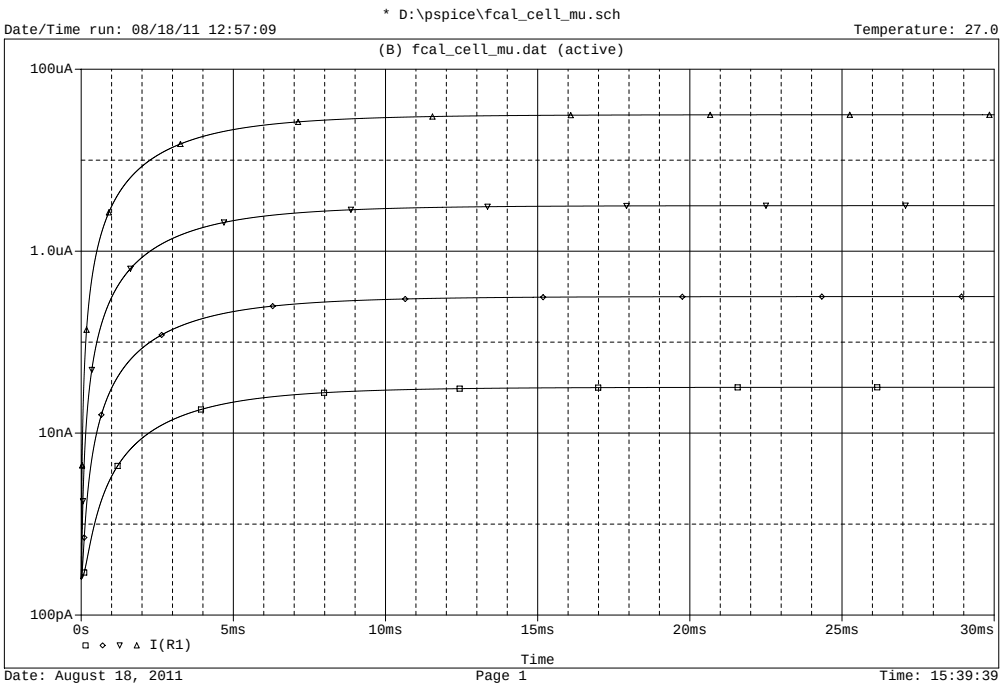

Figure 4.7: Current response at the power supply level for a single FCal-1 high-voltage line in the simulation with μ-dependent pulse amplitude. The four curves correspond to the four simulations with different A-values. See text for details.

A [μA]	0.046	0.46	4.6	46
μ_{eq}	0.01	0.1	1	10
I_{ch} [μA]	0.032	0.316	3.16	31.6

Table 4.3: Parameters and results of fixed period simulation. The period P between each pulse is fixed at 50 ns. The amplitude A corresponds to an average current induced at $\mu = 1$ weighted by μ_{eq}. The DC current expected is for a single FCal-1 high-voltage line.

The results of both simulations are compatible in terms of the order of magnitude of the expected DC currents. They are to be compared with the currents actually measured during data-taking. In the first simulation, the currents measured at a instantaneous luminosity of 10^{32} $cm^{-2}s^{-1}$ range from 1.2 to 1.7 μA, depending on the high-voltage line. The simulation predicts a current of 2.35 μA. In the second simulation, if we look at a fill with a peak μ value of 10, the currents observed in the FCal-1 HV lines range from 25 to 35 μA, whereas the simulation predicts a DC current of 31.6 μA.

To summarise, this proof of concept, which purpose is to demonstrate the birth of a DC current due to minimum bias interactions, rather successfully illustrates the behaviour of the modelled system. DC currents compatible with measurements are predicted over the range of operation of the LHC in 2011. Finally, is also illustrates the lower limit on the instantaneous luminosity required to observe a signal in the FCal-1 high-voltage lines, which is approximately 10^{31} $cm^{-2}s^{-1}$.

4.4 Luminosity calibration

This section describes the absolute calibration of the two ATLAS major luminosity detectors, LUCID and BCM. During the 2010 [33] and 2011 [58] data-taking periods, the ATLAS luminosity algorithms were calibrated using dedicated *van der Meer* [34] (or *beam separation*) scans. It is those calibrated quantities that are used to calibrate the forward calorimeter high-voltage currents.

4.4.1 Luminosity algorithms

Of all of the 3564 LHC slots available for protons bunches, only 2808 can be filled due to the injection and dump gaps. Each of these slots is assigned in Bunch Crossing IDentifier (BCID) synchronised with the ATLAS data acquisition system. By matching their rate measurements with the BCID, the LUCID and BCM detectors are able to provide a bunch-

by-bunch luminosity determination. This quantity depends on whether or not the BCIDs are colliding in ATLAS, and estimating the contribution of non-colliding BCIDs can provide essential information on backgrounds to the luminosity measurements. The LUCID and BCM readouts are configured with online algorithms that provide the Online Luminosity Calculator (OLC) with raw counts based on logical operations (such as a coincidence on the two sides of the detector) of registered events, an event being defined as a signal passing a preset detector threshold. From there the OLC applies the relevant calibrations to the raw counts, provides luminosities to online displays, and allows for their archiving in the COOL conditions database for offline analysis.

The different LUCID and BCM algorithms used throughout the document are briefly described in Table 4.4.

Algorithm name	Description
LUCID Event_OR	A/C inclusive OR
LUCID Event_AND	A/C coincidence
LUCID Event_A	A exclusive OR
LUCID Event_C	C exclusive OR
BCM Event_OR	A/C inclusive OR , horizontal sensors
BCM Event_AND	A/C coincidence , horizontal sensors
BCM Event_OR_V	A/C inclusive OR , vertical sensors
BCM Event_AND_V	A/C coincidence , vertical sensors

Table 4.4: LUCID and BCM algorithms descriptions. With the x-axis of the ATLAS coordinate system pointing towards the inside of the LHC ring, the C-side corresponds to positive z and the A- side to negative z.

4.4.2 van der Meer calibration

The principle of a van der Meer scan, described in length in [59, 33], is to measure simultaneously the luminosity, beam currents, and collision rates during a procedure where one beam moves with respect to the other in the transverse plane.

The luminosity can be written:

$$\mathcal{L} = \frac{\mu n_b f_r}{\sigma_{inel}}$$

where μ is the number of inelastic collisions per bunch crossing, n_b the number of colliding

bunches at IP1, f_r the machine revolution frequency of 11245.5 Hz, and σ_{inel} the inleastic proton-proton cross-section. The problem with this formulation is that μ is not a directly measurable quantity and σ_{inel} has yet to be measured for 7 TeV p-p collisions[4]. However, their ratio can be expressed as follows:

$$\frac{\mu}{\sigma_{inel}} = \frac{\mu_{vis}}{\varepsilon\sigma_{inel}} = \frac{\mu_{vis}}{\sigma_{vis}}$$

where μ_{vis} is the *observed* number of collisions per bunch crossing (i.e. measurable) and $\sigma_{vis} = \varepsilon\sigma_{inel}$ the visible cross-section, which depends on the detector efficiency, acceptance and algorithm used. Therefore, the luminosity can be rewritten:

$$\mathcal{L} = \frac{\mu_{vis} n_b f_r}{\sigma_{vis}}$$

On another hand, using machine parameters such as the transverse beam profiles Σ_x and Σ_y as well as the single bunch currents in each beam n_1 and n_2, the luminosity can also be expressed as follows:

$$\mathcal{L} = \frac{n_b n_1 n_2}{2\pi\Sigma_x\Sigma_y}$$

During the vdM scan, one beam is moved step-wise with respect to the other by a known distance given by the magnet settings, called nominal beam separation, thus allowing for the measurement of Σ_x and Σ_y by fitting the rates, as shown for example on Figure 4.8 during a scan taken in May 2011. The peak rate μ_{vis}^{MAX} can then be compared to the measured luminosity and the visible cross-section extracted as follows:

$$\mu_{vis}^{MAX} = \frac{\mathcal{L}_{MAX}\sigma_{vis}}{n_b f_r} = \frac{n_1 n_2 \sigma_{vis}}{2\pi\Sigma_x\Sigma_y} \quad \Longrightarrow \quad \sigma_{vis} = \mu_{vis}^{MAX}\frac{2\pi\Sigma_x\Sigma_y}{n_1 n_2}$$

In parallel, the numbers of protons per bunch ($n_1 n_2$) are measured by LHC instruments somewhat similar to the return current coils described in the previous chapter and described in detail in [60]. The uncertainty on these bunch currents measurements dom-

[4] ATLAS uses the Pythia value of 71.5 mb

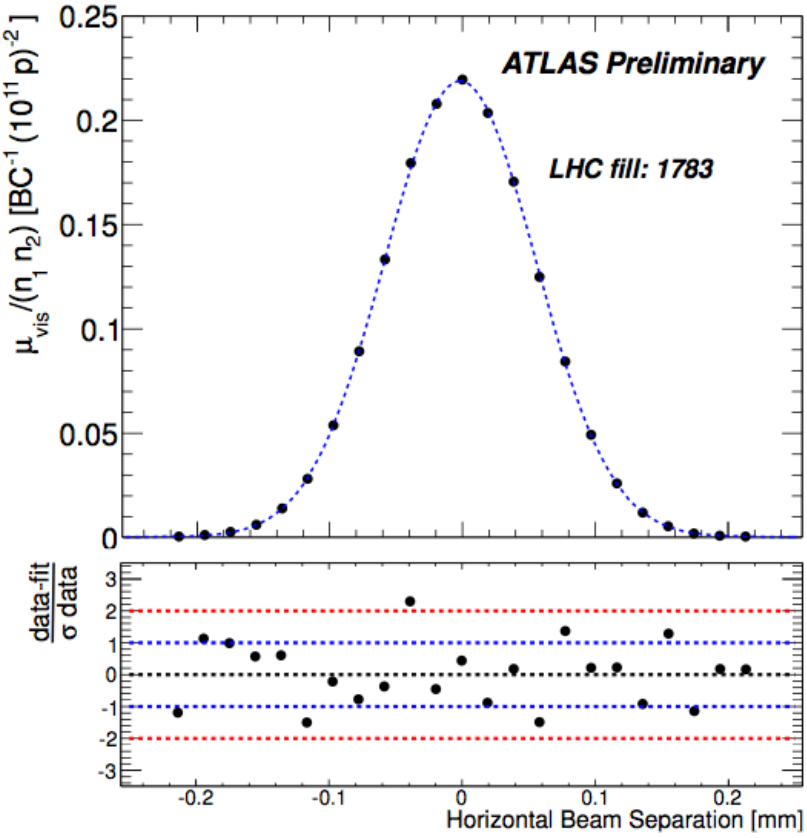

Figure 4.8: Specific interaction rate versus nominal beam separation for the BCM Event_OR algorithm during the May 2011 vdM scan. The residual deviation of the data from the Gaussian plus constant background fit assuming statistical errors only is shown in the bottom panel [58].

inates the total systematic uncertainty on the determination of the visible cross-section, and tremendous efforts from the Beam Current Normalisation Working Group (BCNWG) has helped improve and continues improving this issue.

Now that the visible cross-sections have been determined for each detector algorithm, the remaining calculations involve converting observed event rates during normal physics data-taking into visible numbers of interactions per bunch crossing, and finally into instantaneous luminosities.

In the case of EventOR inclusive algorithms, the probability of detecting such an event, assuming that the probability of detecting none follows a Poisson distribution, can be expressed as follows:

$$P_{EventOR} = \frac{N_{OR}}{N_{BC}} = 1 - \exp\left(-\mu\varepsilon^{OR}\right) = 1 - \exp\left(-\mu_{vis}^{OR}\right)$$

with N_{OR} the number of bunch crossings with an event satisfying the OR conditions amongst the total number of bunch crossing N_{BC}, with an efficiency ε^{OR}.

Therefore, the visible number of interactions per bunch crossing is the following:

$$\mu_{vis}^{OR} = \ln\left(1 - \frac{N_{OR}}{N_{BC}}\right)$$

For the EventAND coincidence algorithms, the probability of observing an event is less trivial and non invertible analytically to express μ_{vis}^{AND} as a function of N_{AND}/N_{BC}. In this case look-up-tables are used in order to find the best value of μ.

Finally, the luminosity is derived from the μ_{vis}^{OR} value and the visible cross-section obtained from the vdM calibration using the well-known relation:

$$\mathcal{L} = \frac{\mu_{vis} n_b f_r}{\sigma_{vis}}$$

Concerning the systematic uncertainty on the luminosity determination using the van

der Meer procedure, it is discussed in length in the references cited in this section. Let us just note that it is dominated by the LHC bunch current measurements and that a total systematic uncertainty of 3.7% has been achieved following vdM scan performed in May 2011 [58]. However some of the contributions to this uncertainty and their implications on the FCal luminosity determination are discussed in the following sections.

This uncertainty will be carried over as the forward calorimeter high-voltage currents are calibrated using vdM-calibrated LUCID and BCM algorithms and will come in addition of other sources of uncertainties.

4.5 FCal high-voltage power supplies currents

Sanity checks have been performed in order to only retain valid high-voltage lines for the luminosity determination by eliminating any biases. These checks are described in the following section.

4.5.1 Shorted tubes

The first issue preventing the use of HV lines is the fact that some of them are connected to tube groups containing one or more shorted tubes. A short occurs when impurities in the liquid argon connect the central rod of the tube to the outer edge of electrode. This effectively closes the circuit and the current fed into this tube by the HV system flows continuously to the ground. Since tubes are fed as a group, the current injected by the HV line includes a DC component if the group contains a shorted tube. This DC current is prone to unpredictable fluctuations due to the very nature of the shorts, hence it is safer to exclude any of these HV lines from the luminosity analysis. In the electromagnetic section of the FCal, a total of 33 HV lines out of 128 feed tube groups containing a shorted tube.

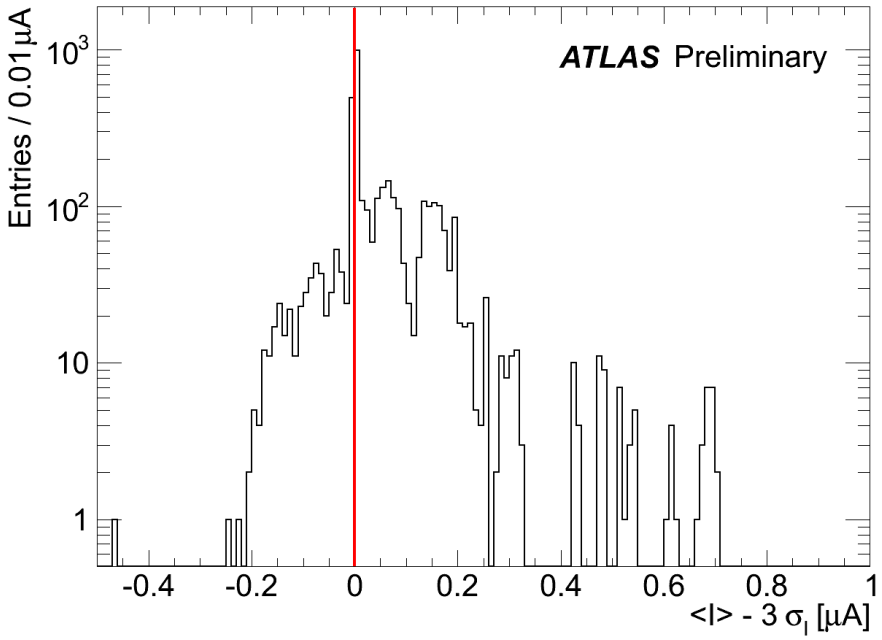

Figure 4.9: Gap $g_{ch} = \langle I_{ch} \rangle - 3 \cdot \sigma_{ch}$ distribution of the 128 EM-FCal high-voltage lines currents during periods with no LHC beam. The vertical line at zero indicates the cut applied on the gap for an HV line to be eligible for the luminosity measurement. Only positive values of g are allowed.

4.5.2 Pedestal measurability

The luminosity measurement is relative and the method is to measure a current varying relative to a pedestal value determined during periods without beam. In many cases, the measurability of the current pedestal is not possible because of ADC calibration drifts of the HV power supply. The power supply has an internal calculation which, from ADC counts, provides only positive calibrated current values. The calibration parameters were put in at the factory during manufacturing and the procedure in described in Appendix E. For some HV lines, this calibration turned out to be slightly shifted so that the pedestal is negative. Therefore an extraction of the pedestal cannot be performed in these cases. To correct for this effect during the 2011 data taking, a new firmware was flashed on the power supplies feeding the EM-FCal shortly after the 2010 winter shutdown. The new firmware artificially offsets all current measurements towards positive values by approximately 2.6 μA (negligible compared to the ADC dynamic range of 0-10 mA), as shown on Figure 4.10. This does not affect the luminosity measurement as the pedestal is subtracted before calibrating the currents, as discussed in section 4.6. A full recalibration

of the power supplies ADC by the constructor is planned at the next shutdown. Since this new feature was not available during the 2010 data taking period, and in order to select HV lines with a measurable pedestal, the quantity $g_{ch} = \langle I_{ch} \rangle - 3 \cdot \sigma_{ch}$ was used as a discriminator, where $\langle I_{ch} \rangle$ is the average current during a period with no LHC beam and σ_{ch} its r.m.s. . If g_{ch} is negative, the current fluctuations around the pedestal are not symmetrical as the tail towards smaller currents is cut away, introducing a bias on the noise estimation. Zero values of g_{ch} indicate cases where only the tail towards larger values of the pedestal fluctuations are readout, hence very small values $\langle I_{ch} \rangle$ and σ_{ch}. Therefore only HV lines with a strictly positive g_{ch} value were selected for the luminosity measurement.

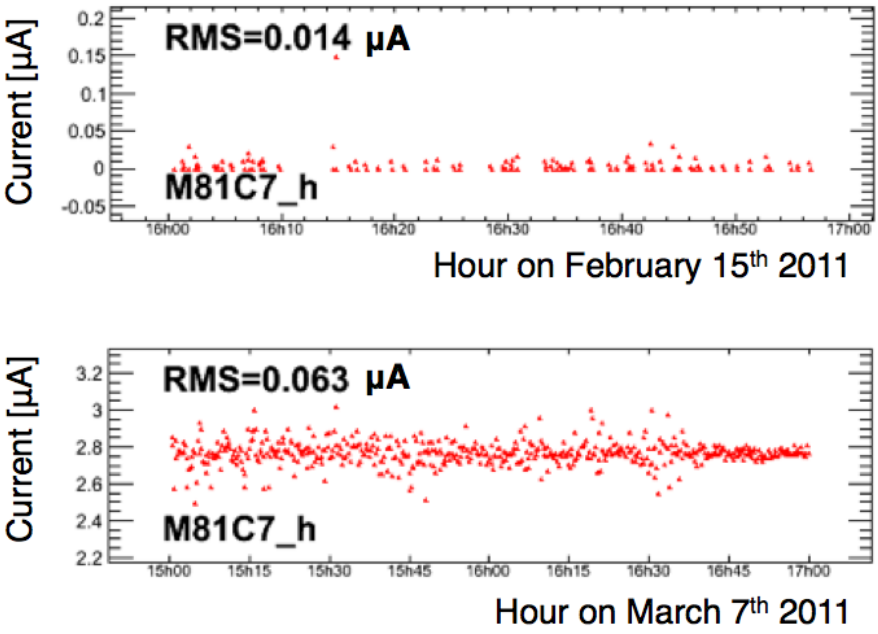

Figure 4.10: One FCal high-voltage line current versus time during periods with no LHC beam presence. Top: Before ADC offset implementation, only the positive tail of the noise fluctuations are read and the pedestal cannot be estimated. Bottom: After new ADC offset, current fluctuates around a positive value and pedestal can be measured.

4.5.3 Pedestal noise

The power supplies are not designed for high precision, low noise current measurements. In order to perform the most accurate luminosity determination, it is first imperative to

ensure that only high-voltage lines with a low current noise are selected. This selection is illustrated in Figure 4.11, which shows the distribution of the root mean square values of all HV lines in the EM FCal over periods with no LHC beam presence. High-voltage lines with a null r.m.s. represent, as discussed previously, extreme cases where only the positive tail of the current pedestal is measured, resulting in a flat current evolution with time. Therefore only high-voltage lines with a current noise between 0.001 μA and 0.015 μA are selected.

For the 2010 data taking period, the combination of these selection criteria bring down the total number of HV lines usable for luminosity to 16 out of 64 in FCal-A and 15 out of 64 in FCal-C. The new ADC offset allows more lines to be used in 2011, with a total of 30 lines on FCal-A and 40 on FCal-C.

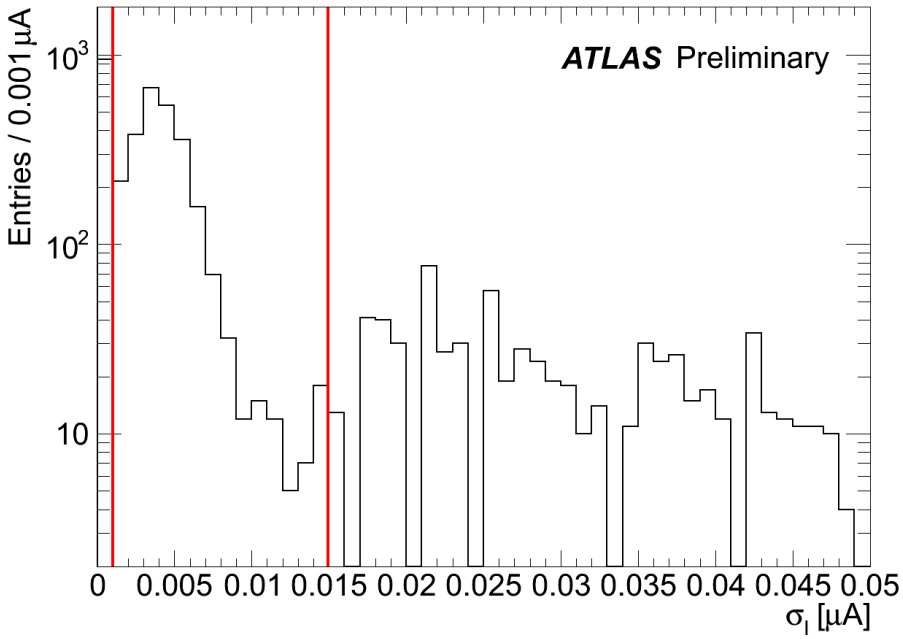

Figure 4.11: Root mean square distribution of the 128 EM-FCal high-voltage lines currents during periods with no LHC beam. The vertical lines at 0.001 μA and 0.015 μA indicate the cuts applied on the noise for an HV line to be eligible for the luminosity measurement.

To summarise, in order for an HV line to be usable for a luminosity determination, it must:

- not be connected to a shorted tube group,

- have a positive pedestal sufficiently above noise,
- have low current noise.

4.6 Luminosity calibration of the FCal high-voltage currents in 2010

4.6.1 Comparing LUCID and FCal data

The LUCID relative luminosity measurement was absolutely calibrated in 2010 during a van der Meer (vdM) scan. However, the technical implementation of the vdM scans could not allow for an absolute calibration of the FCal measurement. Firstly, the instantaneous luminosity during a vdM is significantly lower than during normal LHC operation to avoid emittance blowup, and was below the minimum sensitivity of the FCal high-voltage system. Secondly, the scan steps, at which the rates are recorded in order to perform the calibration, are too short (typically 30 s) for the FCal DC current to set in and provide an accurate measurement. This is worsened by the fact the maximum sampling rate of the FCal HV current is of the order of 0.2 Hz.

There is however another way to calibrate the FCal HV currents. By comparing the FCal currents to an absolutely calibrated LUCID luminosity, it then possible to extract calibration constants for each usable HV line. In 2010, one specific LUCID algorithm was chosen as the default *preferred* luminosity: *LUCID_Event_OR*. It is based on an inclusive OR event counting between the A and C LUCID detectors. In order to verify the stability and robustness of the 2010 FCal calibration, a single ATLAS run was used to extract the calibrations. Run 166786[5], recorded on October 13th 2010, was chosen because of it covers a large range of instantaneous luminosity ($\sim 55-100\ 10^{30}\ cm^{-2}\ s^{-1}$) and contains no oddities.

For one high-voltage line, the calibration procedure consists of the following steps:

[5] http://atlas-runquery.cern.ch/query.py?q=find+run+166786+%2F+show+lhc

- average the measured current by luminosity block (120 s periods),
- calculate the pedestal before the LHC fill (1 h period with no beam present in the machine), as illustrated on Figure 4.12 for a typical selection,
- select "ATLAS "Ready" luminosity blocks (after "STABLE BEAMS" has been declared by the LHC and after warm start of the stand-by subdetectors),
- for the selected luminosity blocks, compare the pedestal-subtracted current to the LUCID luminosity, as shown on Figure 4.13 for the FCal-C selection,
- fit the comparison with a first degree polynomial and extract fit parameters as described by the following relation: $I_{FCal} = a \cdot \mathcal{L}_{LUCID_Event_OR} + b$.

In order to check the validity of the calibration throughout the 2010 data taking period, the constants extracted from the fit on the reference run were applied to a set of runs recorded during October 2010. This period consists of the late 2010 data with high enough instantaneous luminosities to perform a measurement with the forward calorimeters. The quantity $\mathcal{L}_{LUCID}/\mathcal{L}_{FCal}$ can be computed for each high-voltage line and each luminosity block considered. Figure 4.14 shows the evolution of this ratio over time for the 17 runs for each of the 15 FCal-C selected HV lines. The distribution of this quantity for all these runs is shown on Figure 4.15 and displays a root mean square value of $\sim 0.5\%$. The consistency between each run can be check by computing an average ratio per run: $\langle \mathcal{L}_{LUCID}/\mathcal{L}_{FCal} \rangle_{run}$, which is found to be flat over the considered run range as shown on Figure 4.16. Figure 4.17 illustrates the LUCID_Event_OR and FCal calibrated luminosities time evolution during one of the considered runs.

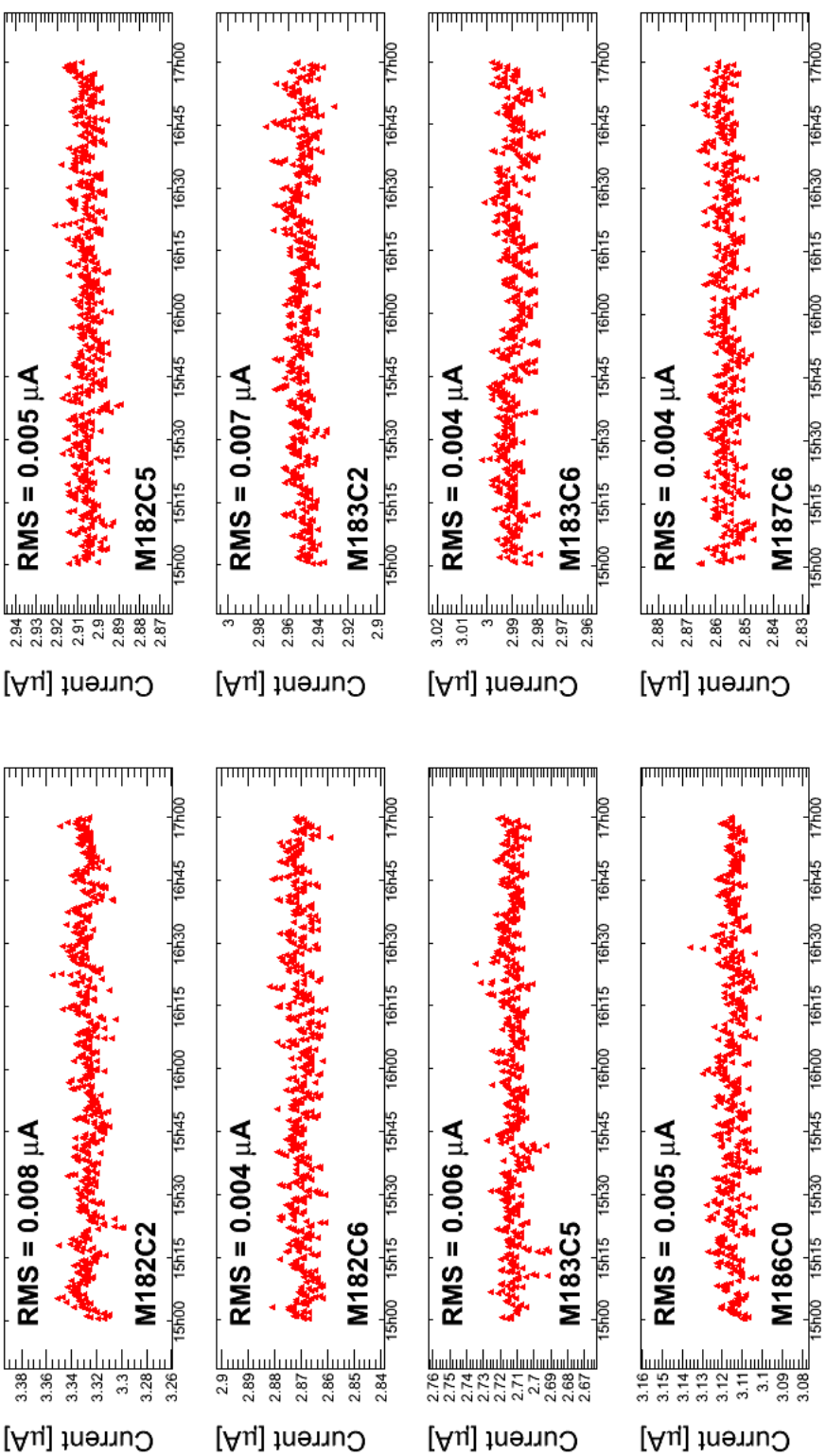

Figure 4.12: Current pedestal versus time for a selection of typical FCal-C HV lines during a one hour period prior to LHC beam injection.

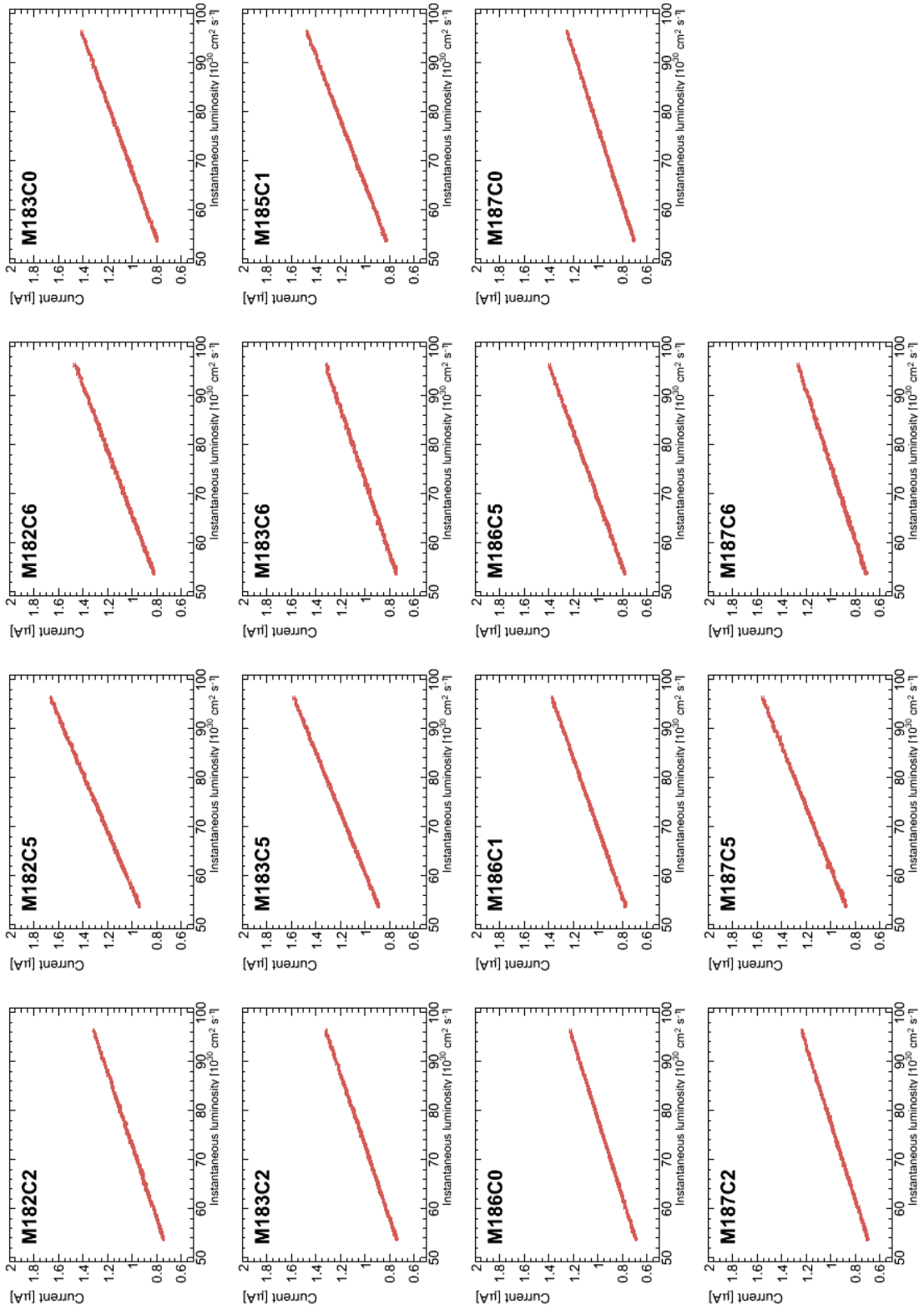

Figure 4.13: Current versus luminosity for a selection of FCal HV lines.

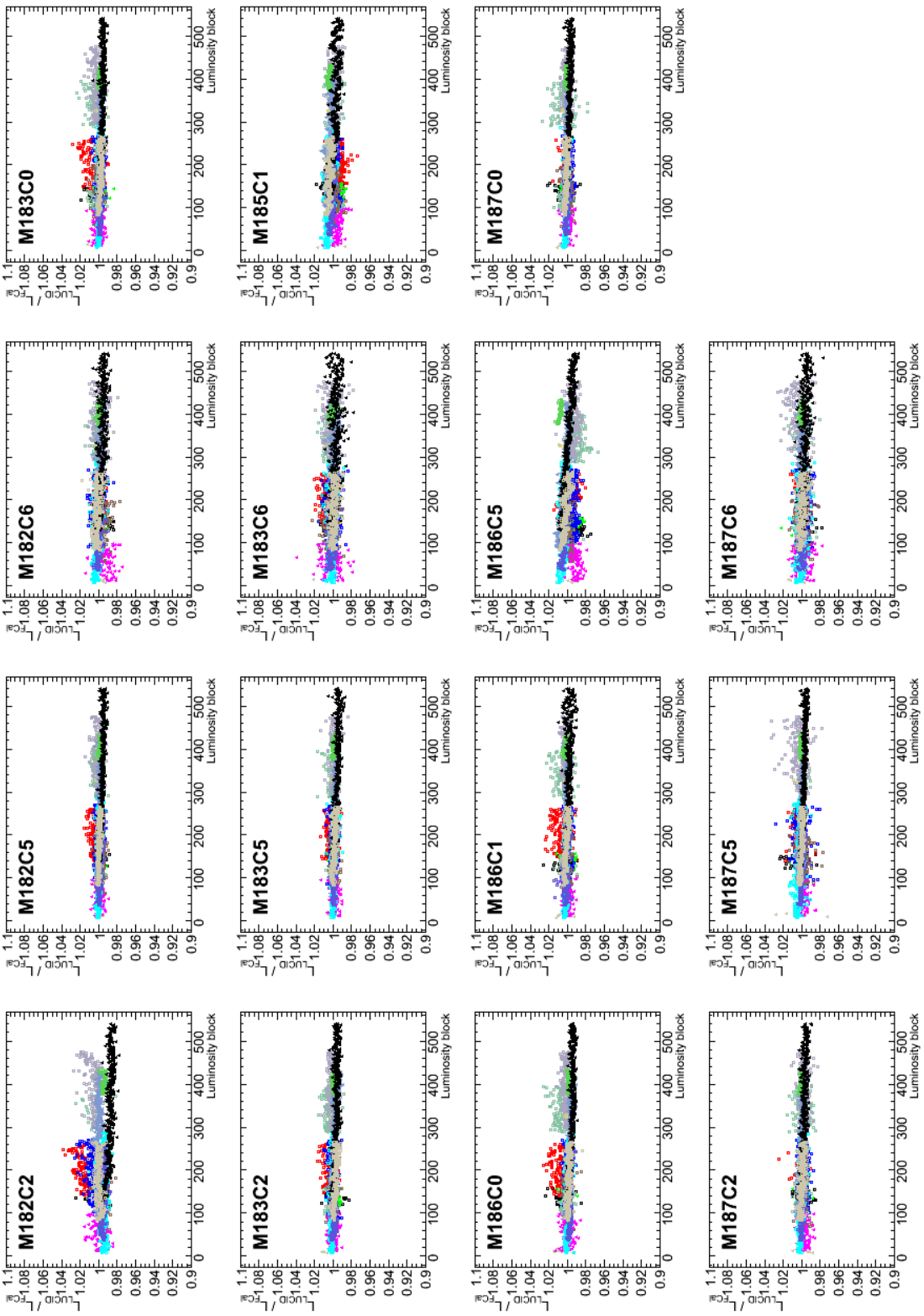

Figure 4.14: Ratio $\mathcal{L}_{LUCID}/\mathcal{L}_{FCal}$ for 17 ATLAS runs in 2010. The ratios are computed and displayed per luminosity block.

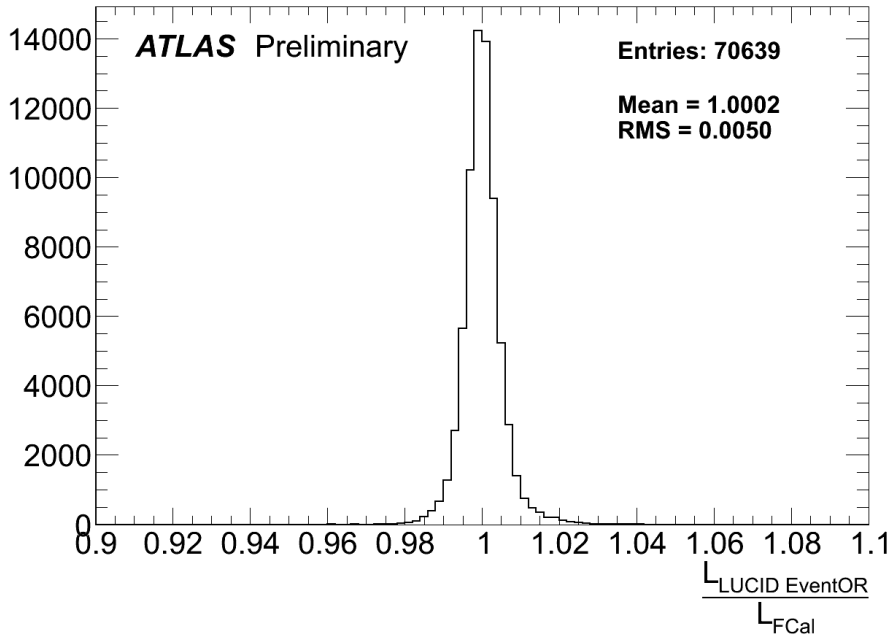

Figure 4.15: Distribution of the ratio $\mathcal{L}_{LUCID}/\mathcal{L}_{FCal}$ for 17 ATLAS runs in 2010. One ratio is computed per luminosity block and high-voltage line.

4.6.2 Systematic uncertainties

The following systematic uncertainties are included in the 0.5% spread of the 2010 calibration, as shown on Figure 4.15.

Current measurement resolution As shown on Figure 4.11, the typical standard deviation of selected high-voltage lines lies between 0.001 μA and 0.015 μA during period with no LHC beam presence. The average pedestal level being approximately 2.6 μA, this leads to a current measurement uncertainty of $\Delta I/I \sim 0.4\%$.

Liquid argon temperature The liquid argon cryostats are kept at a constant temperature of ~88.5 K, which is monitored by ~430 probes as part of the LAr DCS. A temperature variation of 1 K is leads to a 2% variation of the measured signal, due to effects on the argon density and electron drift speed. During the 2010 data taking period, the end-cap cryostats - where the FCal are located - show a temperature stability of ~1.5 mK over time [61]. This value is well below the technical requirement (50-60 mK) and can be

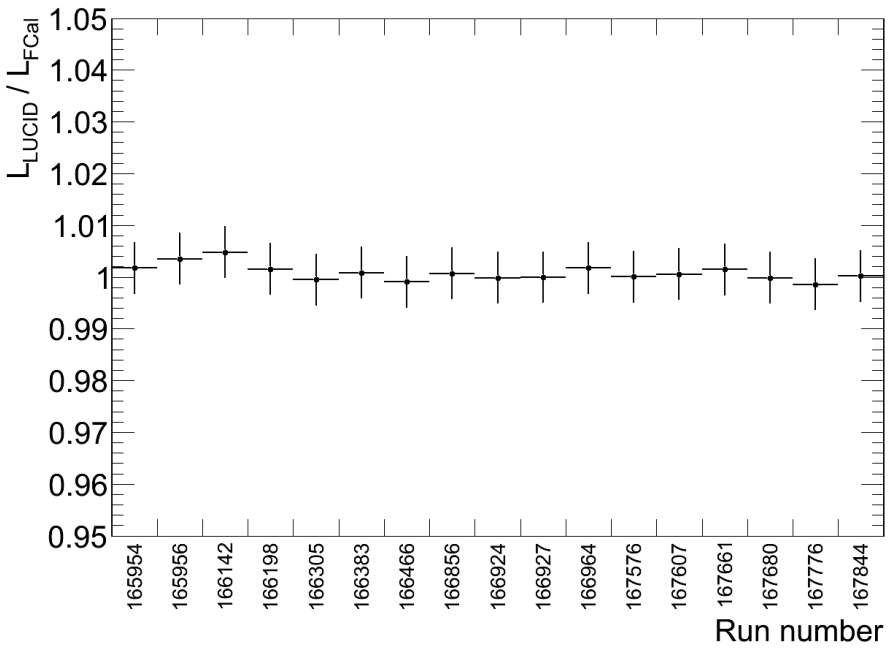

Figure 4.16: Average ratio per run $\langle \mathcal{L}_{LUCID}/\mathcal{L}_{FCal} \rangle_{run}$ for 17 ATLAS runs in 2010.

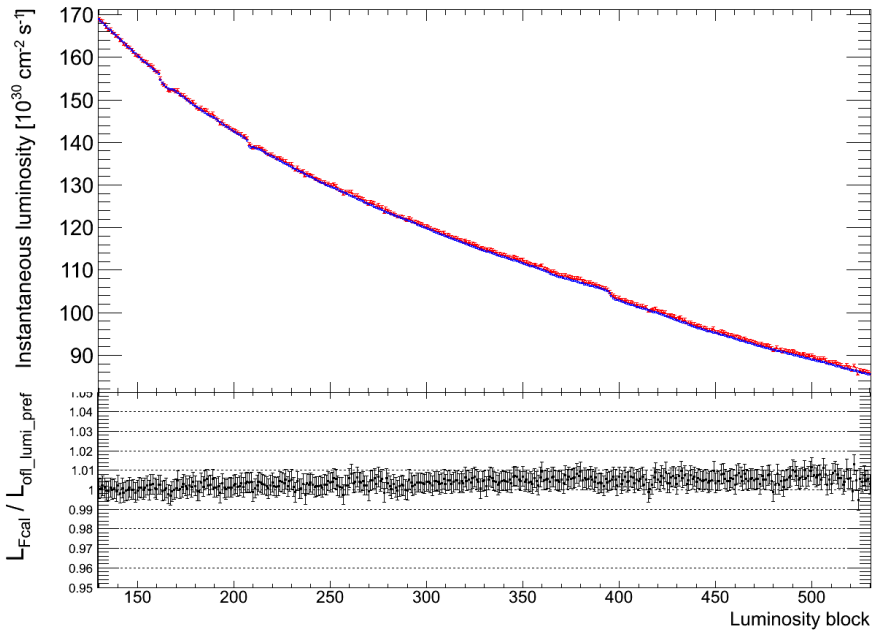

Figure 4.17: FCal calibrated instantaneous luminosity (red) for an ATLAS run taken in 2010. Superimposed is the ATLAS preferred instantaneous luminosity (blue).

therefore considered to have a negligible effect on the stability of the FCal luminosity calibration.

Beam-induced background During proton-proton physics operation, the LHC fill cycle follows a procedure consisting of a series of predetermined steps, from injection to stable collisions, followed by beam dump. A typical LHC physics fill goes as follows:

- INJECTION PHYSICS BEAM: dipole magnets are ramped up to injection energy (450 GeV), injection of proton bunch trains,
- PREPARE RAMP: injection complete, preparing for ramp,
- RAMP: bunch trains are accelerated to collision energy (3.5 TeVper beam), dipole magnets are ramped up accordingly,
- FLAT TOP: immediately after ramp, beams have reached nominal energy,
- SQUEEZE: switch from injection/ramp optics to collision optics using focusing magnets,
- ADJUST: both beams are brought together to collide,
- STABLE BEAMS: colliding beams, stable conditions for physics data-taking,
- BEAM DUMP: both beams are dumped after stable beams period,
- RAMP DOWN: dipole magnets are ramped down to injection energy.

Figure 4.18 illustrates the evolution of the current in one high-voltage line during a physics fill. The FCal HV current shows no significant variation between periods with no beam in the machine (before step 1) until the *ADJUST* phase (step 5), when both beams are brought together to collide at nominal energy. Therefore the high-voltage system appears to be insensitive to beam presence except for colliding beams. This can partly be explained by the fact that the particle flux intensity coming from beam-induced background is orders of magnitude lower than for the minimum bias flux due to collisions.

The following section will focus on changes in the luminosity calibration of the LUCID and BCM detectors between the 2010 and 2011 data taking periods, cross-checks with

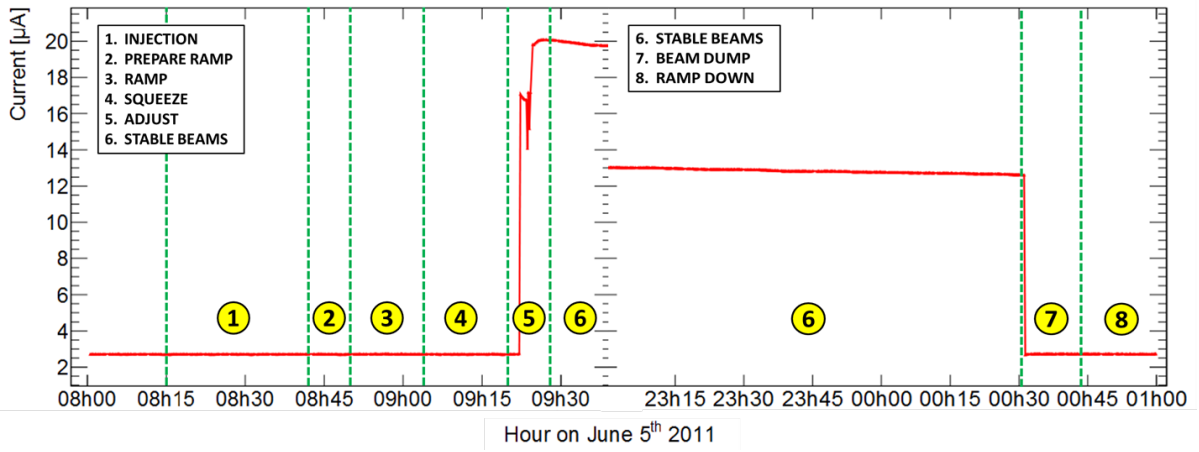

Figure 4.18: Current of one FCal-C HV line versus time for a typical LHC fill on June 5 2011. The left graph, from 8.00AM to 9.45AM, is a zoom of the beginning of the fill from injection to stable beams. The right graph, from 23.00pm to 1.00am, is a zoom of the end of fill and after the beam dump.

the newly calibrated FCal measurement, as well as the consequent rescaling of the LUCID and BCM calibrations.

4.7 FCal luminosity in 2011

During the 2010/2011 winter shutdown, ATLAS-wide hardware and software interventions were performed. Concerning the BCM detector, the analog front-end electronics were modified in order to better accommodate both its luminosity and beam-protection capabilities. Although difficult to quantify, the BCM luminosity calibration was expected to be different from 2010, because of the effect of the modifications on the detector efficiency. However, following these changes, the BCM thresholds were adjusted in order to retrieve a calibration as close as possible to situation in 2010. On the other side, the LUCID strategy during the shutdown was to keep from modifying anything that could affect the luminosity calibration.

Regarding the FCal, a major intervention took place on the detector. Indeed, following analyses with early 2010 collision data, a position shift of the endcap cryostats with respect to the nominal geometry were observed. The analyses were performed by looking at the ϕ-distribution of the energy flow in the forward calorimeters. The most significant

shift observed was in the y-direction, and amounted to approximately 2 mm for each cryostat. In August 2010, an re-alignment in the reconstruction software allowed the recording of the rest of the 2010 collision data with the correct positioning of the endcaps. However, during the winter shutdown, the opportunity to physically raise the cryostats presented itself and was seized. The effect of the positioning on the energy flow was sine-modulated in ϕ and amounted to approximately 2% in amplitude of transverse energy. Concerning the FCal HV currents, as the original 2010 calibration was performed with the old positioning of the cryostats, no modulation is observed in the 2010 data. However, as the procedure was to keep the 2010 calibration and apply it to the 2011 data, the fact that the cryostats were raised gives raise to an ϕ-asymmetry in the FCal luminosities, as depicted in Figure 4.19. There are three ways to cope with this asymmetry:

- re-calibrate the individual FCal high-voltage lines with 2011 data and the new positioning of the cryostats: this cannot be done before the LUCID and BCM are absolutely calibrated
- correct the ϕ-asymmetry by fitting the ϕ-distribution of the 2011 FCal luminosities
- average π-symmetric high-voltage line to cancel the effects of the asymmetry: this method was used in the comparison with the 2011 LUCID and BCM data

4.7.1 Early 2011 data

In 2010, the LUCID and BCM luminosity measurements agree at $\sim 0.5\%$ [33]. Consistency checks between the LUCID and BCM observed luminosity in 2011 show discrepancies at the level of 7 to 12%, depending on the algorithms.

To view this issue from another angle, comparisons with the calibrated FCal luminosity were performed with the LUCID and BCM measurements. The quantity chosen to estimate the discrepancies is the ratio $\mathcal{L}_{alg}/\mathcal{L}_{FCal}$, where *alg* denotes the specific algorithm. Table 4.5 shows these ratios for early 2011 ATLAS runs taken on March 22nd and 23rd. These ratios indicate that from the FCal measurement point of view, the BCM

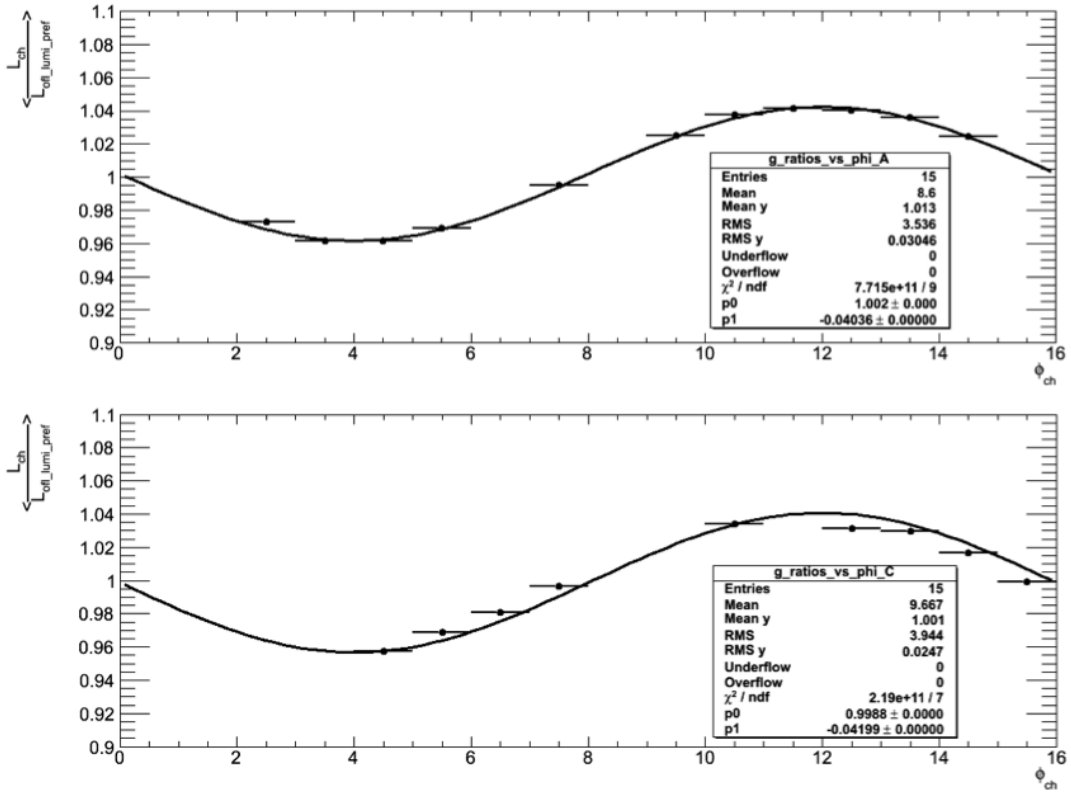

Figure 4.19: Average ratio between FCal A and C HV lines luminosities to the offline preferred luminosity (here LUCID_EventOR) versus the ϕ index of the line in 2011. The calibration of the FCal HV lines is extracted from 2010 data, hence the ϕ modulation. The amplitude of the modulation is approximately 2%.

luminosity calibration in 2011 is comparable to 2010, despite the changes in the BCM analog front-end. However, regarding the LUCID calibration, a difference of the order of 4 to 6% with the FCal is observed.

	178044		178109	
	All	Phys	All	Phys
LUCID Event_OR	1.049	1.030	1.058	1.039
LUCID Event_AND	1.046	1.045	1.059	1.059
BCM Event_OR	1.007	1.001	1.007	1.000
BCM Event_AND	1.000	1.000	1.001	1.000

Table 4.5: Average ratios of LUCID and BCM luminosities to FCal. These two ATLAS runs were recorded on March 22nd and 23rd before the 2011 LUCID and BCM modifications. Ratios labelled *All* are taken over all the BCIDs, and *Phys* only the BCIDs colliding at IP1.

4.7.2 After new LUCID RX cards

Additional interventions were performed in 2011 on the LUCID and BCM detectors. Firstly, in order to enable smooth operation with 50 ns LHC bunch trains, new receiver cards were installed on the LUCID electronics chain. These cards allow for a faster baseline restoration after a signal pulse in the photomultiplier tubes as well as narrower pulse width. The downside of this intervention is that it further impacts the luminosity calibration of the LUCID detector. The same study with the FCal was performed after the new receiver cards were installed, for two ATLAS runs recorded on April 15th and 16th. As shown on Table 4.6, the BCM ratios are comparable to the ones listed in Table 4.5. Regarding LUCID, the ratios have gone up by $\sim 2-3\%$ after the new receiver cards, depending on the algorithm.

4.7.3 BCM thresholds changes

Following a BCM threshold scan in early March 2011, it was decided to adjust these thresholds in order to rejoin the BCM efficiency plateau. This intervention had an expected impact on the BCM luminosity calibration. A third series of ATLAS runs, recorded

	179739		179804	
	All	Phys	All	Phys
LUCID Event_OR	1.078	1.054	1.084	1.060
LUCID Event_AND	1.081	1.081	1.089	1.088
BCM Event_OR	1.008	1.002	1.010	1.004
BCM Event_AND	1.001	1.001	1.003	1.003

Table 4.6: Average ratios of LUCID and BCM luminosities to FCal for two ATLAS runs recorded on April 15th and 16th 2011. These runs were taken after the replacement of the LUCID receiver cards and before the BCM threshold changes. Ratios labelled *All* are taken over all the BCIDs, and *Phys* only the BCIDs colliding at IP1.

in April 2011 was analysed in comparison with the FCal measurement. Tables 4.7 and 4.8 summarise the ratios of the LUCID and BCM algorithms with respect to the FCal for these runs. Averaging over the entire period provides a handle on quantifying the discrepancies. The results show that for this dataset, as illustrated on Figure 4.20, after the new LUCID receiver cards and the new BCM thresholds, the FCal luminosity measurement overestimates the LUCID_Event_OR and BCM_Event_OR algorithms by 6.3% and 3.7% respectively.

	180124	180139	180144	180149	180153	180164	180241	180242	180309	Average
LUCID Event_OR	1.084	1.088	1.077	1.089	1.079	1.088	1.088	1.089	1.098	1.087 ± 0.006
LUCID Event_AND	1.091	1.094	1.079	1.094	1.082	1.094	1.092	1.093	1.104	1.091 ± 0.007
LUCID Event_A	1.095	1.099	1.085	1.100	1.087	1.099	1.095	1.096	1.110	1.096 ± 0.007
LUCID Event_C	1.104	1.110	1.095	1.111	1.097	1.110	1.112	1.113	1.124	1.108 ± 0.008
BCM Event_OR	1.043	1.045	1.043	1.045	1.044	1.044	1.046	1.045	1.045	1.044 ± 0.001
BCM Event_AND	1.040	1.041	1.039	1.041	1.040	1.041	1.042	1.041	1.041	1.041 ± 0.001
BCM Event_OR_V	1.045	1.047	1.044	n/a	1.051	1.046	1.047	1.047	1.047	1.047 ± 0.002
BCM Event_AND_V	1.042	1.044	1.041	1.049	1.043	1.043	1.044	1.044	1.044	1.044 ± 0.002

Table 4.7: Average ratios of LUCID and BCM luminosities to FCal for a set of ATLAS runs recorded in April 2011, after the installation of the new LUCID receiver cards and the BCM thresholds changes. The algorithms used include data from all BCIDs.

	180124	180139	180144	180149	180153	180164	180241	180242	180309	Average
LUCID Event_OR	1.061	1.064	1.054	1.066	1.056	1.065	1.064	1.065	1.072	1.063 ± 0.005
LUCID Event_AND	1.090	1.093	1.079	1.093	1.082	1.093	1.091	1.092	1.103	1.091 ± 0.007
LUCID Event_A	1.076	1.080	1.067	1.081	1.069	1.080	1.076	1.077	1.089	1.077 ± 0.006
LUCID Event_C	1.087	1.092	1.078	1.093	1.081	1.092	1.094	1.095	1.104	1.091 ± 0.007
BCM Event_OR	1.036	1.037	1.035	1.038	1.036	1.037	1.038	1.038	1.037	1.037 ± 0.001
BCM Event_AND	1.040	1.041	1.039	1.041	1.040	1.041	1.041	1.041	1.041	1.041 ± 0.001
BCM Event_OR_V	1.038	1.040	1.037	1.046	1.039	1.039	1.040	1.041	1.040	1.040 ± 0.002
BCM Event_AND_V	1.042	1.044	1.041	1.048	1.043	1.043	1.044	1.044	1.043	1.044 ± 0.002

Table 4.8: Average ratios of LUCID and BCM luminosities to FCal for a set of ATLAS runs recorded in April 2011, after the installation of the new LUCID receiver cards and the BCM thresholds changes. The algorithms used include only data from colliding BCIDs.

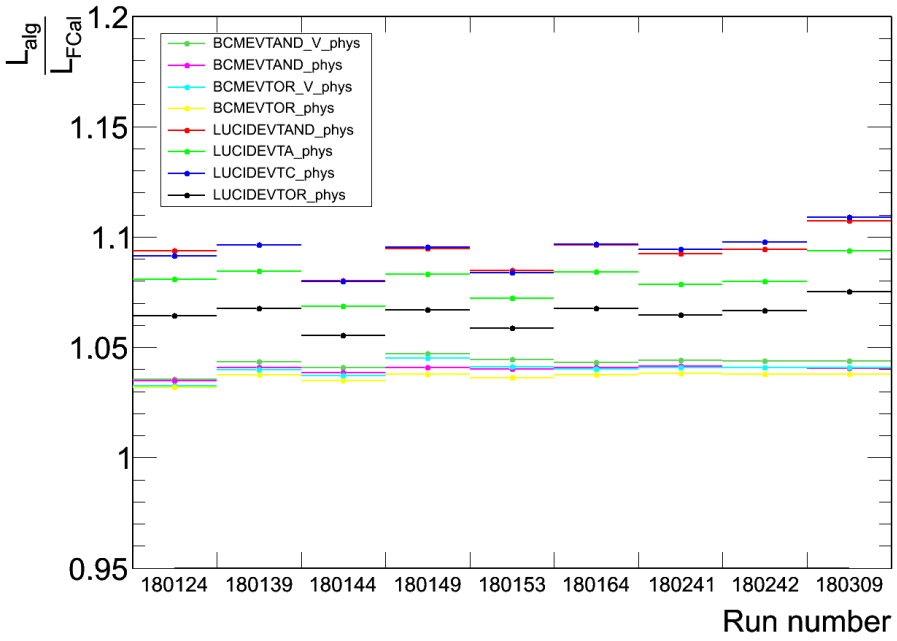

Figure 4.20: Average ratios of LUCID and BCM luminosities to FCal for a set of ATLAS runs recorded in April 2011, after the installation of the new LUCID receiver cards and the BCM thresholds changes. The horizontal axis represents the ATLAS run number.

4.7.4 Rescaling of the 2011 early BCM and LUCID data

Following the discrepancies observed in the comparison between FCal, LUCID, and BCM in early 2011 data, and in addition to the fact that FCal seemed to agree well with BCM before its thresholds changes, the decision was taken to take FCal as a new reference and rescale the BCM and LUCID visible cross-sections. The LUCID and BCM visible cross-sections were rescaled according to several data-taking periods, as listed on Table 4.21. Figure 4.22 illustrates the comparisons between LUCID and BCM after the rescaling. The ratios are centred around 1, with however still a mu-dependence.

The 2010 total systematic uncertainty on the luminosity, 3.4%, had to be revised in early 2011 to take into account the rescaling with respect to the FCal luminosity. The main changes stemmed from the mu-dependence (+1.5%), the long-term consistency (+1%), and the FCal-TileCal discrepancy observed in early 2011 (+2%). This led to a new systematic uncertainty of 4.5%.

Period	Run Range	Lumi (pb^{-1})	Lucid σ_{vis} scale (OR/AND)	BCM σ_{vis} scale (OR/AND)	Notes
A	177531 - 177965	8	1.035/1.08*	1 / 1	Magnets partly off
B	177986 - 178109	17	1.035/1.08*	1 / 1	before RX card swap
D1-D3	179581 - 180122	36	1.06/1.15	1 / 1	after RX card swap
D3-E	180124 - 180710	200	1.06/1.15	1.037 / 1.075	after BCM threshold
F1	180776	1	1 / 1	1 / 1	OLC updated

* Educated guess, not in FCal study
no attempt to correct for magnet-off data

Figure 4.21: FCal-based LUCID and BCM 2011 rescaling factors for different ATLAS data-taking periods, corresponding to different detector statuses.

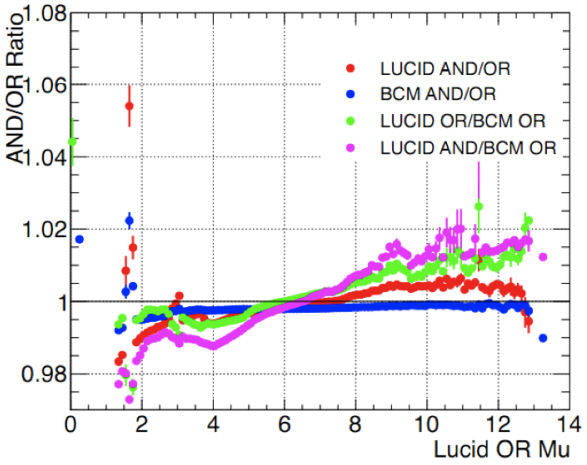

Figure 4.22: Ratios of LUCID and BCM luminosities after FCal-based rescaling, compared to the number of interactions per bunch crossing measured by LUCID.

In order to improve this uncertainty, a vdm scan was performed in May 2011, and the results are described in the following section.

4.7.5 Cross-comparisons after the May 2011 vdM calibration

In May 2011, a new van der Meer scan [58] took place in order to absolutely re-calibrate the LUCID and BCM detectors, as they were shown to have lost their calibrations during the previous winter shutdown. Consequently, new cross-checks with the FCal luminosity measurement (still using the 2010 calibration) could be performed in order to shed light on possible discrepancies. Figure 4.23 shows the ratio between various luminosities per ATLAS run compared to a reference algorithm, BCM_H_EventOR. The relative variations are contain within ±1%, which leads to an additional systematic uncertainty associated with long-term stability of 1%.

A final check consists of comparing the evolution of the luminosity ratios as a function of the number of interactions per bunch crossing, μ. Figure 4.24 illustrates this comparison and all methods agree at the level of 1%, which comes as an additional systematic associated with the μ-dependence.

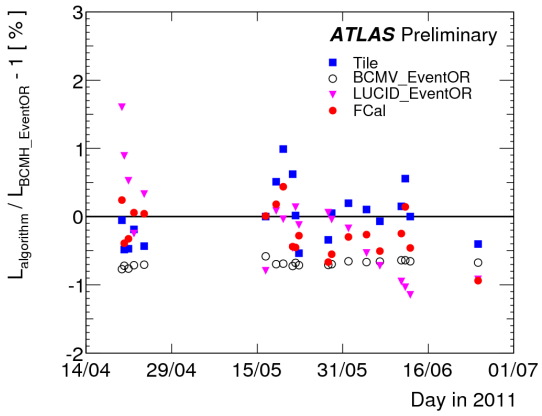

Figure 4.23: Fractional deviation in the integrated luminosity obtained using different algorithms with respect to the BCM_H_EventOR value as a function of time. Each point shows the average deviation for a single ATLAS run. Statistical uncertainties per point are negligible. Extracted from [58].

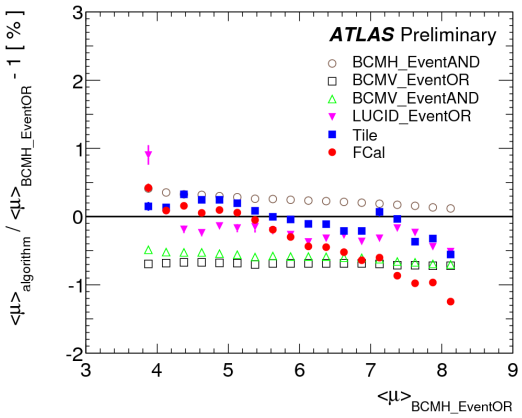

Figure 4.24: Fractional deviation in the average number of interactions per bunch crossing (averaged over BCIDs) obtained using different algorithms with respect to the BCM_H_EventOR value as a function of $\langle\mu\rangle$. Statistical uncertainties per point are negligible. Extracted from [58].

4.8 Conclusion

The feasibility of a relative luminosity measurement using the currents of the forward calorimeter high-voltage system has been demonstrated. It has been shown to be linear up the LHC design luminosity and stable within 0.5% across a two months period in 2010. Cross-checks with the LUCID and BCM luminosity determinations in 2011 have led to a rescaling of their visible cross-sections for part on the 2011 dataset, leading to a temporary re-evaluation of the total systematic uncertainty to 4.5%. In addition, following improvements on the FCal HV system in early 2011 and an absolute calibration of the LUCID and BCM luminosities using the May vdM scans, the total systematic uncertainty has been reduced to 3.7% for the 2011 dataset.

Conclusions and outlook

This document presents a luminosity determination using the currents of the high-voltage system of the ATLAS liquid argon calorimeter. By measuring the currents drawn by the forward calorimeter high-voltage lines, where the minimum bias flux is the highest, it is possible to calibrate them to the absolutely-calibrated LUCID luminosity determination with a precision of 0.5%, not including the 2010 uncertainty of the LUCID calibration of 3.4%.

One of the strongest advantages of using the forward calorimeter as a luminosity monitor is based on the linearity of its response with luminosity, which has been demonstrated during test beam studies by the ATLAS HiLum collaboration, as well as reproduced *in situ* in ATLAS. Simulations based on recorded collision data have also helped defining the limits of the FCal luminosity capabilities.

In 2011, using the 2010 calibration, cross-checks with other luminosity monitors such as the LUCID, BCM, and TileCal detectors helped in deepening the understanding of the luminosity determination within ATLAS.

In order to achieve the full capabilities of the forward calorimeter as a luminosity monitor, we will first need to re-calibrate the FCal high-voltage power supplies. Following this operation, a complete recalibration of the high-voltage currents with respect to an absolutely-calibrated luminosity measurement will have to be performed. In parallel, the online infrastructure has to be completed in order to acquire, calibrate, and publish an FCal luminosity within the official ATLAS framework. This will allow for continuous moni-

toring of the FCal response with respect to other luminosities and a better understanding of the overall ATLAS luminosity determination.

Bibliography

[1] The ATLAS Collaboration. *The ATLAS Experiment at the CERN Large Hadron Collider*. JINST **3**, S08003 (2008).

[2] F. J. Hasert et al. *Observation of neutrino-like interactions without muon or electron in the Gargamelle neutrino experiment*. Phys. Lett. **B46**, 138–140 (1973).

[3] G. Arnison et al. *Experimental observation of isolated large transverse energy electrons with associated missing energy at s**(1/2) = 540-GeV*. Phys. Lett. **B122**, 103–116 (1983).

[4] G. Arnison et al. *Experimental observation of lepton pairs of invariant mass around 95-GeV/c**2 at the CERN SPS collider*. Phys. Lett. **B126**, 398–410 (1983).

[5] M. Banner et al. *Observation of single isolated electrons of high transverse momentum in events with missing transverse energy at the CERN anti-p p collider*. Phys. Lett. **B122**, 476–485 (1983).

[6] G. Duckeck. *Determination of the number of light neutrinos species with the OPAL detector at LEP*. (1997).

[7] O. Adriani et al. *Determination of the number of light neutrino species*. Phys.Lett. **B292**, 463–471 (1992).

[8] D. Decamp et al. *Determination of the Number of Light Neutrino Species*. Phys.Lett. **B231**, 519 (1989).

[9] J. Alcaraz et al. *A Combination of preliminary electroweak measurements and constraints on the standard model*. (2006).

[10] *Updated Combination of CDF and D0 Results for the Mass of the W Boson*. (2009).

[11] F. Abe et al. *Observation of top quark production in anti-p p collisions*. Phys. Rev. Lett. **74**, 2626–2631 (1995).

[12] S. Abachi et al. *Observation of the top quark*. Phys. Rev. Lett. **74**, 2632–2637 (1995).

[13] K. Nakamura et al. *Review of particle physics*. J. Phys. **G37**, 075021 (2010).

[14] F. Englert and R. Brout. *Broken symmetry and the mass of gauge vector mesons*. Phys. Rev. Lett. **13**, 321–322 (1964).

[15] Peter W. Higgs. *Broken symmetries and the masses of gauge bosons*. Phys. Rev. Lett. **13**, 508–509 (1964).

[16] The CDF, D0 Collaborations, the Tevatron New Phenomena and Higgs Working Group. *Combined CDF and D0 Upper Limits on Standard Model Higgs Boson Production with up to 8.6 fb-1 of Data*. (2011).

[17] Lyndon Evans and Philip Bryant. *LHC Machine*. Journal of Instrumentation **3** (08), S08001 (2008).

[18] R. Adolphi et al. *The CMS experiment at the CERN LHC*. JINST **3**, S08004 (2008).

[19] K. Aamodt et al. *The ALICE experiment at the CERN LHC*. JINST **3**, S08002 (2008).

[20] A.Augusto Alves et al. *The LHCb Detector at the LHC*. JINST **3**, S08005 (2008).

[21] H. Burkhardt and P. Grafstrom. *Absolute luminosity from machine parameters*. (2007).

[22] G. Aad et al. *The ATLAS Inner Detector commissioning and calibration*. Eur.Phys.J. **C70**, 787–821 (2010).

[23] Georges Aad et al. *Readiness of the ATLAS Tile Calorimeter for LHC collisions*. Eur.Phys.J. **C70**, 1193–1236 (2010).

[24] G Aad et al. *Readiness of the ATLAS Liquid Argon Calorimeter for LHC Collisions*. Eur.Phys.J. **C70**, 723–753 (2010).

[25] Georges Aad et al. *Commissioning of the ATLAS Muon Spectrometer with Cosmic Rays*. Eur.Phys.J. **C70**, 875–916 (2010).

[26] The ATLAS Collaboration. *ATLAS magnet system: Technical design report*. CERN-LHCC-97-18.

[27] The ATLAS Collaboration. *ATLAS inner detector: Technical design report. Vol. 1*. CERN-LHCC-97-16.

[28] The ATLAS Collaboration. *ATLAS inner detector: Technical design report. Vol. 2*. CERN-LHCC-97-17.

[29] Fabian Hugging and On behalf of the ATLAS Collaboration. *The ATLAS Pixel Insertable B-Layer (IBL)*. (2010).

[30] V. Cindro et al. *The ATLAS Beam Conditions Monitor*. JINST **3**, P02004 (2008).

[31] The ATLAS Collaboration. *ATLAS Forward Detectors for Measurement of Elastic Scattering and Luminosity*. LHCC/2008-004 (2008).

[32] The ATLAS Collaboration. *Zero degree calorimeters for ATLAS*. (2007).

[33] The ATLAS Collaboration. *Luminosity Determination in pp Collisions at sqrt(s)=7 TeV Using the ATLAS Detector at the LHC*. arXiv:1101.2185 [hep-ex] (2010).

[34] S van der Meer. *Calibration of the effective beam height in the ISR*. Technical Report CERN-ISR-PO-68-31 1968.

[35] H Burkhardt and S Cavalier. *Intermediate 90m Optics for ATLAS-ALFA*. (Apr 2011).

[36] The ATLAS Collaboration. *ATLAS liquid argon calorimeter: Technical design report*. CERN-LHCC-96-41.

[37] The ATLAS Collaboration. *ATLAS tile calorimeter: Technical design report*. CERN-LHCC-96-42.

[38] The ATLAS Collaboration. *ATLAS muon spectrometer: Technical design report*. CERN-LHCC-97-22.

[39] Bernard Aubert et al. *Construction, assembly and tests of the ATLAS electromagnetic barrel calorimeter*. Nucl. Instrum. Meth. **A558**, 388–418 (2006).

[40] M. L. Andrieux et al. *Construction and test of the first two sectors of the ATLAS barrel liquid argon presampler*. Nucl. Instrum. Meth. **A479**, 316–333 (2002).

[41] M. Aleksa et al. *Construction, assembly and tests of the ATLAS electromagnetic end-cap calorimeters*. JINST **3**, P06002 (2008).

[42] D. M. Gingrich et al. *Construction, assembly and testing of the ATLAS hadronic end-cap calorimeter*. JINST **2**, P05005 (2007).

[43] A. Artamonov et al. *The ATLAS forward calorimeters*. JINST **3**, P02010 (2008).

[44] N. J. Buchanan et al. *ATLAS liquid argon calorimeter front end electronics*. JINST **3**, P09003 (2008).

[45] N. J. Buchanan et al. *Design and implementation of the Front End Board for the readout of the ATLAS liquid argon calorimeters*. JINST **3**, P03004 (2008).

[46] A. Bazan et al. *ATLAS liquid argon calorimeter back end electronics*. JINST **2**, P06002 (2007).

[47] J. Prast. *The ATLAS liquid argon calorimeters read out drivers (ROD)*. Prepared for 6th Workshop on Electronic for LHC Experiments, Cracow, Poland, 11-15 Sep 2000.

[48] A. Airapetian et al. *ATLAS calorimeter performance*. CERN-LHCC-96-40.

[49] J. Ban et al. *Cold electronics for the liquid argon hadronic end-cap calorimeter of ATLAS*. Nucl. Instrum. Meth. **A556**, 158–168 (2006).

[50] L Di Ciaccio, D Fournier and F Hubaut. *High Voltage corrections for electromagnetic calorimeter*. Technical Report ATL-COM-LARG-2005-003 CERN Geneva Apr 2005.

[51] B. Botchev, G. Finocchiaro, J. Hoffman, R.L. McCarthy, M. Rijssenbeek et al. *The High Voltage Feedthroughs for the ATLAS Liquid Argon Calorimeters*. JINST **2**, T10002 (2007).

[52] G Blanchot. *Grounding of the ATLAS experiment*. Technical Report ATL-ELEC-PUB-2007-002. ATL-COM-ELEC-2007-003 CERN Geneva Dec 2007.

[53] A Barriuso Poy, H Boterenbrood, H J Burckhart, J Cook, V Filimonov, S Franz, O Gutzwiller, B Hallgren, V Khomutnikov, S Schlenker and F Varela. *The detector control system of the ATLAS experiment*. J. Instrum. **3**, P05006 (2008).

[54] G. Aad, J. Adelman, S. Arfaoui, M. Baak, N. Boelaert et al. *Data quality from the detector control system at the ATLAS experiment*. J.Phys.Conf.Ser. **219**, 022037 (2010).

[55] W Bonivento. *Online luminosity monitoring with liquid Argon calorimeters at ATLAS and D0*. Technical Report ATL-LARG-2001-001 2000.

[56] A. Afonin et al. *Relative luminosity measurement of the LHC with the ATLAS forward calorimeter*. JINST **5**, P05005 (2010).

[57] The ATLAS Collaboration. *Measurement of the Inelastic Proton-Proton Cross-Section at $\sqrt{s} = 7$ TeV with the ATLAS Detector*. (2011).

[58] The Luminosity Group. *Luminosity Determination in pp Collisions at sqrt(s) = 7 TeV using the ATLAS Detector in 2011*. Technical Report ATLAS-COM-CONF-2011-130 CERN Geneva Jul 2011.

[59] Simon Mathieu White, H Burkhardt and P Puzo. *Determination of the Absolute Luminosity at the LHC. oai:cds.cern.ch:1308187*. PhD thesis Orsay, UniversitÃ Paris-Sud 11 Orsay 2010. Presented on 11 Oct 2010.

[60] G Anders, N Bacchetta, V Balabara, C Barschel, D Belohrad, D Berge, H Burkhardt, S I Cooper, M Ferro-Luzzi, G Franzoni, C Gabaldon, M Gagliardi, J J Gras, V Halyo, B Heinemann, P Hopchev, A Hunt, W Kozanecki, S Kwan, M Ludwig, D Marlow, P Odier, S Pagan Griso, J Panman, T Pauly, S Thoulet, S White, J C Yun and M Zanetti. *LHC Bunch Current Normalisation for the April-May 2010 Luminosity Calibration Measurements*. (Feb 2011).

[61] J.-B. Blanchard et al. *Performance of the cryogenic regulation and the monitoring system of the liquid argon calorimeter temperature*. Technical Report ATL-LARG-INT-2010-003 CERN Geneva May 2010.

Appendix A

High-voltage system technical specifications

	High Voltage Power Supply System ATLAS Liquid Argon Calorimeter Specification		
ATLAS Project Document. No. *Project - System -- Type – Sequential No.* **EP-ATLAS**	*Institute Document No.*	*Created* 07-Jun-01 *Modified* 4-Sep-01	*Page* 1/27 *VersRev.:* **9**

TECHNICAL SPECIFICATION FOR A MODULAR HIGH VOLTAGE POWER SUPPLY SYSTEM FOR THE ATLAS LIQUID ARGON CALORIMETER

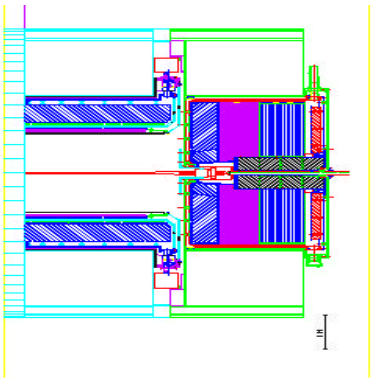

ABSTRACT

This specification concerns the production of a modular High Voltage Power Supply System to be used for the ATLAS Liquid Argon Calorimeter detectors.The system consists of four types of multichannel HV modules housed in 19" subracks (crates) and remotely controlled via CAN bus.

Prepared by:	Checked by:	Approved by:
Helmut Braun		

Distribution List

(EMB, EMB-PS), (EMEC), (HEC), (FCAL), (EMEC-PS), (Purity), (Luminosity), (HV-FT), (Grounding), (TIS)

1. INTRODUCTION

The Large Hadron Collider (LHC) project was approved by the CERN Council in December 1994. The LHC will be the next major research tool for particle physics and it is expected to be commissioned in 2006.

This new proton beam collider facility will be installed in the existing underground ring tunnel of approximately 27 km circumference at CERN.

Within the context of LHC, one of the two major experiments to be built is called ATLAS (A Toroidal LHC ApparatuS).
This experiment, built and funded by an international collaboration between high-energy physics institutes from thirty four countries and by CERN, consists basically of a superconducting magnet system equipped with several particle detectors.

ATLAS will be installed around the LHC interaction point I1 in an underground cavern at a depth of 90 meters. Entrance to this area is made via access shafts from a surface complex called P1, near the main CERN Laboratory 1 site in Switzerland.

The expected lifetime of the experiment is at least 15 years from the LHC commissioning date.

One of the ATLAS detectors is the Liquid Argon Calorimeter (LArg) that uses ionisation chambers immersed in liquid argon to detect energy from penetrating charged particles which ionise the argon.

The ions produced are collected, amplified and sent to the readout chain for further processing.

The ionisation chambers will be biased with a voltage up to 2.5 kVolts. The maximal ion current induced at the highest LHC intensity depends on the location of the chamber with respect to the interaction point of the experiment and ranges from 75μA to 6mA.

A modular High Voltage Power Supply System is foreseen to accomplish such functionality.

The stringent definition of and full compliance with the Technical Specifications is absolutely necessary in order to guarantee that this HV Power Supply System can be used as measurement apparatus to complement the acquisition of physics data.

2. SCOPE OF THE SUPPLY

This technical specification concerns the manufacturing of

- the multichannel High Voltage Modules
- the subracks (crates)
- the monitoring and control system for the components

by matching

- the experiment and detector boundary conditions
- the technical specifications

and fullfilling

- the environmental requirements
- the reliability requirements
- and the calibration requirements

3. TECHNICAL REQUIREMENTS FOR THE HIGH VOLTAGE POWER SUPPLY SYSTEM

3.1. Experiment and Detector Boundary Conditions

The type of multicore HV cable for 32 HV lines and the type of multipin HV connectors used to connect the HV power supply output to the LArg calorimeter detector are described in **Annex 1** and **Annex 2** respectively. The output cable is about 130 m long with a single wire resistance of 147 Ω / km. The connector pin layout is described in **Annex 3**.

Requirement 1: The output connector mounted on the HV module front panel must be compatible with the specifications given in **Annex 2 and 3**.
Requirement 2: The HV applied must be floating with its return (the common leg) connected to the ATLAS-Larg-Cryostat mass connection in the vicinity of the HV rack. A lockable single point connector to the HV return on the backplane of the subrack must be provided in order to implement a cable link to the cryostat mass.
Requirement 3: The HV module housing, the output connector housing, the HV-return and guide pins and the cable shield must all be connected to the HV return.
Requirement 4: The return of the HV supply must be separated from the safety ground of primary power sources, subracks and cabinets which are connected to the safety ground grid in the ATLAS cavern. The potential difference between the HV return and the safety ground must be limited to less than ±30 Volts.

The output load in terms of resistor and capacitance depends on the different ionisation chamber construction for the different subdetectors of the ATLAS LArg calorimeter. The R and C values, as defined in Fig. 1, are summarised in Table 1.

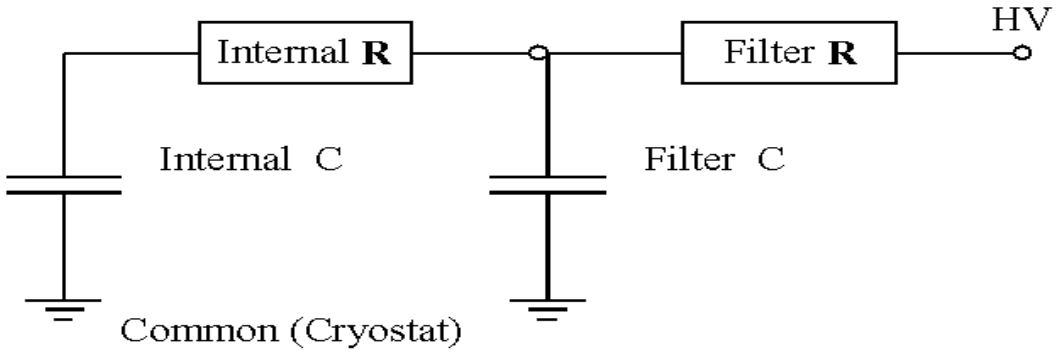

Fig. 1 Simplified Detector Characteristics

	Internal R	**Internal C**	**Filter R**	**Filter C**	**RC time constant via 0Ω to common** *versus* **RC time constant via 50MΩ to common**
Electromagnetic Barrel Detector (EMB)	30 to 60 kΩ	3 μF to 6 μF	100 kΩ	27 nF	0.4 to 1 sec *versus* 150 to 300 sec
Electromagnetic Barrel Detector Presampler (EMB-PS)	10 kΩ	0.3 μF	500 kΩ	27 nF	0.15 sec *versus* 15 sec
Electromagnetic End-Cap Detector (EMEC)	30 kΩ	3.5 μF	100 kΩ	27 nF	0.5 sec *versus* 175 sec
Electromagnetic End-Cap Detector Presampler (EMEC-PS)	100 kΩ	0.03 μF	200 kΩ	27nF	0.01sec *versus* 1.5 sec
Hadronic End-Cap Detector (HEC)	500 kΩ	1.6 μF	200 kΩ	27 nF	1.1 sec *versus* 80 sec
Forward Detector (FCAL)	45 kΩ	0.9 μF	10 kΩ	100 nF	0.055sec *versus* 45 sec
Purity Control Detector (PCD)	20 MΩ	0.001 μF	2 MΩ	27 nF	0.050 sec *versus* 2 sec

Table 1 LArg Calorimeter Subdetectors

3.2. HV Module Requirements

With the maximum current $\mathbf{I_{max}}$ drawn and the maximum high voltage bias $\mathbf{V_{max}}$ defined for the different subdetectors the power supplies needed can be grouped into four supply categories (Table 2).Within these four supply categories different **nominal voltages** are applied:

Supply type	Maximal Voltage V_{max}	Maximal Current I_{max}	Subdetectors and their nominal voltages
1	+ 2.5 kV	75 μA	EMB +2.1 kV EMB-PS +2.1 kV HEC +1.8 kV PosPCD +2.5 kV
2	+ 2.5 kV	200 μA	EMEC between +0.9 kV and +2.5 kV
3	+ 600 Volt	6 mA	FCAL +250 V or +375 V or +500 V
4	- 2.5 kV	75 μA	EMEC-PS –2.5 kV NegPCD –2.5 kV

Table 2 Definition of Supply Categories

Requirement 5: Each HV-circuit must be **insulated ("floating")** and the voltage of each channel must be individually setable and regulated between zero and $\mathbf{V_{max}}$.

Requirement 6: The **voltage output accuracy** compared to an external calibration source must be better than

$$\pm \mathbf{4 \times 10^{-4} V_{max}}$$

which corresponds to ±1V at V_{max} = 2.5 kV and ± 0.25V at V_{max} = 600V.
For the voltage calibration refer to Requirement 15 and 33.

Requirement 7: The **voltage ripple** measured peak to peak at maximum load must be

$\Delta \mathbf{V_{RN}} < \mathbf{10\ mV_{p-p}}$ for type 1,3 and 4
and $< \mathbf{20\ mV_{p-p}}$ for type 2 modules

for frequencies from 10 Hz to 100 MHz and nominal voltages > 400 V for type 1,2 and 4 modules and > 50 V for type 3 modules. Refer also to Requirement 20.

Requirement 8: The **cross talk** of any module channel at nominal voltage and

maximum load onto neighbour channels must be

$$\Delta V_{CT} < 10\ mV_{p\text{-}p}$$

for frequencies from 10 Hz to 100 MHz.

Requirement 9: The **temperature coefficient** in the range **10 to 50 deg.C** must be

$$K_T < 5x10^{-5} / deg.C$$

Requirement 10:
Voltage variations due to **no-load/load effects** and **module input voltage fluctuations** must be

less than $5x10^{-5}$

Requirement 11:
The **voltage setting** and **readout resolution** must be at least
100 mV for type 1,2 and 4 modules
and **20 mV** for type 3 modules.

Requirement 12:
The **measured current I_{meas}** must depend **linearly** on the load I_{true} to better than

$$s = \pm 3x10^{-3}$$

with **s** defined in $(I_{meas} - I_{offset}) = (1+s)\ I_{true}$
and with I_{offset} being the value of I_{meas} at $I_{true} = 0$.
For the linearity calibration refer to Requirement 15 and 33.

Requirement 13: The **current accuracy** must be better than

$\Delta I = \pm 0.5\ \% I_{max}$ for type 1,2 and 4 modules

$\Delta I = \pm 0.06\ \% I_{max}$ for type 3 modules

For the current calibration refer to Requirement 15 and 33.

Requirement 14: The **current measurement resolution** must be at least
20 nA for type 1 and 4 modules,
50 nA for type 2 modules
and **100 nA** for type 3 modules.

Requirement 15: The **voltage** (req. 6), **current** (req. 13) and **linearity** (req. 12) **calibration** must be certified for at least **one year** and the results must be documented .
The calibration procedure must be documented such that recalibration can be performed in situ at CERN.

3.3. Technical Requirements for the HV Subracks (Crates)

Five subracks will be mounted into each **Standard 19" ATLAS 52U Rack with Cooling System** located in the ATLAS control room USA15-Level-2. Rack specifications and a sketched arrangement of subracks within are given in **Annex 4**.

Requirement 16: The subracks must fit the 19" standard in width and must have not more than **6U in height**. For fan tray of 1U height refer to requirement 17,21 and 22.

Requirement 17: The **flow direction** of forced air cooling through the modules housed in rackmounted subracks must be **vertical** upwards.

Requirement 18: The subracks must be mountable on rails in the racks, such that the position of the connector front of the modules allows routing of the **HV-cables within the rack** through the rack top or the rack bottom (**closed door scenario**). Refer to sketch in Annex 4. The minimum bending radius of the multiwire HV cables is about 3 inch.

Requirement 19: Power input for the subracks must be **230 ± 10%VAC 50Hz monophase** using an **IEC connector**. A primary power supply needed within the subrack to drive the modules must use this power input and must be modular and exchangeble in situ.

Requirement 20:
Compliance with "CE" rules (Low Voltage Directives and EMC Directives) must be checked by an independent laboratory certified to do so.

Requirement 21: A modular **fan tray** with integrated dust filter and **1U in height** must be provided for insertion below the subrack. Its functioning must be monitored and ist must cope with Req. 17.

Requirement 22: .
The fan tray (Req. 21) **dust filter** must be removable for cleaning purposes. For the case that the subrack is mounted in the ATLAS standard rack this filter will not be inserted, in order to avoid stopping the cooled air flow within the rack.

3.4. Monitoring and Control Requirements

The ATLAS standard for remote monitoring and control of detector equipment is **CAN bus**.

Requirement 23: The controller interface within a HV module must comply with the CAN standard defined in CAN specification 2.0A.

Requirement 24: A cable must be provided to connect external floating power and the CAN bus to the module supply connector in order to be able to drive and monitor and control a HV module in stand alone mode (out of the subrack).

Requirement 25:

The following **software** and **hardware control and limiting functions** must be implemented:

Req 25. 1: Voltage setting **per channel** from Zero to Umax (ref. to Req. 5)

Req 25. 2: Voltage measuring **per channel**

Req 25. 3: Current measuring **per channel**

Req 25. 4: (Refer also to requirement 36.4)

Overcurrent fast trip for each **channel**.

Trip level setting via potentiometer **per module** for type 1,2 and 4 and **per channel** for type 3 modules. The tripping channel must be indicated in the status information. The **switch time** of the comparator must be ~ **2 µsec** or better.

Req 25. 5: (Refer also to requirement 36.4)

Overvoltage fast trip for each **channel**.

Trip level setting via potentiometer **per module** for type 1,2 and 4 and **per channel** for type 3 modules. The tripping channel must be indicated in the status information.The **switch time** of the comparator must be ~ **2 µsec** or better.

Req 25. 6: (Refer also to requirement 36.4)

Overvoltage and Overcurrent trip level setting **per channel** via **firmware**.

The **switch time** must be ~ **2 msec** or better.

The tripping channel must be indicated in the status information.

Req 25. 7: (Refer also to requirement 36.4)

In case of trip of a channel the module must send an error flag via the CAN bus to the control program.The error flag **generation time** must be ~ **10 msec** or better and the channel status involved must be indicated.

Req 25. 8:

Up/ down **ramping** control **per channel** within steps ranging from 1 to 200 V/sec aswell as channel or module switch off function by discharging according to the enabled mode of Requirement 36.4.

Req 25. 9:

Low frequency (1Hz) **periodic ramping** within a voltage window of **50V** ± **20V**.

Req 25. 10:
The module firmware watchdog must generate auto reset and put channels to zero.
Req 25. 11:
CAN bus connection loss/resume/reset must not change the channel status.
Req 25. 12: Interlock status must be indicated for each module and subrack. Refer to requirement 36.3.
Req 25. 13: Live insertion and extraction of modules must be supported.

Requirement 26: The module temperature must be measured and read out.

Requirement 27: Readout latencies for **125 kbit/sec** CAN bus transfer mode must be better than:
10 sec / 1000 channels in case of 3 values (I,U,Status) read out for every channel
4 sec / 1000 channels in case of 1 packet (I,U,Status) read out for every channel.
The **250 kbit/sec** CAN bus transfer mode must be selectable with correspondingly reduced latencies.

Requirement 28: The internal **refresh cycle** must be better than:
500 msec for 16 bit ADC resolution (type 3 modules)
200 msec for 12 bit ADC resolution (type 1,2 and 4 modules)

Requirement 29: The control software must run on **MS-Windows-2000** PC systems and must be adapted for future **system and SCADA software** upgrades. Adaptation after the guarantee period has elapsed shall be considered as a repair.Refer to Article 3.3 of the Tender Form.

Requirement 30: The PC to CAN bus interface must have optical coupling.

Requirement 31: The collected control and monitoring data must be offered to clients via an **OPC server** implementation into the control software.

Requirement 32: The remote control and monitoring of the subrack and primary power supply parameters must be implemented using CAN bus standard. Parameters must include:
Subrack supply voltages and temperature, On/Off of internal supply voltages.

Requirement 33:
Firmware upgrade and calibration parameters must be downloadable via CAN bus.

3.5. Environmental Conditions and Reliability Requirements

The HV system will be operated at

temperatures of 20 C ± 5 C

and **humidity of < 70%**

controlled environment, within closed racks (cabinets) operating with a controlled, forced airflow cooled by air/water heat exchangers (see Annex 4 and requirements 16 to 20). The maximum cooling power per rack is 9 kWatts.

In test set-up applications, it will be operated in a normal laboratory environment (refer also to requirement 21 and 24).

The system will operate in **normal magnetic** (< 50 Gauss) and **normal radiation environment**.

The **warm-up time** to rated accuracy is **one hour**.

The HV power supply system will be in service for **fifteen years** starting 2005.

Requirement 34:
The calculated **MTTF** for the HV system parts must be **100.000 hours** or more. The system must be protected against dust contamination in case of use outside of the rack (refer to requirement 21).

Requirement 35:
The test, operation and calibration procedures for the system must be documented and must be such, that they can be performed by ATLAS personnel at CERN. This applies especially to all calibration tasks referred to in requirement 15.

Requirement 36:
Failsafe installations to protect the HV system against power failure, control failure and mistaken cable connection must be provided:

Req 36. 1: Watchdog implementation for firmware with auto reset function as cited in requirement 25.10.
Req 36. 2: The channel status must be conserved in case of CAN bus disconnect or control PC failure (refer to requirement 25.11).

Req 36. 3:
Interlock circuitry (Safety Loop) with **status control** (requirement 25.12) must be implemented to be fed by the following external sources:

Source type 1: HV cable disconnect must trip and discharge all channels of the corresponding module. In order to accomplish this function the cable and connectors have a dedicated interlock pair of wires and pins respectively (see Annex 3).
Source type 2: External interlock via optically coupled DC-level fed to module SL-connector must trip and discharge all channels of that module.
Source type 3: External interlock via optically coupled DC-level fed to subrack SL-connector must trip and discharge all modules of that subrack..
Source type 4: Operator interlook via the control software and CAN bus.

For all interlock cases the selected discharge modus according to Requirement 36.4 must apply.

Req 36. 4: A channel must discharge if trip conditions are fulfilled (refer to requirements 25.4, 25.5, 25.6, 25.7).
Two alternatively **selectable discharge modes** must be implemented to achieve the corresponding discharge times cited in **Table 1**:
Mode 1:
Discharge of the concerned channel via the internal **HV module resistor** (~ 50 MOhm) left in after disconnecting from the regulation.
Mode 2: Discharge via **reed relay** (0 Ohm) of a **group of 16 channels** for type 1,2 and 4 modules and a **group of 8 channels** for type 3 modules if the trip channel is a member of the group.

Requirement 37:
The HV system must fulfill the relevant European safety regulations and electrical **EMC** standards.
The HV system must be conform to the **CERN Electrical Safety Code** (**Annex 5**) and to the **CERN Safety Instruction 41** (IS41) regarding " The use of Plastics and other Non-Metallic Materials at CERN with respect to Fire Safety and Radiation Resistance" (see also requirement 20).

Requirement 38:
The voltage difference between the safety ground and the return of the HV lines must be limited via two anti-parallel suppressor-diodes with V_Z = 56 Volt.
Refer also to requirement 2,3 and 4.

3.6. Documentation

Requirement 39:
All Documentation describing the technical characteristics of all the system components must be delivered in English. The documentation must include:

1) The functional diagram of the High Voltage Supply System
2) The organisation of the components of module boards and subracks
3) Description of the control software and CAN bus read out structure

Requirement 40:
Additional documents in English:

1) The instructions for use (user's guide, user's reference manual, etc.)
2) The technical description (functional block diagram, electrical schematics, etc.) of each module type and of the subrack
3) Documents containing the diagrams of the installation
4) Initial test and calibration report
5) Test, operation and calibration instructions
6) Full manufacturing documents conditionally

Annex 1: Multi core 37-fold HV cable specification

KERPEN High Voltage Cable SL – v2YCeH
(multi core) 6 kV (DC) / 70C
screened zero halogen, flame retardant

Application

Used as fixed or flexible installed control cable for high voltage (dc) supply for electrical equipments and control units in research. For indoor and outdoor use in dry and wet locations. With reduced smoke emission, corrosiveness and toxicity of combustion gases acc. to CERN safety instruction IS 23.

Construction

- **Cores**
  Conductor.....Tinned copper, flexible stranded, AWG26/7
  Insulation.....Polyethylene
  Colour Code..Natural-coloured

- **Further Construction**
  Wrapping.....Min. 1 layer of plastic tape, nom. 36µm
  Screen.....Tinned copper wire braid, opt. coverage min. 80 % over tinned copper drain wire, AWG26/7
  Outer Sheath.Zero halogen, flame retardant polymer
  Colour.....Red

- **Cable Marking**
  Imprint.....**KERPENWERK TYPE 6kV(DC) ZERO HALOGEN yyWww Length marking**
  Manufacturer's identification thread

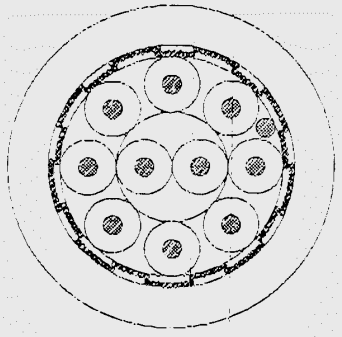

Technical Data

Flame retardancy:	IEC 60332-1	***Temperature range:***	-30°C up to +70°C
Flame propagation:	IEC 60332-3 cat. C	*(during operation)*	
Smoke density:	IEC 61034-1 and -2		-5°C up to +50°C
Amount of halogen acid gas:	IEC 60754-1; 0%	*(during installation)*	
Degree of acidity of gases:	IEC 60754-2		
Outer sheath:		***Min. bending radius:***	
Limiting Oxygen Index (LOI):	**min. 43%** (IEC 60332-3 ann. B)	6 x cable-Ø *(fixed installation)*	
Temperature Index (TI):	**min. 260°C** (ASTM-D-2863)	10 x cable-Ø *(flexible installation)*	

Abbreviations

SL-	high voltage cable
v	tinned copper conductor
2Y	insulation of PE
C	screen
E	drain wire
H	outer sheath of LSZH

Test voltage

	Character	Unit	Values
Core/Core	*nom.*	kV (DC)	12
Core/Screen	*nom.*	kV (DC)	12

High Voltage Cable **SL – v2YCeH**
(multicore) **6 kV (DC) / 70C**
screened **zero halogen, flame retardant**

37xAWG 26/7, red

Geometrical and Electrical Data

Number of Cores	Conductor		Core	Cable				Part Number
	Single-wire-Ø (nom.) mm	Conductor resistance at 20°C (max.) Ω/km	Core-Ø (approx.) mm	Screen-wire-Ø (nom.) mm	Sheath-thickness (nom.) mm	Overall Diameter (approx.) mm	Weight (approx.) kg/km	
Conductor Size AWG26/7								
10	0.16	147	1.3	0.15	1.0	8.1	85	
20	0.16	147	1.3	0.15	1.0	9.7	120	
23	0.16	147	1.3	0.15	1.2	10.7	145	
25	0.16	147	1.3	0.15	1.2	11.2	155	
30	0.16	147	1.3	0.15	1.2	12.0	170	
32	0.16	147	1.3	0.15	1.2	12.0	180	
34	0.16	147	1.3	0.15	1.2	12.4	190	
37	0.16	147	1.3	0.15	1.2	12.4	195	
52	0.16	147	1.3	0.20	1.2	14.4	265	
56	0.16	147	1.3	0.20	1.2	14.8	280	

Annex 2: <u>Multi pin HV connector specification</u>

The specifications below refer to the REDEL Kft **S series**. Please consult the LEMO-REDEL Kft catalog, April 2000, page 16,18,19 and 20 for details.

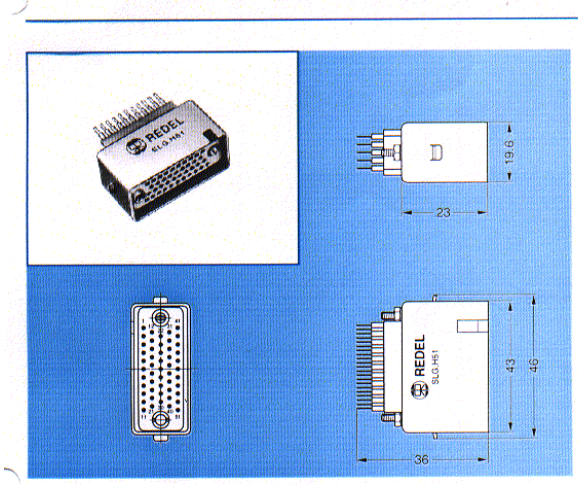

SL● Fixed socket with key (code G or A), two screw fixing

Part Number	Cable Group	Contact Type	Marking
SLG.H51.LLZG	no contact	male	black
SLA.H51.LLZG		female	red
SLG.H51.LLA1G	1	male	black
SLA.H51.LLL1G		female	red
SLG.H51.LLA2G	2	male	black
SLA.H51.LLL2G		female	red

S series chassis panel cut-out

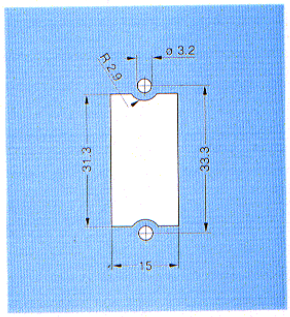

S series

ACCESSORIES

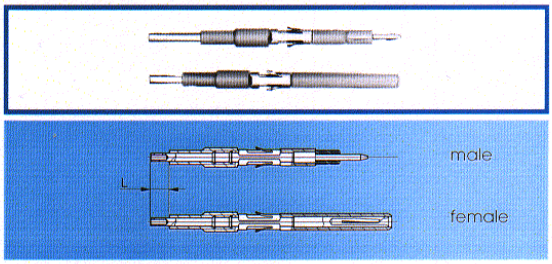

FFA-ERA High Voltage Contacts

Contact Part Number		Cable group	L (mm)
Male contact	Female contact		
FFA.05.403.ZLA1	ERA.05.403.ZLL1	1	4
FFA.05.403.ZLA2	ERA.05.403.ZLL2	2	6

Annex 3: <u>Pin layout for HV chassis connector</u>

The pin assignment for the LEMO-REDEL Kft **S series SLG.H51.LLZG** chassis connector, as mounted on the HV module front panel, is shown below.
HV pins of LEMO type **male FFA.05.403.ZLA1** are numbered from **0 to 31** (HV modules 1,2 and 4).
For HV modules of type 3 only pin position **0 to 15** are used.
Common pins C are of the same type as the HV pins and positionned at the corners.
The gide male pin sits at the top and the gide female pin sits at the bottom.

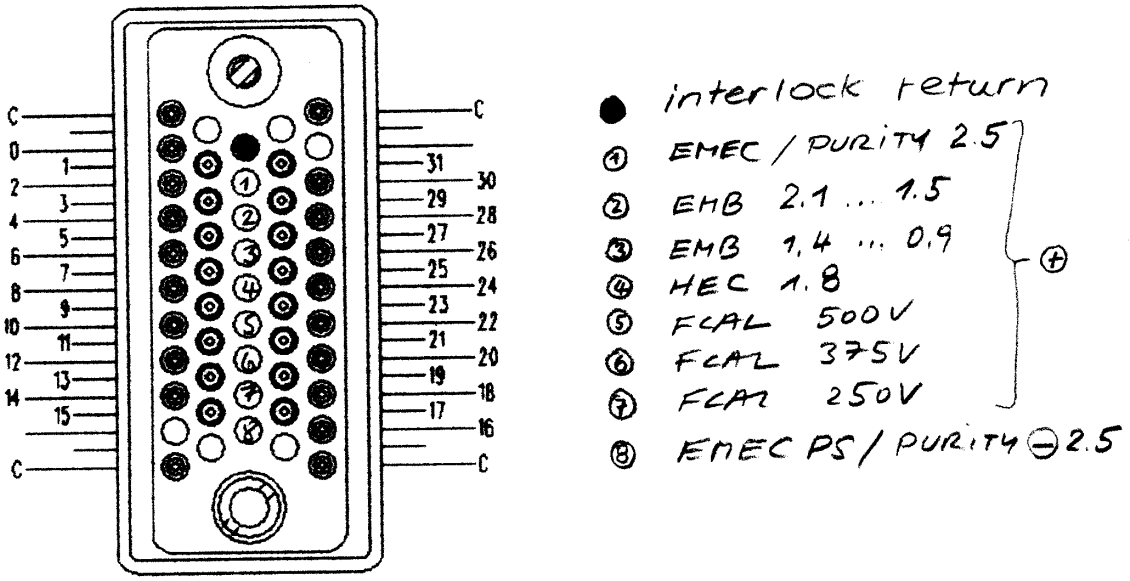

The interlock return pin is sitting at the top of the central pin column.
One of eight interlock key pins attributed to its kind of module sits in the central column (position 1 to 8 counted from below top).
All **male interlock pins** are of LEMO type **FGG.2B.565.ZZC**

EARTHING CONTACT Interlock

Usually, some H.V. contacts are used to connect earthing from the cable shield to the instrument panel. For such earthing connection it is also possible to use L.V. crimp contacts. With a crimp barrel of 1,4 mm, these contacts can be used with wires AWG 18-20.

Connector models	Contact part number	Positioner part number	Crimp tool part number
KAG-KLA-KRA-SAG-SLA-SRA	FGG.2B.565.ZZC	DCE.91.132.BVC	DPC.91.701.V[1)]
KAA-KLG-KRG-SAA-SLG-SRG	EGG.3B.665.ZZM	DCE.91.133.BVM	

M F

Note: 1) according to specification MIL-C-22520/7-01

Termination instructions
Refer to 05 series (page 6 & 7) for each individual H.V. contacts

Annex 4: ATLAS rack specification

The ATLAS Standard racks are 19 inch electronic enclosures in compliance with **IEC-60297 part 1 and 2 (for max weight 500 kg)**.

The external dimensions are:

52U x 600 mm x 900 mm

The front and rear door structure is symmetric to allow opening right or left.

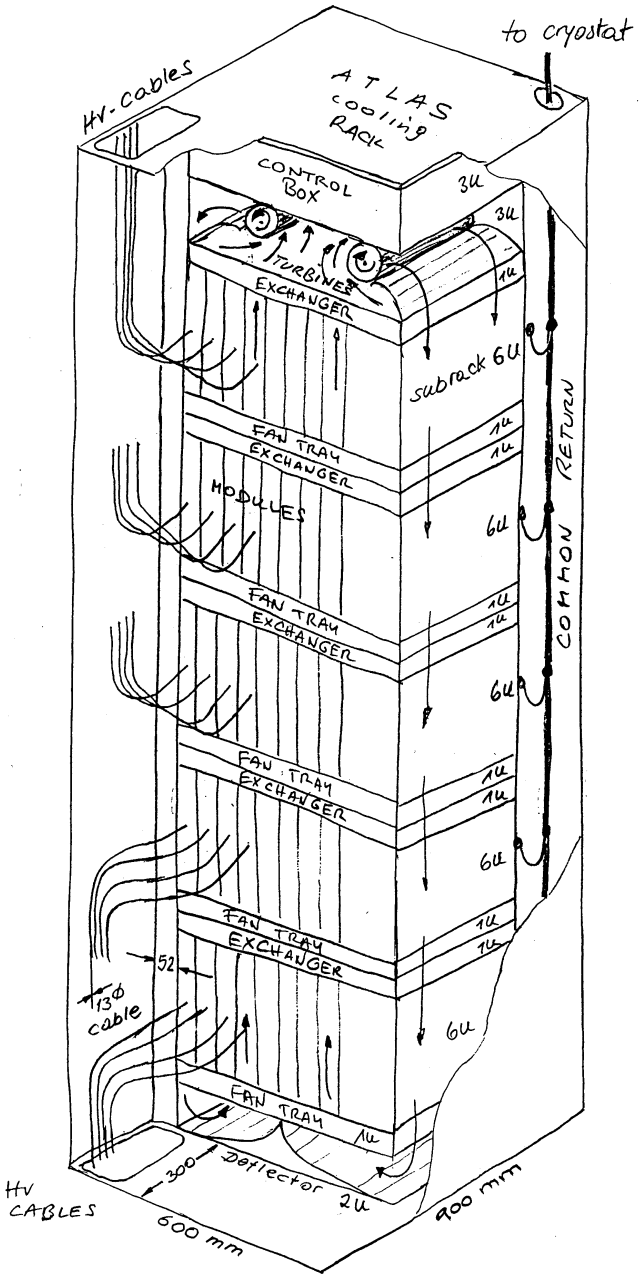

Annex 5: CERN Electrical Safety Code

The CERN **Electrical Safety Code** can be consulted directly by selecting the underlined title or via the following Web-Link to CERN:
http://cern.ch/CERN/Divisions/TIS/safdoc/CODES/C1/electrical_code.html

The printed version can be made available on request.

Annex 6: Glossary of Terms and Abbreviations

ATLAS =
A Toroidal LHC Apparatus

Liquid Argon Calorimeter Detectors:
EMB = Electromagnetic Barrel Detector
EMB-PS = Electromagnetic Barrel Detector Presampler
EMEC = Electromagnetic End-Cap Detector
EMEC-PS = Electromagnetic End-Cap Detector Presampler
HEC = Hadronic End-Cap Detector
FCAL = Forward Calorimeter Detector
PCD = Purity Control Detector

CERN =
Conseil Européen pour la Recherche Nucléaire
which was turned into
"European Organization for Nuclear Research"
as official name.

EMC =
ElectroMagnetic Compatibility

LHC =
Large Hadron Collider

MTTF =
Mean Time To Failure

OPC =
OLE Process Control (a MicroSoft term)

QAP =
Quality Assurance Plan

SL =
Safety Loop

SCADA=
Slow Control and Data Aquisition

Appendix B

FCal high-voltage power supply datasheet

16-channel High Voltage Power Supply EHQ F 006p_605-F

The EHQ F 006p-F is a 16-channel high voltage power supply in 6U Eurocard format. Each single channel is independently controllable. The outputs HV-out (-) - floating HV-GND - and HV-out (+) of each channel are both floating against each other and against ground.
The EHQ F 006p-F is made ready for mounting into a crate. It is also possible to supply the modules separately with the necessary power. The unit is software controlled via CAN Interface directly through a PC or similar controller. The HV output at the EHQ F 006p-F is available with ERNI-Multipin-Connector or with REDEL-Connector.

2. Technical data

	EHQ F 006p_605-F
Output current I_O	max. 6 mA
Output voltage V_O	0 to + 600 V
Floating	Connector HV-out (-) to GND: ≤ |15 V| Connector HV-out (+) to GND: ≤ |15 V| + V_O
Ripple and noise	f = 10 Hz to 100 kHz: < 50 mV (at max. load and f > 100 kHz: < 50 mV V_O > 50 V)
Hardware current limit I_{max}	Potentiometer per channel internal
Interface	CAN-Interface
Voltage setting	Via software, resolution 12 mV
Voltage measurement	Via software, resolution 12 mV
Current measurement	Via software, resolution 120 nA
Accuracy of voltage measurement	< ± 200 mV
Accuracy of current measurement	± (0,01% ∗ I_O + 0,01% ∗ $I_{O\,max}$ + 1 digit)
Temperature coefficient	< 5 ∗ $10^{-5}/_K$
Stability	< 100 mV (no load/load and Δ V_{IN})
Rate of change of output voltage	Via software: 0,2 V/s to 50 V/s resolution 0,5 V
Channel control via software	Status 8 bit: channel error, KILL- enable, channel emergency cut-off, ramp, channel on/off, input error, current trip
8 channels error control via software	Current limit ("Channels are OK" is signalled if these limits do not exceed on each.)
Error signal with green LED	"Channels 0-7 OK" and "Channels 8-15 OK"
Protection loop (I_s) (2 pin Lemo-socket)	5 mA < I_s < 20 mA ⇒ module on I_s < 0,5 mA ⇒ module off
Power requirements V_{IN}	+ 24 V (< 2 A) and + 5 V (< 0,5 A)
Packing	16-channels in 6U Euro cassette (40,64 mm wide and 220 mm deep)
Connector	96-pin connector according to DIN 41612
HV connector	32-pin Erni Multipin-Connector or REDEL-Connector

3. Handling

The supply voltages and the CAN interface is connected to the module via a 96-pin connector on the rear side of the module. The 16 channel version is added with two independently boards.

The maximum output current for each channel is defined through the position of the corresponding internal potentiometer $I_{max}0$ to $I_{max}7$ per board.
The output current will be limited to the setting value after it exceeds the threshold and the green LED on the front panel is 'OFF'.

At the bottom on the right side of the front panel is the socket for the safety loop. If the safety loop is active then output voltage on all channels is only present if a current is flowing in a range of 5 to 20mA of any polarity (i.e. safety loop closed). If the safety loop is opened during operation then the output voltages are shut off without ramp and the corresponding bit in the 'Status module' will be cancelled. After the loop will be closed again the channels must be switched 'ON' and a new set voltage must be given before it is able to offer an output voltage. The pins of the loop are potential free, the internal voltage drop is ca. 3 V. Coming from the factory the safety loop is not active (the corresponding bit is always set). Removing of an internal jumper makes the loop active (s. App. A).

The connector HV-out (-) - floating HV-GND - of each channels should be connected to ground at a certain chosen point. Otherwise it must be sure, that the potential between HV-out (-) and GND should not exceed the amount of $|15\ V|$.

Pin assignment 96-pin connector according to DIN 41612:

PIN		PIN		PIN		Data
a1 a3 a5		b1 b3 b5		c1 c3 c5		+5V +24V GND
a11		b11		c11		@CAN_GND @CANL } potential free @CANH
a13		b13				RESET OFF with ramp (e.g. 10s after power fail)
a30 a31 a32	A4 A2 A0	b30 b31 b32	A5 A3 A1	c30 c31 c32	GND GND GND	} Address field module address (A0 ... A5)

The hardware signal "OFF with ramp" (Pulse High-Low-High, pulse width ≤ 100 µs) on pin b13 will be shut off the output voltage for all channels with a ramp analogue to the Group access "Channel ON/**OFF"**. The ramp speed is defined to V_{OUTmax} / 50 s. This is the actually module ramp speed after "OFF with ramp".
With help of the Group access "Channel **ON**/OFF**"** all channels are switched "ON" again.

With the address field a30/b30 ..... a32/b32 the module address will be coded.
Connected to GND ⇒ A(n) = 0 ; contact open ⇒ A(n) = 1

iseg Spezialelektronik GmbH
Bautzner Landstr. 23
D - 01454 Radeberg/Rossendorf
Email: sales@iseg-hv.de
http://www.iseg-hv.com
Germany
Phone ++ 49 351 / 26 996 - 0
Fax ++ 49 351 / 26 996 - 21

Communication via interface

Device Control Protocol DCP

The communication between the controller and the module works according to the Device Control Protocol DCP, which has been designed for the use of multi-level-hierarchy systems for instruments.

This protocol works according to the master slave principle. Therefore, the controllers who are on higher hierarchy always are masters while devices, which are in lower hierarchy, work as slaves.

In the event of the control of the HV device through a controller the controller will have the master function in this system, while the module (as a Front-end device with intelligence) will be the slave.

The data exchange between the controller and the Front-end (FE) device works with help of data frames. These data frames are assembled of one direction bit DATA_DIR, one identifier bit DATA_ID and further data bytes. The direction bit DATA_DIR defines whether the data frame is a write or read-write access. The DATA_ID carries the information of the type of the data frame and occasionally sub addresses (G0, G1). It is characterised through the first byte of the data frame with bit 7=1. The function of the module as part of a complex system will be defined through the DATA_ID .

In such systems with many hierarchical levels a single function of a single module can be addressed by using group controllers (GC). Then, for each GC on the way to the module the data frame is crated through nesting of the address fields of the GC-addresses followed by the DATA_ID (not necessary in case of control a single module).

EXT_ INSTR	DATA _DIR	DATA_ID Bit								Access
		7	6	5	4	3	2	1	0	
	x	**0**	x	x	x	x	x	x	x	**No** DATA_ID
0/1	**0**	1	0	x	x	x	x	x	x	**Write access** on Front-end device
0/1	**1**	1	0	x	x	x	x	x	x	**Read-write access** on Front-end device (Request at Write)
0/1	**0**	1	1	x	x	x	x	**G1**	**G0**	**Write access** on group
0/1	**1**	1	1	x	x	x	x	**G1**	**G0**	**Read-write access** on group (Request at Write)
										G0, G1 sub address Only needed if group controller (GC) is used

These data frames correspond to a transfer into layer 3 (Network Layer) respectively layer 4 (Transport Layer) of the OSI model of ISO. The transmission medium is CAN Bus according to specification 2.0A, related to level1 (Physical Layer) and level 2 (Data Link Layer).

The Device Control Protocol DCP has been matched to the CAN Bus according to specification CAN 2.0A, but it is also possible to be matched to further transmission media (e.g. RS232). Therefore specials of layer 1 and 2 are only mentioned if absolutely necessary and if misunderstandings of functions between the Transport Layer and functions of the Data Link Layer may be possible. The communication between the controller and a module on the same bus segment will be described as follows.

Summary of CAN data frames

Following list describes the accesses of the DCP made for the 8-channel module EHQ 8005-F.

EXT_ INSTR	DATA_ DIR	DATA_ID Bit								Access	read/ write/ active	DATA - Bytes
ID1	ID0	7	6	5	4	3	2	1	0			
	x	**0**	x	x	x	x	x	x	x	**No DATA_ID**		
x	**x**	**1**	**0**	**C1**	**C0**	**N3**	**N2**	**N1**	**N0**	**Single access CHANNEL:**		
1	1/0	1	0	0	0	N3	N2	N1	N0	Current trip	r/w	4
0	1	1	0	0	0	N3	N2	N1	N0	Actual voltage	r	4
0	1	1	0	0	1	N3	N2	N1	N0	Actual current	r	4
0	1/0	1	0	1	0	N3	N2	N1	N0	Set voltage	r/w	4
0	1	1	0	1	1	N3	N2	N1	N0	Status channel	r	3
		1	**1**	**C3**	**C2**	**C1**	**C0**	**G1**	**G0**	**Group access module**		
1	1	1	1	0	0	0	0	0	0	Voltage supplies and module temperature	r	8
1	1	1	1	0	0	0	1	0	0	offen	r	8
1	1	1	1	0	0	1	0	0	0	Placed hardware channels	r	3
1	1	1	1	0	0	1	1	0	0	Channel works according control	r	3
1	1	1	1	0	1	0	0	0	0	Status4 Sense voltage ≠ Set voltage	r	3
0	1/0	1	1	0	0	0	0	0	0	General status module	r/w a	2
0	1	1	1	0	0	0	1	0	0	Status1 Voltage limit was exceeded at single channel	r	3
0	1	1	1	0	0	1	0	0	0	Status2 Hardware current limit was exceeded at single channel	r	3
0	1/0	1	1	0	0	1	1	0	0	Channel ON / OFF	r/w	3
0	1/0	1	1	0	1	0	0	0	0	Ramp speed	r/w	3
0	0	1	1	0	1	0	1	0	0	Emergency cut-off	w	3
0	1	1	1	0	1	1	0	0	0	Log-on Front-end device in superior layer	a	3
0	0	1	1	0	1	1	0	0	0	Log-off superior layer at Front-end device	w	3
0	1/0	1	1	0	1	1	1	0	0	Bit rate	r/w	3
0	1/0	1	1	1	0	0	0	0	0	Serial number, software release and CAN message configuration	r/w	7/2
0	0	1	1	1	0	0	1	0	0	Set voltage for all channels	w	4
0	1/0	1	1	1	0	1	1	0	0	KILL-enable	r/w	3
0	1/0	1	1	1	1	0	0	0	0	ADC filter setting	r/w	3
0	1	1	1	1	1	0	1	0	0	Module nominal values	r	5
0	1	1	1	1	1	1	0	0	0	Status3 Software current trip was exceeded at single channel	r	3

C_i: Accesses	N_i 0 to 15: Channel 0 to 15
G_i 0 to 3: Group 0 to 3 Only needed if group controller (GC) used	

Appendix C

High-voltage crates manual

Manual extension

Crate ECH 228 to

Crate ECH 238 and option UPS

with CAN-Control

The crates ECH 238 are supplied with a controller for remote and monitoring control via CAN-bus.

Option UPS:
together with an UPS and a battery back up, short term power failure (<10s) can be bridged and in case of longer AC power failure a defined shut down procedure for the HV modules is guaranteed.

Installation

After unpacking the crate has to be installed under the described condition.
For crates with UPS option the 16A fuse which is included has to put into the fuse holder on the rear side.
Afterwards the battery is activated.
With AC line ON the crate is in Stand-by mode.

Technical Data version 1.	
CAN bus speed	20, 50, 100, 125 and 250 kbit/s
Analogue functions	ADC with 10-Bit resolution, control of supplies voltages and temperature of this crate.
Digital functions	ON – and OFF switch of internal supply voltages via CAN-Bus in Stand-by mode
Power-ON/OFF	Power cable connected and AC line is ON, now the crate is in Stand-by mode. In Stand-by mode the internal DC supply voltages can be switched ON and OFF with help of a push button, even if no CAN-control is present.
With option UPS	In case of AC power failure the internal voltages are saved by the acc. battery. If the power is failing more than 10 sec. a signal will be provided , which is going to start a defined shut down procedure. (HLH- impulses on each module-slot, Pin b13). The bridge time for the battery is 1 min at least.

CAN-Interface

The CAN-control is completely configurable via software. The Structures is following to CAN-Open (CAL-based Draft Standard 301 / release 3.0).

After Power_ON-Reset the controller is running into CAN-Status “Initialisation“. During this state Write access is possible to all EEPROM-cells via the sub identifier. If control is already configured (e.g. from factory), control is running into CAN-status “Pre-operational”.

Only in these both states it is possible to work with services Network-Management (NMT) and Distribution - Management (DBT).

iseg Spezialelektronik GmbH
Bautzner Landstr. 23
D - 01454 Radeberg / Rossendorf
Email: sales@iseg-hv.de
http://www.iseg-hv.com
Germany
Phone ++ 49 (0)351 / 26 996 - 0
Fax ++ 49 (0)351 / 26 996 - 21

CAN-Status “Pre-operational“ is necessary for the further description.

In order to allow the control of the crate via CAN-Bus, with global command „START“ the CAN-Status „Pre-operational“ will be switched into CAN-Status “Operational“:

Services	ID (with RTR =0)	DLC	DATA_1
Network - Management (NMT)			
START / STOP / RESET global broadcast message to all ECH CAN nodes	0	1	Bit 0 = 1 ⇒ Start Bit 1 = 1 ⇒ Stop Bit 2 = 1 ⇒ Reset CAN-interf. Bit 3 = 1 ⇒ Reset Controller

Now control can work via two identifier (see ID - Distribution):

1. Control (EMCY-ID)

The internal supply voltages will be controlled cyclically (V_{Meas} ca all 100 ms). The voltage control is factory fixed with $\Delta V = \pm$ 5% given through tolerance values $V_{Trehsold}$ in an EEPROM. If the thresholds of voltage and/or temperature will be exceeding then the controller is sending a message with EMCY-ID to the Bus (send only).

Controls of EMCY-ID´s are working only after the controller has been set into Operational mode with NMT-Start.

ID	RTR	DLC	Voltage	DATA_2	DATA_3	DATA_4	DATA_5	
EMCY-ID	0	5	0 0 0 0 0 0 x x x	12-bit unsigned ADC-word: V_{Meas}		12-bit unsigned ADC-word: $V_{Threshold}$		xxx: 000 + 24 V = $V_{Nominal\ 0}$ 001 + 5 V = $V_{Nominal\ 1}$ 010 $24V_{Battery}$ = $V_{Nominal\ 2}$
				V_{Meas} resp. $V_{Threshold} = V_{Nominal\ x} * ADC\text{-word} / 2048$				

ID	RTR	DLC	Temperature	DATA_2	DATA_3	DATA_4	DATA_5	
EMCY-ID	0	5	0 0 0 0 0 0 x x x	0	T_{Meas} [°C]	0	$T_{Threshold}$ [°C]	xxx: 011 temperature sensor 1 (24V-DC PS) 100 temperature sensor 2 (Back plane) 101 temperature sensor 3 110 temperature sensor 4 (3 and 4: reserved)

ID	RTR	DLC	AC line power failure signal	DATA_2	DATA_3	DATA_4	DATA_5	
EMCY-ID	0	5	0 0 0 0 0 0 x x x	0	0	7	7c	xxx: 111 AC line power failure

2. Subidentifier (Sub-ID)

E-command	ID	RTR	DLC	r/w	Command							DATA_n	Remarks
Multiplex-command	Sub-ID	0	x	x	0	x	x	x	x	x	x		multiplexed DAC/ADC – work on channels of selected module (Sub-ID)
ADC	Sub-ID	0	1	1	0	1	0	0	x	x	x		Read Access, (call from host)
	Sub-ID	0	3	1	0	1	0	0	x	x	x	2 Byte ADC-word	$V_{Meas} = V_{Nominal\ x} * ADC\text{-word} / 2048$ xxx: 000 + 24 V = $V_{Nominal\ 0}$ 001 + 5 V = $V_{Nominal\ 1}$ 010 $24V_{Battery}$ = $V_{Nominal\ 2}$
	Sub-ID	0	4	1	0	1	0	0	x	x	x	2 Byte ADC-value + 1 Byte fan status	ADC-value = Temperature [°C] Byte fan status = 0: stage 1, 1: stage 2, full cooling xxx: 011 temperature sensor 1 (Back plane) 100 temperature sensor 2 (24V-DC Power supply) 101 temperature sensor 3 110 temperature sensor 4 (3 and 4: not installed)
	Sub-ID	0	3	1	0	1	0	0	1	1	1	1. Byte AC line power status 2. Byte crate power status	Status AC line power 1: AC line power OK 0: AC line power wrong Capture status if voltages were out of range. Bit b7=1 temperature to high Bit b5=1 +24V to high Bit b4=1 +24V to low Bit b3=1 +5V to high Bit b2=1 +5V to low Bit b1=1 24V battery voltage to high Bit b0=1 24V battery voltage to low
	Sub-ID	0	3	0	0	1	0	0	1	1	1	1. Byte AC line power status 2. Byte crate power status	In order to reset the AC power line status it have to be set bit 0 to one in DATA_1. In order to reset the corresponding bit of the crate status it have to be set in the DATA_2.

<table>
<tr><td rowspan="2">Module-command</td><td>Sub-ID</td><td>0</td><td>x</td><td>x</td><td>1</td><td>x</td><td>x</td><td>x</td><td>x</td><td>x</td><td>x</td><td></td><td colspan="5">Use module functions of selected module (Sub-ID)</td></tr>
<tr><td>EEPROM</td><td>Sub-ID</td><td>0</td><td>2</td><td>1</td><td>1</td><td>0</td><td>0</td><td>0</td><td>0</td><td>0</td><td>0</td><td>EEPROM-address</td><td colspan="5">Read / Write access, (call from host)</td></tr>
<tr><td rowspan="5">/Tolerances</td><td rowspan="4">Sub-ID</td><td rowspan="4">0</td><td rowspan="4">3</td><td rowspan="4">1</td><td rowspan="4">1</td><td rowspan="4">0</td><td rowspan="4">0</td><td rowspan="4">0</td><td rowspan="4">0</td><td rowspan="4">0</td><td rowspan="4">0</td><td rowspan="4">Data_1:
EEPROM-address</td><td colspan="5">Byte oriented reading of tolerances from EEPROM-address:</td></tr>
<tr><td>V</td><td colspan="2">Higher ADC-threshold</td><td colspan="2">Lower ADC-threshold</td></tr>
<tr><td></td><td>High</td><td>low</td><td>high</td><td>low</td></tr>
<tr><td>+ 24 V
+ 5 V
$24V_{Battery}$</td><td>0x3d
0x41
0x45</td><td>0x3e
0x42
0x46</td><td>0x3f
0x43
0x47</td><td>0x40
0x44
0x48</td></tr>
<tr><td>Sub-ID</td><td>0</td><td>3</td><td>0</td><td>1</td><td>0</td><td>0</td><td>0</td><td>0</td><td>0</td><td>0</td><td>Data_1:
EEPROM-address
Data_2:
tolerance high/low</td><td colspan="5">-byte oriented writing of tolerances on above EEPROM-address, tolerance = word ADC-threshold
-tolerance = (calculated set-ADC-value) $*$ $(1 \pm \Delta V)$</td></tr>
</table>

E-command	ID	RTR	DLC	r/w	Command							DATA_n																Remarks
Module-commands	Sub-ID	0	x	x	1	x	x	x	x	X	x																	Use module function of selected modules (Sub-ID)
ON/OFF	Sub-ID	0	1	1	1	0	0	0	0	0	1																	Read / Write Access, (call from host)
	Sub-ID	0	3	1	1	0	0	0	0	0	1	0	0	0	0	0	0	0	x	0	0	0	0	0	0	0	1	x=0... switched on x=1... switched off Read/Write Access
ON/OFF	Sub-ID	0	3	0	1	0	0	0	0	0	1	0	0	0	0	0	0	0	x	0	0	0	0	0	0	0	1	x=0... switched on x=1... switched off Write Access
Bit rate	Sub-ID	0	1	1	1	0	0	0	0	1	1																	Read / Write Access, (call from host)
	Sub-ID	0	2	1	1	0	0	0	0	1	1	Data_0																Bit rate [kBit/s] Read/Write Access
Bit rate	Sub-ID	0	2	0	1	0	0	0	0	1	1	Data_0																New bit rate: only 20, 50, 100, 125 for bit rate [kBit/s] is allowed! Write Access
Unit-ID	Sub-ID	0	6	1	1	0	0	0	1	1	0	3 Byte BCD-unit-no. and 2 Byte BCD-software-release																

These identifiers will be fixed by ID - Distribution (DBT) Service:

ID - Distribution (DBT) Service	ID	DLC	DATA_1	DATA_n	remarks
DBT - Master - Request	2024d 7E8h (RTR=1)	0			Call from host only by connected module: message address and ID´s of module
DBT - Slave - Service	2023d 7E7h (RTR=0)	8	mod.-addr.	2 3 4 5 6 7 8	Message with module address and corresponding ID´s
DBT - Master - Service	2024d 7E8h (RTR=0)	8	mod.-addr.	0 0 EMCY -ID | Sub -ID | 0	
DBT - Master - Service ⇓	2024d 7E8h (RTR=0)	2	0x80	module-addr.	Call from host to module address: message of ID´s to address
DBT - Slave - Service	2023d 7E7h (RTR=0)	8	mod.-addr.	2 3 4 5 6 7 8	Message with module address and the corresponding ID´s

Example:	DBT-Master-Request	ID	RTR	DLC	Data
	send to crate	0x7E8	1	0	
	recive from crate	0x7E8	0	8	0x30 0x00 0x00 0x40 0x80 0x60 0x80 0x00
					mod.-addr. 0x30
					EMCY-ID 0x408 (left justified)
					SUB-ID 0x608 (left justified)

The remote control module will be configured with help of Network-Management (NMT) Service:

Network - Management (NMT)	ID	DLC	DATA_1	remark
NMT - Slave – Service (only in initialising mode)	2025d 7E9h	2	Mod.-addr. (0xFF)	After stop of CAN-Status (0x20): 0x80: Operational 0x40: Pre-operational 0x20: Initialisation
NMT - Master - Service	2026d 7EAh	2	Mod.-addr. old	Mod.-Adr. new, **Addr. 0x80 forbidden !**
Start / Stop / Reset global broadcast message to all ECH CAN nodes	0	1	Bit 0 = 1 ⇒ Start Bit 1 = 1 ⇒ Stop Bit 2 = 1 ⇒ Reset CAN-Interf. Bit 3 = 1 ⇒ Reset Controller	

Maintenance

The crate and the included battery are free from any support. If the crate is not in use for more than half a year it has to be connected to mains and switched ON for at least 8 hours, so that the batteries will be charged to full capacity again. After 5 years time the batteries have to be replaced by new ones.

Appendix D

OPC server manual

Chapter II

The isegHVOPCServer for iseg Multi-Channel HV systems

Document: **isegHVOPCServer.odt** Version: 5.01.0003 Date: **10/ August 2010 16:35**

iseg Spezialelektronik GmbH
Bautzner Landstr. 23
D - 01454 Radeberg / Rossendorf
Email: sales@iseg-hv.de
http://www.iseg-hv.com
Germany
Phone ++ 49 (0)351 / 26 996 - 0
Fax ++ 49 (0)351 / 26 996 - 21

Table of Contents

The isegHVOPCServer for iseg Multi-Channel HV systems....1
OLE for Process Control (OPC) for the iseg Multi-Channel HV systems....5
1 Introduction....5
2 Modules....6
3 Crates....6
4 Software....7
4.1 General information....7
5 OPC Server part for Multi-Channel HV devices....7
5.1 Configuration....7
5.2 Data Access Server and Alarm and Events Server....8
5.2.1 Data Access Server....8
5.2.1.1 Item's properties....9
5.2.1.2 Items of the status from the server components....10
5.2.1.3 Items of Data Access to the channel properties....12
5.2.1.4 Items of Data Access to the module properties....13
5.2.1.5 Items to signal an alarm from the HV devices via Data Access....14
5.2.1.6 Notes to the item Status channel (EHQ)....15
5.2.1.7 Notes to the item Channel status (EHS)....16
5.2.1.8 Notes to the items of the Channel control (EHS)....16
5.2.1.9 Notes to the item Channel event status (EHS)....17
5.2.1.10 Notes to the item Channel event mask (EHS)....17
5.2.1.11 Notes to the item Module status (EHS)....18
5.2.1.12 Notes to the items of the Module control (EHS)....18
5.2.1.13 Notes to the item Module event status (EHS)....19
5.2.1.14 Notes to the item Module event mask (EHS)....19
5.2.1.15 Notes to the item Event channel status (EHS)....19
5.2.1.16 Notes to the item Event channel mask (EHS)....19
5.2.1.17 Notes to the item General status (EHQ)....20
5.2.1.18 Notes to the items VsetAllChannels, ITripAllChannels and ISetAllChannels....21
5.2.1.19 Notes to the item Configuration of the relay and regulation error....21
5.2.1.20 Notes to GroupNumber and GroupVariable (EHS)....22
5.2.1.21 Notes to the item Alarm information....25
5.2.1.22 Notes to the item Option (EHS)....25
5.2.1.23 Notes to OptionSingleSpec (EHS)....25
5.2.1.24 Items for public groups defined by the OPC server:....26

5.2.2 Alarms and Events server....28
5.2.2.1 Simple events....28
5.2.2.2 Tracking events....28
6 OPC server part for iseg system crate ECHx38....29
6.1 Configuration....29
6.2 Data Access Server and Alarm and Event Server....29
6.2.1 Data Access Server....29
6.2.1.1 Items of the releases from the server components....30
6.2.1.2 Items of Data Access....30
6.2.1.3 Crate power status....31
6.2.2 Alarm and Events Server....31
Appendix A 32

iseg Spezialelektronik GmbH
Bautzner Landstr. 23
D - 01454 Radeberg / Rossendorf
Email: sales@iseg-hv.de
http://www.iseg-hv.com
Germany
Phone ++ 49 (0)351 / 26 996 - 0
Fax ++ 49 (0)351 / 26 996 - 21

OLE for Process Control (OPC) for the iseg Multi-Channel HV systems

The isegHVOPCServer as a part of OLE process control is the link between the OPC client, the iseg Multi-Channel HV modules and / or the iseg system crates.

1 Introduction

The **iseg** Multi-Channel HV system is made of several devices of hardware and software components. The hardware devices are as follows:

- Multi-Channel HV power supply modules
- System crates carrying the HV modules

Each module and each crate offers a microprocessor-based intelligence. The interface which controls and monitors the hardware is the CAN bus. It is following the CAN 2.0B (passive) specification. The data points for the accesses to the module and the crate properties comes together in one executable file and can work on one CAN bus or on different CAN buses in conformity with the configuration files.
The system software interface is made by an OPC server, which follows the rules defined by the OPC Foundation (DA 3.0, 2.0 and 1.0 are supported). Therefore the users of the system must not know the internal protocols in detail.
In order to understand the OPC interface (server namespace), the relevant details of the modules and the crates are described as follows:

2 Modules

Each modules offers up to 32 channels, made of one or two internal cards (PCB). Each internal card represents one CAN node (the most of the modules have 16 channels per card, some modules comes also with another number of channels per card – see instruction "Placed hardware channels" of the EHQ Multi-Channel CAN operators manual). Each channel of the module offers individual properties (see below).
In addition there are properties as groups that summarize a property for all channels and which are controlled by one CAN node.

Properties of one channel:

- set voltage write / read
- current trip write / read
- actual current read
- actual voltage read
- status read

Properties of a channel group (some examples):

- sum error read
- ramp speed read / write
- set voltage for all channels write
- emergency cut-off write

3 Crates

Properties of a crate (some examples):

- actual voltage of single lines read
- temperature read
- Power ON / OFF read / write
- Status read / write
- StatusACLinePower read

The most important information of the crate is the status of the power supplies.

4 Software

4.1 General information

The ***isegCANHVControl.exe*** control software performs all basic monitor and control tasks for modules and crates. It provides a HMI (human machine interface) for all properties of the modules and crates using the proprietary driver of the CAN interface (PEAK). It can be used in order to configure the modules and crates before the work with the ***isegHVOPCServer***. Such configurations are the flash update, changing the bit rate and identifiers for crates, the offset calibration of the module temperature and the permanent saving of setting values inside of the modules.
An alternative and more general control software is based on the standardized OPC interface. With means of the OPC tools is it possible to establish a sever client system in order to access the iseg Multi-Channel HV system, too. The properties of the Multi-Channel HV hardware can be accessed via the item data points.

5 OPC Server part for Multi-Channel HV devices

The OPC server has been developed using the following tools:

- Softing OPC Toolkit, Ver. 4.10, DA 3.0, AE1.01
- Microsoft's Visual C++, Ver. 6.01
- PEAK System's CAN device driver

The OPC server for Multi-Channel HV system is divided into 'Data Access' part and an 'Alarms and Events' part.

5.1 Configuration

First the OPC server has to be configured. It must get all information about the kind of **iseg** HV hardware connected to the CAN bus. This information is stored in the configuration file ***isegHVOPCServer.ini***. The tool ***isegHVOPCcfg.exe*** is used to create this configuration file. It performs a scan on the CAN bus and collects information from the connected CAN nodes (modules and crates). Also it supports the graphical access to the initialising file ***isegHVOPCServer.ini***.
For further details see the configuration manual ***isegHVOPCSetup.pdf***.

5.2 Data Access Server and Alarm and Events Server

5.2.1 Data Access Server

The OPC DA server is made to work with more than one crate. Therefore each item has to be addressed in a geographical way to build a fully qualified item ID that means:

STATUS.COMPONENT	iseg OPC server components (software releases and status of CAN bus)
CANBUS.NODE.CHANNEL.ITEMNAME	data point for channel depending properties
CANBUS.NODE.ITEMNAME	data point for module depending properties

By the use of a special namespace text file – ***isegHVOPCServer.nsp*** – can build user defined fully qualified item IDs. The description is placed in the file ***isegHVOPCUserNameSpace.pdf***. The program ***isegHVOPCUserNameSpace.exe*** is able to make a scan over the namespace and save the information prepared to read by the ***isegHVOPCServer*** from the namespace file.

The properties of Multi-Channel HV system in the OPC server are defined as items. In the simplest case, such an item is directly coupled to a read or write via CAN bus. The ‘set voltage’ is one example.
Some OPC items have to be built up from data read results via CAN. The ‘status current limit’ is one example, which is read as an unsigned integer (2 bytes). Each bit of these 2 bytes represents the status of the current limit of one channel. This bit is interpreted as Boolean. All channels result in an array with 16 elements of Boolean, the ‘StatHwILimitBoolArray’.

There is a feature of ranking these many requests because a client can send many of them. First priority is assigned to emergency off ‘Emcy’, second priority to the command set voltage ‘VSet’. All other requests are under normal (lowest) priority.
A background loop process can be used to update the cache of the changeable channel items continuously. This process reads all measurement data and channel status data from the HV modules and fills the cache of the OPC server namespace. To implement a background loop process the “ReadSync” entry in the OPC initialising file “EHQ3216Srv.ini” have to be a different value from zero. The advantages of this mechanism is a very fast update of the really interesting module properties (Vmeas, Imeas and Stat item) because the group update of this items of an OPC client will cause no device reads if the time stamps of the items are as newer as the last update of the group.

iseg Spezialelektronik GmbH
Bautzner Landstr. 23
D - 01454 Radeberg / Rossendorf
Email: sales@iseg-hv.de
http://www.iseg-hv.com
Germany
Phone ++ 49 (0)351 / 26 996 - 0
Fax ++ 49 (0)351 / 26 996 - 21

5.2.1.1 Item's properties

The items own a sum of the same and a sum of specific item properties.

Each item has as standard properties:
- Item Canonical Data Type
- Item Value
- Item Quality
- Item Time Stamp
- Item Access Rights
- Server Scan Rate
- Item Description

Specific item properties:
- Item EU Type
- Item EU
- Item High EU (the maximum value that the device will accept and/or return)
- Item Low EU (the minimum value that the device will accept and/or return)
- Application Description

5.2.1.2 Items of the status from the server components

fully qualified identifier	device class	description	access	variant type
Status.release_isegHVOPCServer	all	isegHVOPCServer.EXE	readable	VT_BSTR
Status.HeartBeat	all	heart beat of the server	readable	VT_UI1
Status.release_isegCAN	all	iseg[p/s]can.DLL	readable	VT_BSTR
Status.CAN	all	status of CAN bus	readable	VT_BSTR
Status.Force	all	0=mode1 1=mode2	readable	VT_BOOL
Status.Refresh	all	mode1=0	Readable	VT_UI1

Status.CAN Actual status of the CAN line
Possible values are "OK"
"BUSHEAVY" bus errors e.g. when there is a mix of different bit rates
"BUSOFF" bus error e.g. a short on the bus
"OVERRUN" overflow of the buffer of the CAN driver
In order to select another CAN line for evaluation or to make a reset of the interface hardware of the corresponding CAN line, the number of the real hardware line has to be written to this item (not the number of the user namespace file).

A parallelization of the send and receive thread can be made with the items Force and Refresh to increase:
the update rate of the item cache.
the CAN busload without a noticeable increasing of the system load.

Status.Force

Force=false Mode1
An access to the item cache via an OPC client will be made with a request to the device hardware through the event handler of the item tag connected with a delay until the answer from the device or the time out.

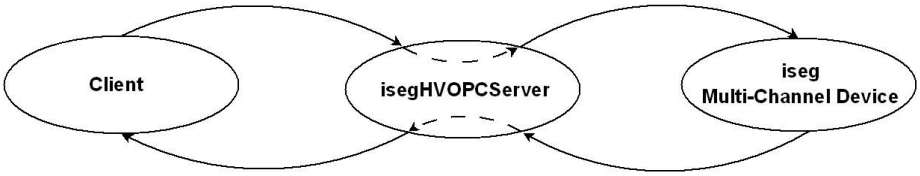

Force=true Mode2 (for Multi-Channel devices and crate monitoring units, not for crate monitoring units only)
An access to the item cache via an OPC client will be made without a request to the device hardware. The update of the item cache can be adjusted with the item Refresh.

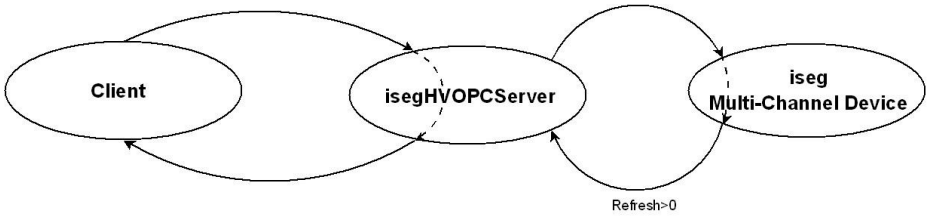

iseg Spezialelektronik GmbH
Bautzner Landstr. 23
D - 01454 Radeberg / Rossendorf
Email: sales@iseg-hv.de
http://www.iseg-hv.com
Germany
Phone ++ 49 (0)351 / 26 996 - 0
Fax ++ 49 (0)351 / 26 996 - 21

Status.Refresh

The Items listed in Appendix A will refreshed as fast as possible in background.

Useful values are: Refresh=0 - no update of the item cache in background
Refresh>0 up to 32 - update of the item cache in background

A higher value of the item “Refresh” means that more data will request in background with that a higher update rate of the OPC groups is possible, but which increase also the CAN bus load.

A possible handling is:

The client reads all stable items such as can*x*.m*tyy*.ch*zz*.NominalV after the OPC server has been started. In a next step the item “Force” will be set on true value and the group update rate for instance of the items to measurement data points will decrease. The background refresh can be started now with set the “Refresh” item to a value unequal to zero.

5.2.1.3 Items of Data Access to the channel properties

Syntax:	*t* Є [a|p]	module type (active or passive)
	x Є [0..15]	number of the CAN bus
	yy Є [0..63]	number of the CAN node
	zz Є [0..15]	number of the channel

fully qualified identifier	device class	description	access	variant type
can*x*.m*tyy*.ch*zz*.VSet	all	set voltage	write-/ readable	VT_R4
can*x*.m*tyy*.ch*zz*.VMeas	all	actual voltage	readable	VT_R4
can*x*.m*tyy*.ch*zz*.NominalV	all	nominal voltage	readable	VT_R4
can*x*.m*tyy*.ch*zz*.ISet	(all)	set current / set current trip	write-/ readable	VT_R4
can*x*.m*tyy*.ch*zz*.ITrip	all	(set current) / set current trip	write-/ readable	VT_R4
can*x*.m*tyy*.ch*zz*.IMeas	all	actual current	readable	VT_R4
can*x*.m*tyy*.ch*zz*.NominalI	all	nominal current	readable	VT_R4
can*x*.m*tyy*.ch*zz*.Stat	all	status channel in the kind of EHQ	readable	VT_UI2
can*x*.m*tyy*.ch*zz*.On	all	set on = -1, set off = 0	writeable	VT_BOOL
can*x*.m*tyy*.ch*zz*.Emergency	all	set emergency = -1, reset emergency = 0	writeable	VT_BOOL
can*x*.m*tyy*.ch*zz*.doClear	all	reset the errors (EHQ), events (EHS) of the channels	writeable	VT_BOOL
can*x*.m*tyy*.ch*zz*.Status	all (< 20 without any function)	status channel (OPC quality is bad, when it is not an EHS module in EHS mode	readable	VT_UI2
can*x*.m*tyy*.ch*zz*.EventStatus	>20 / (all)	channel event status	write-/ readable	VT_UI2
can*x*.m*tyy*.ch*zz*.EventMask	>20 / (all)	channel event mask	write-/ readable	VT_UI2

iseg Spezialelektronik GmbH
Bautzner Landstr. 23
D - 01454 Radeberg / Rossendorf
Email: sales@iseg-hv.de
http://www.iseg-hv.com
Germany
Phone ++ 49 (0)351 / 26 996 - 0
Fax ++ 49 (0)351 / 26 996 - 21

5.2.1.4 Items of Data Access to the module properties

fully qualified identifier	device class	description	access	type
canx.mtyy.GeneralStat	all	general status	readable	VT_UI1
canx.mtyy.GeneralSafetyLoop	all	safety loop is closed	write-/ readable	VT_BOOL
canx.mtyy.GeneralHwVLimitLow	0 / (all)	hardware voltage limit is to low	write-/ readable	VT_BOOL
canx.mtyy.Status	>20 / (all)	module status (EHS)	readable	VT_UI2
canx.mtyy.EventStatus	>20 / (all)	module event status	write-/ readable	VT_UI2
canx.mtyy.EventMask	>20 / (all)	module event mask	write-/ readable	VT_UI2
canx.mtyy.EventChannelStatus	>20 / (all)	event channel status	write-/ readable	VT_UI2
canx.mtyy.EventChannelMask	>20 / (all)	event channel mask	write-/ readable	VT_UI2
canx.mtyy.setAdjust	all	Adjust of the HV on = -1 Adjust of the HV off = 0	writeable	VT_BOOL
canx.mtyy.setKillEnable	all	hardware kill enable = -1 hardware kill disable = 0	writeable	VT_BOOL
canx.mtyy.doClear	all	Clear all events / errors of the whole HV module	writeable	VT_BOOL
canx.mtyy.GroupNumber	>20 / (all)	Index of the variable groups 0 to 31	write-/ readable	VT_UI1
canx.mtyy.GroupVariable	>20 / (all)	extended and flexible range of group functions	write-/ readable	VT_UI4
canx.mtyy.StatHardwareVLimit	all	status voltage limit – corresponding channel voltage limit = 1	write-/ readable	VT_UI2
canx.mtyy.StatHardwareILimit	all	status current limit – corresponding channel current limit = 1	write-/ readable	VT_UI2
canx.mtyy.StatINHIBIT	7 / (all)	status INHIBIT – corresponding INHIBIT = 1	write-/ readable	VT_UI2
canx.mtyy.StatITrip	all	status current trip – corresponding channel current trip = 1	write-/ readable	VT_UI2
canx.mtyy.StatRegulationErr	0, 1, 2 / (all)	status regulation error – corres-ponding channel error = 1	write-/ readable	VT_UI2
canx.mtyy.On	all	corresponding channel set on = 1 or set off = 0	write-/ readable	VT_UI2
canx.mtyy.VSetAllChannels	all	set voltage of all channels	write-/ readable	VT_R4
canx.mtyy.ISetAllChannels	all	set current of all channels	write-/ readable	VT_R4
canx.mtyy.ITripAllChannels	0-5, 8 / (all)	set current trip of all channels	write-/ readable	VT_R4
canx.mtyy.RampSpeed	all	speed of the voltage ramp in per-cent of the nominal voltage of the channel per second	write-/ readable	VT_R4
canx.mtyy.IRampSpeed	all	speed of the current ramp in per-cent of the nominal current of the channel per second (OPTION)	write-/ readable	VT_R4
canx.mtyy.Emcy	all	emergency - corresponding channel set emergency = 1 reset emergency = 0	write-/ readable	VT_UI2
canx.mtyy.ADCSmplsPScnd	>20	ADC samples per second	write-/ readable	VT_UI2
canx.mtyy.DigitalFilter	>20	Digital filter	write-/readable	VT_UI2
canx.mtyy.DeviceID	all	device identifier	readable	VT_BSTR
canx.mtyy.SoftwareID	all	software release	readable	VT_BSTR
canx.mtyy.BitRate	all	bit rate	readable	VT_UI2
canx.mtyy.Option	>20 / (all)	options	readable	VT_BSTR
canx.mtyy.OptionSingleSpec	>20 / (all)	option single specification	write-/ readable	VT_BSTR
canx.mtyy.OptionSpec	>20 / (all)	specification	readable	VT_UI1
canx.mtyy.HardwareILimit	all	hardware current limit	readable	VT_R4
canx.mtyy.HardwareVLimit	all	hardware voltage limit	readable	VT_R4
canx.mtyy.Supply24V	all	supply 24V	readable	VT_R4
canx.mtyy.Supply5V	all	supply 5V	readable	VT_R4
canx.mtyy.BoardTemp	all	board temperature	readable	VT_R4

fully qualified identifier	device class	description	access	type
canx.mtyy.ErrThreshold	all	threshold of error evaluation in percent of the nominal voltage	write-/ readable	VT_R4
canx.mtyy.ConfigRelFErr	0, 1, 2 / (all)	configuration mask of relay and regulation error	write-/ readable	VT_UI1
canx.mtyy.Polarity	5 / (all)	electronical polarity switch	write-/ readable	VT_UI1
canx.mtyy.Alive	all	module is alive	readable	VT_BOOL
canx.mtyy.DeviceClass	all	device class	readable	VT_UI1

5.2.1.5 Items to signal an alarm from the HV devices via Data Access

fully qualified identifier	device class	description	access	type
canx.mtyy.Alarm	all	alarm status	readable	VT_BOOL
canx.mtyy.AlarmInformation	all	alarm information	readable	VT_UI1

The items “Alarm” and “AlarmInformation” are implemented as event driven update inside of the ***isegHVOPCServer***. These two items are included (on request of Cern) in order to have an access to the fast alarm messages of the modules. The better way is to use the faster “Alarm & Event” part of the ***isegHVOPCServer***. Since version 4.01 the items as there are “Alarm” and “AlarmInformation” can be cleared by reset of the corresponding status bit. If an error occurs the “alarm status” will become to a *true* value. The error of the modules can be reset only by a reset of the reason of the error followed by writing a *‘1’* to the corresponding status bit.

The item “AlarmInformation” describes the kind of the alarm (see Hints to the item alarm information). The server refreshes „Alarm“ and „AlarmInformation“ if a new alarm is attempted but the client will register the new alarm only if the DA-value has been changed.

iseg Spezialelektronik GmbH
Bautzner Landstr. 23
D - 01454 Radeberg / Rossendorf
Email: sales@iseg-hv.de
http://www.iseg-hv.com
Germany
Phone ++ 49 (0)351 / 26 996 - 0
Fax ++ 49 (0)351 / 26 996 - 21

5.2.1.6 Notes to the item *Status channel (EHQ)*

device classes 0, 1, 2

DATA_1 to DATA_0 bool array UI2

b15	b14	b13	b12	b11	b10	b9	b8	b7	b6	b5	b4	b3	b2	b1	b0
v	c	k	e	r	o	p	x	x	x	x	x	x	x	s	t

device class 6

DATA_1 to DATA_0 bool array UI2

b15	b14	b13	b12	b11	b10	b9	b8	b7	b6	b5	b4	b3	b2	b1	b0
v	c	x	e	r	o	p	x	x	x	x	x	x	x	x	t

device class 7

DATA_1 to DATA_0 bool array UI2

b15	b14	b13	b12	b11	b10	b9	b8	b7	b6	b5	b4	b3	b2	b1	b0
v	c	x	e	r	o	p	x	i	x	x	x	x	x	x	t

t	current trip	t = 0	channel is ok
		t = 1	V_O shut of 0V because software current trip has been exceeded
s	sum error	s = 0	channel is ok
		s = 1	detection of a sum error - consist of an OR between current and voltage limit error in time slots of 1ms, which means that it exists an error in the regulation of the channel, see to [(1)]
x	no information		
I	INHIBIT	i = 0	no INHIBIT channel is ok
		i = 1	detection of an INHIBIT if the HV is above the threshold to arm the error detection
p	input-error	p = 0	no input-error
		p = 1	wrong message to control the module
o	switch channel to	o = 0	channel OFF
		o = 1	channel ON
r	ramping	r = 0	voltage is stable
		r = 1	voltage ramps
e	emergency cut-off	e = 0	channel works
		e = 1	cut-off V_O shut off to 0V without ramp
k	kill function	k = 0	disable (see hardware current limit and software current trip)
		k = 1	enable (see hardware current limit and software current trip)
c	current limit error	c = 0	channel is ok
		c = 1	V_O shut off 0V because hardware current limit has been exceeded
v	voltage limit error	v = 0	channel is ok
		v = 1	V_O shut of permanently because voltage limit has been exceeded

For detection of a current or voltage limit error flag the firmware must evaluate the channel voltage at first.

5.2.1.7 Notes to the item *Channel status (EHS)*

can*x*.m*tyy*.ch*zz*.Status channel status readable VT_UI2

Bit15	Bit14	Bit13	Bit12	Bit11	Bit10	Bit9	Bit8	Bit7	Bit6	Bit5	Bit4	Bit3	Bit2	Bit1	Bit0
isVLIM	isCLIM	isTRP	isEINH	isVBND	isCBND	res	res	isCV	isCC	isEMCY	isRAMP	isON	IERR	res	res

isVLIM	IsVoltageLimitExceeded	voltage limit set by V_{max} is exceeded
isCLIM	IsCurrentLimitExceeded	current limit set by I_{max} is exceeded
isTRP	IsTripExceeded	Trip is set when Voltage or Current limit or Iset has been exceeded (when KillEnable=1)
isEINH	IsExtInhibit	External Inhibit
isVBND	IsVoltageBoundsExceeded	Voltage out of bounds
isCBND	IsCurrentBoundsExceeded	Current out of bounds
isCV	IsControlledVoltage	Voltage control active
isCC	IsControlledCurrent	Current control active
isEMCY	IsEmergencyOff	Emergency off without ramp
isON	IsOn	On
isRAMP	IsRamping	Ramp is running
IERR	InputError	Input error
res	Reserved	

isVLIM=0 channel is ok
isVLIM=1 the hardware voltage limit is exceeded
isCLIM=0 channel is ok
isCLIM=1 the hardware current limit is exceeded
(to detect a hardware voltage or current limit error flag the firmware has to evaluate the channel voltage and current at first)
isTRP=0 channel is ok
isTRP=1 V_O is shut off to 0V without ramp because the channel has been tripped.
isEINH=0 channel is ok
isEINH=1 External Inhibit was scanned
isVBND=0 channel is ok
isVBND=1 |Vmeas-Vset| > Vbounds
isCBND=0 channel is ok
isCBND=1 |Imeas-Iset| > Ibounds (to detect a voltage or current out of bound flag the firmware has to ramp the channel voltage Vset at first)
isCV=1 channel is in state of voltage control
isCC=1 channel is in state of current control
isEMCY=1 channel is in state of emergency off, VO has been shut off to 0V without ramp
isON=0 channel is off
isON=1 channel voltage follows the Vset value
isRAMP=0 no voltage is in change
isRAMP=1 voltage is in change with the stored ramp speed value
IERR=0 no input-error
IERR=1 incorrect message to control the module

5.2.1.8 Notes to the items of the *Channel control (EHS)*

setOn	Set on channel
setEemergencyY	Set Emergency
doClear	Do clear events (EHS) or errors signals (EHQ) of the channel.

setEmergency = 0 reset Emergency
setEmergency =1 set Emergency (cut-off V_O shut off to 0V without ramp)

setOn = 0 switch the channel to OFF
setOn = 1 switch the channel to ON
(When Vset has been set to a value unequal to zero (0V) before the status bit 'isOn' is changed from (1) one to (0) zero a ramp down of the voltage to zero (0V) will be started.)

doClear=0 do nothing
doClear=1 reset the errors (EHQ), events (EHS) of the channels

iseg Spezialelektronik GmbH
Bautzner Landstr. 23
D - 01454 Radeberg / Rossendorf
Email: sales@iseg-hv.de
http://www.iseg-hv.com
Germany
Phone ++ 49 (0)351 / 26 996 - 0
Fax ++ 49 (0)351 / 26 996 - 21

5.2.1.9 Notes to the item *Channel event status (EHS)*

can*x*.m*tyy*.ch*zz*.EventStatus channel event status write-/ readable VT_UI2

Bit15	Bit14	Bit13	Bit12	Bit11	Bit10	Bit9	Bit8	Bit7	Bit6	Bit5	Bit4	Bit3	Bit2	Bit1	Bit0
EVLIM	ECLIM	ETRP	EEINH	EVBNDs	ECBNDs	res	res	ECV	ECC	EEMCY	EEOR	EOn2Off	EIER	res	res

EVLIM	EventVoltageLimit	Event: Hardware- voltage limit has been exceeded
ECLIM	EventCurrentLimit	Event: Hardware- current limit has been exceeded
ETRP	EventTrip	Event: Trip is set when Voltage or Current limit or Iset has been exceeded (when KillEnable=1)
EEINH	EventExtInhibit	Event external Inhibit
EVBNDs	EventVoltageBounds	Event: Voltage out of bounds
ECBNDs	EventCurrentBounds	Event: Current out of bounds
ECV	EventControlledVoltage	Event: Voltage control
ECC	EventControlledCurrent	Event: Current control
EEMCY	EventEmergencyOff	Event: Emergency off
EEOR	EventEndOfRamp	Event: End of ramp
EOn2Off	EventOnToOff	Event: Change from state "On" to "Off"
EIER	EventInputError	Event: Input Error
res	Reserved	

An event bit is permanently set if the status bit is 1 or is changing to 1. Different to the status bit an event bit isn't automatically reset. A reset has to be done by the user by writing an 1 to this event bit.

5.2.1.10 Notes to the item *Channel event mask (EHS)*

can*x*.m*tyy*.ch*zz*.EventMask channel event mask write-/ readable VT_UI2

Bit15	Bit14	Bit13	Bit12	Bit11	Bit10	Bit 9	Bit 8	Bit7	Bit6	Bit 5	Bit4	Bit3	Bit2	Bit 1	Bit0
MEVLIM	MECLIM	MECTRP	MEEINH	MEVBNDs	MECBNDs	res	res	MECV	MECC	res	MEEOR	MEOn2Off	MEIERR	res	res

MEVLIM	MaskEventVoltageLimit	EventMask: Hardware- voltage limit has been exceeded
MECLIM	MaskEventCurrentLimit	EventMask: Hardware- current limit has been exceeded
METRIP	MaskEventTrip	EventMask: Voltage limit or Current limit or Iset has been exceeded (when KillEnable=1)
MEEINH	MaskEventExtInhibit	EventMask: External Inhibit
MEVBNDs	MaskEventVoltageBounds	EventMask: Voltage out of bounds
MECBNDs	MaskEventCurrentBounds	EventMask: Current out of bounds
MECV	MaskEventControlledVoltage	EventMask: Voltage control
MECC	MaskEventControlledCurrent	EventMask: Current control
MEEMCY	MaskEventEmergencyOff	EventMask: Emergency off
MEEOR	MaskEventEndOfRamp	EventMask: End of ramp
MEOn2Off	MaskEventOnToOff	EventMask: Change from state on to off
MEIER	MaskEventInputError	EventMask: Input Error
res	Reserved	

5.2.1.11 Notes to the item *Module status (EHS)*

can*x*.m*tyy*.Status module status readable VT_UI2

Bit15	Bit14	Bit13	Bit12	Bit11	Bit10	Bit9	Bit8	Bit7	Bit6	Bit5	Bit4	Bit3	Bit2	Bit1	Bit0
isKILena	isTMPgd	isSPLYgd	isMODgd	isEVNTact	isSFLPgd	isnoRAMP	isnoSERR	res	res	isHwVLIMgd	isSrvc	res	res	res	isAdj

IsKILena	IsKillEnable	Module state of kill enable
isTMPgd	IsTemperatureGood	Module temperature good
isSPLYgd	IsSupplyGood	Power supply good
isMODgd	IsModuleGood	Module in state good
isEVNTact	IsEventActive	Any event is active and mask is set
isSFLPgd	IsSafetyLoopGood	Safety loop closed
isnoRAMP	IsNoRamp	All channels stable, no ramp active .
isnoSERR	IsNoSumError	Module without failure
isHwVLIMgd	IsHardwareVoltageLimitGood	Hardware voltage limit in proper range, only for HV distributor modules with current mirror;
IsSrvc	IsService	Hardware failure detected (consult iseg Spezialelektronik GmbH)
isADJ	IsFineAdjustment	Mode of the fine adjustment
res	Reserved	

isKILLena=0 Module in state kill disable
isKILLena=1 Module in state kill enable
isTMPgd=0 if module temperature is higher than 55°C then all channel are switched off permanently
isTMPgd=1 module temperature is within working range
isSPLYgd=0 supply voltages are out of range (range of 24V +/-10% and of 5V +/-5%)
isSPLYgd=1 supply voltages are within range
isMODgd=0 module is not good, that means (isnoSERR AND (ETMPngd OR ESPLYngd OR ESFLPngd))==0
isMODgd=1 module is good, that means (isnoSERR AND NOT(ETMPngd OR ESPLYngd OR ESFLPngd))==1
(see module event status also)
isEVNTact=0 no Event is active
isEVNTact=1 any Event is active
isSFLPgd=0 safety loop is broken -V_O bas been shut off,
isSFLPgd=1 safety loop is closed
isnoRAMP=0 V_O is ramping in at least one channel
isnoRAMP=1 no channel is ramping
isnoSERR=0 voltage limit, current limit, trip, voltage bound or current bound has been exceeded in at least one of the channels or external INHIBIT ⇒ error, reset by reset of the corresponding flag of the 'Channel Status'
isnoSERR=1 evaluation of the 'Channel Status' over all channels to a sum error flag
⇒ VLIM&CLIM&CTRP&EINH&VBND&CBND=0 ⇒ no errors
isHwVLIMgd=0 hardware voltage limit not in proper range
isHwVLIMgd=1 hardware voltage limit in proper range
isADJ=0 Fine adjustment is off.
isADJ=0 Fine adjustment is on (default)

5.2.1.12 Notes to the items of the *Module control (EHS)*

setAdjust	Set adjust	Switch ON of fine adjustment
setKillEnable	Set kill enable	Kill function
doClear	Clear events (EHS) and errors (EHQ)	Clear event (EHS) or error signals (EHQ) in the channels and the module

setAdjust = 0 fine adjustment OFF
setAdjust = 1 fine adjustment ON

setKillEnable = 0 kill function disable
setKillEnable = 1 kill function enable

doClear=0 do nothing
doClear=1 reset the errors (EHQ), events (EHS) of the channels

iseg Spezialelektronik GmbH
Bautzner Landstr. 23
D - 01454 Radeberg / Rossendorf
Email: sales@iseg-hv.de
http://www.iseg-hv.com
Germany
Phone ++ 49 (0)351 / 26 996 - 0
Fax ++ 49 (0)351 / 26 996 - 21

5.2.1.13 Notes to the item *Module event status (EHS)*

can*x*.m*tyy*.EventStatus module event status write-/ readable VT_UI2

Bit15	Bit14	Bit13	Bit12	Bit11	Bit10	Bit9	Bit8	Bit7	Bit6	Bit5	Bit4	Bit3	Bit2	Bit1	Bit0
res	ETMPngd	ESPLYngd	res	res	ESFLPngd	res	res	res	res	res	res	res	res	res	res

ETMPngd	EventTemperatureNotGood	Event: Temperature is above 55°C
ESPLYngd	EventSupplyNotGood	Event: at least one of the supplies is not good
ESFLPngd	EventSafetyLoopNotGood	Event: Safety loop is open
res	Reserved	

5.2.1.14 Notes to the item *Module event mask (EHS)*

can*x*.m*tyy*.EventMask module event mask write-/ readable VT_UI2

Bit15	Bit14	Bit13	Bit12	Bit11	Bit10	Bit9	Bit8	Bit7	Bit6	Bit5	Bit4	Bit3	Bit2	Bit1	Bit0
res	METMPngd	MESPLYngd	res	res	MESFLPngd	res	res	res	res	res	res	res	res	res	res

METMPngd	MaskEventTemperatureNotGood	MEventMask: Temperature is above 55°C
MESPLYngd	MaskEventSupplyNotGood	MEventMask: at least one of the supplies is not good
MESFLPngd	MaskEventSafetyLoopNotGood	MEventMask: Safety loop (SL) is open
res	Reserved	

5.2.1.15 Notes to the item *Event channel status (EHS)*

can*x*.m*tyy*.EventChannelStatus event channel status write-/ readable VT_UI2

Bit15	Bit14	Bit13	Bit12	Bit11	Bit10	Bit9	Bit8	Bit7	Bit6	Bit5	Bit4	Bit3	Bit2	Bit1	Bit0
CH15	CH14	Ch13	CH12	CH11	CH10	CH9	CH8	CH7	CH6	CH5	CH4	CH3	CH2	CH1	CH0

The n-th bit of the register is set, if an event is active in the n-th channel and the associated bit in the EventMask register of the n-th channel is set too.

CHn = EventStatus[n] & EventMask[n]

Reset of a bit is done by writing a 1 to this bit.

5.2.1.16 Notes to the item *Event channel mask (EHS)*

can*x*.m*tyy*.EventChannelMask event channel mask write-/ readable VT_UI2

Bit15	Bit14	Bit13	Bit12	Bit11	Bit10	Bit9	Bit8	Bit7	Bit6	Bit5	Bit4	Bit3	Bit2	Bit1	Bit0
CH15	CH14	Ch13	CH12	CH11	CH10	CH9	CH8	CH7	CH6	CH5	CH4	CH3	CH2	CH1	CH0

This register decides whether a pending event leads to the sum event flag of the module or not. If the n-th bit of the mask is set and the n-th channel has an active event in the EventChannelStatus the bit isEventActive in the ModuleStatus register is set

5.2.1.17 Notes to the item *General status (EHQ)*

can*x*.m*tyy*.GeneralStat general status readable VT_UI1

b7	b6	b5	b4	b3	b2	b1	b0
save	killena/ hwVLimNoExceed	vsply	avad	stbl	sloop	nramp	sum

sum	sum error flag	sum = 0	voltage limit, current limit or trip were exceeded in the module
		sum = 1	status channel flags v & c & t = 0 for all channels
nramp	no ramp flag	nramp = 0	V_O is ramping at least one channel
		nramp = 1	no channel is ramping
sloop	safety loop flag	sloop = 0	safety loop is broken -V_O has been shut off, clear this bit by reading the general status information
		sloop = 1	safety loop is closed
stbl	stable	stbl = 0	all channels are stable with programmable ADC filter frequency f_N (ADC conversion time =1 / f_N, see 'ADC filter frequency setting', default f_N = 50 Hz)
		stbl = 1	at least one channel is ramping V_O or not yet stable after ramping (with ADC filter frequency f_N = 100 Hz)
avad	average adjust	avad=0	fine adjustment OFF for device classes 0, 6 and 7 average of voltage and current measurement OFF for device classes 1, 2 and 7
		avad=1	fine adjustment ON for device classes 0, 6 and 7 average of voltage and current measurement ON for device classes 1, 2 and 7
vsply	supply voltages	vsply=0	supply voltages or module temperature are out of range
		vsply=1	supply voltages and module temperature are in range
killena	kill enable	killena=0	kill function disable, only at modules of device class 6 and 7
		killena=1	kill function enable only at modules of device class 6 and 7
hwVLimNoExceed		=0	hardware voltage limit to "Low", only at modules of device class 0
		=1	hardware voltage limit in a proper range, only at modules of device class 0
save	save set values	save=0	no write access to EEPROM
		save=1	store all set values to EEPROM (time to save ca. 10s)

sn. serial numbers

iseg Spezialelektronik GmbH
Bautzner Landstr. 23
D - 01454 Radeberg / Rossendorf
Email: sales@iseg-hv.de
http://www.iseg-hv.com
Germany
Phone ++ 49 (0)351 / 26 996 - 0
Fax ++ 49 (0)351 / 26 996 - 21

5.2.1.18 Notes to the items *VsetAllChannels*, *ITripAllChannels* and *ISetAllChannels*

All items are readable since isegHVOPCServer release 4.10. The item VsetAllChannels, ITripAllChannels and IsetAllChannels has been implemented for a fast possibility to set all channel items of the same kind such as VSet on a value. The read access of the OPC items VsetAllChannels, ITripAllChannels and IsetAllChannels deliver only the value from cache of the OPC server, which has been written as last. The really value of the channel items can be differ for instance in case of a mix module or a hardware limit and others but the channel items VSet, ITrip and ISet contain always the proper values.

5.2.1.19 Notes to the item *Configuration of the relay and regulation error*

canx.m*t*yy.ConfigRelFErr configuration of relay and regulation error write-/readable VT_UI1

b7	b6	b5	b4	b3	b2	b1	b0
x	dcRACRO	dcRACSO	dcRREr	dcRSLp	dcRTErr	dcRVErr	dcRIErr

dcRIErr 1 discharge if the hardware current limit was exceeded for at least one channel
0 no discharging with help of the relay

dcRVErr 1 discharge if the hardware voltage limit was exceeded for at least one channel
0 no discharging with help of the relay

dcRTErr 1 discharge if the software current trip was exceeded for at least one channel
0 no discharging with help of the relay

dcRSLp 1 discharge if the safety loop has been disconnected, the output voltages are shut off without ramp
0 no discharging with help of the relay
(If the safety loop has been disconnected, the set voltages are shut off with the actual ramp speed.)

dcRREr 1 discharge if the regulation was out of order for at least one channel (reaction >= 1ms)
0 no discharging with help of the relay

dcRACSO 1 discharge if all channels set to “OFF”(Group access module “Channel ON/OFF” or “Emergency cut-off”) - ***is working only if the dcRACRO bit has been set also***
0 no discharging with help of the relay
(ramp down the set voltages with the actual ramp speed)

dcRACRO 1 discharge if all channels set to “OFF” (Group access module “Channel ON/OFF” and the end of ramping has been reached or “Emergency cut-off”)
0 no discharging with help of the relay
(when the set voltages of all channels are set to “OFF”)

Under the setting of one of these conditions and the corresponding error occurs following will happen:

- shut off the HV without ramp in all channels and the set voltage in all channels to 0V by software.
- close contact of discharge relay.

The relay contacts will discharge capacities connected to the output with help of an integrated load resistor (see Appendix B Operators Manual - Multi-channel High Voltage Power Supply EHQ). This item configures the conditions of how this does work.

Under the setting of one of these conditions and the corresponding error occurs following will happen:

- shut off the HV without ramp in all channels and the set voltage in all channels to 0V by software.

- close contact of discharge relay.

5.2.1.20 Notes to *GroupNumber* and *GroupVariable (EHS)*

With mean of the item GroupNumber is it possible to access to one of the 32 variable group functions.

Each variable group definition will set via the item GroupVariable. The item GroupVariable consists out of 2 words each of 16 bits. In variable groups one word carries the information about the members of the group or gives an overview about a selected situation in all channels, the other word carries the information about type and characteristics of the goup.

Set group:

Set groups will be used in order to set channels to a same value, which happen to carry the identical channel value. Therefore within the group following will be defined:

- Member of the group: Each member will be activated in the channel setting list **ChSetLst**
- Type of the group: Set group type **TypeSet**
- Channel characteristics: Coding of characteristics, which have to be set commonly
- Control mode: Divides between a one-time setting of the slave channel property and a permanently copying of the Master channel's property to the slave channels
- Master channel: Number of the channel, which characteristics will be transferred to the other channels. Is just necessary for Set groups which set a value. If functions have to be initialized e.g. start of ramp then there is no Master channel

ChSetLst				ChannelSettingList											UI2
Bit31	Bit30	Bit29	Bit28	Bit27	Bit26	Bit25	Bit24	Bit23	Bit22	Bit21	Bit20	Bit19	Bit18	Bit17	Bit16
CH15	CH14	CH13	CH12	CH11	CH10	CH9	CH8	CH7	CH6	CH5	CH4	CH3	CH2	CH1	CH0
TypeSet				DATA_0 to DATA_1 TypeSet											UI2
Bit15	Bit14	Bit13	Bit12	Bit11	Bit10	Bit9	Bit8	Bit7	Bit6	Bit5	Bit4	Bit3	Bit2	Bit1	Bit0
TYPE1	TYPE0	res	res	res	res	res	MOD0	SET3	SET2	SET1	SET0	MCH3	MCH2	MCH1	MCH0

TYPE1	TYPE0	Value	
0	0	SetGroupType	Group is defined as Set group

MOD0	Value	
0	0	The group function is done one time
1	1	The group function is done permanently

SET3	SET2	SET1	SET0	Value	
0	0	0	1	SetVset	Copy Vset from MCH to all members
0	0	1	0	SetIset	Copy Iset from MCH to all members
0	1	0	0	SetVbnds	Copy Vbounds from MCH to all members
0	1	0	1	SetIbnds	Copy Ibounds from MCH to all members
1	0	1	0	SetOn	Switch ON/OFF all members depending on setON in MCH
1	0	1	1	SetEmrgCutOff	Switch OFF all members (Emergeny OFF)
1	1	1	1	Cloning	Set all properties of members like MCH properties *(in preparation)*

MCH3	MCH2	MCH1	MCH0	Value	
0	0	0	0	0	1: Channel 0 is MasterChannel MCH
0	0	0	1	1	1: Channel 1 is MasterChannel MCH
...	...	...	...	...	...
1	1	1	1	15	1: Channel 15 ist MasterChannel MCH

Status group:
Status groups are used to report the status of a single characteristic of all channels simultaneously. No action is foreseen. Therefore within the group following has to be defined :
Members of the group: Each member will be activated in the channel status list **ChStatLst.**
Type of the group: Status group type **TypeStat**
Channel characteristics:Coding of characteristics , which is to be reported.

ChStatLst					ChannelStatusList											UI2
Bit31	Bit30	Bit29	Bit28	Bit27	Bit26	Bit25	Bit24	Bit23	Bit22	Bit21	Bit20	Bit19	Bit18	Bit17	Bit16	
CH15	CH14	CH13	CH12	CH11	CH10	CH9	CH8	CH7	CH6	CH5	CH4	CH3	CH2	CH1	CH0	
TypeStat					DATA_0 to DATA_1 TypeStatus											UI2
Bit15	Bit14	Bit13	Bit12	Bit11	Bit10	Bit9	Bit8	Bit7	Bit6	Bit5	Bit4	Bit3	Bit2	Bit1	Bit0	
TYPE1	TYPE0	res	res	res	res	res	res	STAT3	STAT2	STAT1	STAT0	res	res	res	res	

TYPE1	TYPE0	Value	
0	1	StatusGroupType	Group will be defined as Status group

STAT3	STAT2	STAT1	STAT0	Value	
0	0	1	1	ChkIsOn	check channel Status.isON (is on)
0	1	0	0	ChkIsRamping	check channel Status.isRAMP (is ramping)
0	1	1	0	ChkIsControlledCurrent	check channel Status.isCC (is current control)
0	1	1	1	ChkIsControlledVoltage	check channel Status.isCV (is voltage control)
1	0	1	0	ChkIsCurrentBounds	check channel Status.isCBNDs (is current bounds)
1	0	1	1	ChkIsVoltageBounds	check channel Status.isVBNDs (is voltage bounds)
1	1	0	0	ChkIsExternalInhibit	check channel Status.isEINH (is external inhibit)
1	1	0	1	ChkIsTrip	check channel Status.isTRIP(is trip)
1	1	1	0	ChkIsCurrentLimit	check channel Status.isCLIM (is current limit exceeded)
1	1	1	1	ChkIsVoltageLimit	check channel Status.isVLIM (is voltage limit exceeded)

Monitoring group:
Monitoring groups are used to observe a single characteristic of selected channels simultaneously and in case of need take action. Therefore the group has to be defined :
Members of the group: Each member will be activated in the channel monitoring list **ChMonLst.**
Type of the group: Monitoring group type **TypeMon**
Channel characteristics:Coding of characteristics , which is to be monitored.
Control mode: Coding of the control function, i.e. which kind of change in the group-image shall cause a signal.
Activity: Define , which activity has to happen after the event.

ChMonLst					ChannelMonitoringList											UI2
Bit31	Bit30	Bit29	Bit28	Bit27	Bit26	Bit25	Bit24	Bit23	Bit22	Bit21	Bit20	Bit19	Bit18	Bit17	Bit16	
CH15	CH14	CH13	CH12	CH11	CH10	CH9	CH8	CH7	CH6	CH5	CH4	CH3	CH2	CH1	CH0	
TypeMon					DATA_0 to DATA_1 TypeMonitoring											UI2
Bit15	Bit14	Bit13	Bit12	Bit11	Bit10	Bit9	Bit8	Bit7	Bit6	Bit5	Bit4	Bit3	Bit2	Bit1	Bit0	
TYPE1	TYPE0	ACT1	ACT0	res	res	res	MOD0	MON3	MON2	MON1	MON0	res	res	res	res	

TYPE1	TYPE0	Value	
1	0	MonitoringGroupType	Group will be defined as Monitoring group

ACT1	ACT0	Value	
0	0	0	No special action ; EventGroupStatus[grp] will be set
0	1	1	Ramp down of group EventGroupStatus[grp] will be set
1	0	2	Switch OFF of group without ramp; EventGroupStatus[grp] will be set
1	1	3	Switch OFF of module without ramp; EventGroupStatus[grp] will be set

MOD0	Value	
0	0	event will happen if at least one Channel == 0
1	1	event will happen if at least one Channel == 1

MON3	MON2	MON1	MON0	Value	
0	0	1	1	MonitorIsOn	monitor channel Status.isON (is on)
0	1	0	0	MonitorIsRamping	monitor channel Status.isRAMP (is ramping)
0	1	1	0	MonitorIsControlledCurrent	monitor channel Status.isCC (is current control)
0	1	1	1	MonitorIsControlledVoltage	monitor channel Status.isCV (is voltage control)
1	0	1	0	MonitorIsCurrentBounds	monitor channel Status.isCBNDs (is current bounds)
1	0	1	1	MonitorIsVoltageBounds	monitor channel Status.isVBNDs (is voltage bounds)
1	1	0	0	MonitorIsExternalInhibit	monitor channel Status.isEINH (is external inhibit)
1	1	0	1	MonitorIsTrip	monitor channel Status.isTRIP (is trip)
1	1	1	0	MonitorIsCurrentLimit	monitor channel Status.isCLIM (is current limit exceeded)
1	1	1	1	MonitorIsVoltageLimit	monitor channel Status.isVLIM (is voltage limit exceeded)

Delayed Trip group:
Trip timeout groups are necessary to keep the timing for the time controlled delayed Trip function and to define the action which has to happen after a Trip.

Therefore in the group following will be defined:

- Members of group: Each member will be activated in a word channel trip timeout list **ChTrpTotLst.**
- Type of the group: Time out group type **TypeTime**
- Activity: Define , which activity has to happen after time controlled Trip
- Timeout: Coding of Timeout-time as 12 Bit Integer.

Timeout groups have to stay unchanged for the whole time as long they are used.
An overwriting will cause the definition of a new group. An overlay of the channels of multiple Trip groups is not allowed.

ChTrpTotLst				ChannelTripTimoutList											UI2
Bit31	Bit30	Bit29	Bit28	Bit27	Bit26	Bit25	Bit24	Bit23	Bit22	Bit21	Bit20	Bit19	Bit18	Bit17	Bit16
CH15	CH14	CH13	CH12	CH11	CH10	CH9	CH8	CH7	CH6	CH5	CH4	CH3	CH2	CH1	CH0
TypeTime				DATA_0 to DATA_1 TypeTimeOut											UI2
Bit15	Bit14	Bit13	Bit12	Bit11	Bit10	Bit9	Bit8	Bit7	Bit6	Bit5	Bit4	Bit3	Bit2	Bit1	Bit0
TYPE1	TYPE0	ACT1	ACT0	TOT11	TOT10	TOT9	TOT8	TOT7	TOT6	TOT5	TOT4	TOT3	TOT2	TOT1	TOT0

TYPE1	TYPE0	Value	
1	1	TimeOutGroupType	Group will be defined as Timeout group

ACT1	ACT0	Action	
0	0	0	No special action; EventGroupStatus[grp] will be set.
0	1	1	Ramp down of group with ramp; EventGroupStatus[grp] will be set
1	0	2	Switch OFF the group without ramp; EventGroupStatus[grp] will be set
1	1	3	Switch OFF the module without ramp; EventGroupStatus[grp] will be set

TOT[11..0]:	Binary coded Timeout-time in ms (8..4088ms) resolution is 8ms

5.2.1.21 Notes to the item *Alarm information*

canx.mtyy.AlarmInformation alarm status readable VT_UI1

b7	b6	b5	b4	b3	b2	b1	b0
$HwV_{Limit_to_low}$ / INHIBIT	M_{Temp}	V_{Supl}	S_{Loop}	V_{Limit}	C_{Limit}	R_{Error}	C_{Trip}

C_{Trip}	current trip	C_{Trip} = 0 ⇒ no channel has tripped C_{Trip} = 1 ⇒ software current trip at least one of the channels
R_{Err}	regulation error	R_{Error} = 0 ⇒ no channel has a regulation error (see channel status) R_{Error} = 1 ⇒ at least one of the channels has detected a regulation error
C_{Limit}	current limit	C_{Limit} = 0 ⇒ no channel has exceeded the hardware current limit C_{Limit} = 1 ⇒ at least one of the channels has exceeded the current limit
V_{Limit}	voltage limit	V_{Limit} = 0 ⇒ no channel has exceeded the voltage limit V_{Limit} = 1 ⇒ at least one of the channels has exceeded the voltage limit
S_{Loop}	safety loop	S_{Loop} = 0 ⇒ safety loop is closed S_{Loop} = 1 ⇒ safety loop is broken
V_{supl}	voltage supplies	V_{supl} = 0 ⇒ supply voltages are in range V_{supl} = 1 ⇒ supply voltages are out of range
M_{Temp}	module temperature	M_{Temp} = 0 ⇒ module temperature <= 60°C, no action M_{Temp} = 1 ⇒ module temperature > 60°C, HV has been switched off
$HwV_{Limit_to_low}$	(device class 0 only)	$HwV_{Limit_to_low}$ = 0 ⇒ hardware voltage limit in range $HwV_{Limit_to_low}$ = 1 ⇒ hardware voltage limit to low - it is not possible to switch on any channel
INHIBIT (device class 7 only)		INHIBIT = 0 ⇒ no channel has detected an INHIBIT INHIBIT = 1 ⇒ at least one of the channels has detected an INHIBIT

5.2.1.22 Notes to the item *Option (EHS)*

canx.mtyy.Option option readable VT_BSTR

Option	Description	Specification
“EDCP”	Enhanced Device Control Protocol	no
“HVBM”	HV boards per (CAN nodes) module	no
“CLIM”	hardware current limit	no
“VLIM”	hardware voltage limit	no
”INHB”	external INHIBIT signals	no
“RELY”	discharge relay	no
“FRMP”	fast ramp	yes (1 - 25% of Nominal V, 2 - 50% of Nominal V, 3 - 75% of Nominal V)
“NIPL”	not implemented	

5.2.1.23 Notes to *OptionSingleSpec (EHS)*

In order to request the specification of one option item *OptionSpec* the corresponding option string have to be written to the item *OptionSingleSpec.*

5.2.1.24 Items for public groups defined by the OPC server:

GroupDeviceID	list of all device identifiers	readable	VT_BSTR
GroupSoftwareID	list of all software identifiers	readable	VT_BSTR
GroupStatHardwareILimit	list of all status current limits	readable	VT_UI2
GroupStatHardwareVLimit	list of all status voltage limits	readable	VT_UI2
GroupStatITrip	list of all status current trips	readable	VT_UI2
GroupStatRegulationErr	list of all status regulation errors	readable	VT_UI2
GroupGeneralSumError	list of all sum errors	readable	VT_BOOL
GroupGeneralStable	list of all stable status	readable	VT_BOOL
GroupGeneralSafetyLoop	list of all safety loop status	readable	VT_BOOL
GroupGeneralFineAdjust	list of all fine adjustment flags	readable	VT_BOOL
GroupGeneralHwVLimitLow	list of all HW voltage limit tow low flags	readable	VT_BOOL
GroupBitRate	list of bit rates that are stored in modules	readable	VT_UI2
GroupErrThreshold	list error thresholds	readable	VT_UI2
GroupConfigRelFErr	list of bit mask for relay configurations	readable	VT_UI2
GroupAlarm	list of all alarm status information	readable	VT_BOOL
GroupAlive	list of all alive information	readable	VT_BOOL

If an error occurs it will be signalled by the item *alarm status* in connection with the check of the sum error flag from the item GeneralStat (GeneralStatSumError). These items will catch the errors by read and they will cancel the errors by write with the corresponding channel flag is set to “1”.

OPC alarm events under Data Access via EHQ3216Srv

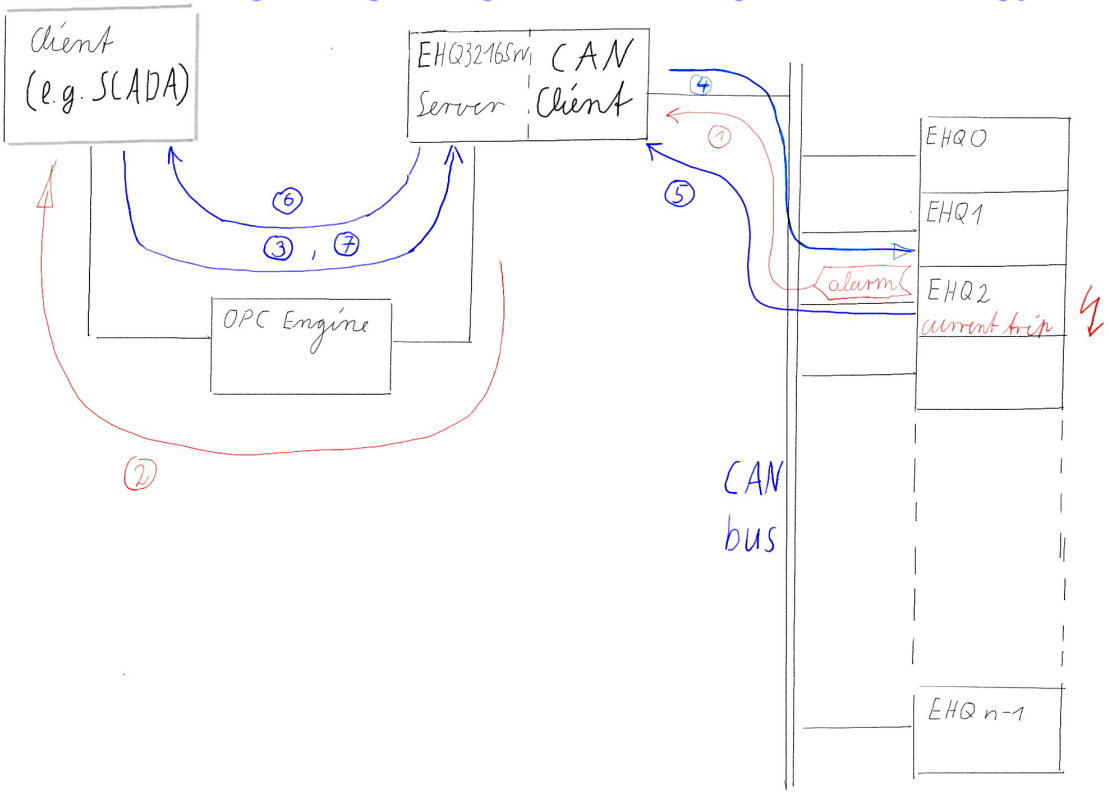

(1) A current trip happens and will generate one CAN alarm message with higher priority as the normal messages of the data transfer.

(2) The ***isegHVOPCServer*** sets the item Alarm to TRUE and gives a note of the kind of the alarm by the item “AlarmInformation” (both were build as a reported item in the name space).

(3, 4, 5, 6) The Client has to read which channel has tripped and is able to cancel the error flag by a write of the item “StatITrip” with the corresponding channel flag is set to “1”.

(7) Not necessary up to version 4.0.

5.2.2 Alarms and Events server

The OPC server offers the “Alarms & Events” feature built into the same executable in order to let the OPC client act quickly on a single event or an alarm.

The following alarms and events have been defined:

5.2.2.1 Simple events

canx.ErrorSafetyLoop	error status of safety loop	readable
canx.ErrorSupply	error status of supply voltages	readable
canx.ErrorSumError	error status of general sum status	readable

5.2.2.2 Tracking events

Computer.KeyboardPressed	access to local keyboard on server	readable
Computer.MouseActivity	access to local mouse on server	readable

iseg Spezialelektronik GmbH
Bautzner Landstr. 23
D - 01454 Radeberg / Rossendorf
Email: sales@iseg-hv.de
http://www.iseg-hv.com
Germany
Phone ++ 49 (0)351 / 26 996 - 0
Fax ++ 49 (0)351 / 26 996 - 21

6 OPC server part for iseg system crate *ECHx38*

The OPC server has been developed using the following tools:

- Softing OPC Toolkit, Ver. 4.0 DA3.0
- Microsoft Visual C++, Ver. 6.01
- PEAK System CAN device driver

The executable is included in ***isegHVOPCServer.exe*** also as OPC “Data Access” server and “Alarm and Event” server.

6.1 Configuration

The OPC server has to be configured at the beginning. It must get all information about the kind of **iseg** HV hardware connected to the CAN bus. This information is stored into the configuration file. The tool ***isegHVOPCcfg.exe*** is used to create this configuration file. It performs a scan on the CAN bus and collects information from the connected CAN nodes (modules and crates). Also it supports the graphical access to the initialising file ***isegHVOPCServer.ini***.
For further details see the configuration manual ***isegHVOPCSetup.pdf***.

6.2 Data Access Server and Alarm and Event Server

6.2.1 Data Access Server

The OPC (DA) server is made to work with more than one crate. Therefore each property of the **iseg** system crate has to be addressed in a geographical way to build a fully qualified item ID that means:

CANBUS.CRATE.ITEMNAME

The properties in the OPC server are defined as items. In the simplest case, such an item is directly coupled to a read or write via CAN bus. The “On” is an example. The OPC “Data Access” method is working via request queues.

6.2.1.1 Items of the releases from the server components

6.2.1.2 Items of Data Access

Syntax: *x* Є [0..15] number of the CAN bus
yy Є [0..63] number of the CAN node

can*x*.crate*yy*.Supply24V	crate power 24V	readable	VT_R4
can*x*.crate*yy*.Supply5V	crate power 5V	readable	VT_R4
can*x*.crate*yy*.Battery	battery voltage for the UPS ca. 24V	readable	VT_R4
can*x*.crate*yy*.TempBackPlane	temperature on the back plane	readable	VT_R4
can*x*.crate*yy*.TempPowerSupply	temperature on the DC/DC converter	readable	VT_R4
can*x*.crate*yy*.FanStageBackPlane	stage on the back plane fan unit	readable	VT_UI1
can*x*.crate*yy*.FanStagePowerSupply	stage on the crate power supply fan unit	readable	VT_UI1
canx.crate*yy*.Status	crate power status	write-/readable	VT_UI1
canx.crate*yy*.StatusACLinePower	status of the AC line power	write-/readable	VT_BOOL
can*x*.crate*yy*.On	status of the power	write-/readable	VT_BOOL
can*x*.crate*yy*.DeviceID	device identifier	readable	VT_BSTR
can*x*.crate*yy*.SoftwareID	software release	readable	VT_BSTR
can*x*.crate*yy*.BitRate	bit rate	readable	VT_UI2
can*x*.crate*yy*.Alive	crate is alive	readable	VT_BOOL
canx.crate*yy*.AlarmFlag	alarm status	readable	VT_BOOL
canx.crate*yy*.AlarmInformation	alarm information	readable	VT_BSTR

When the AlarmFlag goes true the item value of AlarmInformation will get one of the following strings:
“EMCY supply 24V”
“EMCY supply 5V”
“EMCY battery 24V”
“Temperature PS”
“Temperature BP”
“AC line power”

If there are more than one alarm sources the item value will display the latest received alarm. With help of the status items it will display all received alarms. It has to reset an alarm by write a one to the corresponding status bit of the Status item or a true to the StatusACLinePower item.

canx.crate*yy*.AlarmValue	alarm value	readable	VT_R4

alarm information – “EMCY supply 24V”	*measurement supply 24V*
alarm information – “EMCY supply 5V”	*measurement supply 5V*
alarm information – “EMCY battery 24V”	*measurement 24V battery voltage*
alarm information – “Temperature PS”	*measurement Temperature PS*
alarm information – “Temperature BP”	*measurement Temperature BP*
alarm information – “AC line power”	*nothing - 0*

The items “AlarmFlag”, “AlarmInformation” and “AlarmValue” are implemented as event driven update inside of the ***isegHVOPCServer***. The “AlarmFlag” will become a true if an error occurs. The “AlarmValue” is the corresponding measurement to the “AlarmInformation” item. The “AlarmInformation” describes the kind of the alarm (see Hints to the item AlarmInformation). The alarm will be generated with help of EMCY ID (see manual ***ECH-CANwithUPS_eng.pdf***). The crate will repeat the alarm trigger until the error will go away. These items are included (on request of Cern) in order to have an access to the fast alarm messages of the crates. The better way is to use the faster “Alarm & Event” part of the ***isegHVOPCServer***. Since version 4.01 the items as there are “AlarmFlag”, “AlarmInformation” and “AlarmValue” can be cleared by reset of the corresponding status

iseg Spezialelektronik GmbH
Bautzner Landstr. 23
D - 01454 Radeberg / Rossendorf
Email: sales@iseg-hv.de
http://www.iseg-hv.com
Germany
Phone ++ 49 (0)351 / 26 996 - 0
Fax ++ 49 (0)351 / 26 996 - 21

bit. The error of the crate can be reset only by a reset of the reason of the error followed by writing a *'1'* to the corresponding status bit.

The "Alarm Flag", "AlarmInformation" and "AlarmValue" will refreshed by the server if a new alarm is attempted but the client will register the new alarm only if the DA-value has been changed.

6.2.1.3 Crate power status

Capture status if voltages were out of range.

b7	b6	b5	b4	b3	b2	b1	b0
temperature to high		+24V to high	+24V to low	+5V to high	+5V to low	24V battery to high	24V battery to low

6.2.2 Alarm and Events Server

The OPC server offers the 'Alarms & Events' feature built into the same executable in order to let the OPC client act quickly on a single event or an alarm.

The following alarms and events have been defined:

Simple events:

canx.ErrorSupply24V	error of supply 24V	readable
canx.ErrorSupply5V	error of supply 5V	readable
canx.ErrorBattery24V	error of battery 24V (possible only if the crate power is off)	readable
canx.ErrorTemperaturePS	error of temperature senor on power supply 24V-DC-PS	readable
canx.ErrorTemperatureBP	error of temperature sensor on pack plane	readable
canx.ErrorACline_power	error of AC line power	readable

Tracking events:

Computer.KeyboardPressed	access to local keyboard on server	readable
Computer.MouseActivity	access to local mouse on server	readable

Appendix A

Following items will refreshed via the background cycle:

canx.mtyy.GeneralStat
canx.mtyy.Status
canx.mtyy.EventStatus
canx.mtyy.EventMask
canx.mtyy.EventChannelStatus
canx.mtyy.EventChannelMask
canx.mtyy.RampSpeed
canx.mtyy.IRampSpeed
canx.mtyy.On
canx.mtyy.Emcy
canx.mtyy.StatHardwareVLimit
canx.mtyy.StatHardwareILimit
canx.mtyy.StatITrip
canx.mtyy.StatINHIBIT
canx.mtyy.StatRegulationErr
canx.mtyy.HardwareVLimit
canx.mtyy HardwareILimit
canx.mtyy.Supply24V
canx.mtyy.Supply5V
canx.mtyy.BoardTemp
canx.mtyy.ErrThreshold
canx.mtyy.ConfigRelFErr

canx.mtyy.chzz.Vset
canx.mtyy.chzz.VMeas
canx.mtyy.chzz.Iset
canx.mtyy.chzz.Itrip
canx.mtyy.chzz.IMeas
canx.mtyy.chzz.Stat
canx.mtyy.chzz.Status
canx.mtyy.chzz.EventStatus
canx.mtyy.chzz.EventMask

canx.crateyy.Supply24V
canx.crateyy.Supply5V
canx.crateyy.Battery
can*x*.crate*yy*.TempBackPlane
can*x*.crate*yy*.TempPowerSupply
can*x*.crate*yy*.FanStageBackPlane
can*x*.crate*yy*.FanStagePowerSupply
can*x*.crate*yy*.On
canx.crate*yy*.Status
canx.crate*yy*.StatusACLinePower

Appendix E

Power supply calibration manual

Chapter V

iseg EHQ Calibration

Contents

Calibration of *iseg* Multi-Channel HV systems 4
1 Hardware equipment of the calibration unit 4
2 Software parts for the calibration unit 4
2.1 Program for re-calibration EHQCAL 4
2.2 Database *EHQDB* 5
2.3 OPC Server *EHQ3216Srv* 6
2.4 Program *Setohm* 6
2.5 Program *isegHVM* 6
3 Preparations before the start of a calibration 6
3.1 How to connect the iseg-Multi-channel HV devices to the calibration equipment 6
3.2 How to start program CALEHQ 6
4 Calibrating an iseg-Multi-channel HV module 7
4.1 Basic calibration 7
4.2 Visualization and manual adjustment 9
4.3 Measurement specifications 10
4.4 Offline visualization 10
5 Restoration of the original device configuration 11
6 Check the calibration 11

iseg Spezialelektronik GmbH
Bautzner Landstr. 23
D - 01454 Radeberg / Rossendorf
Email: sales@iseg-hv.de
http://www.iseg-hv.com
Germany
Phone ++ 49 (0)351 / 26 996 - 0
Fax ++ 49 (0)351 / 26 996 - 21

iseg Spezialelektronik GmbH
Bautzner Landstr 23
D - 01454 Radeberg / Rossendorf
Email: sales@iseg-hv.de
http://www.iseg-hv.com
Germany
Phone ++ 49 (0)351 / 26 996 - 0
Fax ++ 49 (0)351 / 26 996 - 21

Calibration of *iseg* Multi-Channel HV systems

1 Hardware equipment of the calibration unit

- iseg system CALIBRATION CRATE (CAN-IF / RS232-IF)
- load unit for 16 channel HV modules (Inputs 1:1 / 1:400, GPIB IF)
- KETHLEY 2001 Multimeter
- Pentium PC (delivered Compaq Intel Pentium III 1GHz)
- PEAK CAN PCI card
- National Instruments GPIB card

2 Software parts for the calibration unit

- OS WIN2000 SP2 or higher
- Calibration program CALEHQ
- OPC server for EHQ Multi-channel HV modules EHQ3216Srv
- Program SETOHM to test the calibration of modules to control the load unit separately
- Program to control the modules after the calibration

The last four programs will be installed during the set up of iseg OPC software package.
The set up of iseg OPC software package copies the database twice to disk in order to have a copy of the factory database:

- "[INSTALLDIR]\HVCAL\DB\EHQDB.MDB" – database to recalibration with the program EHQCAL
- "[INSTALLDIR]\EHQDB.MDB" – database without ODBC connection

2.1 Program for re-calibration EHQCAL

2.1.1 General description

The program EHQCAL provides an easy to handle tool for calibration of ***iseg*** Multi-Channel EHQ HV devices.

2.1.2 The calibration procedure

The purpose of this calibration is, on the one hand to ensure a correct voltage setting, and on the other hand to enable the device for precise measurements of the voltage and the current.

iseg Spezialelektronik GmbH
Bautzner Landstr. 23
D - 01454 Radeberg / Rossendorf
Email: sales@iseg-hv.de
http://www.iseg-hv.com
Germany
Phone ++ 49 (0)351 / 26 996 - 0
Fax ++ 49 (0)351 / 26 996 - 21

The first point ('DAC-calibration') determines the transformation of voltages into an integer DAC-value. The second ('ADC-calibration') is to determine a transformation from the values, measured by the ADC into physical voltages and currents respectively. All transformations are linear and in general given by

$$DAC = U * N_{DAC} - O_{DAC} \qquad (1)$$

$$U = (ADC_U - O_U) * N_U \qquad (2)$$

$$I = (ADC_I - O_I) * N_I - U * K_I, \qquad (3)$$

where N_{DAC}, O_{DAC}, N_U, O_U, N_I, O_I and K_I are the calibration values to be determined. U and I are physical voltages and currents.

The calibration is performed in two separate steps:

1. **DAC- / Voltage measurement calibration:** For a set of DAC-values the corresponding voltages and their ADC-values are measured. Since two constants are to be determined, two points would be the minimum. By default three points are used and the best fit is calculated.
2. **Current measurement calibration:** In order to determine the three constants NI, OI and KI, at least three independent measurements with two different resistors must be performed. Here by default at three different voltages for each of both resistors the current and it's ADC-value are measured. Note, that also the voltage must be measured. This is done using the results of the first calibration step.

2.2 Database *EHQDB*

All information of the calibration are stored to the database "ehqdb.mdb".

First location is in directory "[INSTALLDIR]\hvcal\db\ehqdb.mdb" to which also the ODBC is linked.

The second copy of this is in directory "[INSTALLDIR]\opc\ehqdb.mdb".

The MS Access database EHQDB contains complete calibration and configuration data of all HV-devices.

The data is structured in 6 tables:

1. Device Data
2. Device Properties
3. Channel Data
4. Measurement Specification
5. Voltage Measurement Data
6. Current Measurement Data

Device Data stores general specifications and properties that are applicable to every device type. Examples are the number of channels, device type, nominal voltage and current. There is exactly one entry per device. It is referenced by the ID number of the device.

Device Properties: specific properties, depending on the device type. For internal use only.

Channel Data contains the calibration values and errors (relative deviations between the fit and measured points). A complete set for one device implies one entry per channel. For each device there can be up to two sets, a master set (generated by ***iseg***) and a user set to store your calibration results.
Measurement Specifications stores the location of measurement points (voltages and resistors).
Voltage / Current Measurement Data: the raw data of a calibration (all measurement results during calibration). Only the latest data will be stored, a new calibration overwrites the previous.

Caution: The database is not intended for any direct editing (outside *EHQCAL*)!

2.3 OPC Server *EHQ3216Srv*

Set up and registration see “isegOPCSetup.pdf”.

2.4 Program *Setohm*

Control of the load unit

2.5 Program *isegHVM*

See manual “isegHVM220_eng.pdf”

3 Preparations before the start of a calibration

3.1 How to connect the iseg-Multi-channel HV devices to the calibration equipment

The iseg system CALIBRATION CRATE was build to calibrate and heat up EHQ modules before calibration. All slots can be equipped with EHQ modules during the calibration, but it is necessary that only one of the switches above the modules shows up. The switch in the line of the calibrating board have to switched up all others down. The correct set up of the switches must be done before power on.

3.2 How to start program CALEHQ

Start CALEHQ from folder START→Programs→HVCalib→CALEHQ.
Before a calibration procedure can be started, the name or ID of the operator must be entered. This is for bookkeeping purposes and the name will be saved into the database together with the results of the calibration.

iseg Spezialelektronik GmbH
Bautzner Landstr. 23
D - 01454 Radeberg / Rossendorf
Email: sales@iseg-hv.de
http://www.iseg-hv.com
Germany
Phone ++ 49 (0)351 / 26 996 - 0
Fax ++ 49 (0)351 / 26 996 - 21

4 Calibrating an iseg-Multi-channel HV module

4.1 Basic calibration

The dialog bar that appears below the pull-down menus summarizes the calibration procedure.

Step 1: Preparation

- Start *Open Device* from the dialog bar or via Database→Open Device. When delivered, the database contains a master set of calibration data. If the device has been calibrated before, it will also contain a user set. In this case an extra dialog will ask, which set to load.
- Enter the 6 digit device ID
- All information, necessary for calibration including current calibration data is loaded from the database *EHQDB*
- Button *Hardware Setup* or Setup→Hardware shows the measurement devices and the resistor that are intended to use for calibration. If not done yet, please connect them with the PC interface and to the resistor unit. Plug the voltmeter into the resistor socket with the shown ratio.

Step 2: Calibration

- Start *Calibration* from the dialog bar or via Device→Run Calibration.
- First of all, the interfaces to all contributing devices (HV unit, resistor unit, measurement devices) will be tested. If a test fails, an error message is shown. If this happens, please check that everything is connected properly and try again.
- Now the main calibration dialog appears:

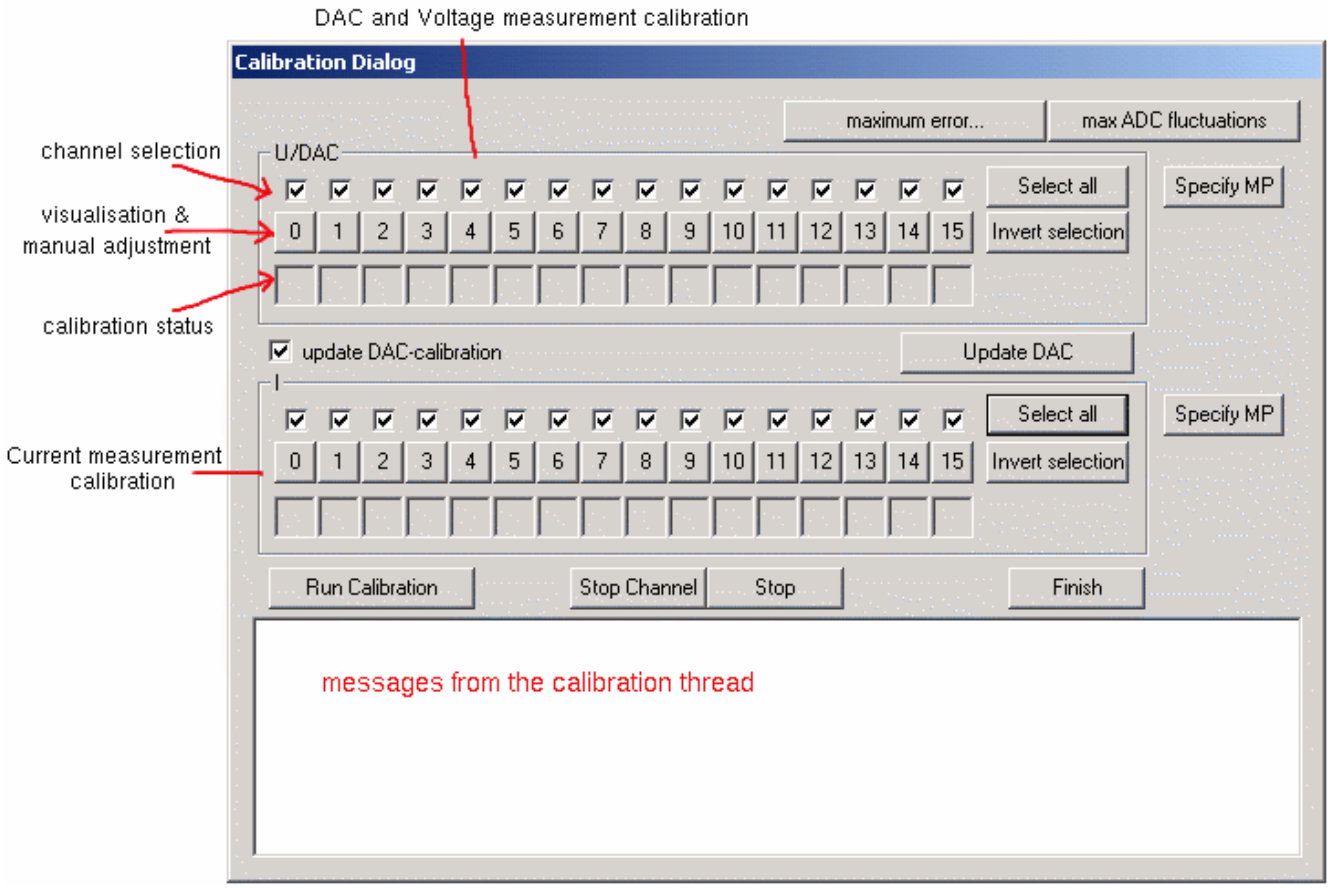

- Make your selection within the channels and calibration tasks.
- *Run Calibration* starts the calibration thread in the background.
- To stop the thread before finishing, press *Stop* or *Stop channel*. *Stop* will interrupt the calibration immediately (although this may take a few seconds), while *Stop channel* finish's the currently calibrated channel first. The thread can be stopped and restarted any time.
- For the status the following abbreviations are used:

  cal currently calibrating

  OK successfully calibrated

  ~ calibrated, but with deviations larger than the maximum allowed error (see device specification)

  err serious error, calibration had to be stopped
- When all calibration is done, press *Finish*

Step 3:

- Button *Data>>Database* or *Database→Save* updates the data base with the new measurement and calibration results.
- *Data>>Device* or *Device→Cal Data->EEPROM* writes the new calibration values into the device.

iseg Spezialelektronik GmbH
Bautzner Landstr. 23
D - 01454 Radeberg / Rossendorf
Email: sales@iseg-hv.de
http://www.iseg-hv.com
Germany
Phone ++ 49 (0)351 / 26 996 - 0
Fax ++ 49 (0)351 / 26 996 - 21

4.2 Visualization and manual adjustment

The visualization dialogs are opened from the main calibration dialog via the channel buttons. A plot gives an overview of the calibration. Manual changes of the calibration values are possible there. If such a dialog is opened for a channel that was not calibrated yet, the data from database is displayed.

4.2.1 The visualization dialog for DAC / Voltage calibration

Along the X-axis of the diagram we have the voltage of the measured points, starting from 0 V in the origin, up to the nominal voltage of the device. In the case of the blue plot, the Y-axis is the difference between the voltage, measured by the external voltmeter, and the voltage that by eq. (1) would lead to the DAC-value which was given for the point. The green plot shows the difference between the voltage, measured by the voltmeter and the ADC (together with the transformation in eq. (2)). Both plots are scaled by their maximum allowed errors that are given in the device specification.

On the right the calibration values can be modified. *Redraw* will update the plot for the changes. To restore the originally obtained values (which are the best fit, if every point has the same weight), press *Reset*. Via *Values from DB* previous values can be loaded from the data base, in order to check if they are still compatible with the new points. *Drop Measurement* will remove the points permanently.

4.2.2 The visualization dialog for Current measurement calibration

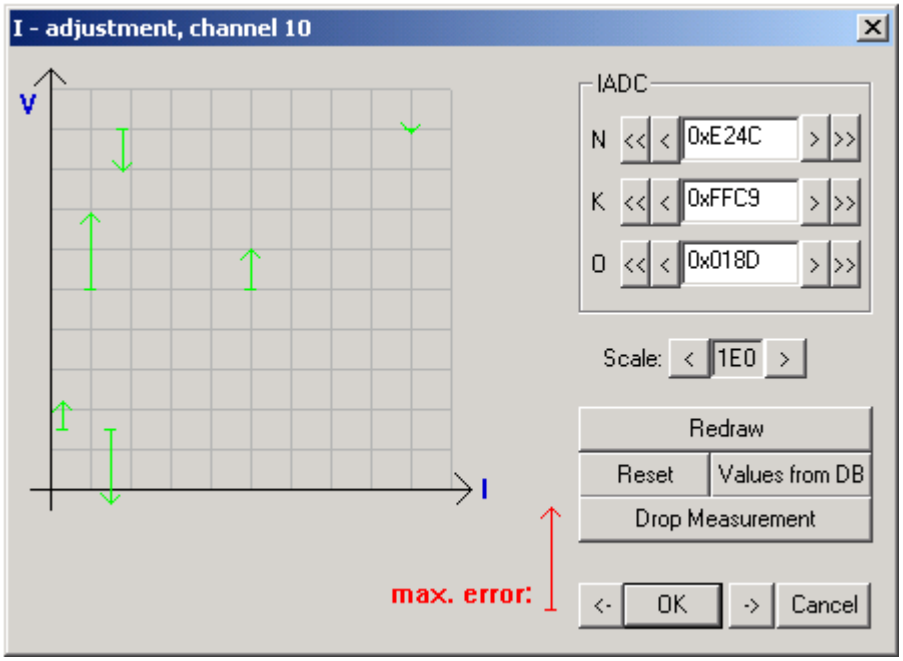

Here the measurement points are specified by the voltage and the current, since the transformation from the ADC-value to the current explicitly depends on the voltage (eq. 3). The axes range from 0 to the nominal current and voltage, respectively. The length of the arrows correspond to the difference between the current, measured by the external ampermeter, and the current, obtained by the transformed ADC-value. The scale is again relative to the maximum allowed error (shown by the arrow on the bottom). Points with larger deviation are drawn in red color.
Manual changes are analogous to the previous section.

4.3 Measurement specifications

Via the buttons *SpecMP* in the main calibration dialog it is possible to change the number of measurement points and their voltages.
For the DAC / Voltage calibration, select the number by the radio buttons and enter the voltage for each point. For the Current measurement calibration, two numbers (one for each resistor) can be changed on the left side in the dialog. The corresponding voltages must be entered on the right side.
In both cases make sure, that the selected voltages and corresponding currents are safely below the hardware limits (at least 5-10%).

4.4 Offline visualization

It is possible to view the measurement data from previous calibrations with the device and the calibration hardware offline. To do so, *Open* a device and select *Device→View* Calibration in the main menu. The main

iseg Spezialelektronik GmbH
Bautzner Landstr. 23
D - 01454 Radeberg / Rossendorf
Email: sales@iseg-hv.de
http://www.iseg-hv.com
Germany
Phone ++ 49 (0)351 / 26 996 - 0
Fax ++ 49 (0)351 / 26 996 - 21

calibration dialog appears. Go through the channels to view and change calibration data. It is not possible to start a calibration in this mode.

5 Restoration of the original device configuration

- Press *Open Device* and enter the ID-number. Load the master set.
- *Data>>Device* to restore the EEPROM settings.

6 Check the calibration

To check the calibration use the delivered program “setohm.exe” and the monitor program “icanHVcontrol.exe.”

Resumé

Les principaux objectifs du programme scientifique de l'experience ATLAS sont l'observation ou l'exclusion de physique au-delà du Modèle Standard, ainsi que la mesure de sections efficaces de production de processus du Modèle Standard. Pour ce faire, il est important de mesurer la luminosité au point d'interaction avec une grande précision. Dans l'experience ATLAS, la luminosité est extraite à l'aide de plusieurs détecteurs possédant des efficacités et acceptances géométriques variées. Différentes méthodes, telles que le comptage inclusif (ou en coïncidence) d'événements, ainsi que des mesures de courants intégrés provenant des calorimètres, sont calibrées et comparées afin d'assurer une détermination précise de la luminosité. Afin de permettre une comparaison additionelle et un meilleur contrôle sur les incertitudes systématiques liées à la détermination de la luminosité, une mesure indépendante utilisant le compartiment avant du calorimètre électromagnétique, basé sur la mesure du courant de son système haute-tension, a été développée. Ce document décrit comment la mise en route dud système haute-tension du calorimètre à argon liquide du détecteur ATLAS, ainsi que son application à une mesure de luminosité.

Abstract

The main goals of the ATLAS scientific programme are the observation or exclusion of physics beyond the Standard Model (SM), as well as the measurement of production cross-sections of SM processes. In order to do so, it is important to measure the luminosity at the interaction point with great precision. The ATLAS luminosity is extracted using several detectors with varying efficiencies and acceptances. Different methods, such as inclusive - or coincidence - event counting and calorimeter integrated current measurements, are calibrated and cross-compared to provide the most accurate luminosity determination. In order to provide more cross-checks and a better control on the systematic uncertainties, an independent measurement using the liquid argon (LAr) forward calorimeter (FCal), based on the readout current of its high-voltage system, has been developed. This document describes how the LAr calorimeter high-voltage system has been installed and commissioned, as well as its application to a relative luminosity determination.